# Macrodiversity MIMO Transceivers

by

Dushyantha A. Basnayaka

A dissertation submitted for the degree of

**Doctor of Philosophy**

in

Electrical and Electronic Engineering


University of Canterbury

New Zealand

Jun 2012

To my parents

# Abstract

In wireless systems, radio signals are corrupted due to fading, interference and noise. In order to handle the effects of fading and interference, modern systems employ various techniques including multi-antenna transceivers. Initially, multi-antenna systems were proposed only for point-point communication. More recently, multi-antenna transceivers have been proposed for multiuser (MU) wireless systems. There are various topologies in which multi-antenna transceivers can be used in a multiuser wireless environment. Among them, macrodiversity is an important concept driven by many scenarios, including base station cooperation, coordinated multipoint (CoMP) transmission and network multiple input multiple output (MIMO).

A communication system where antenna elements at both source and receiver are widely (geographically) separated is described as a macrodiversity communication system. For these macrodiversity systems, every link may have a different average signal to noise ratio (SNR) since the sources and the receive antennas are all in different locations. This variation in average SNR across the links makes the performance analysis of such systems more complex. For this reason, most of the results currently available are based on simulation. However, the value of analytical results can be immense for efficient computation and optimized operation. Therefore, in this thesis we present a comprehensive, and rigorous analytical investigation of various aspects of multiuser macrodiversity MIMO systems.

Two main aspects of macrodiversity MIMO systems are considered: the multiple access channel (MAC) and uplink user scheduling. In the earlier chapters of the thesis, we inves-

tigate the performance of uplink transmission employing multi-antenna transmitters and receivers. We analyze the signal-to-interference plus noise ratio (SINR) performance, symbol error rate (SER) and ergodic sum capacity etc. In a later chapter, we consider multiuser scheduling issues in macrodiversity multiuser MIMO systems. The primary emphasis is on the MIMO-MAC where we present some systematic performance metrics and approaches to multiuser scheduling which only require the long term channel state information (CSI). These methods provide a double advantage over scheduling using instantaneous CSI. First, the computational burden is lower and secondly, the delay between obtaining and using channel estimation is reduced.

# Acknowledgements

During my doctoral studies my work has benefited from many different people and institutions. I would like to express my heartiest gratitude to everyone who gave their hand to me. Above all, the shadow of the University of Canterbury was a huge support for me. She stood by me and my colleagues amidst the unprecedented troubles of the September 2010, earthquake that rattled Christchurch. Furthermore, I would like to acknowledge her for supporting me through a University of Canterbury International Doctoral Scholarship.

I am extremely grateful to my principal supervisor Associate Prof. Peter J. Smith for his directions and support. If I am going into detail, I greatly appreciate his suggestions for my PhD topic. Naturally I enjoy working on hard problems and the difficulty of the problems is an extra motivation for me to go further. I would also like to thank him for being patient, helpful and encouraging. I would also like to thank my co-supervisor Dr. Philippa A. Martin, for her support throughout my tenure as a PhD student.

Next, I am thankful to Adjunct Prof. Mansoor Shafi for introducing me to Peter and for believing in me. That single decision changed my career forever. If I have to say whose single decision has made the biggest impact on my career so far, the answer should definitely be Prof. Mansoor Shafi's. I wish him all the best in his life to be there for many more students like me around the world.

Further, I am very grateful to Senior Prof. Nimal Ekanayake at the University of Peradeniya for continuously encouraging me to pursue my post graduate studies and US based Prof. S. R. H. Hoole for the guidance, advice and help he extended me in times when I have given

up doing my post graduate studies which undoubtedly was a huge support.

Next, I should remind my friend, Dr. Abdulla Firag, whose support and experience as a recent doctoral graduate was enormously helpful to me.

I should mention my many colleagues across the School of Engineering at the University of Canterbury for their company and exchanging their ideas, thoughts and opinions on various subjects such as politics, economics, research towards changing the world. Those friends and ideas were undoubtedly inspirational and were an escape for me.

Last, but not least, I would like to thank my parents, to whom I dedicate this work, for their love, sacrifices and support and more importantly for implanting the value of education in my soul. Further, I am grateful to my beloved wife, Ruvini for her courage throughout my studies in New Zealand. Next I like to remind my little daughter, Sanumi, for making my life full of joy and excitement especially in times when I was deeply disappointed and drained due to my studies.

**Maha Basnayaka Mudiyanselage Pahala Walawwe Dushyantha Anuruddha Basnayaka**[a]

[a]D. A. Basnayaka is also known in his full name as Maha Basnayaka Mudiyanselage Pahala Walawwe Dushyantha Anuruddha Basnayaka. Then the name with initials becomes M. B. M. P. W. D. A. Basnayaka.

# Contents

# List of Figures

# List of Tables

# Abbreviations

| | |
|---|---|
| AWGN | additive white Gaussian noise. |
| BPSK | binary phase shift keying. |
| BS | base station. |
| cdf | cumulative distribution function. |
| CoMP | coordinated multi point transmission. |
| CSCG | circularly symmetric complex gaussian. |
| CDI | channel distribution information. |
| CSI | channel state information. |
| esf | elementary symmetric function. |
| FER | frame error rate. |
| iid | independent and identically distributed. |
| id | identically distributed. |
| LTE | long term evaluation. |
| MAC | multiple access channel. |
| mgf | moment generating function. |
| MIMO | multiple input multiple output. |
| ML | maximum likelihood. |
| MLD | maximum likelihood detection. |
| MMSE | minimum mean squared error. |
| $M$-PSK | $M$-ary phase shift keying. |

| | |
|---|---|
| $M$-QAM | $M$-ary quadrature amplitude modulation. |
| MRC | maximal ratio combing. |
| MS | mobile station. |
| MU | multiuser. |
| pdf | probability density function. |
| PEP | pairwise error probability. |
| QPSK | quadrature phase shift keying. |
| SER | symbol error rate. |
| SINR | signal to interference plus noise ratio. |
| SNR | signal to noise ratio. |
| ZF | zero forcing. |
| ZMCSCG | zero mean circularly symmetric complex Gaussian. |

# List of Symbols

| | |
|---|---|
| $j$ | $\sqrt{-1}$. |
| Re(z), Im(z) | Real and Imaginary parts of z. |
| lim | Limit. |
| ln,e | Natural logarithm, Euler's constant. |
| $\log_n$ | Logarithm base n. |
| $\mathcal{R}, \mathcal{C}, \mathcal{Z}$ | Set of real numbers, complex numbers and integers. |
| $\mathcal{R}^{m\times 1}, \mathcal{C}^{m\times 1}$ | Real, complex $m \times 1$ vectors. |
| $\mathcal{R}^{m\times n}, \mathcal{C}^{m\times n}$ | Real, complex $m \times n$ matrices. |
| $\mathrm{Tr}(\boldsymbol{X})$ | Trace of the matrix $\boldsymbol{X}$. |
| $\mathrm{etr}(\boldsymbol{X})$ | Shorthand form for $e^{\mathrm{Tr}\boldsymbol{X}}$. |
| $\det(\boldsymbol{X})$, $\lvert\boldsymbol{X}\rvert$ | Determinant of the matrix $\boldsymbol{X}$. |
| Perm (.) | Permanent of a rectangular matrix. |
| perm (.) | Permanent of a square matrix. |
| $\boldsymbol{X}^H$ | Conjugate transform of $\boldsymbol{X}$. |
| $\boldsymbol{X}^+$ | Moore-Penrose pseudo inverse of $\boldsymbol{X}$. |
| $\boldsymbol{I}_n, \boldsymbol{I}$ | $n \times n$ Identity matrix. |
| $\boldsymbol{O}_{n\times m}$ | $n \times m$ matrix of all zeros. |
| $(a_{ik})$ | Matrix whose entry in the ith row and kth column is $a_{ik}$. |
| $(.)^T, (.)^H$ | Transpose, conjugate-transpose. |
| $\bar{X}$ | Complex conjugate of complex scalar $X$. |

| | |
|---|---|
| $\text{diag}(a_1, \ldots, a_N)$ | Square diagonal matrix with $a_1, \ldots, a_N$ on the main diagonal. |
| $\boldsymbol{X} > 0, \boldsymbol{X} \geq 0$ | Positive-definite, positive-semidefinite matrix $\boldsymbol{X}$. |
| $\|.\|$ | (vector argument): Euclidian vector norm, i.e., $\|\boldsymbol{x}\|^2 = \boldsymbol{x}^H\boldsymbol{x}$. |
| $\|.\|$ | (matrix argument): Frobenius norm, i.e., $\|\boldsymbol{X}\|^2 = \text{Tr}(\boldsymbol{X}^H\boldsymbol{X})$. |
| $\boldsymbol{X}^{\frac{1}{2}}$ | Symmetric square root of $\boldsymbol{X}$. |
| $\boldsymbol{X}^{\circ\frac{1}{2}}$ | Element wise square root of $\boldsymbol{X}$. |
| $\boldsymbol{X} \circ \boldsymbol{Y}$ | Hadamard product of matrix $\boldsymbol{X}$ and $\boldsymbol{Y}$. |
| Pr(.) | Probability of (.). |
| f(.) | Function of (.). |
| $\sim$ | Is distributed as. |
| $\simeq$ | Approximately equal to. |
| $\approx$ | Approximately distributed as. |
| $E_X\{.\}$ | Mean of random variable X. |
| $\text{Var}_X\{.\}$ | Variance of random variable X. |
| $\mathcal{N}(\mu, \sigma^2)$ | Real Gaussian random variable with mean $\mu$ and variance $\sigma^2$. |
| $\mathcal{CN}(\mu, \sigma^2)$ | CSCG random variable with mean $\mu$ and variance $\sigma^2$. |
| $\mathcal{M}_X(t)$ | Moment generating function of random variable X. |
| $\phi_X(t)$ | Characteristic function of random variable X. |

## Notes

All vectors are designated with italic bold lower case while matrices are given in italic bold upper case.

# Chapter 1

# Introduction

From the date when animals on earth started to live in small groups, communication between individuals became very important. This communication helped the individuals to form and expand their groups which became the building blocks of animal civilization. Among such animal groups, humans developed complex languages and communication methods. Until recently, these communication techniques were extremely tribal.

Since the late 19th century, humans have successfully performed long-haul communication with the help of technological support. This has gradually expanded and broadened the knowledge among different groups of people. Ever since this time, the desire for more and more sophisticated communication technologies has been growing. Among notable milestones, the electrical telegraph, telephone, radio and television are in the forefront.

In the early 1980s, analog wireless mobile cellular communication systems started to emerge. Soon after, digital wireless mobile systems were developed, which have pushed modern telecommunications into a whole new dimension. Digital communication was widely adopted due to its remarkable capabilities to evolve, on an unprecedented scale. It is now being used not only for voice services but also for many different services such as data, multimedia etc. Due to these applications, digital wireless systems have now become an integral part of our life. Since communication became personal, the demand for high data rates, more reliability and portability has grown rapidly. Today, wireless communication has grown to a sophisticated space and time communication architecture

which has enabled engineers to support the growing demand for wireless resources [1]. Many modern wireless systems have very high spectral efficiency and diversity. One of the techniques used to achieve such a high spectral efficiency and reliability is multiple input multiple output (MIMO) technology along with smart signal processing to communicate over time varying wireless channels [1, 2].

MIMO technology is being used and proposed in the near future for many modern wireless systems in many different scenarios to combat against fading and to improve performance. There are many different ways to implement MIMO technology in wireless systems. For example, MIMO is used to improve the spectral efficiency of point to point wireless links by employing multiple co-located antennas at the transmitter and the receiver. On the other hand, multiple co-located antenna base stations (BS) are used to improve the link reliability of cellular mobile wireless systems. Recently, cooperative multipoint (CoMP) transmission and network MIMO concepts have given rise to macrodiversity MIMO techniques to improve spectral efficiency further in cellular networks [3, 4, 5]. The benefits of MIMO technology comes at the price of complex transceiver technologies which need to be designed carefully according to the operating conditions and priorities.

Innovative MIMO designs come as a result of system understanding. Wireless systems, including MIMO systems, suffer from a phenomenon called multipath fading and it is very important to quantify their performance in practical fading environments [6, 7]. Performance measures such as the signal to interference plus noise ratio (SINR), bit error rate (BER), symbol error rate (SER) and capacity are some of the common measures found in the wireless literature [8, 9]. Analyzing system performance in general is very important, because it broadens our understanding of the system.

## 1.1 Problem Statement and Focus

Performance results for the legacy single input single output (SISO) system are well-known for a wide variety of scenarios [10]. However, performance analysis of MIMO links is considerably different from the legacy SISO systems, because it involves vectors and matrices as explained in Sec. 2.1.3 [11]. Therefore, performance analysis has to go in parallel with linear algebra [12]

and multivariate statistical theory [13, 14, 15, 16]. Fortunately, we have a very rich and vibrant multivariate statistical theory which has directly influenced wireless research over many decades. Because this theory has developed a coherent methodology, the performance analysis of many conventional MIMO systems is now well developed. Multivariate statistical theory, which has been developed since the early $20^{\text{th}}$ century [17], must be directly credited for some of the rapid development in MIMO wireless research. In contrast, performance analysis for macrodiversity MIMO becomes extremely difficult or impossible due to the lack of coherent, well established resources to handle the channel matrices that arise in macrodiversity MIMO systems. Simulation results are possible, but there is a major drawback in simulation results as they do not allow us to identify important contributing factors. Understanding these contributing factors is very important, because it allows us to optimize system performance. Therefore, analytical results for SINR, SER and ergodic capacity are invaluable for understanding, optimized design and rapid evaluation. Hence, the prime objective of this thesis is to obtain analytical results for the performance of macrodiversity MIMO systems. Therefore, this thesis contains a rigorous investigation of the performance of macrodiversity MIMO systems in various practically important settings.

## 1.2 Thesis Outline and Contributions

Despite the lack of a coherent statistical approach to deal with the channel matrices that arise in macrodiversity multiuser (MU) MIMO systems, we are able to analyze several practically important macrodiversity MIMO systems, quantifying the link level performance of these systems in terms of channel distribution information (CDI). These results comprise the first rigorous analytical investigation in this area of wireless communication for finite system sizes and has led to the solution of several long standing research problems. In particular, our contributions are as follows.

### 1.2.1 Macrodiversity Maximal Ratio Combining

The performance of maximal ratio combining (MRC) in Rayleigh channels with co-channel interference (CCI) is well-known for receive arrays which are co-located, i.e., where the antennas are

close enough to experience equal average signal to noise ratio (SNRs) from a given source. However, for macrodiversity systems the situation is much less clear. Hence, in Chapter 3, we consider MRC performance in Rayleigh channels with CCI and a macrodiversity architecture. We derive approximate and exact symbol error rate results for $M$-ary quadrature amplitude modulation ($M$-QAM)/binary phase shift keying (BPSK) modulations and use the analysis to provide a simple power metric and error floor results. The analysis can be applied to wide range of modulations where the SER can be written in terms of an expected value of the Gaussian $Q$-function and $Q^2$-function. Numerical results, verified by simulations, are used in conjunction with the analysis to gain insight into the effects of the link powers on performance.

### 1.2.2 Ergodic Sum Capacity of Macrodiversity MIMO Systems

In Chapter 4, we consider a macrodiversity MIMO multiple access channel (MAC) where all sources and receive antennas are widely separated and all links experience independent Rayleigh fading. For this system, we consider the ergodic sum capacity, under the assumption of no channel state information (CSI) at the transmitters. For two sources, we derive the exact ergodic sum capacity. The result is given in closed form, but the details are complicated and for more than two sources, it would appear that an exact approach is too complex to be useful. Hence, we develop an approximation and a bound for the general case. The first technique is very accurate, but the functional form is awkward to interpret. Hence, a second, less accurate but simple bound is developed which has a familiar and appealing structure. This bound leads to insight into capacity behavior and its relationship with the average link SNRs.

Note that the methodology developed is for the case of arbitrary powers for the entries in the channel matrix. There is no restriction due to particular cellular structures. Hence, the results and techniques may also have applications in multivariate statistics.

### 1.2.3 Dual User Macrodiversity MIMO Systems with Linear Receivers

The performance of linear receivers in the presence of co-channel interference in Rayleigh channels is a fundamental problem in wireless communications. Performance evaluation for these systems is well-known for receive arrays which are co-located. In contrast, there are no analytical results available for macrodiversity systems (such as network MIMO) for finite system sizes (see Sec. 2.1.3) where both the sources and receive antennas are widely separated. In this macrodiversity layout, receive antennas experience unequal average SNRs from a given source and a single receive antenna receives a different average SNR from each source. In general, this appears to be an extremely difficult problem. However, progress is possible for the two-user scenario. In Chapter 5, we derive exact closed form results for the probability density function (pdf) and cumulative distribution function (cdf) of the output SINR and SNR of minimum mean squared error (MMSE) and zero forcing (ZF) receivers in independent Rayleigh channels with arbitrary numbers of receive antennas. The results are verified by Monte Carlo simulations and high SNR approximations for the SER of MMSE and ZF receivers are also derived. These results lead to a simple metric

$$\frac{\operatorname{Tr} \boldsymbol{P}_2}{|\boldsymbol{P}_1| \operatorname{Tr}\left(\boldsymbol{P}_1^{-1}\boldsymbol{P}_2\right)}, \tag{1.1}$$

which relates system performance, in particular the SER of user 1, to the average link SNRs (contained in the $\boldsymbol{P}_1$, $\boldsymbol{P}_2$ matrices) and therefore provides insight into the effect of these SNRs. Definitions of $\boldsymbol{P}_1$ and $\boldsymbol{P}_2$ are given in Chapter 5. The results enable further system analysis such as the evaluation of outage probability, BER and capacity.

### 1.2.4 Multiuser Macrodiversity MIMO Systems with Linear Receivers

In Chapter 5, we considered the statistical properties of the output SINR/SNR of MMSE and ZF receivers in dual user scenarios. How the macrodiversity affects the system performance is

quantified through a simple performance metric which is only dependent on the average link SNRs. In Chapter 6, we extend the results in Chapter 5 to the case of arbitrary numbers of sources. For this general situation, we derive the approximate pdf and cdf of the SINR/SNR for MMSE/ZF receivers. The final pdf approximation shall be shown to have a remarkably simple form as a generalized mixture of exponentials. Further, we derive high SNR SER results for MMSE/ZF receivers. Similar to the dual user analysis, the high SNR analysis leads to a compact metric

$$\frac{\mathrm{Perm}\left(\boldsymbol{Q}_2\right)}{|\boldsymbol{P}_1|\,\mathrm{Perm}\left(\boldsymbol{P}_1^{-1}\boldsymbol{Q}_2\right)}, \tag{1.2}$$

which relates the system performance, particularly SER, to the average link SNRs. This metric provides insight into the effect of these SNRs in general antenna and user configurations. Definitions of $\boldsymbol{P}_1$, $\boldsymbol{Q}_2$ are given in Chapter 6.

### 1.2.5 Maximum Likelihood Detection in Macrodiversity MIMO Systems

In Chapter 7, we present a performance analysis of maximum likelihood detection in a macrodiversity MIMO system. First, we consider the base line scenario where an uncoded system operates in a Rayleigh flat fading environment. Secondly, we consider the extension to a Rician fading environment. The performance analysis builds on an exact evaluation of the pairwise error probability (PEP) for both flat Rayleigh and Rician fading which leads to a union bound for SER. The SER results are shown, as well as diversity order, a high SNR analysis and an investigation of the impact of macrodiversity.

### 1.2.6 Uplink Macrodiversity MU-MIMO Scheduling

In Chapter 8, we consider the idea of using long term CSI for user scheduling in a macrodiversity MU MIMO-MAC channel. In particular, channel distribution information based user scheduling is beneficial in CoMP systems where a limited backhaul interconnection network is present and the use of instantaneous CSI is restricted. Despite the analytical difficulty in deriving scheduling

metrics for user scheduling using CDI, in this chapter we propose several user scheduling criteria based on information theoretical capacity, linear multiuser receiver processing and maximum likelihood decoding. Furthermore, we derive several systematic group scheduling metrics and individual scheduling metrics which may allow system designers to design novel scheduling algorithms based on these scheduling metrics for improved system throughput and user fairness.

## 1.3 Publications

The following is a list of journal and conference publications produced during my PhD studies.

- Journal articles

    1. **D. A. Basnayaka**, P. J. Smith and P. A. Martin, "Performance analysis of dual-user macrodiversity MIMO systems with linear receivers in flat Rayleigh fading," accepted for publication in *IEEE Trans. on Wireless Commun.*
    2. **D. A. Basnayaka**, P. J. Smith and P. A. Martin, "The effect of macrodiversity on the performance of MLD in flat Rayleigh/Rician fading," accepted for publication in *IEEE Commun. Lett.*.
    3. **D. A. Basnayaka**, P. J. Smith and P. A. Martin, "The effect of macrodiversity on the performance of maximal ratio combining in flat Rayleigh fading," submitted to *IEEE Trans. on Commun.*
    4. **D. A. Basnayaka**, P. J. Smith and P. A. Martin, "Ergodic sum capacity of macrodiversity MIMO systems in flat Rayleigh fading," submitted to *IEEE Trans. Inform. Theory*
    5. **D. A. Basnayaka**, P. J. Smith and P. A. Martin, "Performance analysis of macrodiversity MIMO systems with MMSE and ZF receivers in flat Rayleigh fading," submitted to *IEEE Trans. on Wireless Commun.*
    6. **D. A. Basnayaka**, P. J. Smith and P. A. Martin, "On optimum linear transceivers in the presence of imperfect channel state information and codebook feedback," in preparation

for submission to *IEEE Trans. on Wireless Commun.*

7. A. Firag, P. J. Smith, A. Papathanassiou, M. Shafi, **D. A. Basnayaka** and P. A. Martin, "A comparison of transceiver techniques in multi-user MIMO broadcast systems," in preparation for submission to *IEEE Trans. on Wireless Commun.*

- Conference papers

1. **D. A. Basnayaka**, P. J. Smith and P. A. Martin, "Ergodic sum capacity of macrodiversity MIMO systems in flat Rayleigh fading," *IEEE ISIT*, MA, USA, pp. 2181–2185, Jul. 2012.

2. **D. A. Basnayaka**, P. J. Smith and P. A. Martin, "Exact dual-user macrodiversity performance with linear receivers in flat Rayleigh fading," *IEEE ICC*, Ottawa, Canada, pp. 5626–5631, Jun. 2012.

1. **D. A. Basnayaka**, P. J. Smith and P. A. Martin, "Symbol error rate performance of macrodiversity maximal ratio combining in flat Rayleigh fading," *IEEE AusCTW*, Wellington, New Zealand, pp. 25–30, Feb. 2012.

2. A. Firag, P. J. Smith, A. Papathanassiou, M. Shafi, **D. A. Basnayaka** and P. A. Martin, "A comparison of transceiver techniques in multi-user MIMO broadcast systems," *IEEE AusCTW*, Wellington, New Zealand, pp. 31–36 , Feb. 2012.

- Patents

1. P. J. Smith and **D. A. Basnayaka** "Multiuser scheduling for radio resource allocation," US provisional patent application 61/648505, filed May 17, 2012.

# Chapter 2

# System Background and Assumptions

When analyzing complex engineering systems, it is usually impossible to consider all the system parameters. Instead, we consider an appropriate model that captures the most important properties of the system for a particular problem of interest. This approach is also true for the wireless communication systems considered in this thesis. Therefore, in this chapter we present the background information and assumptions used throughout the thesis. First, the models used for the time varying wireless channel and the fading environment are described. Then, various wireless MIMO topologies are described followed by a description of the macrodiversity MU-MIMO topologies which form the heart of this thesis.

## 2.1 Wireless Channel and Models

In this section, we explain the basic characteristic of wireless channels using a conventional SISO wireless link as shown in Fig. 2.1. In Sec. 2.1.3, we extend this to a discussion of MIMO wireless channels. There are wireless channel characterizations available for over-the horizon communications [18], digital mobile communication [19] and indoor communication [20]. In this thesis, we primarily consider digital mobile channel characterization as discussed in [19]. Unlike the additive white Gaussian noise (AWGN) channel [10], wireless channels suffer from fading which creates a whole new set of challenges in system design.

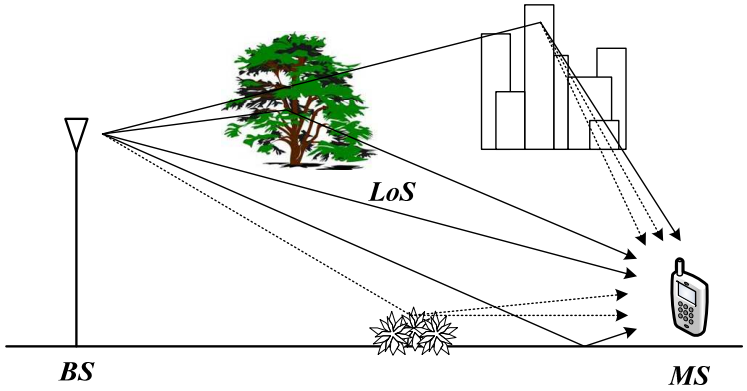


Figure 2.1: Typical outdoor wireless link between a single transmitter and a single receiver.

Consider an electromagnetic (EM) wave with constant power which is equivalent to an unmodulated carrier (say $A\cos(2\pi f_c t)$) that is being transmitted from the BS in Fig. 2.1. After propagating through the atmosphere a distance of typically several kilometers, the transmitted wave reaches the mobile station (MS) on the ground. The received signal in the absence of noise may be expressed as

$$y(t) = A\sum_n \alpha_n(t)\cos\left(2\pi f_c\left(t-\tau_n(t)\right)\right), \tag{2.1}$$

where $\alpha_n(t)$ is the time-variant attenuation factor associated with the nth propagation path and $\tau_n(t)$ is the corresponding propagation delay. We may view the received signal $y(t)$ in equation (2.1) as the sum of a number of signals each of which has a time-variant amplitude, $\alpha_n(t)$, and delay, $\tau_n(t)$. Also, the delays and amplitudes associated with the different signal paths change at different rates in a random manner. However, we are able make some fundamental observation as follows. There is a mean signal strength at the MS along with noise like, rapid variations due to delayed and scattered signal components. The mean signal strength is present regardless of the presence of a line of sight (LoS) path. Scattering creates multiple signal paths which are subsequently received by the MS constructively or destructively causing a highly random fluctuation of signal power around the mean signal strength. On the other hand, if there is a LoS path between BS and MS, then there is a non-faded signal component as well. However, the LoS path is not common in urban wireless mobile systems. The characteristics of receive power vs distance are

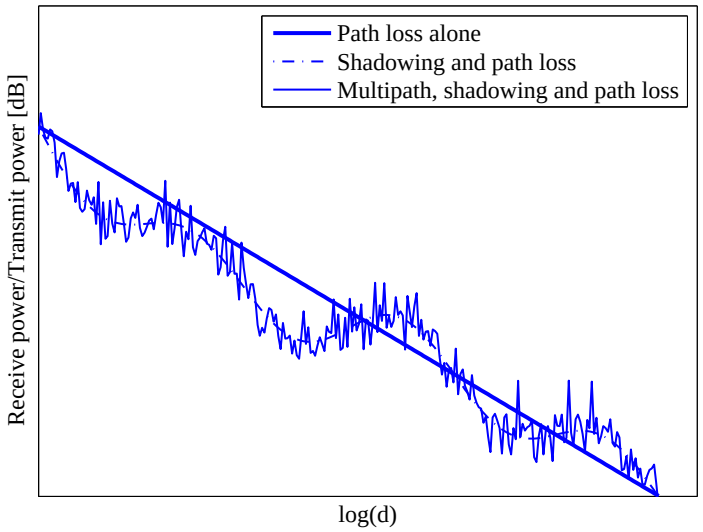


Figure 2.2: Combined path loss, shadowing and multipath fading.

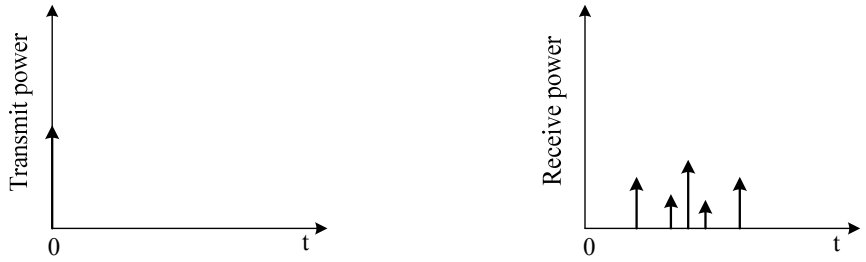


Figure 2.3: Illustration of a power delay profile.

illustrated in Fig. 2.2. The distance from BS to MS is $d$. This simple example demonstrates some of the most fundamental limitations of the wireless channel such as large-scale fading (shadowing) and the small-scale fading, which is commonly known as multipath fading. Large-scale fading is the change in mean receive power due to the path loss and shadowing [8]. On the other hand, multipath fading is the rapid fluctuation of instantaneous signal strength around the mean power. Due to changes in path loss, shadowing and multipath, the strength of the received signal varies with time. Therefore, the wireless channel is a time varying system.

There are several critical measures in time varying wireless channel characterization which directly influence data transmission strategies. A wireless channel is completely characterized by its power delay profile [10]. A typical power delay profile is illustrated in Fig. 2.3. A single impulse at the

transmitter results in multiple impulses at the receiver at different times. In practice, radarlike pulses which have a width of the order of nano seconds, are used instead of impulses to measure the power delay profile. Received impulses are also not exactly impulses but resolvable pulses with certain widths. A more comprehensive discussion of channel sounding can be found in [20, 21]. If the wireless channel is considered as a system, which is the case in most analysis, the power delay profile closely resembles the channel transfer function. An important measure deduced from the power delay profile is called delay spread. The delay spread is the difference between the time of arrival of the earliest significant multipath component and the time of arrival of the last multipath component [22, pp. 31]. There are two more important measures which can be deduced from the power delay profile: channel coherence bandwidth and coherence time. The coherence bandwidth is the frequency range over which the fading process is correlated. If the transmitted signal bandwidth is smaller than the channel coherence bandwidth, then the fading is referred to as frequency flat. If not, the fading is called frequency selective. Inter-symbol interference occurs in frequency selective channels due to the larger delay spread. In contrast, there is only one impulse in the power delay profile of frequency flat fading channels. The coherence time determines the time duration over which the channel impulse response remains unchanged. This in turn gives rise to the notions of slow fading and fast fading [22, pp. 30]. This thesis consider frequency flat wireless channels.

Due to the large number of influencing factors on a wireless channel, physical modeling of a generic link is difficult. There is a large body of research in this area and many standards where wireless channel models appear [23, 20, 24, 25]. A fairly comprehensive study of physical channel models can be found in [26]. In this thesis, a simple yet widely accepted stochastic channel modeling is considered [27]. This is discussed in Sec. 2.1.1. A comparison between complex industrial spatial channel models and simple stochastic channel models can be found in [28].

### 2.1.1 Statistical Channel Models

#### Path Loss and Shadowing

Transmit power attenuation due to path loss alone is often modeled as

$$P_r = A\frac{P_t}{d^\gamma}, \tag{2.2}$$

where $P_t$ and $P_r$ are transmit power and received power respectively, $\gamma$ is the path loss exponent and $A$ is a unitless constant that accounts for all other contributing factors. In this simplified path loss model, $\gamma$ is different from the free space path loss exponent which is equal to 2. In this thesis, it is taken to be in the range from 2.5 to 4 which models environments from rural to dense urban areas.

Shadowing due to the shadowing effects of large obstacles such as buildings, is often modeled as a log normal random variable [8, 19, 29]. Hence, it has the following representation as

$$\Psi = 10^{\frac{U}{10}}, \tag{2.3}$$

where $U \sim \mathcal{N}\left(0, \sigma_{SF}^2\right)$ and $\sigma_{SF}$ is the standard deviation of the shadowing in dB. Then, the power falloff due to both path loss and shadowing can be given by

$$P_r = A\frac{P_t}{d^\gamma}\Psi. \tag{2.4}$$

In this thesis, the power attenuation due to long-term fading is assumed to be known. In digital communication systems, a wireless channel is observed as a snapshot of a real wireless link between a transmitter and a receiver in a small time duration which is of the order of microseconds. This smallest transmission duration in digital wireless communication is called a channel use or a time slot which has a duration represented by $T_s$. In such a small time window, the power variation due to long-term fading is negligible which justifies the deterministic assumption of long-term fading. Typically long-term fading affect the average link SNRs as the MS moves a distance of the order of the cell size. Due to fast moving mobile users in rich scattering environment, the multipath

fading can not be considered as deterministic. Hence it is treated as a random phenomenon which is more influencing to the design of reliable and efficient communication systems. That is the focus of following discussion.

### Rayleigh Fading

A Rayleigh fading model is commonly used to describe the receive power where there is no line of sight between transmitter and receiver but there is a dense urban environment containing a large number of scattering sources which generate a large number of scattered waves at the receiver. Due to the large number of contributing waves, it is hard to develop a functional relationship for received power due to multipath fading in such an environment. Hence, in this thesis the standard statistical model is used. In the Rayleigh fading case, the channel fading amplitude, $Y$, is distributed according to

$$f_Y(y) = 2ye^{-y^2}, \quad y \geq 0. \tag{2.5}$$

Here it is assumed that $E\left\{Y^2\right\} = 1$.

### Rician Fading

A Rician fading model is commonly employed in describing scenarios where a LoS path is present. In Rician fading, the channel fading amplitude, $Y$, is distributed according to the pdf

$$f_Y(y) = \frac{2y}{\Theta} e^{-\frac{y^2}{\Theta} - \nu^2} I_0\left(\frac{2y}{\Theta} v\right), \quad y \geq 0, \tag{2.6}$$

where $\Theta$ and $\nu^2$ are the power of the scattered paths and direct path respectively. An important parameter in the Rician probability density function is the $K$ factor which is defined as

$$K = \frac{\nu^2}{\Theta}. \tag{2.7}$$

Clearly, the average link power, $E\left\{Y^2\right\} = \Theta + \nu^2$. There is another representation of the Rician fading amplitude, in which the average link power is normalized to unity to give $\Theta + \nu^2 = 1$. This constraint along with the constraint in (2.7) gives $\Theta = 1/(1+K)$ and $\nu^2 = K/(1+K)$. These values for $\Theta$ and $\nu^2$ give a slightly modified Rician fading amplitude distribution where the average link power is normalized to unity. So $E\left\{Y^2\right\} = 1$. In this thesis we may use both representations interchangeably.

### 2.1.2 Modeling SISO Channels

A block diagram of the SISO channel shown in Fig. 2.1 is given in Fig. 2.4. Consider a digital communication scenario in which the source transmits digital data across a frequency flat slow fading wireless channel. If the source and the destination stations are assumed to be perfectly synchronized, the received signal at the receiver in the $\tau^{th}$ time slot is given in complex baseband representation as [8, 30]

$$r(\tau) = h(\tau)\, s(\tau) + n(\tau), \tag{2.8}$$

where $s$ is the transmitted complex data signal, $r$ is the complex receive signal, $n$ is the zero mean circularly symmetric complex Gaussian (ZMCSCG) thermal noise and $h$ is the complex channel response. The channel response, $h$, represents the fading in the wireless channel. In an AWGN channel, the channel coefficient, $h$, is essentially equal to unity. In Fig. 2.4, $P$ gives the average link power. From the previous discussion, it is apparent that both long-term and multipath fading contribute to the instantaneous link power. Since the long-term fading is assumed to be a deterministic value in this thesis, the channel response can be decomposed into a product of the long-term fading and multipath fading. Hence, the channel coefficient in the $\tau^{th}$ time slot becomes

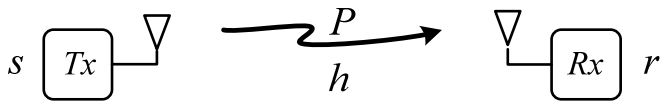


Figure 2.4: A block diagram of a SISO channel.

$$h(\tau) = \sqrt{P} h_w(\tau), \tag{2.9}$$

where $h_w(\tau)$ represents the normalized multipath fading. In a Rayleigh fading environment, $h_w$ is complex Gaussian with zero mean and $E\left\{|h_w|^2\right\} = 1$. We say that $h_w \sim \mathcal{CN}(0,1)$. Therefore, $h_w(\tau)$ is called the normalized channel coefficient. In Rician fading, $h_w(\tau) \sim \mathcal{CN}\left(\sqrt{\frac{K}{1+K}}\Omega, \frac{1}{1+K}\right)$, where $\sqrt{\frac{K}{1+K}}\Omega$ is the complex mean which accounts for the power of the direct path. For the normalized channel coefficient, $|\Omega|^2$ is set to unity. Therefore $E\left\{|h_w(\tau)|^2\right\} = 1$ which give rise to $E\left\{|h(\tau)|^2\right\} = P$. Hence, the power of the LoS path from transmitter to receiver is equal to $\frac{PK}{1+K}$.

### 2.1.3 Modeling MIMO Channels

In the previous section, wireless links between a single transmitter and a receiver were discussed. In this section, MIMO links [1, 31, 32] are discussed in a frequency flat fading environment. Consider a situation where $N$ transmit antennas transmit multiple data symbols (say $s_i$ for $i = 1, \ldots N$) in the same resource unit (i.e., the same time slot and frequency) which are received by $n_R$ receive antennas as in Fig. 2.5. In a situation like this, the wireless link between transmit antenna $k$ and receive antenna $i$ can be modeled in the same way as in (2.8). Then, the set of observations in the $\tau^{th}$ time slot at the $n_R$ receivers can be given by [22],

$$\boldsymbol{r}(\tau) = \boldsymbol{H}(\tau)\,\boldsymbol{s}(\tau) + \boldsymbol{n}(\tau), \tag{2.10}$$

where $\boldsymbol{s}$ is a vector of $N$ transmitted data signals, $\boldsymbol{r}$ is a vector of $n_R$ received signals, $\boldsymbol{n}$ is a ZMCSCG noise vector with variance $\sigma^2$ and $\boldsymbol{H}$ is a $n_R \times N$ channel matrix defined by

$$\boldsymbol{H}(\tau) = \begin{pmatrix} h_{11}(\tau) & h_{12}(\tau) & \ldots & h_{1N}(\tau) \\ h_{21}(\tau) & h_{22}(\tau) & \ldots & h_{2N}(\tau) \\ \vdots & \vdots & \ddots & \vdots \\ h_{n_R 1}(\tau) & h_{n_R 2}(\tau) & \ldots & h_{n_R N}(\tau) \end{pmatrix}. \tag{2.11}$$

The entries of $\boldsymbol{H}(\tau)$, $h_{ik}(\tau)$, are complex baseband equivalents of the channel coefficients between the $k^{th}$ transmit antenna and the $i^{th}$ receive antenna. The channel matrix, $\boldsymbol{H}(\tau)$, completely describes the fading characteristics of the entire MIMO link. The system size of the MIMO link is defined as $n_R \times N$. Note that there are $Nn_R$ SISO links in a $N \times n_R$ MIMO link. Therefore, according to the geographical distribution of these transmit and receive antennas, each individual SISO link may have a different average link power as discussed in the SISO link example. In general, the average link powers can be given by

$$\boldsymbol{P} = \begin{pmatrix} P_{11} & P_{12} & \cdots & P_{1N} \\ P_{21} & P_{22} & \cdots & P_{2N} \\ \cdots & \cdots & \ddots & \cdots \\ P_{n_R N} & P_{n_R N} & \cdots & P_{n_R N} \end{pmatrix}. \tag{2.12}$$

The matrix $\boldsymbol{P}$ contains the power information of the MIMO system and is referred to as the power matrix or power profile. As will be discussed later in the chapter, this power profile play a major role in the analysis of the MIMO system. Equation (2.10) can be rewritten as

$$\boldsymbol{r}(\tau) = \left(\boldsymbol{P}^{\circ\frac{1}{2}} \circ \boldsymbol{H}_w(\tau)\right)\boldsymbol{s}(\tau) + \boldsymbol{n}(\tau). \tag{2.13}$$

The matrix $\boldsymbol{H}_w(\tau)$ is a normalized matrix that captures the multipath fading phenomenon of the MIMO link. In an uncorrelated transmitters and receivers in flat Rayleigh environment, the entries of $\boldsymbol{H}_w(\tau)$ are independent, identically distributed ZMCSCG variables with unit magnitude variance. Hence, the entries of $\boldsymbol{H}_w(\tau)$, satisfy $h_{w,ik}(\tau) \sim \mathcal{CN}(0,1)$. In Rician multipath fading, $h_{w,ik}(\tau) \sim \mathcal{CN}\left(\sqrt{\frac{K_{ik}}{1+K_{ik}}}\Omega_{ik}, \frac{1}{1+K_{ik}}\right)$. Here, in the normalized channel coefficient, $|\Omega_{ik}|^2$ is set to

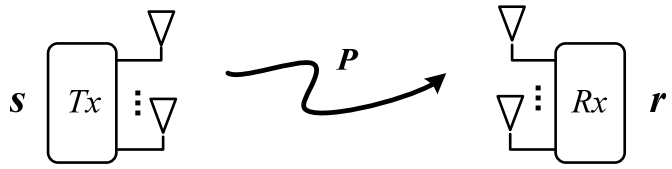


Figure 2.5: A block diagram of a MIMO channel.

unity. Therefore $E\left\{|h_{w,ik}(\tau)|^2\right\} = 1$ which gives rise to $E\left\{|h_{ik}(\tau)|^2\right\} = P_{ik}$. Hence, the power of the LoS path from transmitter $k$ to receiver $i$ equal to $\frac{K_{ik}P_{ik}}{1+K_{ik}}$. The envelope of the channel entries then follow the Rayleigh distribution or Rician distribution accordingly as in Sec. 2.1.1. Note that the time index $\tau$ in (2.10), (2.11) and (2.13) is usually dropped for brevity.

## 2.2 Multiuser MIMO Channels

One important deployment scenario for MIMO technology is the multiuser environment. These are called MU-MIMO scenarios. For example, consider a multiple antenna deployment at the BS to support multiple users with multiple antennas each. These multiple users have completely independent and confidential data to be transmitted and received. This is a common and easily understandable example of many MU-MIMO scenarios. Before moving to the MU-MIMO channels, some conventional space time (ST) configurations are given in Fig. 2.6 for the sake of completeness. All the ST configurations in Fig. 2.6 may be used in point to point single user communication systems. SISO is the legacy system. SIMO is used to introduce receive antenna diversity [2, 33] while MISO is used to introduce transmit diversity [34, 35]. Single user (SU) MIMO can be used in diversity mode and spatial multiplexing mode [1, 31]. The power profile that arises in the SU-MIMO system in Fig. 2.6-(d) is given by

$$\boldsymbol{P} = \begin{pmatrix} P & P & \cdots & P \\ P & P & \cdots & P \\ \cdots & \cdots & \ddots & \cdots \\ P & P & \cdots & P \end{pmatrix}, \tag{2.14}$$

where $P_{ik} = P \ \forall i, k$. Now consider MU-MIMO systems [30, 11]. Practical multiuser network MIMO systems can also be divided into two main categories, MAC and broadcast channel (BC). Figures 2.7 and 2.8 show block diagrams of MIMO-MAC and MIMO-BC layouts. These MU configurations refer to the case where a base station with multiple antennas communicates with multiple distributed users in the uplink for MIMO-MAC and in the downlink for MIMO-BC. Note

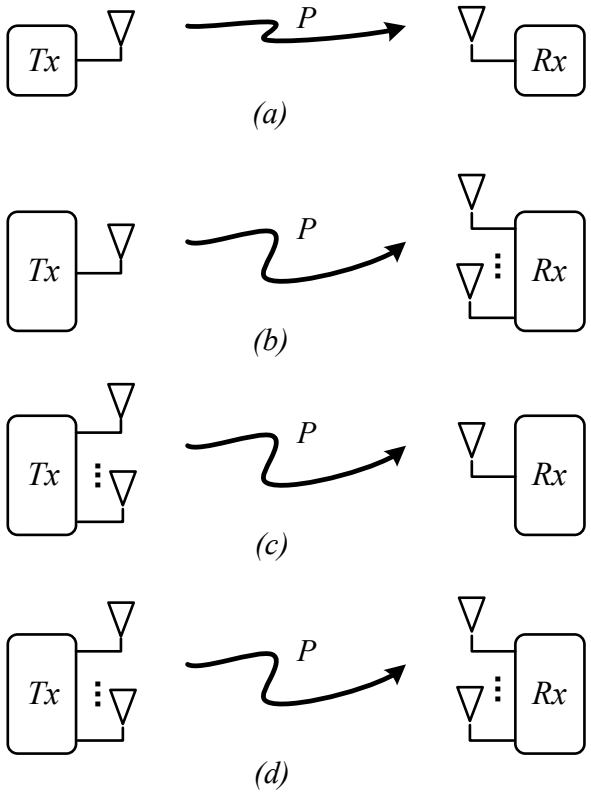


Figure 2.6: (a) SISO system. (b) SIMO system. (c) MISO system. (d) MIMO system. Note that all antennas are reasonably closely packed (microdiversity) so that the average link SNR, P, is constant on all branches.

that in both MIMO-MAC and MIMO-BC, the average link powers across the users are different while the powers across the branches of each user are constant. This is due to the collocated nature of the antenna elements of the distributed users. Due to the multi element antennas at each end, each link between a user and the BS creates a MIMO link as in Sec. 2.1.3. Considering all such links with the BS then creates a larger MIMO link which is called a MIMO-MAC or MIMO-BC.

In a typical microdiversity MAC scenario, distributed users communicate with a single access point where a collocated multi element receiver is employed. In the BC scenario, an access point with collocated multi-element transmit antennas, communicates with multiple distributed users. Hence, these are called microdiversity MIMO-MAC and microdiversity MIMO-BC. The power profile that arises in the MIMO-MAC system shown in Fig. 2.7 is given in (2.15), where we have

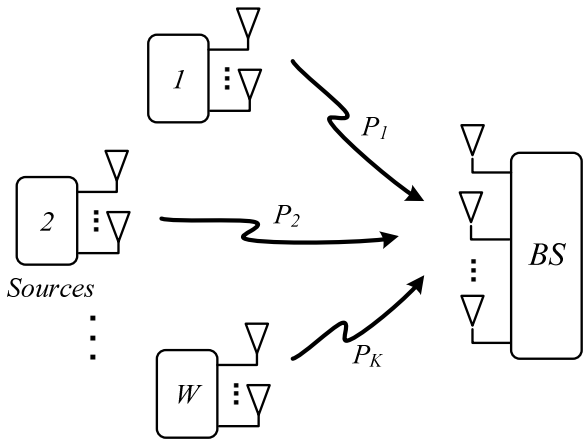


Figure 2.7: Multiple access channel with multiple element antennas at both base station and users.

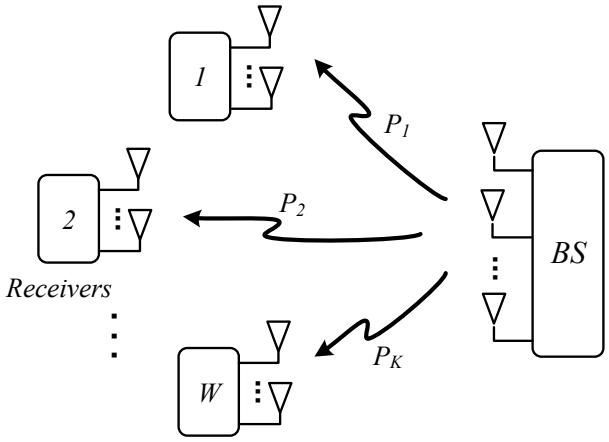


Figure 2.8: Broadcast channel with multiple element antennas at both base station and users.

assumed that user $k$ for $k = 1, \ldots W$ has one antenna, giving $P_{ik} = P_k$ for $k = 1, \ldots W$. Hence,

$$\boldsymbol{P} = \begin{pmatrix} P_1 & P_2 & \cdots & P_W \\ P_1 & P_2 & \cdots & P_W \\ \cdots & \cdots & \ddots & \cdots \\ P_1 & P_2 & \cdots & P_W \end{pmatrix}. \tag{2.15}$$

Note that in the MAC, joint processing at the receiver is possible, while in the BC only joint processing at the transmitter is possible [30, 36]. In this thesis, the MIMO communication systems discussed so far are referred to as conventional systems. Network MIMO systems which

form the backbone of the latest 3rd generation partnership project (3GPP) long term evolution (LTE)-Advanced standards, on which this thesis focuses, will be discussed next.

**Definition 2.1.** *A MIMO communication system where both sources and receivers are widely (geographically) separated is called a macrodiversity communication system, regardless of whether the sources/receivers belong to a single user or multiple users. Both the sources and the receivers may have multiple co-located antennas elements.*

In this thesis, it is assumed that either the transmit or receive antennas are connected together by means of some interconnection mechanism to a backhaul processing unit (BPU) to establish a collaboration for transmission and/or reception. There is a lot of debate about suitable interconnection links in macrodiversity MU-MIMO systems. Technologies like optical fibre, high power radio frequency (RF) and Gigabit ethernet links are among the leading candidates, but there are limitations to such interconnections such as the cost of optical fibre links and the limited capacity of RF links etc. However, this work assumes there are error free infinite bandwidth interconnection links to create a perfect virtual distributed antenna system. As far as the level of collaboration and the capacity and reliability of interconnection links are concerned, there are considerable differences between the latest proposals. A brief description about practical macrodiversity MU-MIMO systems is given in Sec. 2.3. Similar to conventional MIMO systems, macrodiversity MIMO systems also have two main categories, the macrodiversity MIMO-MAC and macrodiversity MIMO-BC system. In the BC scenario, the sources, and in the MAC scenario, the receivers are in collaboration to create a virtual multi element antenna array as shown in Figs. 2.9 and 2.10. To reduce the clutter, links from a single user are shown. In this thesis, the macrodiversity MIMO-MAC is the main focus. In macrodiversity terminology, the locations from where RF signaling starts and ends, are called transmission points (TPs) and receiving points (RPs) respectively. Hence in the MIMO-MAC, we may use TPs as users and RPs as BSs, as in the conventional cellular MAC channel. The type of power profile that arises in a macrodiversity MIMO-MAC system is given in

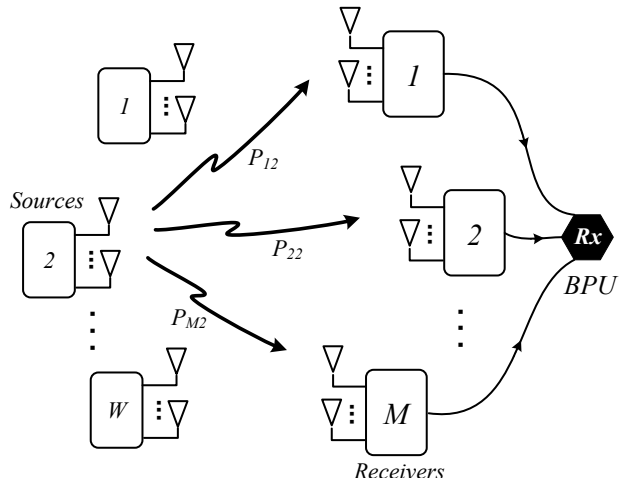


Figure 2.9: Macrodiversity MAC with multiple element antennas at receiver end and source end.

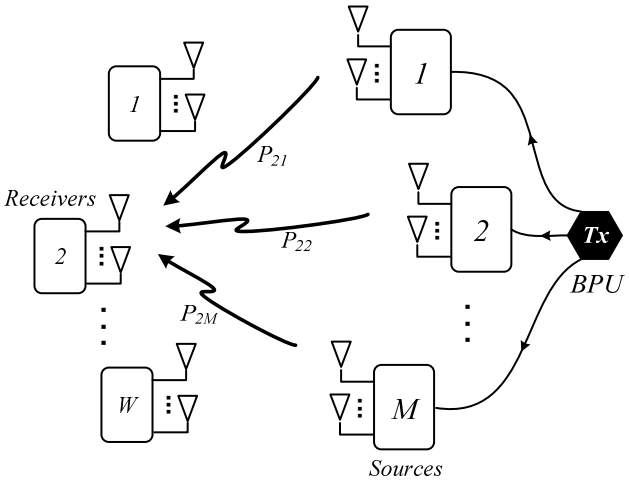


Figure 2.10: Macrodiversity BC with multiple element antennas at receiver end and source end.

(2.16) where we have assumed receive BS $i$ and user $k$ have a single antenna each for $\forall i, k$,

$$\boldsymbol{P} = \begin{pmatrix} P_{11} & P_{12} & \cdots & P_{1W} \\ P_{21} & P_{22} & \cdots & P_{2W} \\ \cdots & \cdots & \ddots & \cdots \\ P_{M1} & P_{M2} & \cdots & P_{MW} \end{pmatrix}. \tag{2.16}$$

A single user, point to point MIMO scenario similar to Fig. 2.6-(d), in a macrodiversity en-

vironment is not common. However, if distributed sources and receivers do belong to a single transmitter/receiver pair and are connected for joint transmission and reception, then a virtual point to point macrodiversity MIMO wireless link is created.

## 2.3 Macrodiversity MIMO Applications

In this section, we summarize some macrodiversity MIMO deployment scenarios. The discussion so far has been based on general macrodiversity systems where practical scenarios were deliberately omitted in order to maintain generality. However, in this section we present some more system specific descriptions of the kind of macrodiversity MU-MIMO systems proposed in the latest releases of the 3GPP LTE Advanced standards, namely CoMP transmission. There are various deployment scenarios and transmission modes identified and proposed in [37, 38, 39, 40, 41]. These deployment scenarios and transmission modes are described next. In order to facilitate our discussion, we assume a traditional, homogenous, hexagonal, cellular based mobile wireless communication system as our baseline system. Furthermore, cells with a relatively small coverage area are referred to as microcells while cells with larger coverage areas are referred to as macrocells henceforth.

### 2.3.1 CoMP Deployment Scenarios

- Scenario 1: A typical cell BS site is usually comprised of 3 or more sectors. In this scenario, the macrocell BS controls each of the sectors. This collaboration method is easy to implement as no backhaul communication to other entities is needed. At the same time, there is a downside to this method as no coordination with other BSs, diminishes the advantages of full cooperation.

- Scenario 2: Several microcell BSs (usually 3 or 7) are connected together by a macro network to form a macrocell. This macro network is likely be a fibre network. Though this approach can coordinate transmission points in a much larger area than the first approach, its practical implementation is difficult as a fiber infrastructure must be put in place to connect the participating BSs with the central BS. This is a homogeneous network topology and is depicted in Fig. 2.11 for a 3 cell collaboration.

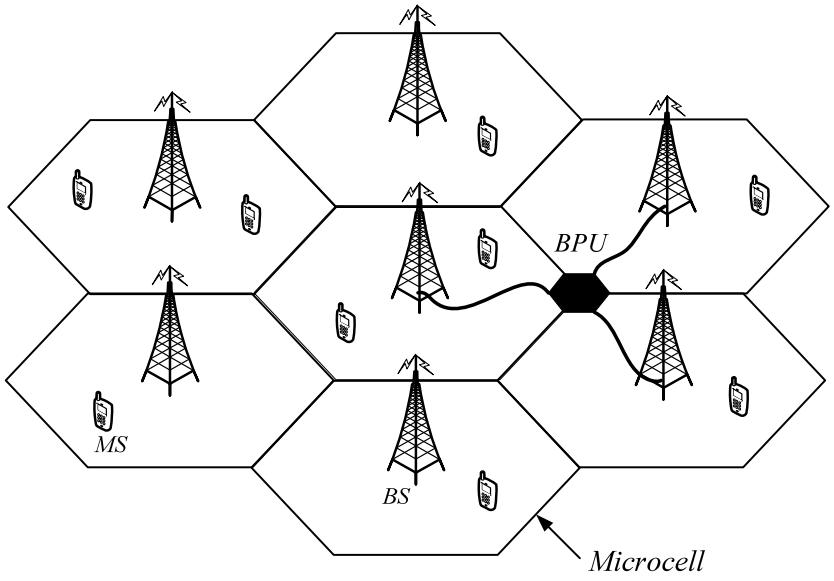


Figure 2.11: Illustration of deployment Scenario 2. Only the interconnection links of a single coordination unit is shown for clarity

- Scenario 3: There are many low power remote radio heads (RRH) distributed across a macrocell to cover certain hotspots. These points have their own cell identity and therefore act as independent cells. These transmit/receive points are connected to the central macrocell BS in a coordination unit. This is a heterogeneous network topology and is depicted in Fig. 2.12.

- Scenario 4: This is the same deployment as in Scenario 3, except the transmit/receive points (RRHs) do not have independent cell identities and create a distributed antenna array under the control of the macrocell BS.

The above deployment scenarios have not been finalized by standardization bodies like the 3GPP, but are currently being investigated for LTE-Advanced.

### 2.3.2 CoMP Transmission Modes

Unlike conventional MU-MIMO systems, macrodiversity MU-MIMO may have some limitations in transmitting and receiving technologies due to the limitations imposed by the backhaul interconnection links. Due to those limitations, transmission modes in the downlink CoMP and combining modes in the uplink CoMP have to be designed accordingly. A comprehensive description on var-

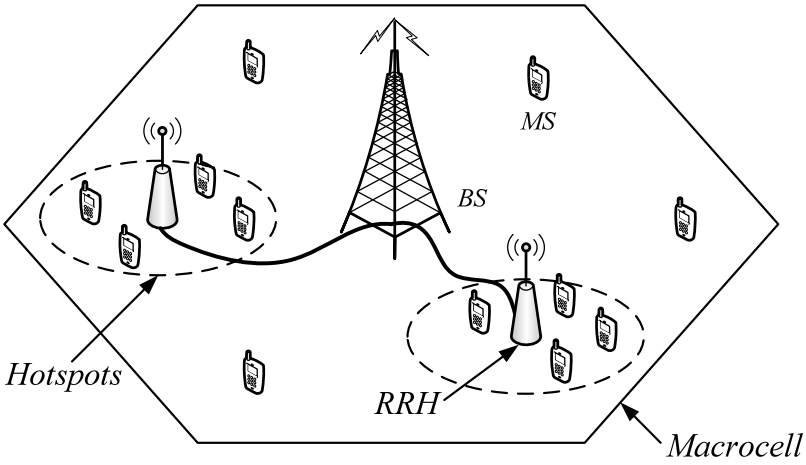


Figure 2.12: Illustration of deployment Scenario 3. Only a single macrocell is shown for clarity

ious transmission modes for both downlink and uplink CoMP is found in [42]. Since our major focus is on macrodiversity MIMO uplink in this thesis, we only consider uplink CoMP systems in this section. Currently, there are two major uplink CoMP processing modes under consideration.

- Joint Processing (JP): This is also called MIMO cooperation. In this scenario, received data at all BSs are transmitted to a central processing unit through high capacity delay free links. Data processing is done at the central processing unit jointly on received data. Therefore, very advanced joint signal processing techniques can be used to extract the greatest benefits out of this form of cooperative communication.

- Coordinated scheduling/coordinated processing (CS/CP): In this processing mode, all the participating distributed BSs share channel state information, but user data remains unshared. This technique approaches the ideal JP gains [43, 44].

Actual implementations of CoMP may be combinations of the above deployment scenarios and transmission modes depending upon the priorities of manufacturers. Academically, there is a large body of research devoted to many aspects of the above scenarios. Interested readers are directed to [40] for a fairly comprehensive overview. However, in this thesis we have made the following assumption in order to make our analysis more general and in some sense fundamental.

**Assumption 2.2.** *In this thesis, we assume the MIMO cooperation processing mode (JP) where all the participating distributed BSs are connected by infinite capacity, delay free interconnection links and employ coherent reception/transmission, so that all the BSs and MSs create a macrodiversity MU-MIMO system as defined in Def. 2.1.*

# Chapter 3

# Macrodiversity Maximal Ratio Combining.

Maximum ratio combining is a well-known linear combining technique that maximizes the SNR in noise limited systems [9]. In the presence of co-channel interferers, MRC is sub-optimal compared to MMSE combining. However, MMSE combining requires instantaneous channel knowledge of both the desired source and the interfering sources. In contrast, MRC only requires a knowledge of the desired source and hence is simpler to implement. For this reason, there is still interest in MRC processing in the presence of interference. In [45], MRC is investigated for large systems where it was shown that in the limit as the number of antennas increases, intercell interference effects disappear. In [46], a switched MRC/MMSE receiver is proposed where the simplicity of MRC is preferred when the interference levels drop below a threshold. The performance of MRC systems with co-located antenna arrays is well known for Rayleigh fading channels with multiple co-channel interferers [47]. The performance of microdiversity MRC systems with imperfect channel estimation in the presence of CCI with an arbitrary power interference-to-noise ratio (INR) has been investigated in [48, 49]. In [50, 51], studies on the performance of MRC diversity schemes with various fading scenarios (Rician and Nakagami) and cochannel interference were reported, but macrodiversity MRC makes performance analysis more complex and to the best of our knowledge no analytical results are currently available for such finite size systems. Hence, in this chapter,

we analyze the SER of macrodiversity MRC systems. In particular, we consider a distributed antenna array performing MRC combining for a single antenna desired source in the presence of an arbitrary number of single antenna co-channel interferers. The analysis also covers the case where both the desired and interfering sources may have multiple antennas. Since the sources and the receive antennas are not co-located, the channels are normally independent and so the focus is on independent Rayleigh fading channels where each link has a different SNR. In the scenario where some sources have multiple antennas, there may be spatial correlation in the channels corresponding to that position. This is beyond the scope of the current work where independent channels are considered. However, receiver correlation due to co-located antennas at each BS can also be handled, but the transmit side correlation due to multiple antennas at each user is not covered by the current analysis. We provide specific results for BPSK and quadrature phase shift keying (QPSK) modulations, but the analysis can be applied to M-ary quadrature amplitude modulation and a wide range of modulations where the SER can be written in terms of an expected value of the Gaussian $Q$-function and $Q^2$-function.

## 3.1 System Model

Consider $N$ single-antenna distributed users communicating with $n_R$ distributed BS [38] each with a single receive antenna over an independent flat fading Rayleigh channel. The system diagram is given in Fig.3.1. The received signal is given by

$$\boldsymbol{r} \;=\; \boldsymbol{H}\boldsymbol{s}+\boldsymbol{n}, \tag{3.1}$$

where $\boldsymbol{r}=(r_1,r_2,\ldots,r_{n_R})^T$ is the $\mathcal{C}^{n_R\times 1}$ receive vector, $\boldsymbol{H}=(h_{ik})$ is the $\mathcal{C}^{n_R\times N}$ channel matrix, $\boldsymbol{s}=(s_1,s_2,\ldots,s_N)^T$ is the $\mathcal{C}^{N\times 1}$ signal vector and $\boldsymbol{n}=(n_1,n_2,\ldots,n_{n_R})^T$ is the $\mathcal{C}^{n_R\times 1}$ AWGN vector at the receive antennas such that $\boldsymbol{n}\sim\mathcal{CN}\left(\boldsymbol{0},\sigma^2\boldsymbol{I}\right)$. The signals are normalized to be zero-mean, unit power variables so that $E\left\{|s_i|^2\right\}=1$ for $i=1,2,\ldots,N$. The channel matrix, $\boldsymbol{H}$, has independent zero-mean, complex Gaussian elements such that $E\left\{|\boldsymbol{H}_{ik}|^2\right\}=P_{ik}$. Hence, equation (3.1) can be rewritten as

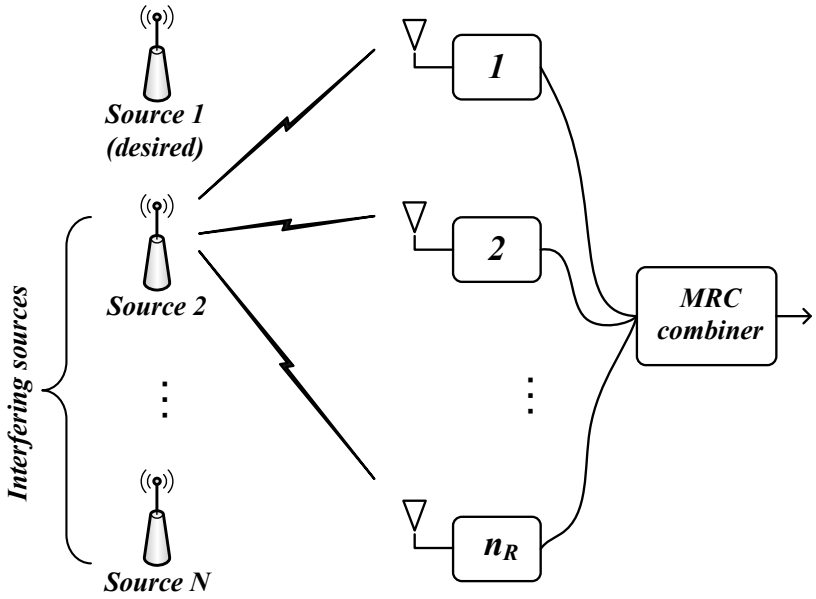


Figure 3.1: System diagram. To reduce clutter, only paths from source 2 are shown.

$$\boldsymbol{r} = \left(\boldsymbol{H}_w \circ \boldsymbol{P}^{\circ\frac{1}{2}}\right)\boldsymbol{s} + \boldsymbol{n}, \tag{3.2}$$

where $\boldsymbol{P} = (P_{ik})$ and the elements, $\boldsymbol{H}_{w,ik}$, of $\boldsymbol{H}_w$ satisfy $\boldsymbol{H}_{w,ik} \sim \mathcal{CN}(0,1) \quad \forall i,k$. The matrix, $\boldsymbol{P}$, is the global power matrix for the system and for the $k^{th}$ source, an individual power matrix is also defined by $\boldsymbol{P}_k = E\left\{\boldsymbol{h}_k \boldsymbol{h}_k^H\right\} = \text{diag}\left(P_{1k}, P_{2k}, \ldots, P_{n_R k}\right)$, for $k = 1, 2, \ldots, N$. In the microdiversity case, $\boldsymbol{P}_k \propto \boldsymbol{I}$. In macrodiversity scenarios, $\boldsymbol{P}_k$ is no longer proportional to the identity and these more general power matrices make the analysis more complex. Assume, without loss of generality, that user 1 is the desired user. For the purpose of decoding user 1, (3.1) can be rewritten as

$$\boldsymbol{r} = \boldsymbol{h}_1 s_1 + \tilde{\boldsymbol{H}}\tilde{\boldsymbol{s}} + \boldsymbol{n} \tag{3.3}$$

$$= \boldsymbol{h}_1 s_1 + \boldsymbol{i}, \tag{3.4}$$

where $\boldsymbol{h}_1$ is the first column of $\boldsymbol{H}$, $\tilde{\boldsymbol{H}}$ is all columns of $\boldsymbol{H}$, excluding the first column, meaning $\boldsymbol{H} = \left(\boldsymbol{h}_1, \tilde{\boldsymbol{H}}\right)$, and $\tilde{\boldsymbol{s}} = (s_2, \ldots, s_N)^T$. The $n_R \times 1$ vector, $\boldsymbol{i}$ is the interference and noise vector. With MRC processing, the output of the combiner is given by [10]

$$\tilde{\boldsymbol{r}} = \frac{\boldsymbol{h}_1^H \boldsymbol{r}}{\boldsymbol{h}_1^H \boldsymbol{h}_1} = s_1 + \frac{\boldsymbol{h}_1^H \boldsymbol{i}}{\boldsymbol{h}_1^H \boldsymbol{h}_1}. \tag{3.5}$$

The interference and noise term in (3.5) can be written as

$$Z = \frac{\boldsymbol{h}_1^H \boldsymbol{i}}{\boldsymbol{h}_1^H \boldsymbol{h}_1} = \frac{\boldsymbol{h}_1^H \left(\tilde{\boldsymbol{H}}\tilde{\boldsymbol{s}} + \boldsymbol{n}\right)}{\boldsymbol{h}_1^H \boldsymbol{h}_1}. \tag{3.6}$$

Following the standard approach [10], we develop a conditional Gaussian representation for $Z$ as follows. Since $\tilde{\boldsymbol{H}}$ and $\boldsymbol{n}$ are zero-mean Gaussian and independent of $\boldsymbol{h}_1$ and $\tilde{\boldsymbol{s}}$, it follows that $Z$ is also zero-mean Gaussian conditioned on $\boldsymbol{h}_1$ and $\tilde{\boldsymbol{s}}$. The conditional variance of $Z$ is given by

$$E\left\{|Z|^2 \,|\boldsymbol{h}_1, \tilde{\boldsymbol{s}}\right\} = E\left\{ \frac{\boldsymbol{h}_1^H \left(\tilde{\boldsymbol{H}}\tilde{\boldsymbol{s}} + \boldsymbol{n}\right)\left(\tilde{\boldsymbol{s}}^H \tilde{\boldsymbol{H}}^H + \boldsymbol{n}^H\right)\boldsymbol{h}_1}{\left(\boldsymbol{h}_1^H \boldsymbol{h}_1\right)^2} \middle| \boldsymbol{h}_1, \tilde{\boldsymbol{s}} \right\}, \tag{3.7}$$

$$= \frac{\boldsymbol{h}_1^H E\left\{\tilde{\boldsymbol{H}}\tilde{\boldsymbol{s}}\tilde{\boldsymbol{s}}^H \tilde{\boldsymbol{H}}^H + \sigma^2 \boldsymbol{I}\right\}\boldsymbol{h}_1}{\left(\boldsymbol{h}_1^H \boldsymbol{h}_1\right)^2}, \tag{3.8}$$

$$= \frac{\boldsymbol{h}_1^H \left(\sum_{k=2}^N \boldsymbol{P}_k |s_k|^2 + \sigma^2 \boldsymbol{I}\right)\boldsymbol{h}_1}{\left(\boldsymbol{h}_1^H \boldsymbol{h}_1\right)^2}. \tag{3.9}$$

Hence, $Z$ has the exact representation

$$Z = \frac{\sqrt{\boldsymbol{h}_1^H \left(\sum_{k=2}^N \boldsymbol{P}_k |s_k|^2 + \sigma^2 \boldsymbol{I}\right)\boldsymbol{h}_1}}{\boldsymbol{h}_1^H \boldsymbol{h}_1} U, \tag{3.10}$$

where $U \sim \mathcal{CN}(0,1)$. Using this representation in (3.5) gives the combiner output in simplified signal plus noise form as

$$\tilde{\boldsymbol{r}} = s_1 + \frac{\sqrt{Y}}{X} U, \tag{3.11}$$

where $X = \boldsymbol{h}_1^H \boldsymbol{h}_1$, $Y = \boldsymbol{h}_1^H \boldsymbol{D}(\tilde{\boldsymbol{s}})\boldsymbol{h}_1$ and $\boldsymbol{D}(\tilde{\boldsymbol{s}}) = \sum_{k=2}^N \boldsymbol{P}_k |s_k|^2 + \sigma^2 \boldsymbol{I}$.

## 3.2 Performance Analysis

### 3.2.1 A Simple SER Analysis

With the combiner output given by (3.11), SERs for many modulations can be obtained using standard methodology [10]. As an example, for BPSK, we have the SER

$$P_s = \Pr\left(-1 + \frac{\sqrt{Y}}{X}\mathrm{Re}\left(U\right) > 0\right), \tag{3.12}$$

$$= E\left\{Q\left(\sqrt{\frac{2X^2}{Y}}\right)\right\}, \tag{3.13}$$

where $Q\left(x\right) = \frac{1}{\sqrt{2\pi}}\int_x^\infty e^{-\frac{t^2}{2}}dt$ is the Gaussian Q-function defined in [52]. Defining $\gamma = X^2Y^{-1}$ gives the BPSK SER as $E\left\{Q\left(\sqrt{2\gamma}\right)\right\}$. Note that in general $\gamma$ is a function of $\tilde{\boldsymbol{s}}$ but this dependence is not shown for convenience. For BPSK, each element of $\tilde{\boldsymbol{s}}$ has unit modulus and so there is no dependence on $\tilde{\boldsymbol{s}}$ and the SER in (3.13) is valid for any values of $\tilde{\boldsymbol{s}}$. For many modulations [8, 53], SERs are constructed from similar functions of the form

$$\mathcal{W}_1\left(a, b, \tilde{\boldsymbol{s}}\right) = E\left\{aQ\left(\sqrt{b\gamma}\right)\right\}, \tag{3.14}$$

$$= \int_0^\infty aQ\left(\sqrt{b\gamma}\right) f\left(\gamma\right) d\gamma, \tag{3.15}$$

where $f\left(\gamma\right)$ is the probability density function of $\gamma$. For some modulations, such as BPSK, the SER can be given exactly in terms of $\mathcal{W}_1\left(a, b, \tilde{\boldsymbol{s}}\right)$, whereas for other modulations it will provide an approximation. Using integration by parts on (3.15) gives

$$\mathcal{W}_1\left(a, b, \tilde{\boldsymbol{s}}\right) = \frac{a}{\sqrt{2\pi}}\int_0^\infty e^{-\frac{w^2}{2}} F_\gamma\left(\frac{w^2}{b}\right) dw, \tag{3.16}$$

where $F\left(.\right)$ is the cumulative distribution function of $\gamma$. Hence, SER performance for MRC relies on the evaluation of (3.16) which in turn relies on the cdf of $\gamma$.

In the microdiversity case, all the $\boldsymbol{P}_i$ matrices are proportional to the identity and $\gamma$ reduces to a simplified expression, $\gamma \propto \chi^2$, where $\chi^2$ is a chi-squared random variable [54]. In the macrodiversity

case, this reduction does not occur and $\gamma$ is proportional, not to a simple chi-squared random variable, but to a ratio of powers of correlated quadratic forms. This is the novel analytical challenge posed by the macrodiversity scenario. The derivation of the cdf is based on the joint distribution of $X, Y$. From [55], the joint distribution of $X$ and $Y$ becomes

$$f_{X,Y}(x,y) = \sum_{i=1}^{n_R} \sum_{k \neq i}^{n_R} \xi_{ik} e^{-\frac{x}{P_{i1}}} e^{-\beta_{ik}\left(y - \frac{Q_i x}{P_{i1}}\right)} \begin{cases} u\left(y - \frac{Q_i}{P_{i1}} x\right) u(x) & \text{for } \beta_{ik} > 0 \\ -u\left(\frac{Q_i}{P_{i1}} x - y\right) u(x) & \text{for } \beta_{ik} < 0, \end{cases} \tag{3.17}$$

where $u(x)$ is the standard unit step function defined as

$$u(x) = \begin{cases} 0 & x < 0 \\ 1 & x > 0, \end{cases} \tag{3.18}$$

and

$$\xi_{ik} = \frac{P_{i1}^{n_R - 2} \, \upsilon_{ik}{}^{n_R - 3}}{\prod_{l \neq i,k}^{n_R} (\upsilon_{ik} \nu_{il} - \nu_{ik} \upsilon_{il})}, \tag{3.19}$$

$$\beta_{ik} = \frac{\nu_{ik}}{\upsilon_{ik}}, \tag{3.20}$$

$$\upsilon_{ik} = P_{i1} Q_k - Q_i P_{k1}, \tag{3.21}$$

$$\nu_{ik} = P_{i1} - P_{k1}, \tag{3.22}$$

$$\boldsymbol{Q} = \boldsymbol{D}(\tilde{\boldsymbol{s}}) \boldsymbol{P}_1 = \operatorname{diag}(Q_1, Q_2, \ldots, Q_{n_R}). \tag{3.23}$$

Note that each term in the summation of (3.17) has its own region of validity depending on the algebraic sign of $\beta_{ik}$. The $\beta_{ik} = 0$ condition has been ignored since the case of distributed users with a single antenna always yields $\beta_{ik} \neq 0$.

The cdf of $\gamma$ is defined by

$$F_\gamma(r) = \Pr(\gamma < r) = \Pr\left(\frac{X^2}{Y} < r\right), \tag{3.24}$$

$$= \Pr\left(X^2 - rY < 0\right), \tag{3.25}$$

$$= \iint_{\mathcal{D}} f_{X,Y}(x,y)\, dxdy, \tag{3.26}$$

where the domain of integration is defined by $\mathcal{D} = \left\{x, y : x \geq 0, y \geq 0 \text{ and } x^2 - ry < 0\right\}$. In Appendix B.1, the integral in (3.26) is computed giving

$$F_\gamma(r) = \sum_{i=1}^{n_R} \sum_{k \neq i}^{n_R} F_{ik}(r), \tag{3.27}$$

where $F_{ik}(r) = F_{ik}^1(r)$ for $\beta_{ik} > 0$ and $F_{ik}(r) = F_{ik}^2(r)$ for $\beta_{ik} < 0$, where $F_{ik}^1(r)$ and $F_{ik}^2(r)$ are given in (B.4) and (B.9) and $\beta_{ik}$ is given in (3.20). For convenience, we expand $\beta_{ik}$ in (3.20) and also give the result here as

$$\beta_{ik} = \frac{\frac{1}{P_{i1}} - \frac{1}{P_{k1}}}{\sum_{u=2}^{N} (P_{ku} - P_{iu}) |s_u|^2}. \tag{3.28}$$

Note that the case of $\beta_{ik} = 0$ is not considered as this is the case when $P_{i1} = P_{k1}$, an event which occurs with probability zero when the receive antennas are not co-located. As for the cdf, the SER analysis is performed separately according to the algebraic sign of $\beta_{ik}$. Therefore, substituting (3.27) into (3.16), the final result is

$$\mathcal{W}_1(a, b, \tilde{\boldsymbol{s}}) = \sum_{i=1}^{n_R} \sum_{k \neq i}^{n_R} P_{s_{ik}}, \tag{3.29}$$

where $P_{s_{ik}} = P_{s_{ik}}^1$ for $\beta_{ik} > 0$ and $P_{s_{ik}} = P_{s_{ik}}^2$ for $\beta_{ik} < 0$, where $P_{s_{ik}}^1$ and $P_{s_{ik}}^2$ are given in (3.30)

and (3.31).

$$P_{s_{ik}}^{1}=\frac{a}{\sqrt{2}}\left(\frac{P_{i1}\xi_{ik}}{\beta_{ik}}\left(\frac{1}{\sqrt{2}}-\frac{1}{2\sqrt{\left(\frac{1}{2}+\frac{Q_i}{bP_{i1}^2}\right)}}\right)+\sqrt{\frac{b}{\beta_{ik}}}\frac{\xi_{ik}}{\left(\omega_{ik}^2-2b\beta_{ik}\right)}\left(\sqrt{\frac{\beta_{ik}}{b\left(\frac{1}{2}+\frac{Q_i}{bP_{i1}^2}\right)}}\alpha_{ik}-1\right)\right). \tag{3.30}$$

---

$$P_{s_{ik}}^{2}=\frac{a}{\sqrt{2}}\left(\frac{P_{i1}\xi_{ik}}{\beta_{ik}}\left(\frac{1}{\sqrt{2}}-\frac{1}{2\sqrt{\left(\frac{1}{2}+\frac{Q_i}{bP_{i1}^2}\right)}}\right)+\sqrt{\frac{b}{-\beta_{ik}}}\frac{\xi_{ik}}{\left(\omega_{ik}^2-2b\beta_{ik}\right)}\left(\sqrt{\frac{-\beta_{ik}}{b\left(\frac{1}{2}+\frac{Q_i}{bP_{i1}^2}\right)}}\alpha_{ik}+\frac{\omega_{ik}}{\sqrt{-2b\beta_{ik}}}\right)\right). \tag{3.31}$$

The results in (3.30) and (3.31) are obtained using the following three standard integral identities [52]

$$\int_0^\infty e^{\mu x}\left(1-\Phi\left(\sqrt{\alpha x}\right)\right)dx=\frac{1}{\mu}\left(\sqrt{\frac{\alpha}{\alpha-\mu}}-1\right),\quad \text{for}\quad \mathrm{Re}\left(\alpha\right)>0;\mathrm{Re}\left(\mu\right)<\mathrm{Re}\left(\alpha\right), \tag{3.32}$$

$$\int_0^\infty xe^{-\mu x^2}\Phi\left(jax\right)dx=\frac{ja}{2\mu\sqrt{\mu-a^2}},\quad \text{for}\quad a>0;\mathrm{Re}\left(\mu\right)>\left(\mathrm{Re}\left(a\right)\right)^2, \tag{3.33}$$

$$\int_0^\infty e^{-q^2x^2}dx=\frac{\sqrt{\pi}}{2q}\quad \text{for}\quad q>0, \tag{3.34}$$

where $\Phi\left(x\right)$ in (3.32) and (3.33) is the standard error function [52]. For multi-level constellations, the values of $\tilde{\boldsymbol{s}}$ affect $\boldsymbol{D}\left(\tilde{\boldsymbol{s}}\right)$ and therefore $\gamma$. Hence, SER results must average (3.29) over all possible values of $\tilde{\boldsymbol{s}}$. This gives

$$\mathcal{W}_1\left(a,b\right)=\sum_{\tilde{\boldsymbol{s}}}\mathcal{W}_1\left(a,b,\tilde{\boldsymbol{s}}\right)\Pr\left(\tilde{\boldsymbol{s}}\right), \tag{3.35}$$

where (3.35) may be an exact or approximate SER result, the summation is over all possible $\tilde{\boldsymbol{s}}$ and

$\Pr(\tilde{\boldsymbol{s}})$ is the probability of a particular $\tilde{\boldsymbol{s}}$ value. Finally for BPSK modulation the SER in (3.13) becomes

$$P_s = \mathcal{W}_1(1, 2, \tilde{\boldsymbol{s}}). \tag{3.36}$$

### 3.2.2 Extended SER Analysis

For $M$-QAM, first order SER approximations can be found via expressions of the form in (3.14). Exact results involve expectation over the $Q^2(.)$ function in addition to (3.14). As an example, consider 4-QAM where the SER is given by

$$P_s = \Pr\left(-\frac{1}{\sqrt{2}} + \frac{1}{\sqrt{\gamma}}\mathrm{Re}(U) > 0 \quad \text{or} \quad -\frac{1}{\sqrt{2}} + \frac{1}{\sqrt{\gamma}}\mathrm{Im}(U) > 0\right) \tag{3.37}$$

$$P_s = 1 - \Pr\left(\mathrm{Re}(U) < \sqrt{\frac{\gamma}{2}}\right)^2 \tag{3.38}$$

$$= 1 - E\left\{\left(1 - Q\left(\sqrt{\gamma}\right)\right)^2\right\} \tag{3.39}$$

$$= 2E\left\{Q\left(\sqrt{\gamma}\right)\right\} - E\left\{Q^2\left(\sqrt{\gamma}\right)\right\}. \tag{3.40}$$

Here, the $2E\left\{Q\left(\sqrt{\gamma}\right)\right\} = \mathcal{W}_1(2, 1, \tilde{\boldsymbol{s}})$ term in (3.40) is a good approximation to $P_s$ [10] and the remaining term, $E\left\{Q^2\left(\sqrt{\gamma}\right)\right\}$, makes only a small adjustment. However, in other variations of $M$-QAM modulation schemes the contribution from $Q^2(.)$ is not negligible [10]. Therefore, for general $M$-QAM, the exact SER is useful and this can be written in terms of $\mathcal{W}_1(a, b, \tilde{\boldsymbol{s}})$ and $\mathcal{W}_2(a, b, \tilde{\boldsymbol{s}}) = E\left\{aQ^2\left(\sqrt{b\gamma}\right)\right\}$. The first expectation is found in (3.29). The second expectation can be derived as follows. Let,

$$\mathcal{W}_2(a, b, \tilde{\boldsymbol{s}}) = a\int_0^\infty Q^2\left(\sqrt{b\gamma}\right) f(\gamma)\, d\gamma. \tag{3.41}$$

Using integration by parts on (3.41) gives

$$\mathcal{W}_2\left(a,b,\tilde{\boldsymbol{s}}\right)=a\sqrt{\frac{2}{\pi}}\int_0^{\infty}e^{-\frac{w^2}{2}}Q\left(w\right)F_{\gamma}\left(\frac{w^2}{b}\right)dw. \tag{3.42}$$

In order to facilitate our analysis we need two fundamental probability integrals. To the best of our knowledge, there are no equivalent integral forms in the literature. Therefore, we derive both integrals in Appendix B.2, since they may have applications in other communication problems. As for the simple SER analysis, the extended analysis is also performed separately according to the algebraic sign of $\beta_{ik}$. Therefore, substituting (3.27) into (3.42), the final result is derived in Appendix B.2 as

$$\mathcal{W}_2\left(a,b,\tilde{\boldsymbol{s}}\right)=\sum_{i=1}^{n_R}\sum_{k\neq i}^{n_R}\tilde{P}_{s_{ik}}, \tag{3.43}$$

where $\tilde{P}_{s_{ik}}=\tilde{P}^1_{s_{ik}}$ for $\beta_{ik}>0$ and $\tilde{P}_{s_{ik}}=\tilde{P}^2_{s_{ik}}$ for $\beta_{ik}<0$, where $\tilde{P}^1_{s_{ik}}$ and $\tilde{P}^2_{s_{ik}}$ are given in (3.44) and (3.45), respectively.

$$\tilde{P}^1_{s_{ik}}=\frac{a}{\sqrt{2}}\left(\frac{P_{i1}\xi_{ik}}{\beta_{ik}}\left(\frac{1}{\sqrt{8}}-\frac{\tan^{-1}\left(\sqrt{1+\frac{2Q_i}{bP^2_{i1}}}\right)}{\pi\sqrt{\left(\frac{1}{2}+\frac{Q_i}{bP^2_{i1}}\right)}}\right)+\frac{\xi_{ik}}{\sqrt{b\beta_{ik}}\beta_{ik}}I_2\left(\alpha_{ik}\sqrt{\frac{\beta_{ik}}{b}},\frac{\omega^2_{ik}}{4b\beta_{ik}}-\frac{1}{2}\right)\right). \tag{3.44}$$

$$\begin{aligned}\tilde{P}^2_{s_{ik}}=\frac{a}{\sqrt{2}}\Bigg(&\frac{P_{i1}\xi_{ik}}{\beta_{ik}}\left(\frac{1}{\sqrt{8}}-\frac{\tan^{-1}\left(\sqrt{1+\frac{2Q_i}{bP^2_{i1}}}\right)}{\pi\sqrt{\left(\frac{1}{2}+\frac{Q_i}{bP^2_{i1}}\right)}}\right)-\frac{1}{j}\frac{\xi_{ik}}{\sqrt{-b\beta_{ik}}\beta_{ik}}\\&\times\left(I_1\left(\alpha_{ik}\sqrt{\frac{-\beta_{ik}}{b}},\frac{1}{2}-\frac{\omega^2_{ik}}{4b\beta_{ik}}\right)+I_1\left(\frac{\omega_{ik}}{2\sqrt{-b\beta_{ik}}},\frac{1}{2}-\frac{\omega^2_{ik}}{4b\beta_{ik}}\right)\right)\Bigg).\end{aligned} \tag{3.45}$$

Hence, the exact SERs are computable using (3.29) and (3.43) for any $M$-QAM modulation. As in Sec. 3.2.1, for multi-level constellations the SER results depend on $\mathcal{W}_1\left(a,b\right)$ and $\mathcal{W}_2\left(a,b\right)$ results

where $\mathcal{W}_1(a,b)$ is given in (3.35) and

$$\mathcal{W}_2(a,b) = \sum_{\tilde{\boldsymbol{s}}} \mathcal{W}_2(a,b,\tilde{\boldsymbol{s}}) \Pr(\tilde{\boldsymbol{s}}). \tag{3.46}$$

For QPSK modulation the SER in (3.40) becomes

$$P_s = \mathcal{W}_1(2,1,\tilde{\boldsymbol{s}}) - \mathcal{W}_2(1,1,\tilde{\boldsymbol{s}}). \tag{3.47}$$

### 3.2.3 A Simple Power Metric

The SER and any other performance metrics are functions of the power matrices $\boldsymbol{P}_1, \boldsymbol{P}_2, \ldots, \boldsymbol{P}_N$. Although (3.29) and (3.43) give the exact SER as a function of these powers, the result is complex and does not offer any simple insights into the relationship between performance and the powers. Hence, we consider (3.5) and (3.9) which give the mean SINR of the combiner as

$$\tilde{m}_P \triangleq E\left\{ \frac{\left(\boldsymbol{h}_1^H \boldsymbol{h}_1\right)^2}{\boldsymbol{h}_1^H \left(\sum_{k=2}^N \boldsymbol{h}_k \boldsymbol{h}_k^H + \sigma^2 \boldsymbol{I}\right) \boldsymbol{h}_1} \right\}, \tag{3.48}$$

where $\tilde{m}_P$ is a performance metric based on the link powers and we have used $E\left\{|s_i|^2\right\} = 1$. Exact evaluation of (3.48) is possible but it is rather involved and produces complex expressions. Hence, we prefer the compact approximation based on the first order delta method, similar to the Laplace approximation [56], given by

$$m_P = \frac{E\left\{\left(\boldsymbol{h}_1^H \boldsymbol{h}_1\right)^2\right\}}{E\left\{\boldsymbol{h}_1^H \left(\sum_{k=2}^N \boldsymbol{h}_k \boldsymbol{h}_k^H + \sigma^2 \boldsymbol{I}\right) \boldsymbol{h}_1\right\}}. \tag{3.49}$$

Using established results for the moments of quadratic forms [54, pp. 119], we obtain

$$m_P = \frac{\mathrm{Tr}\left(\boldsymbol{P}_1\right)^2 + \mathrm{Tr}\left(\boldsymbol{P}_1^2\right)}{\mathrm{Tr}\left(\sum_{i=2}^N \boldsymbol{P}_1 \boldsymbol{P}_i + \sigma^2 \boldsymbol{P}_1\right)}. \tag{3.50}$$

From (3.50), we observe that while a $\boldsymbol{P}_1$ matrix with large entries boosts the numerator, hence improving performance, it also interacts with the interferers in the denominator. Since MRC is based on weighting the strongest signal, the most advantageous interference profile is for the stronger interferers to line up with the weaker desired signals and vice-versa. This intuitive result is precisely captured by (3.50) which increases with $\mathrm{Tr}\,(\boldsymbol{P}_1)$ and also increases as $\mathrm{Tr}\,(\boldsymbol{P}_1\boldsymbol{P}_i)$ decreases, for $i = 2, 3, \ldots, N$.

Although $m_P$ captures some of the important relationships between performance and the power matrices, it is not always an accurate predictor of performance. As the SINR grows, the mean becomes further from the lower tail which governs error rate performance. Hence, we expect the mean to carry less information about SER at high SINR. This is discussed in more detail in Sec. 3.3.

### 3.2.4 Remarks on Systems with Multiple Co-located Receive Antennas at BSs

The analysis in Sec. 3.2 is restricted to situations where the BSs have a single antenna each. However, if the receiver, for example has two co-located antennas at any BS, the system analysis still can be handled by the same method, but will result in a different joint distribution for (3.17). Thus, every new scenario for co-located antennas gives a new joint distribution and in turn this gives a different error rate expression. A pragmatic solution is to use a perturbation approach. If $P_{i1} = P_{r1}$ (corresponding to receive antennas $i$ and $r$ of the desired user, being co-located at $i^{\text{th}}$ BS) then we can use $P_{i1}$ and $P_{i1} + \epsilon$ for the two powers where $\epsilon$ is a small perturbation. This approach provides stable and accurate results as will be shown in Sec. 3.3.

## 3.3 Numerical and Simulation Results

For the numerical results, we consider a system with three distributed receive antennas and also a larger system with 6 receive antennas deployed in three sets of co-located pairs. Hence, there are three positions at which one or two antennas are deployed and these are refereed to as locations.

Note that the number of interferers in the system is irrelevant, since, from (3.10), their effect is governed by $\sum_{k=2}^{N} \boldsymbol{P}_k |s_k|^2$. Hence, one interferer with a power matrix equal to $\sum_{k=2}^{N} \boldsymbol{P}_k |s_k|^2$ is equivalent to $N-1$ interferers with power matrices $\boldsymbol{P}_2 |s_2|^2, \ldots, \boldsymbol{P}_N |s_N|^2$. Hence, we consider a single interferer throughout. In this section we consider BPSK and 4-QAM results where $|s_i|^2 = 1$ $\forall i$. Hence, for both systems, we parameterize the performance by three parameters which are independent of the transmit symbols. The average received signal to noise ratio is defined by $\rho = \mathrm{Tr}(\boldsymbol{P}_1)/n_R\sigma^2$. The total signal to interference ratio is defined by $\varsigma = \mathrm{Tr}(\boldsymbol{P}_1)/\mathrm{Tr}(\boldsymbol{P}_2)$. The spread of the signal power across the three locations is assumed to follow an exponential profile, as in [57], so that a range of possibilities can be covered with only one parameter. The exponential profile is defined by

$$P_{ik} = K_k(\alpha)\,\alpha^{i-1}, \tag{3.51}$$

for receive location i and source k where

$$K_k(\alpha) = \mathrm{Tr}(\boldsymbol{P}_k) / \left(1 + \alpha + \alpha^2\right), \quad k = 1, 2, \tag{3.52}$$

and $\alpha > 0$ is the parameter controlling the uniformity of the powers across the antennas. Note that as $\alpha \to 0$ the received power is dominant at the first location, as $\alpha$ becomes large ($\alpha \gg 1$) the third location is dominant and as $\alpha \to 1$ there is an even spread, as in the standard microdiversity scenario. In Figs. 3.2-3.3 we show SER results for the ten scenarios (S1-S10) given in Table 3.1.

Note that an error floor occurs as $\rho \to \infty$ $\left(\sigma^2 \to 0\right)$ for fixed $\varsigma$. The value of the error floor is obtained by substituting $\sigma^2 = 0$ in (3.29). In Table 3.1 we report the values of $m_P$ and the error floor for the ten scenarios considered. Note that $m_p$ is given for a $\sigma^2$ value corresponding to $\rho = 20$ dB.

Figures 3.2 and 3.3 verify the analytical results in (3.29) for BPSK modulation with simulations and also explore the effect of different power profiles. In Fig. 3.2, a low SIR is considered with $\varsigma = 1$. Here, S1 is the worst case since the desired signal profile is aligned with the interferer and the profile is rapidly decaying giving little diversity. S3 is the best since the profiles are opposing

Table 3.1: Parameters for Figures 3.2 and 3.3

| Sc. No. | $\varsigma$ | Decay Parameter: Desired | Decay Parameter: Interfering | $m_P$ (dB) | Err. Floor |
|---|---|---|---|---|---|
| S1 | 1 | $\alpha = \frac{1}{65}$ | $\alpha = \frac{1}{65}$ | 3.06 | 1.36e-1 |
| S2 | 1 | $\alpha = \frac{1}{65}$ | $\alpha = 1$ | 7.68 | 6.26e-2 |
| S3 | 1 | $\alpha = \frac{1}{65}$ | $\alpha = 65$ | 28.64 | 1.80e-3 |
| S4 | 1 | $\alpha = 1$ | $\alpha = 1$ | 5.97 | 2.49e-2 |
| S5 | 1 | $\alpha = 1$ | $\alpha = \frac{1}{65}$ | 5.97 | 2.76e-2 |
| S6 | 10 | $\alpha = \frac{1}{65}$ | $\alpha = \frac{1}{65}$ | 12.93 | 1.42e-2 |
| S7 | 10 | $\alpha = \frac{1}{65}$ | $\alpha = 1$ | 17.30 | 4.90e-3 |
| S8 | 10 | $\alpha = \frac{1}{65}$ | $\alpha = 65$ | 27.62 | 1.68e-4 |
| S9 | 10 | $\alpha = 1$ | $\alpha = 1$ | 15.60 | 1.21e-4 |
| S10 | 10 | $\alpha = 1$ | $\alpha = \frac{1}{65}$ | 15.60 | 2.57e-4 |

Table 3.2: Parameters for Figure 3.4

| Sc. No. | $\varsigma$ | Decay Parameter: Desired | Decay Parameter: Interfering | $m_P$ (dB) | Err. Floor |
|---|---|---|---|---|---|
| S11 | 30 | $\alpha = \frac{1}{65}$ | $\alpha = \frac{1}{65}$ | 17.42 | 1.54e-2 |
| S12 | 30 | $\alpha = \frac{1}{65}$ | $\alpha = 1$ | 21.34 | 5.20e-3 |
| S13 | 30 | $\alpha = \frac{1}{65}$ | $\alpha = 65$ | 27.68 | 1.99e-4 |
| S14 | 30 | $\alpha = 1$ | $\alpha = 1$ | 19.65 | 7.68e-5 |
| S15 | 30 | $\alpha = 1$ | $\alpha = \frac{1}{65}$ | 19.64 | 1.72e-4 |

and the best desired signal aligns with the weakest interference. Since Fig. 3.2 has a low SIR the major impact on performance is caused by the presence or absence of a high SIR or low SIR at each antenna. In Fig. 3.3, the same power profiles are considered but at higher SIR, $\varsigma = 10$, the order is changed. S6 is still the worst as this scenario has high interference at all antennas and little diversity. In contrast S8 is no longer the best with S9 now giving better performance. Note that S9 has greater diversity with an even spread of power across the antennas and this becomes more important at high SIR.

Another comparison between scenarios can be seen in Table 3.1. Note that in Fig. 3.2 the ordering based on $m_P$ correctly identifies the best and worst scenarios whereas in Fig. 3.3 the $m_p$ metric suggest that S8 is best whereas S9 is better. The $m_p$ metric gives some intuition about macrodiversity MRC performance, especially at low SIR, but it doesn't accurately capture diversity effects (seen in the lower tail of the combiner output) which are needed for accurate performance

Table 3.3: Parameters for Figure 3.5

| Sc. No. | $\varsigma$ | Decay Parameter | | $m_P$ (dB) | Err. Floor |
|---|---|---|---|---|---|
| | | Desired | Interfering | | |
| S16 | 20 | $\alpha = \frac{1}{65}$ | $\alpha = \frac{1}{65}$ | 17.57 | 1.50e-3 |
| S17 | 20 | $\alpha = \frac{1}{65}$ | $\alpha = 1$ | 21.69 | 1.61e-4 |
| S18 | 20 | $\alpha = \frac{1}{65}$ | $\alpha = 65$ | 29.32 | 5.51e-7 |
| S19 | 20 | $\alpha = 1$ | $\alpha = 1$ | 20.57 | 1.54e-7 |
| S20 | 20 | $\alpha = 1$ | $\alpha = \frac{1}{65}$ | 19.96 | 1.04e-6 |

prediction.

In Fig. 3.4, the same power profiles are considered for QPSK transmission. Here, the exact results from Sec. 3.2.2 are verified by simulation. In particular, the SER expression in (3.40) for QPSK modulation is used along with (3.29) and (3.43). The relative performance provided by the 5 scenarios is the same as in Fig. 3.3 except that the cross over of S13 and S15 in Fig. 3.4 (equivalent to the cross over of S8 and S10 in Fig. 3.3) does not occur until SNR $> 30$ dB.

Finally, in Fig. 3.5 we consider the six antenna receiver where antennas 1,2 are co-located, antennas 3,4 are co-located elsewhere and antennas 5,6 are also co-located and separated from antennas 1-4. Here, the long term receive SNR of a source at antennas 1 and 2 will be the same. Hence, we use the perturbation approach of Sec. 3.2.4 to obtain results. Fig. 3.5 validates the perturbation approach by simulation and shows a large performance improvement relative to Fig. 3.4 due to the increased number of antennas. Again, the results due to the five scenarios follow the same order as in Figs. 3.3 and 3.4. Note that when $\alpha = 1$ for both desired and interfering sources, the system layout is microdiversity. Hence, scenarios S4, S9, S14 and S19 provide microdiversity results.

## 3.4 Summary

Exact SER results are derived for BPSK and $M$-QAM modulations in a Rayleigh fading macrodiversity system employing MRC. The results have applications to several systems of current interest in communications including network MIMO and cooperative communications. The analysis is used to study the effects of the macrodiversity power profiles on MRC performance. It is shown that simple power metrics may capture several features of MRC performance but the impact of

diversity in a distributed system is important at realistic SINR values. Here, the exact results are necessary to provide an accurate performance measure. In general, performance improves as the desired signal dominates the interferer at some antennas and as the desired power is spread more evenly over the receive antennas. The exact balance between these two key features is difficult to obtain in a simple form but is provided by the exact solutions given.

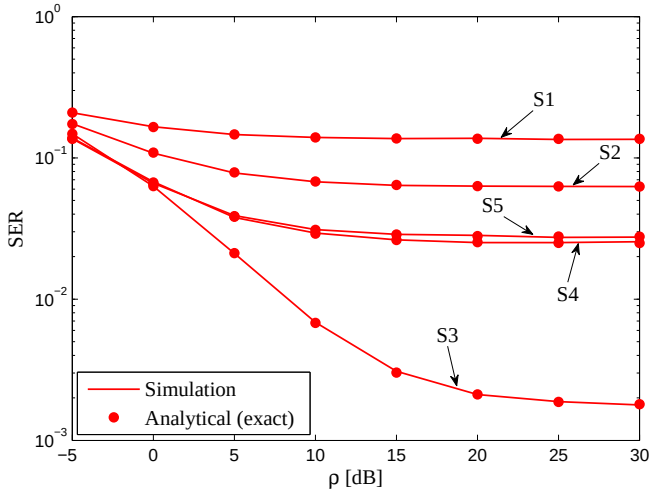


Figure 3.2: Analytical and simulated SER values for a MRC receiver with BPSK modulation in flat Rayleigh fading for scenarios S1-S5 with parameters: $n_R = 3$ and $\varsigma = 1$.

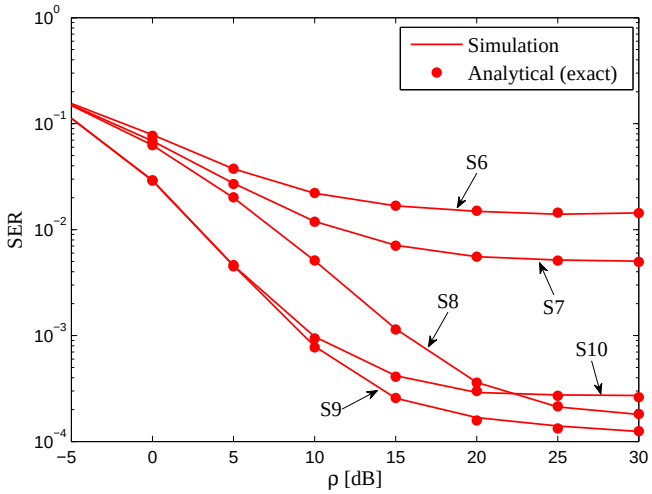


Figure 3.3: Analytical and simulated SER values for a MRC receiver with BPSK modulation in flat Rayleigh fading for scenarios S6-S10 with parameters: $n_R = 3$ and $\varsigma = 10$.

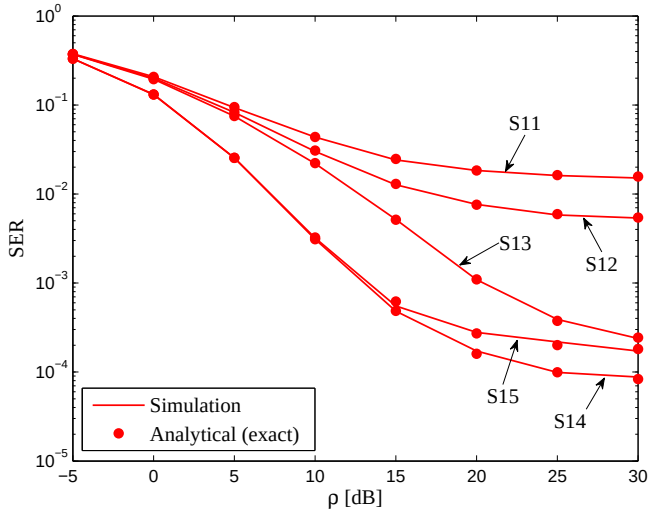


Figure 3.4: Analytical and simulated SER values for a MRC receiver with QPSK modulation in flat Rayleigh fading for scenarios S11-S15 with parameters: $n_R = 3$ and $\varsigma = 30$.

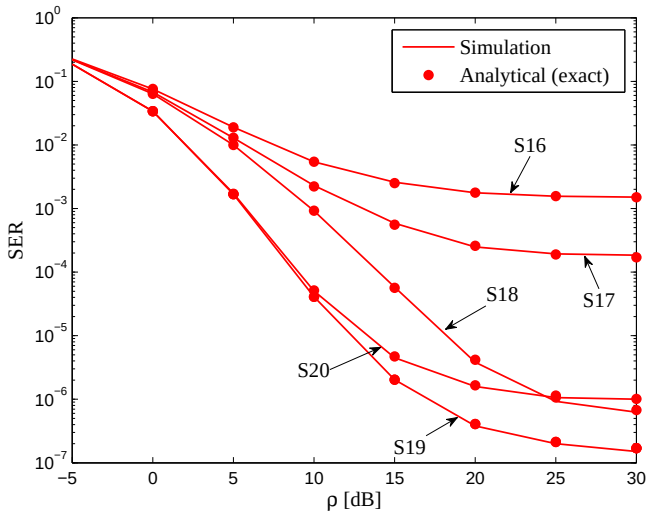


Figure 3.5: Analytical and simulated SER values for a MRC receiver with QPSK modulation in flat Rayleigh fading for scenarios S16-S20 with parameters: $n_R = 6$ and $\varsigma = 20$.

# Chapter 4

# Ergodic Sum Capacity of Macrodiversity MIMO Systems

The information capacity is a fundamental measure which quantify the maximum amount of information transferable across a channel reliably [1, 31]. Despite our knowledge on the capacity of other MU-MIMO systems [58], little is known analytically in the macrodiversity MU-MIMO scenario. There appears to be no work currently available on the capacity of general systems of this type. Similar work includes the capacity analysis of Rayleigh channels with a two-sided Kronecker correlation structure [59, 60]. However, the Kronecker structure is much too restrictive for a macrodiversity layout and such results cannot be leveraged here. Also, there is interesting work on system capacity for particular cellular structures, including Wyner's circular cellular array model [61] and the infinite linear cell-array model [62]. Despite these contributions, the general macrodiversity model appears difficult to handle [58]. In [63], the ergodic capacity is calculated using an asymptotic large random matrix approach for point-to-point MIMO systems. Similarly, an asymptotic approach is used to study cellular systems with multiple correlated BS and US antennas in [64]. The analytical difficulties are caused by the geographical separation of the antennas which results in different entries of the channel matrix having different powers with an arbitrary pattern. Also, these powers can vary enormously when shadowing and path loss are considered. Note that this type of channel model also occurs in the work of [65].

In this chapter, we consider a MIMO-MAC where all sources and receive antennas are widely separated and all links experience independent Rayleigh fading. For this system, we consider the ergodic sum capacity, under the assumption of no CSI at the transmitters. For two sources, we derive the exact ergodic sum capacity. The result is given in closed form, but the details are complicated and for more than two sources, it would appear that an exact approach is too complex to be useful. Hence, we develop a compact approximation and a bound for the general case. The first technique is very accurate, but the functional form is awkward to interpret. Hence, a second, less accurate but simple bound is developed which has a familiar and appealing structure. This bound leads to insight into capacity behavior and its relationship with the channel powers. Results are verified by Monte Carlo simulations and the impact on capacity of various channel power profiles is investigated.

Note that, the methodology developed is for the case of arbitrary powers for the entries in the channel matrix. There is no restriction due to particular cellular structures. Hence, the results and techniques may also have applications in multivariate statistics.

## 4.1 System Model

Consider a MIMO-MAC link with $M$ base stations and $W$ users operating over a Rayleigh channel where BS $i$ has $n_{R_i}$ receive antennas and user $i$ has $n_i$ antennas. The total number of receive antennas is denoted $n_R = \sum_{i=1}^{M} n_{R_i}$ and the total number of transmit antennas is denoted $N = \sum_{i=1}^{W} n_i$. An example of such a system is shown in Fig. 4.1, where three BSs are linked by a backhaul processing unit and communicate with multiple, mobile users. All channels are considered to be independent since the correlated channel scenario can be transformed into the independent case as shown in Sec. 4.1.1. The system equation is given by

$$\boldsymbol{r} = \boldsymbol{H}\boldsymbol{s} + \boldsymbol{n}, \tag{4.1}$$

where $\boldsymbol{r}$ is the $\mathcal{C}^{n_R \times 1}$ receive vector, $\boldsymbol{s}$ is the combined $\mathcal{C}^{N \times 1}$ transmitted vector from the $W$ users, $\boldsymbol{n}$ is an additive white Gaussian noise vector, $\boldsymbol{n} \sim \mathcal{CN}\left(\boldsymbol{0}, \sigma^2 \boldsymbol{I}\right)$, and $\boldsymbol{H} \in \mathcal{C}^{n_R \times N}$ is the composite

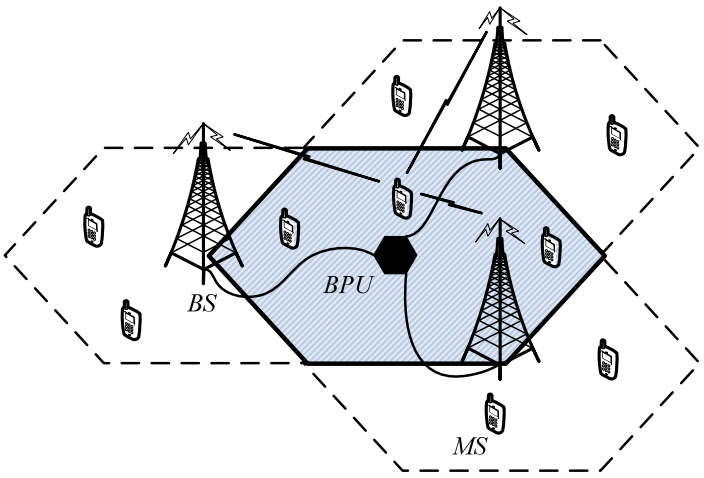


Figure 4.1: A network MIMO system with a 3 sector cluster. To reduce the clutter, only paths from a single source are shown.

channel matrix containing the $W$ channel matrices from the $W$ users. The ergodic sum capacity of the link depends on the availability of channel state information at the transmitter side. In particular, if no CSI at the transmitter is assumed, the corresponding ergodic sum capacity is [30, pp. 57]

$$E\{C\} = E\left\{\log_2\left|\boldsymbol{I} + \frac{1}{\sigma^2}\boldsymbol{H}\boldsymbol{H}^H\right|\right\}, \tag{4.2}$$

where $E\left\{|s_i|^2\right\} = 1$, $i = 1, 2, \ldots, N$, is the power of each transmitted symbol. It is convenient to label each column of $\boldsymbol{H}$ as $\boldsymbol{h}_i$, $i = 1, 2, \ldots, N$, so that $\boldsymbol{H} = (\boldsymbol{h}_1, \boldsymbol{h}_2, \ldots, \boldsymbol{h}_N)$. The covariance matrix of $\boldsymbol{h}_k$ is defined by $\boldsymbol{P}_k = E\left\{\boldsymbol{h}_k\boldsymbol{h}_k^H\right\}$ and $\boldsymbol{P}_k = \text{diag}\,(P_{1k}, P_{2k}, \ldots, P_{n_R k})$. Hence, the $ik^{th}$ element of $\boldsymbol{H}$ is $\mathcal{CN}(0, P_{ik})$. Using this notation, we can also express $\boldsymbol{h}_k$ as $\boldsymbol{h}_k = \boldsymbol{P}_k^{\frac{1}{2}}\boldsymbol{u}_k$, where $\boldsymbol{u}_k \sim \mathcal{CN}(\boldsymbol{0}, \boldsymbol{I})$. Note that, for convenience, all the power information is contained in the $\boldsymbol{P}_k$ matrices so that there is no normalization of the channel and, in (4.2), the scaling factor in the capacity equation is simply $1/\sigma^2$.

### 4.1.1 Correlated Channels

Consider the general scenario where sources and/or BSs have multiple co-located antennas for transmission and reception. Here, spatial correlation may be present due to the co-located antennas

[66, 67]. If a Kronecker correlation model is assumed, then the composite channel matrix is given by

$$\boldsymbol{H} = \begin{pmatrix} \boldsymbol{R}_{r1}^{\frac{1}{2}} & & \boldsymbol{0} \\ & \ddots & \\ \boldsymbol{0} & & \boldsymbol{R}_{rM}^{\frac{1}{2}} \end{pmatrix} \begin{pmatrix} \boldsymbol{H}_{w,11} & \dots & \boldsymbol{H}_{w,1W} \\ \vdots & \ddots & \vdots \\ \boldsymbol{H}_{w,M1} & \dots & \boldsymbol{H}_{w,MW} \end{pmatrix} \begin{pmatrix} \boldsymbol{R}_{t1}^{\frac{1}{2}} & & \boldsymbol{0} \\ & \ddots & \\ \boldsymbol{0} & & \boldsymbol{R}_{tW}^{\frac{1}{2}} \end{pmatrix}, \tag{4.3}$$

where the $\mathcal{C}^{n_{R_k} \times n_i}$ matrix, $\boldsymbol{H}_{w,ik}$, has iid elements since all the channel powers from user $k$ to BS $i$ are the same. The matrix $\boldsymbol{R}_{ri}$ is the receive correlation matrix at BS $i$ and the matrix $\boldsymbol{R}_{tk}$ is the transmit correlation matrix at source $k$ as defined in [66]. Using the spectral decompositions, $\boldsymbol{R}_{ri} = \boldsymbol{\Phi}_{ri}\boldsymbol{\Lambda}_{ri}\boldsymbol{\Phi}_{ri}^H$ and $\boldsymbol{R}_{tk} = \boldsymbol{\Phi}_{tk}\boldsymbol{\Lambda}_{tk}\boldsymbol{\Phi}_{tk}^H$ and substituting (4.3) into (4.2) it is easily shown that the capacity with the channel in (4.3) is statistically identical to the capacity with channel

$$\boldsymbol{H} = \begin{pmatrix} \boldsymbol{\Lambda}_{r1}^{\frac{1}{2}} & & \boldsymbol{0} \\ & \ddots & \\ \boldsymbol{0} & & \boldsymbol{\Lambda}_{rM}^{\frac{1}{2}} \end{pmatrix} \begin{pmatrix} \boldsymbol{H}_{w,11} & \dots & \boldsymbol{H}_{w,1W} \\ \vdots & \ddots & \vdots \\ \boldsymbol{H}_{w,M1} & \dots & \boldsymbol{H}_{w,MW} \end{pmatrix} \begin{pmatrix} \boldsymbol{\Lambda}_{t1}^{\frac{1}{2}} & & \boldsymbol{0} \\ & \ddots & \\ \boldsymbol{0} & & \boldsymbol{\Lambda}_{tW}^{\frac{1}{2}} \end{pmatrix}. \tag{4.4}$$

Denoting (4.4) by $\boldsymbol{H} = \boldsymbol{\Lambda}_r^{\frac{1}{2}}\boldsymbol{H}_w\boldsymbol{\Lambda}_t^{\frac{1}{2}}$, we see that correlation is equivalent to a scaling of the channel powers by the relevant eigenvalues in $\boldsymbol{\Lambda}_r$ and $\boldsymbol{\Lambda}_t$. In particular, the $(u,v)^{th}$ element of $\boldsymbol{H}$ has power $\boldsymbol{\Lambda}_{r,uu}\boldsymbol{\Lambda}_{t,vv}P_{uv}$, where $P_{uv}$ is the single link power from transmit antenna $v$ to receive antenna $u$. Hence, correlation can be handled by the same methodology developed in Secs. 4.3-4.5, with suitably scaled power values [1].

## 4.2 Preliminaries

In this section we derive some useful results which will be used extensively throughout the chapter.

[1] Arbitrary fixed transmit power control techniques can also be handled in the same way as for the correlated scenario.

**Lemma 4.1.** *Let* $\boldsymbol{X}$ *be an* $n \times n$ *complex random matrix with,*

$$\boldsymbol{A} = E\left\{\boldsymbol{X} \circ \boldsymbol{X}\right\} \triangleq \begin{pmatrix} E\left\{|X_{11}|^2\right\} & \dots & E\left\{|X_{1n}|^2\right\} \\ E\left\{|X_{21}|^2\right\} & \dots & E\left\{|X_{2n}|^2\right\} \\ \dots & \dots & \dots \\ E\left\{|X_{n1}|^2\right\} & \dots & E\left\{|X_{nn}|^2\right\} \end{pmatrix}, \tag{4.5}$$

*where* $\circ$ *represents the Hadamard product. With this notation, the following identity holds.*

$$E\left\{\left|\boldsymbol{X}^H\boldsymbol{X}\right|\right\} = \operatorname{perm}\left(\boldsymbol{A}\right), \tag{4.6}$$

*where* perm(.) *is the permanent of a square matrix defined in [68].*

*Proof.* From the definition of the determinant of a generic matrix, $\boldsymbol{X} = \{X_{i,k}\}_{i,k=1\dots n}$, we have

$$E\left\{\left|\boldsymbol{X}^H\boldsymbol{X}\right|\right\} = E\left\{\left[\sum_{\sigma} \operatorname{sgn}(\sigma) \prod_{i=1}^{n} \bar{X}_{\sigma_i,i}\right] \times \left[\sum_{\mu} \operatorname{sgn}(\mu) \prod_{i=1}^{n} X_{\mu_i,i}\right]\right\}, \tag{4.7}$$

where $\sigma = (\sigma_1, \sigma_2, \dots, \sigma_n)$ is a permutation of the integers $1, \dots, n$, the sum is over all permutations, and $\operatorname{sgn}(\sigma)$ denotes the sign of the permutation. The permutation, $\mu$, in the second summation of (4.7) is defined similarly. Since all the elements of $\boldsymbol{X}$ are independent, the only terms giving non-zero value expectations are $\prod_{i=1}^{n} \bar{X}_{a_i,i} \prod_{i=1}^{n} X_{b_i,i}$, where permutation $a = b$. Hence, using the permanent definition in [68] we have

$$E\left\{\left|\boldsymbol{X}^H\boldsymbol{X}\right|\right\} = \sum_{\sigma} \prod_{i=1}^{n} A_{\sigma_i,i} = \operatorname{perm}\left(\boldsymbol{A}\right). \tag{4.8}$$

□

**Corollary 4.2.** *Let* $\boldsymbol{X}$ *be an* $m \times n$ *random matrix with,* $E\left\{\boldsymbol{X} \circ \boldsymbol{X}\right\} = \boldsymbol{A}$*, where* $\boldsymbol{A}$ *is an* $m \times n$ *deterministic matrix and* $m > n$*. Then, the following identity holds.*

$$E\left\{\left|\boldsymbol{X}^H\boldsymbol{X}\right|\right\} = \operatorname{Perm}\left(\boldsymbol{A}\right), \tag{4.9}$$

*where* $\mathrm{Perm}(\boldsymbol{A})$ *is the permanent of the rectangular matrix* $\boldsymbol{A}$ *as defined in [68].*

*Proof.* Using the Cauchy-Binet formula for the determinant of the product of two rectangular matrices, we can expand $\left|\boldsymbol{X}^H\boldsymbol{X}\right|$ as a sum of products of two square matrices. Each product of square matrices can be evaluated using Lemma 4.1. The resulting expression is seen to be the permanent of the rectangular matrix, $\boldsymbol{A}$, which completes the proof. □

**Corollary 4.3.** *Let* $\boldsymbol{X}$ *be an* $m \times n$ *random matrix with,* $E\{\boldsymbol{X} \circ \boldsymbol{X}\} = \boldsymbol{A}$*, where* $\boldsymbol{A}$ *is an* $m \times n$ *deterministic matrix and* $m > n$*. If the* $m \times m$ *deterministic matrix* $\boldsymbol{\Sigma}$ *is diagonal, then the following identity holds.*

$$E\left\{\left|\boldsymbol{X}^H\boldsymbol{\Sigma}\boldsymbol{X}\right|\right\} = \mathrm{Perm}\left(\boldsymbol{\Sigma}\boldsymbol{A}\right). \tag{4.10}$$

*Proof.* The result follows directly from Lemma 4.1, and the fact that $\boldsymbol{\Sigma}^{\frac{1}{2}} \circ \boldsymbol{\Sigma}^{\frac{1}{2}} = \boldsymbol{\Sigma}$ for any diagonal matrix. □

## 4.3 Exact Small System Analysis

In this section, we derive the exact ergodic sum capacity in (4.2) for the $N = 2$ case. This corresponds to two single antenna users or a single user with two distributed antennas. Here, the channel matrix becomes $\boldsymbol{H} = (\boldsymbol{h}_1, \boldsymbol{h}_2)$ and it is straightforward to write (4.2) as

$$\begin{aligned} E\{C\}\ln 2 &= E\left\{\ln\left|\boldsymbol{I} + \frac{1}{\sigma^2}\boldsymbol{h}_1\boldsymbol{h}_1^H\right|\right\} \\ &\quad + E\left\{\ln\left|\boldsymbol{I} + \frac{1}{\sigma^2}\left(\boldsymbol{I} + \frac{1}{\sigma^2}\boldsymbol{h}_1\boldsymbol{h}_1^H\right)^{-1}\boldsymbol{h}_2\boldsymbol{h}_2^H\right|\right\} \\ &\triangleq C_1 + C_2. \end{aligned} \tag{4.11}$$

Both $C_1$ and $C_2$ can be expressed as scalars [36], [69, pp. 48], so the capacity analysis simply requires

$$C_1 = E\left\{\ln\left(1+\frac{1}{\sigma^2}\boldsymbol{h}_1^H\boldsymbol{h}_1\right)\right\}, \tag{4.12}$$

$$C_2 = E\left\{\ln\left(1+\frac{1}{\sigma^2}\boldsymbol{h}_2^H\left(\boldsymbol{I}+\frac{1}{\sigma^2}\boldsymbol{h}_1\boldsymbol{h}_1^H\right)^{-1}\boldsymbol{h}_2\right)\right\}. \tag{4.13}$$

In order to facilitate our analysis, it is useful to avoid the logarithm representations in (4.12) and (4.13). We exchange logarithms for exponentials as follows. First, we note the identity,

$$\frac{1}{a} = \int_0^\infty e^{-at}dt, \quad \text{for} \quad a > 0. \tag{4.14}$$

Now equation (4.14) can be used to find $\ln a$ as below:

$$\frac{\partial \ln a}{\partial a} = \int_0^\infty e^{-at}dt, \tag{4.15}$$

$$\int_0^{\ln a} d\ln a = \int_1^a\int_0^\infty e^{-at}dtda, \tag{4.16}$$

$$\ln a = \int_0^\infty \frac{e^{-t}-e^{-at}}{t}dt. \tag{4.17}$$

This manipulation is useful because there are many results which can be applied to exponentials of quadratic forms, whereas few results exist for logarithms. As an example, using (4.17) in (4.12) gives

$$C_1 = E\left\{\int_0^\infty \frac{e^{-t}-e^{-\left(1+\frac{1}{\sigma^2}\boldsymbol{h}_1^H\boldsymbol{h}_1\right)t}}{t}dt\right\}. \tag{4.18}$$

Note that $a = 1+\frac{1}{\sigma^2}\boldsymbol{h}_1^H\boldsymbol{h}_1$ has been used in (4.17). Since $a \geq 1$, it follows that the integrand in (4.18) is non-negative. Also, the expected value, $C_1$, is clearly finite and so, by Fubini's theorem, the order of expectation and integration in (4.18) may be interchanged. Using the Gaussian integral

identity (A.18), the expectation in (4.18) can be computed to give

$$C_1 = \int_0^\infty \frac{e^{-t}}{t} - \frac{e^{-t}}{t\,|\boldsymbol{\Sigma}_1|} dt, \tag{4.19}$$

where $\boldsymbol{\Sigma}_1 = \boldsymbol{I} + \frac{t}{\sigma^2}\boldsymbol{P}_1$. Hence, the log-exponential conversion in (4.17) leads to a manageable integral for $C_1$. Using the same approach and applying (4.17) in (4.13) gives

$$C_2 = E\left\{ \int_0^\infty \frac{e^{-t}}{t} - \frac{e^{-t-\frac{t}{\sigma^2}\boldsymbol{h}_2^H\left(\boldsymbol{I}+\frac{1}{\sigma^2}\boldsymbol{h}_1\boldsymbol{h}_1^H\right)^{-1}\boldsymbol{h}_2}}{t} dt \right\}. \tag{4.20}$$

The expectation in (4.20) has to be calculated in two stages. First, the expectation over $\boldsymbol{h}_2$ can be solved using the Gaussian integral identity (A.18) and, with some simplifications, we arrive at

$$C_2 = \int_0^\infty \frac{e^{-t}}{t} - E_{\boldsymbol{h}_1}\left\{ \frac{e^{-t}\left(\sigma^2 + \boldsymbol{h}_1^H\boldsymbol{h}_1\right)}{t\,|\boldsymbol{\Sigma}_2|\left(\sigma^2 + \boldsymbol{h}_1^H\boldsymbol{\Sigma}_2^{-1}\boldsymbol{h}_1\right)} \right\} dt, \tag{4.21}$$

where $\boldsymbol{\Sigma}_2 = \boldsymbol{I} + \frac{t}{\sigma^2}\boldsymbol{P}_2$. Interchange of the expectation and integral in (4.21) follows from the same arguments used for $C_1$. Equation (4.21) can be further simplified to give

$$C_2 = \int_0^\infty \frac{e^{-t}}{t} - \frac{e^{-t}}{t\,|\boldsymbol{\Sigma}_2|} dt - E_{\boldsymbol{h}_1}\left\{ \frac{1}{\sigma^2}\int_0^\infty \frac{e^{-t}\boldsymbol{h}_1^H\boldsymbol{P}_2\boldsymbol{\Sigma}_2^{-1}\boldsymbol{h}_1}{t\,|\boldsymbol{\Sigma}_2|\left(\sigma^2 + \boldsymbol{h}_1^H\boldsymbol{\Sigma}_2^{-1}\boldsymbol{h}_1\right)} dt \right\}. \tag{4.22}$$

Defining the third term in (4.22) as $I_b$, the ergodic sum capacity, $E\,(C) = C_1 + C_2$, becomes

$$E\,\{C\} = \frac{1}{\ln 2}\left\{ \sum_{k=1}^{2} I_{a_k} - I_b \right\}, \tag{4.23}$$

where

$$I_{a_k} = \int_0^\infty \left( \frac{e^{-t}}{t} - \frac{e^{-t}}{t\,|\boldsymbol{\Sigma}_k|} \right) dt. \tag{4.24}$$

Substituting for $\boldsymbol{\Sigma}_k$ in (4.24) and expanding $(t\,|\boldsymbol{\Sigma}_k|)^{-1}$ gives

$$I_{a_k} = \sum_{i=1}^{n_R} \eta_{ik} \int_0^\infty \frac{e^{-t}}{t + \frac{\sigma^2}{P_{ik}}} dt, \tag{4.25}$$

where

$$\eta_{ik} = \frac{P_{ik}^{n_R-1}}{\prod_{l\neq i}^{n_R} (P_{ik} - P_{lk})}. \tag{4.26}$$

Note that the first $e^{-t}/t$ term in (4.24) cancels out with one of the terms in the partial fraction expansion leaving only the linear terms shown in the denominator of (4.25). The integrals in (4.25) can be solved in closed form [52] to give

$$I_{a_k} = \sum_{i=1}^{n_R} \eta_{ik} e^{\frac{\sigma^2}{P_{ik}}} E_1\left(\frac{\sigma^2}{P_{ik}}\right). \tag{4.27}$$

In order to compute $I_b$ we use Lemma 5.1 to give

$$I_b = -\int_0^\infty \int_0^\infty \frac{e^{-t}}{|\boldsymbol{\Sigma}_2|} \left.\frac{\partial E\left\{e^{-\theta_1 z_1 - \theta_2 z_2}\right\}}{\partial \theta_1}\right|_{\theta_1=0} d\theta_2 dt, \tag{4.28}$$

where $z_1 = \boldsymbol{h}_1^H \boldsymbol{P}_2 \boldsymbol{\Sigma}_2^{-1} \boldsymbol{h}_1$ and $z_2 = \sigma^2 + \boldsymbol{h}_1^H \boldsymbol{\Sigma}_2^{-1} \boldsymbol{h}_1$. The expectation in (4.28) can be solved using (A.18), and with some manipulations we arrive at

$$I_b = -\int_0^\infty \int_0^\infty \frac{\partial}{\partial \theta_1} \left[\frac{e^{-\sigma^2 t - \sigma^2 \theta_2}}{|\boldsymbol{I} + t\boldsymbol{P}_2 + \theta_1 \boldsymbol{P}_1 \boldsymbol{P}_2 + \theta_2 \boldsymbol{P}_1|}\right]_{\theta_1=0} d\theta_2 dt. \tag{4.29}$$

In Appendix C.1, $I_b$ in (4.29) is calculated in closed form and the final result is given by

$$I_b = -\frac{1}{|\boldsymbol{P}_1 \boldsymbol{P}_2|} \left\{ \sum_{i=1}^{n_R} \sum_{k\neq i}^{n_R} \sum_{l\neq i,k}^{n_R} \frac{\xi_{ikl}\left(\tilde{M}_{b_{ikl}} - \tilde{N}_{b_{ikl}}\right)}{J_i} \right\}, \tag{4.30}$$

where $\tilde{M}_{b_{ikl}}$, $\tilde{N}_{b_{ikl}}$, $J_i$ and $\xi_{ikl}$ are given in (C.30), (C.31), (C.8) and (C.18) respectively. Then, the final result becomes

$$E\{C\} = \frac{1}{\ln 2}\left\{\sum_{k=1}^{2}\sum_{i=1}^{n_R}\eta_{ik}e^{\frac{\sigma^2}{P_{ik}}}E_1\left(\frac{\sigma^2}{P_{ik}}\right) + \frac{1}{|\boldsymbol{P}_1\boldsymbol{P}_2|}\left[\sum_{i=1}^{n_R}\sum_{k\neq i}^{n_R}\sum_{l\neq i,k}^{n_R}\frac{\xi_{ikl}\left(\tilde{M}_{b_{ikl}} - \tilde{N}_{b_{ikl}}\right)}{J_i}\right]\right\}. \quad (4.31)$$

## 4.4 Approximate General Analysis

In this section, we present an approximate ergodic sum rate capacity analysis for the case where $n_R \geq N > 2$. Extending this to $N \geq n_R$ is a simple extension of the current analysis. We use the following notation for the channel matrix,

$$\begin{aligned}\boldsymbol{H} &= \left(\tilde{\boldsymbol{H}}_N, \boldsymbol{h}_N\right) && (4.32a)\\ &= \left(\tilde{\boldsymbol{H}}_k, \boldsymbol{h}_k \ldots, \boldsymbol{h}_{N-1}, \boldsymbol{h}_N\right) && (4.32b)\\ &= \quad \vdots \\ &= (\boldsymbol{h}_1, \boldsymbol{h}_2, \ldots, \boldsymbol{h}_N), && (4.32c)\end{aligned}$$

where the $n_R \times (k-1)$ matrix, $\tilde{\boldsymbol{H}}_k$, comprises the $k-1$ columns to the left of $\boldsymbol{h}_k$ in $\boldsymbol{H}$. Using the same representation as in (4.11), the ergodic sum capacity is defined by [30] as,

$$E\{C\}\ln 2 \triangleq \sum_{k=1}^{N} C_k, \quad (4.33)$$

where

$$\begin{aligned}C_k &= E\left\{\ln\left|\boldsymbol{I} + \frac{1}{\sigma^2}\left(\boldsymbol{I} + \frac{1}{\sigma^2}\tilde{\boldsymbol{H}}_k\tilde{\boldsymbol{H}}_k^H\right)^{-1}\boldsymbol{h}_k\boldsymbol{h}_k^H\right|\right\} && (4.34)\\ &= E\left\{\ln\left(1 + \frac{1}{\sigma^2}\boldsymbol{h}_k^H\left(\boldsymbol{I} + \frac{1}{\sigma^2}\tilde{\boldsymbol{H}}_k\tilde{\boldsymbol{H}}_k^H\right)^{-1}\boldsymbol{h}_k\right)\right\}. && (4.35)\end{aligned}$$

Applying (4.17) to (4.35) gives

$$C_k = \int_0^\infty \frac{e^{-t}}{t} - E\left\{ \frac{e^{-t}\left|\sigma^2 \boldsymbol{I} + \tilde{\boldsymbol{H}}_k^H \tilde{\boldsymbol{H}}_k\right|}{t\left|\boldsymbol{\Sigma}_k\right|\left|\sigma^2 \boldsymbol{I} + \tilde{\boldsymbol{H}}_k^H \boldsymbol{\Sigma}_k^{-1} \tilde{\boldsymbol{H}}_k\right|} \right\} dt, \tag{4.36}$$

where $\boldsymbol{\Sigma}_k = \boldsymbol{I} + \frac{t}{\sigma^2}\boldsymbol{P}_k$. In order to calculate the second term in (4.36), the following expectation needs to be calculated,

$$\tilde{I}_k(t) = \frac{1}{|\boldsymbol{\Sigma}_k|} E\left\{ \frac{\left|\sigma^2 \boldsymbol{I} + \tilde{\boldsymbol{H}}_k^H \tilde{\boldsymbol{H}}_k\right|}{\left|\sigma^2 \boldsymbol{I} + \tilde{\boldsymbol{H}}_k^H \boldsymbol{\Sigma}_k^{-1} \tilde{\boldsymbol{H}}_k\right|} \right\}. \tag{4.37}$$

Exact analysis of $\tilde{I}_k(t)$ is cumbersome, and even the $N = 2$ case (see the $I_b$ calculation in (4.29)) is complicated. Hence, we employ a Laplace type approximation [56], so that $\tilde{I}_k(t)$ can be approximated by

$$\tilde{I}_k(t) \simeq \frac{1}{|\boldsymbol{\Sigma}_k|} \frac{E\left\{\left|\sigma^2 \boldsymbol{I} + \tilde{\boldsymbol{H}}_k^H \tilde{\boldsymbol{H}}_k\right|\right\}}{E\left\{\left|\sigma^2 \boldsymbol{I} + \tilde{\boldsymbol{H}}_k^H \boldsymbol{\Sigma}_k^{-1} \tilde{\boldsymbol{H}}_k\right|\right\}}. \tag{4.38}$$

Note that the Laplace approximation is better known for ratios of scalar quadratic forms [56]. However, the identity in both the numerator and denominator of (4.37) can be expressed as the limit of a Wishart matrix as in [57]. This gives (4.37) as ratio of determinants of matrix quadratic forms which in turn can be decomposed to give a product of scalar quadratic forms as in Appendix C.4. Hence, the Laplace approximation for (4.37) has some motivation in the work of [56, 70]. It can also be thought of as a first order delta expansion [71]. From Appendix C.2, the expectation in the numerator of (4.38) is given by

$$E\left\{\left|\sigma^2 \boldsymbol{I} + \tilde{\boldsymbol{H}}_k^H \tilde{\boldsymbol{H}}_k\right|\right\} = \sum_{i=0}^{k-1} \sum_{\sigma} \mathrm{Perm}\left((\boldsymbol{Q}_k)^{\sigma_{i,k-1}}\right)\left(\sigma^2\right)^{k-i-1}, \tag{4.39}$$

where $\boldsymbol{Q}_k$ is defined in (C.36). From Appendix C.3, the expectation in the denominator of (4.38) is given by

$$|\boldsymbol{\Sigma}_k| \, E\left\{\left|\sigma^2 \boldsymbol{I} + \tilde{\boldsymbol{H}}_k^H \boldsymbol{\Sigma}_k^{-1} \tilde{\boldsymbol{H}}_k\right|\right\} = \sum_{l=0}^{n_R} t^l \, \varphi_{kl}, \tag{4.40}$$

where $\varphi_{kl}$ is given in (C.46). Therefore, $\tilde{I}_k(t)$ becomes

$$\tilde{I}_k(t) \simeq \frac{\Theta(\boldsymbol{Q}_k)}{\sum_{l=0}^{n_R} t^l \, \varphi_{kl}} \tag{4.41}$$

$$= \frac{\Theta(\boldsymbol{Q}_k)}{\varphi_{kn_R} \sum_{l=0}^{n_R} \left(\frac{\varphi_{kl}}{\varphi_{kn_R}}\right) t^l} \tag{4.42}$$

$$= \frac{\Theta(\boldsymbol{Q}_k)}{\varphi_{kn_R} \prod_{l=1}^{n_R} (t + \omega_{kl})}, \tag{4.43}$$

where

$$\Theta(\boldsymbol{Q}_k) = \sum_{i=0}^{k-1} \sum_{\sigma} \mathrm{Perm}\left((\boldsymbol{Q}_k)^{\sigma_{i,k-1}}\right) \left(\sigma^2\right)^{k-i-1}. \tag{4.44}$$

Note that $\omega_{kl} > 0$ for all $l, k$ from Descartes' rule of signs as all the coefficients of the monomial in the denominator of (4.42) are positive. Also note that, from (C.46), we have $\Theta(\boldsymbol{Q}_k) = \varphi_{k0}$. Applying (4.43) in (4.36) gives

$$C_k \simeq \int_0^{\infty} \frac{e^{-t}}{t} - \frac{\varphi_{k0}}{\varphi_{kn_R}} \frac{e^{-t}}{t \prod_{l=1}^{n_R} (t + \omega_{kl})} dt. \tag{4.45}$$

Using a partial fraction expansion for the product in the denominator of the second term of (4.45) gives

$$\frac{1}{t \prod_{l=1}^{n_R} (t + \omega_{kl})} = \frac{\zeta_{k0}}{t} - \sum_{l=1}^{n_R} \frac{\zeta_{kl}}{t + \omega_{kl}}, \tag{4.46}$$

where

$$\zeta_{k0} = \frac{1}{\prod_{u=1}^{n_R} \omega_{ku}} = \frac{\varphi_{kn_R}}{\varphi_{k0}} \tag{4.47}$$

and

$$\zeta_{kl} = \frac{1}{\omega_{kl} \prod_{u \neq l}^{n_R} (\omega_{ku} - \omega_{kl})}. \tag{4.48}$$

Applying (4.46) in (4.36) gives

$$C_k \simeq \frac{\varphi_{k0}}{\varphi_{kn_R}} \sum_{l=1}^{n_R} \int_0^{\infty} \frac{\zeta_{kl}}{t + \omega_{kl}} dt \tag{4.49}$$

$$= \frac{\varphi_{k0}}{\varphi_{kn_R}} \sum_{l=1}^{n_R} \zeta_{kl} e^{\omega_{kl}} E_1(\omega_{kl}). \tag{4.50}$$

Then, applying (4.50) in (4.33) gives the final approximate ergodic sum rate capacity as

$$E\{C\} \triangleq \frac{1}{\ln 2} \sum_{k=1}^{N} \left( \frac{\varphi_{k0}}{\varphi_{kn_R}} \sum_{l=1}^{n_R} \zeta_{kl} e^{\omega_{kl}} E_1(\omega_{kl}) \right). \tag{4.51}$$

Note the simplicity of the general approximation in (4.51) in comparison to the two-user exact results in (4.31).

## 4.5 A Simple Capacity Bound

In this section, we derive an extremely simple upper-bound for the ergodic capacity in (4.2). This provides a simpler relationship between the average link powers and ergodic sum capacity at the expense of a loss in accuracy. Using Jensen's inequality [72] and $\bar{\gamma} = \frac{1}{\sigma^2}$, equation (4.2) leads to

$$E\{C\} \leq \log_2 \left( E\left\{ \left| \boldsymbol{I} + \bar{\gamma} \boldsymbol{H}^H \boldsymbol{H} \right| \right\} \right). \tag{4.52}$$

From Appendix C.2, (4.52) can be given as

$$E\{C\} \leq \log_2 \left( \sum_{i=0}^{N} \sum_{\sigma} \mathrm{Perm}\left(\boldsymbol{P}^{\sigma_{i,N}}\right) \bar{\gamma}^i \right), \tag{4.53}$$

$$= \log_2 \left( \sum_{i=0}^{N} \vartheta_i \bar{\gamma}^i \right). \tag{4.54}$$

where $\boldsymbol{P} = (P_{ik})$. The simplicity of (4.53) is hidden by the permanent form. For small systems, expanding the permanent reveals the simple relationship between the upper bound and the channel powers. For $n_R = N = 2$ and $n_R = N = 3$, (4.54) gives the upper bounds in (4.55) and (4.56) respectively.

$$E\{C\} \leq \log_2\left(1 + \bar{\gamma}\left(P_{11} + P_{12} + P_{21} + P_{22}\right) + \bar{\gamma}^2\left(P_{11}P_{22} + P_{12}P_{21}\right)\right). \tag{4.55}$$

$$\begin{aligned} E\{C\} \leq \log_2 (1 + \bar{\gamma} (&P_{11} + P_{12} + P_{13} + P_{21} + P_{22} + P_{23} + P_{31} + P_{32} + P_{33}) \\ &+ \bar{\gamma}^2 (P_{11}P_{22} + P_{11}P_{32} + P_{21}P_{12} + P_{21}P_{32} + P_{31}P_{12} + P_{31}P_{22} + P_{11}P_{23} + P_{11}P_{33} + P_{21}P_{13} \\ &+ P_{21}P_{33} + P_{31}P_{13} + P_{31}P_{23} + P_{12}P_{23} + P_{12}P_{33} + P_{22}P_{13} + P_{22}P_{33} + P_{32}P_{13} + P_{32}P_{23}) \\ &+ \bar{\gamma}^3 (P_{11}P_{22}P_{33} + P_{11}P_{23}P_{32} + P_{12}P_{21}P_{33} + P_{12}P_{31}P_{23} + P_{13}P_{21}P_{32} + P_{13}P_{22}P_{31})). \end{aligned} \tag{4.56}$$

These bounds show the simple pattern where cross products of $L$ channel powers scale the $\bar{\gamma}^L$ term. Hence, at low SNR where the $\bar{\gamma}$ term is dominant, $\log_2(1 + P_T\bar{\gamma})$, where $P_T = \sum_i \sum_k P_{ik}$, is an approximation to (4.54). Similarly, at high SNR, the $\bar{\gamma}^N$ term is dominant and $\log_2\left(1 + \mathrm{Perm}(\boldsymbol{P})\,\bar{\gamma}^N\right)$ is an approximation. These approximations show that capacity is affected by the sum of the channel powers at low SNR, whereas at high SNR, the cross products of $N$ powers becomes important.

## 4.6 Numerical and Simulation Results

For the numerical results, we consider three distributed BSs with either a single receive antenna or two antennas. For a two-source system, we parameterize the system by three parameters [73, 74]. The average received signal to noise ratio is defined by $\rho = P_T/\sigma^2$. In particular for a two-source system, $\rho = \left(\mathrm{Tr}(\boldsymbol{P}_1) + \mathrm{Tr}(\boldsymbol{P}_2)\right)/\sigma^2$. The total signal to interference ratio is defined by $\varsigma = \mathrm{Tr}(\boldsymbol{P}_1)/\mathrm{Tr}(\boldsymbol{P}_2)$. The spread of the signal power across the three BS locations is assumed to follow an exponential profile, as in [57], so that a range of possibilities can be covered with only

one parameter. The exponential profile is defined by

$$P_{ik} = K_k(\alpha)\,\alpha^{i-1}, \tag{4.57}$$

for receive location $i \in \{1,2,3\}$ and source $k$ where

$$K_k(\alpha) = \mathrm{Tr}(\boldsymbol{P}_k) / \left(1+\alpha+\alpha^2\right), \quad k = 1,2, \tag{4.58}$$

and $\alpha > 0$ is the parameter controlling the uniformity of the powers across the antennas. Note that as $\alpha \to 0$ the received power is dominant at the first location, as $\alpha$ becomes large ($\alpha \gg 1$) the third location is dominant and as $\alpha \to 1$ there is an even spread, as in the standard microdiversity scenario. Using these parameters, eight scenarios are given in Table 5.1 for the case of two single antenna users. In Fig. 4.2, we explore the capacity of scenarios S1-S4 where $n_R = 3$. The capacity result in (4.31) agrees with the simulations for all scenarios, thus verifying the exact analysis. Furthermore, the approximation in (4.51) is shown to be extremely accurate. All capacity results are extremely similar except for S1, where both sources have their dominant path at the first receive antenna. Here, the system is largely overloaded (two strong signals at a single antenna) and the performance is lower. The similarity of S3 and S4 is interesting as they represent very different systems. In S3, the two users are essentially separate with the dominant channels being at different antennas. In S4, both users have power equally spread over all antennas so the users are sharing all available channels. Figure 4.3 follows the same pattern with S6 (the overloaded case) being lower and the other scenarios almost equivalent. In Fig. 4.3, the overall capacity level is reduced in comparison to Fig. 4.2 as $\varsigma = 10$ implies a weaker second source.

Figures 4.4 and 4.5 show results for a random drop scenario with $M = n_R = 3, W = N = 3$ and $n_R = 6, M = 3, W = N = 6$ respectively. In each random drop, uniform random locations are created for the users and lognormal shadow fading and path loss are considered where $\sigma_{SF} =$ 8dB (standard deviation of shadow fading) and $\gamma = 3.5$ (path loss exponent). The transmit power of the sources is scaled so that all locations in the coverage area have a maximum received SNR greater than 3dB, at least 95% of the time. The maximum SNR is taken over the 3 BSs.

Hence, each drop produces a different $\boldsymbol{P}$ matrix and independent channels are assumed. The excellent agreement between the approximation in (4.51) and the simulations in both Fig. 4.4 and Fig. 4.5 is encouraging as this demonstrates the accuracy of (4.51) over different system sizes as well as over completely different sets of channel powers. Note that at high SNR, Fig. 4.5 gives much higher capacity values than Fig. 4.4 since there are 6 receive antenna rather than 3. In this high SNR region, the $\bar{\gamma}^N$ term in (4.54) dominates and capacity can be approximated by $\log_2\left(1+\mathrm{Perm}\left(\boldsymbol{P}\right)\bar{\gamma}^N\right)$. With $n_R = N = 3$ there are 6 cross products in $\mathrm{Perm}\left(\boldsymbol{P}\right)$ whereas with $n_R = N = 6$ there are 720 cross products. Hence, the bound clearly demonstrates the benefits of increased antenna numbers. In practice there is a trade-off between the costs of increased collaboration between possibly distant BSs and the resulting increase in system capacity. In Figs. 4.2 - 4.5, at low SNR the capacity is controlled by $P_T$. Hence, since $\rho = P_T/\sigma^2$, all four drops have similar performance at low SNR and diverge at higher SNR where the channel profiles affect the results. The upper bound and associated approximations are shown in Figs. 4.6 and 4.7 both for a two user scenario (S3) and a random drop. In Fig. 4.6, the upper bound is shown for scenario S3 as well as the high and low SNR approximations. The results clearly show the loss in accuracy resulting from the use of the simple Jensen bound. However, the bound is quite reasonable over the whole SNR range. The low SNR approximations are quite reasonable below 0 dB and the high SNR version is as accurate as the bound above 15 dB. In Fig. 4.7, similar results are shown for a random drop with $M = n_R = 6, W = N = 6$. Here, similar patterns are observed but the low and high SNR approximations become reasonable at more widely spread SNR values. For example, the low SNR results are accurate below 0 dB and the high SNR results are poor until around 30 dB. In contrast, the upper bound is reasonable throughout. Hence, although there is a noticeable capacity error at high SNR, the cross-product coefficients in (4.55) and (4.56) are seen to explain the large majority of the ergodic capacity behavior.

## 4.7 Summary

In this chapter, we have studied the ergodic sum capacity of a Rayleigh fading macrodiversity MIMO-MAC. The results obtained are shown to be valid for both independent channels and

Table 4.1: Parameters for Figures 4.2 and 4.3

| Sc. No. | Decay Parameter | | $\varsigma$ |
|---|---|---|---|
| | User 1 | User 2 | |
| S1 | $\alpha = 0.1$ | $\alpha = 0.1$ | 1 |
| S2 | $\alpha = 0.1$ | $\alpha = 1$ | 1 |
| S3 | $\alpha = 0.1$ | $\alpha = 10$ | 1 |
| S4 | $\alpha = 1$ | $\alpha = 1$ | 1 |
| S5 | $\alpha = 0.1$ | $\alpha = 0.1$ | 10 |
| S6 | $\alpha = 0.1$ | $\alpha = 1$ | 10 |
| S7 | $\alpha = 0.1$ | $\alpha = 10$ | 10 |
| S8 | $\alpha = 1$ | $\alpha = 0.1$ | 10 |

correlated channels, which may occur when some of the distributed transmit/receive locations have closely spaced antennas. In particular, we derive exact results for the two-source scenario and approximate results for the general case. The approximations have a simple form and are shown to be very accurate over a wide range of channel powers. In addition, a simple upper bound is presented which demonstrates the importance of various channel power cross products in determining capacity.

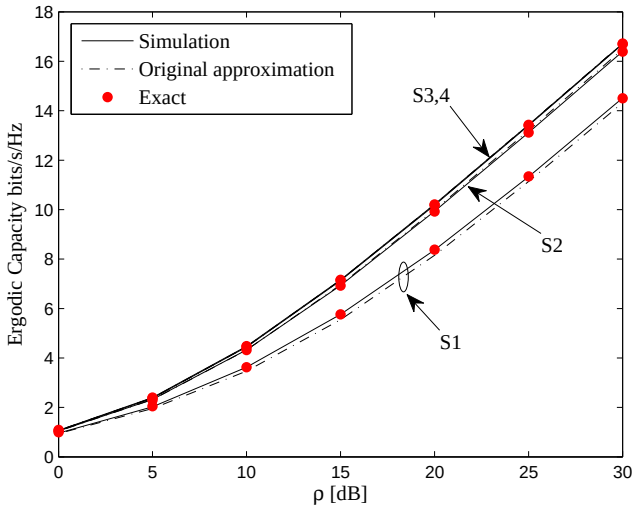


Figure 4.2: Exact, approximated and simulated ergodic sum capacity in flat Rayleigh fading for scenarios S1-S4 with parameters: $n_R = 3$, $N = W = 2$ and $\varsigma = 1$.

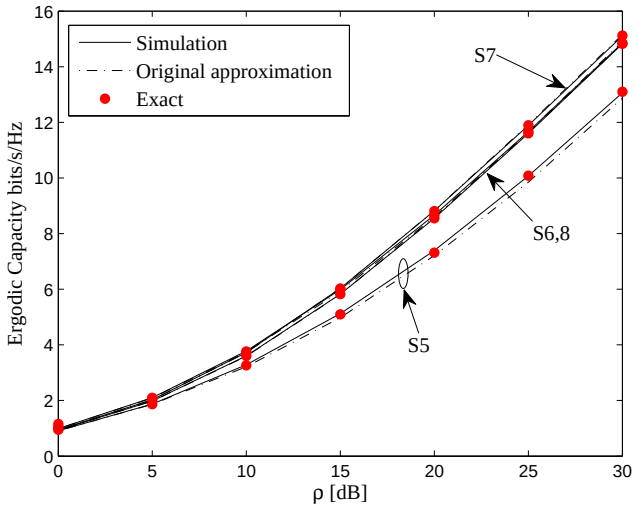


Figure 4.3: Exact, approximated and simulated ergodic sum capacity in flat Rayleigh fading for scenarios S5-S8 with parameters: $n_R = 3$, $N = W = 2$ and $\varsigma = 10$.

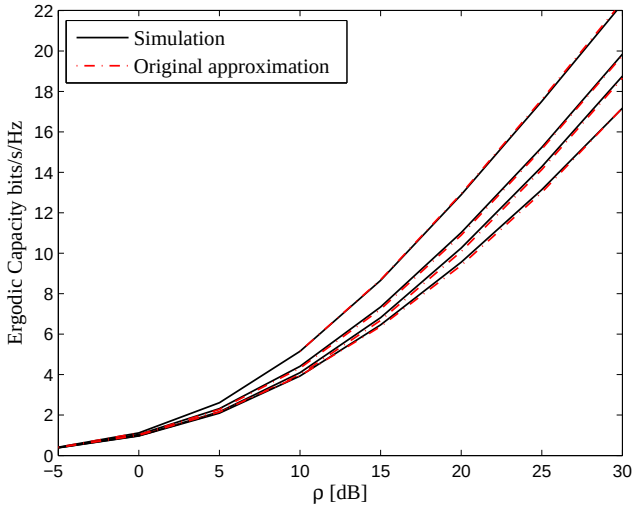


Figure 4.4: Approximated and simulated ergodic sum capacity in flat Rayleigh fading for $M = n_R = 3$, $W = N = 3$ and four random drops.

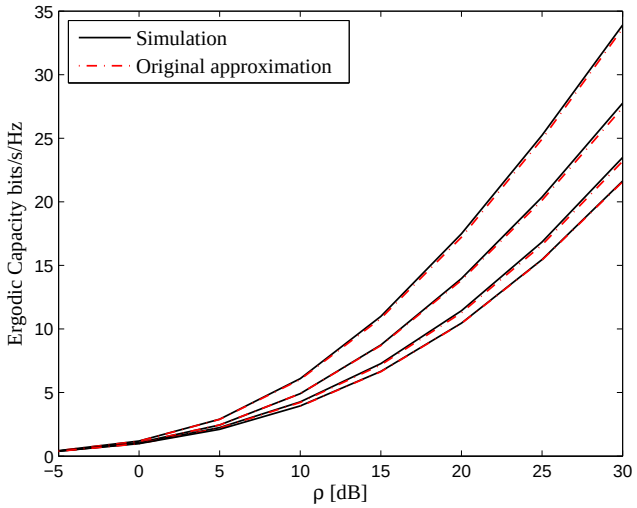


Figure 4.5: Approximated and simulated ergodic sum capacity in flat Rayleigh fading for $n_R = 6$, $M = 3$, $W = N = 6$ and four random drops.

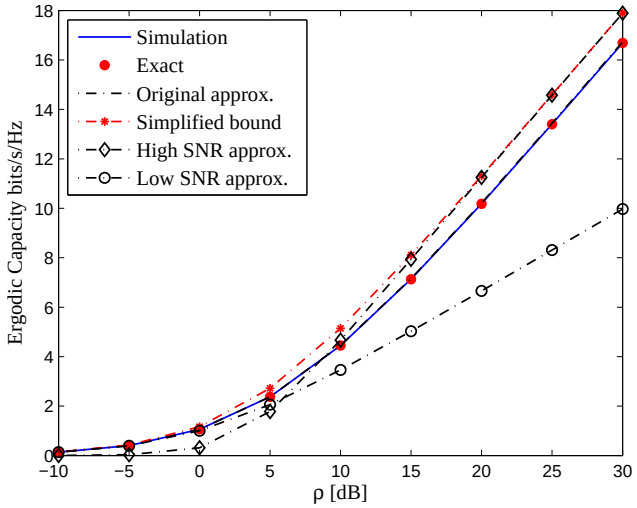


Figure 4.6: Ergodic sum capacity in flat Rayleigh fading for scenario S3 with parameters: $M = n_R = 3$, $W = N = 2$ and $\varsigma = 1$.

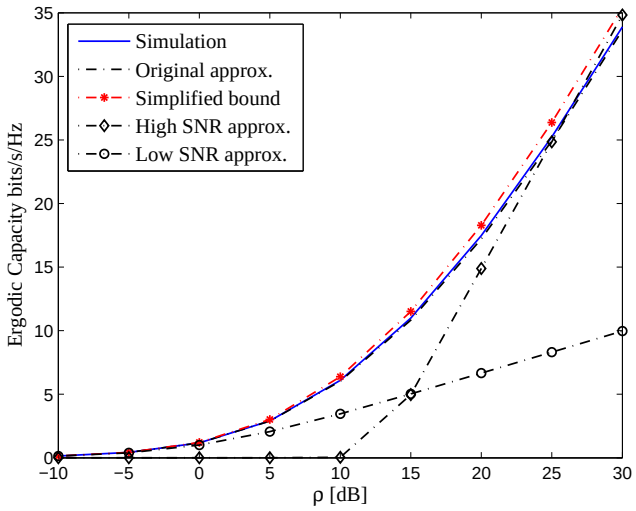


Figure 4.7: Ergodic sum capacity in flat Rayleigh fading for a random drop with parameters: $n_R = 6$, $M = 3$ and $W = N = 6$.

# Chapter 5

# Dual User Macrodiversity MIMO Systems with Linear Receivers

Performance analysis of uncoded MIMO systems with linear receivers is a rich branch of research where many interesting results can be found [57, 75]. Linear combining systems are particularly common due to their low complexity [76, 77]. However, the performance analysis of macrodiversity MIMO systems with linear receivers is believed to be a very difficult problem due to the inherent complexity of the channel matrices that arise in macrodiversity scenarios despite their growing importance in industry standards like the 3GPP LTE-Advanced [37].

The performance of linear receivers in such a macrodiversity system has been investigated via simulation [78, 79], but very few analytical results appear to be available. Hence, in this chapter we consider an analytical treatment of SINR performance for the two user case with two types of linear receivers: MMSE and ZF receivers. We focus on the baseline case of an uncoded multiuser macrodiversity MIMO system in a flat fading Rayleigh channel, where the links are all independent but have different SNRs due to the geographical separation. This subject has been well studied in the microdiversity case [33, 53, 57, 80] where there may be distributed sources, but the receive antennas are closely spaced. In [81], the performance of MMSE in Rician fading is studied while, in [82] the SINR is analyzed using an asymptotic large random matrix approach. The performance metric of interest is the SINR/SNR distribution, since this also leads to results for BER, SER,

outage probability and capacity, etc.

For this dual user scenario, the sources are two single antenna users or a single user with two widely separated transmit antennas. The sources communicate with an arbitrary number of base stations each with a single receive antenna or a single base station with an arbitrary number of widely distributed receive antennas. A particular example of this scenario is also considered, where a three sector cluster in a network MIMO system communicates with two single antenna users. For the general two-user scenario, we are able to derive the exact closed form SINR/SNR distribution for both MMSE and ZF receivers. In addition to the exact SINR/SNR analysis, we also derive high SNR results for the SER of MMSE and ZF receivers. These results lead to a simple metric which relates system performance to the average link SNRs and therefore provides insight into the effect of these SNRs.

## 5.1 System Model and Receiver Types

### 5.1.1 System Model

Consider two single-antenna users communicating with $n_R$ distributed receive antennas in an independent flat Rayleigh fading environment. The $\mathcal{C}^{n_R \times 1}$ received vector is given by

$$\boldsymbol{r} \;=\; \boldsymbol{H}\boldsymbol{s} + \boldsymbol{n}, \tag{5.1}$$

where $\boldsymbol{n}$ is the $\mathcal{C}^{n_R \times 1}$ AWGN vector, $\boldsymbol{s} = (s_1, s_2)^T$ contains the two transmitted symbols from user 1 and user 2 and $\boldsymbol{H}$ is the $\mathcal{C}^{n_R \times 2}$ channel matrix. The complex transmit vector, $\boldsymbol{s}$, is normalized so that $E\left\{|s_1|^2\right\} = E\left\{|s_2|^2\right\} = 1$. The Gaussian noise vector, $\boldsymbol{n} \sim \mathcal{CN}\left(\boldsymbol{0}, \sigma^2\boldsymbol{I}\right)$, has independent entries with $E\left\{|n_i|^2\right\} = \sigma^2$, for $i = 1, 2, \ldots, n_R$. The channel matrix contains independent elements, $\boldsymbol{H}_{ik} \sim \mathcal{CN}\left(0, P_{ik}\right)$, where $E\left\{|\boldsymbol{H}_{ik}|^2\right\} = P_{ik}$.

A particular example of this scenario is shown in Fig. 5.1, where three BSs collaborate via a central BPU in the shaded three sector cluster to serve two single antenna users. In Fig. 5.1, it is clear that the geographical spread of users and receivers gives rise to a $3 \times 2$ channel matrix, $\boldsymbol{H}$,

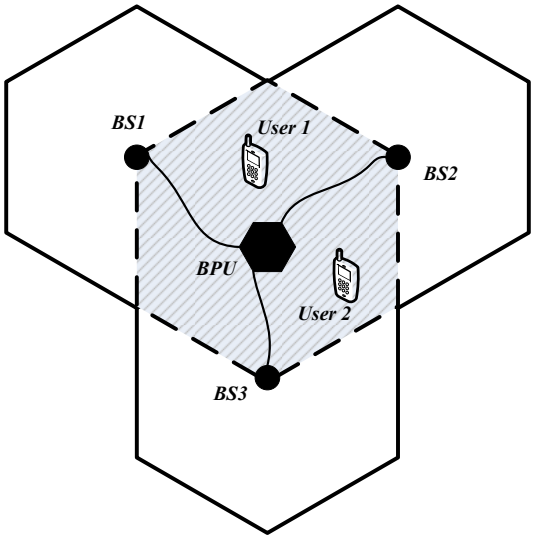


Figure 5.1: A network MIMO system with a 3 sector cluster.

where all the $P_{ik}$ values are different.

### 5.1.2 Receiver Types

At the receiver, the $n_R$ distributed antennas perform linear combining. Hence, the output of the combiner is $\tilde{\boldsymbol{r}} = \boldsymbol{V}^H \boldsymbol{r}$, where $\boldsymbol{V}$ is an $n_R \times 2$ weight matrix. The form of $\boldsymbol{V}$ and the resulting output SINR/SNR are well known for MMSE and ZF receivers. These results are summarized below. Without loss of generality, we assume that the index of the desired user is $i = 1$ and we denote the first column of $\boldsymbol{V}$ by $\boldsymbol{v}_1$. From [57, 33, 83] the combining vector and output SINR of the MMSE receiver are given by

$$\boldsymbol{v}_1 = \boldsymbol{R}^{-1}\boldsymbol{h}_1, \tag{5.2}$$

$$\text{SINR} = \boldsymbol{h}_1^H \boldsymbol{R}^{-1} \boldsymbol{h}_1, \tag{5.3}$$

where $\boldsymbol{R} = \boldsymbol{h}_2 \boldsymbol{h}_2^H + \sigma^2 \boldsymbol{I}$ and $\boldsymbol{h}_1, \boldsymbol{h}_2$ denote columns 1 and 2 of $\boldsymbol{H}$. From [33, 84] the combining

matrix $\boldsymbol{V} = \boldsymbol{H}\left(\boldsymbol{H}^H\boldsymbol{H}\right)^{-1}$ and output SNR of the ZF receiver for $n_R \geq 2$ are given by

$$\text{SNR} = \frac{1}{\sigma^2\left[\left(\boldsymbol{H}^H\boldsymbol{H}\right)^{-1}\right]_{11}}, \tag{5.4}$$

where $[\boldsymbol{B}]_{11}$ indicates the $(1,1)^{th}$ element of matrix $\boldsymbol{B}$.

## 5.2 System Analysis

In this section, we derive the CDFs of the output SINR/SNR of MMSE and ZF receivers. First, we present some useful results as follows.

### 5.2.1 Background

The following lemma gives a compact method to calculate the expected value of a ratio of random variables with arbitrary integer powers [85].

**Lemma 5.1.** *Let $U_1$, $U_2$ and $Z$ be three continuous random variables such that $P(U_2 > 0) = 1$, $Z \geq 0$ and $Z = \frac{U_1^m}{U_2^n}$. Assuming that there exists a joint moment generating function (mgf) for $U_1$ and $U_2$, denoted $\mathcal{M}(\theta_1, \theta_2) = E\left(e^{\theta_1 U_1 + \theta_2 U_2}\right)$, then, for all positive integer values of $m$ and $n$, the expected value of $Z$ is given by*

$$E\left\{\frac{U_1^m}{U_2^n}\right\} = \frac{1}{(n-1)!}\int_0^\infty z^{n-1}\left.\frac{\partial^m \mathcal{M}(\theta, -z)}{\partial\theta^m}\right|_{\theta=0} dz.$$

### 5.2.2 ZF Analysis

Let $\tilde{Z}$ be the output SNR of a ZF receiver as given in (5.4). $\tilde{Z}$ can be written as [83]

$$\tilde{Z} = \frac{1}{\sigma^2}\boldsymbol{h}_1^H\boldsymbol{M}\boldsymbol{h}_1, \tag{5.5}$$

where $\boldsymbol{M} = \boldsymbol{I} - \boldsymbol{h}_2 \left(\boldsymbol{h}_2^H \boldsymbol{h}_2\right)^{-1} \boldsymbol{h}_2^H$. The characteristic function (cf) of $\tilde{Z}$ is [13, 10]

$$\phi_{\tilde{Z}}(t) \quad = \quad E\left\{e^{jt\tilde{Z}}\right\} = E\left\{e^{\frac{jt}{\sigma^2}\boldsymbol{h}_1^H \boldsymbol{M} \boldsymbol{h}_1}\right\}. \tag{5.6}$$

Note that $\boldsymbol{M}$ and $\boldsymbol{h}_1$ are independent and the pdfs of $\boldsymbol{h}_1$ and $\boldsymbol{h}_2$ are given by from (A.21)

$$f(\boldsymbol{h}_k) = \frac{1}{\pi^{n_R}\left|\boldsymbol{P}_k\right|} e^{-\boldsymbol{h}_k^H \boldsymbol{P}_k^{-1} \boldsymbol{h}_k}, \quad \text{for} \quad k = 1, 2, \tag{5.7}$$

where the $n_R \times n_R$ matrix $\boldsymbol{P}_k = \text{diag}(P_{1k}, P_{2,k}, \ldots, P_{n_R,k})$. Next, by using integral identity in (A.18), the cf conditioned on $\boldsymbol{h}_2$ becomes

$$\phi_{\tilde{Z}}(t|\boldsymbol{h}_2) = \frac{1}{\left|\boldsymbol{I} - jt\frac{1}{\sigma^2}\boldsymbol{M}\boldsymbol{P}_1\right|}. \tag{5.8}$$

Substituting $\boldsymbol{M}$ in (5.8) and rearranging gives

$$\phi_{\tilde{Z}}(t|\boldsymbol{h}_2) = \frac{\boldsymbol{h}_2^H \boldsymbol{h}_2}{|\boldsymbol{D}|\left(\boldsymbol{h}_2^H \boldsymbol{D}^{-1} \boldsymbol{h}_2\right)}, \tag{5.9}$$

where $\boldsymbol{D} = \boldsymbol{I} - \frac{1}{\sigma^2} jt\boldsymbol{P}_1$. From [10], the full cf can be obtained by averaging the conditional cf in (5.9) over $\boldsymbol{h}_2$. Using Lemma 5.1, the full cf is given by

$$\phi_{\tilde{Z}}(t) = -\frac{1}{|\boldsymbol{D}|}\int_0^\infty \left.\frac{\partial E\left\{e^{-\theta_1 z_1 - \theta_2 z_2}\right\}}{\partial \theta_1}\right|_{\theta_1 = 0} d\theta_2, \tag{5.10}$$

where $z_1 = \boldsymbol{h}_2^H \boldsymbol{h}_2$ and $z_2 = \boldsymbol{h}_2^H \boldsymbol{D}^{-1} \boldsymbol{h}_2$. Note that the dummy variables are $\theta_1, \theta_2 \geq 0$ and we have used a slight variation of Lemma 5.1, in which the joint mgf has negative coefficients, for convenience. Using the pdf of $\boldsymbol{h}_2$ in (5.7) to evaluate the expectation in (5.10) and using the Gaussian integral identity in (A.18) and a few simplifications, we obtain the following result.

$$\phi_{\tilde{Z}}(t) = -\int_0^\infty \frac{\partial}{\partial \theta_1}\left[\frac{1}{|\boldsymbol{D}_1 - jt\boldsymbol{D}_2|}\right]_{\theta_1 = 0} d\theta_2, \tag{5.11}$$

where $\boldsymbol{D}_1 = \boldsymbol{I} + \theta_1\boldsymbol{P}_2 + \theta_2\boldsymbol{P}_2$ and $\boldsymbol{D}_2 = \frac{1}{\sigma^2}\boldsymbol{P}_1\,(\boldsymbol{I} + \theta_1\boldsymbol{P}_2)$. From [10], the pdf and cdf of $\tilde{Z}$ are

$$f_{\tilde{Z}}(z) = \frac{1}{2\pi}\int_{-\infty}^{\infty}\phi_{\tilde{Z}}(t)e^{-jtz}dt, \tag{5.12}$$

and

$$F_{\tilde{Z}}(z) = \frac{1}{2\pi}\int_{0}^{z}\int_{-\infty}^{\infty}\phi_{\tilde{Z}}(t)e^{-jtx}dtdx. \tag{5.13}$$

By substituting (5.11) into (5.12) and (5.13) multiple integral forms for the pdf and cdf of $\tilde{Z}$ are obtained as

$$f_{\tilde{Z}}(z) = -\frac{1}{2\pi}\int_{-\infty}^{\infty}\int_{0}^{\infty}\frac{\partial}{\partial\theta_1}\left[\frac{e^{-jtz}}{|\boldsymbol{D}_1 - jt\boldsymbol{D}_2|}\right]_{\theta_1=0}d\theta_2 dt, \tag{5.14}$$

$$F_{\tilde{Z}}(z) = -\frac{1}{2\pi}\int_{0}^{z}\int_{-\infty}^{\infty}\int_{0}^{\infty}\frac{\partial}{\partial\theta_1}\left[\frac{e^{-jtx}}{|\boldsymbol{D}_1 - jt\boldsymbol{D}_2|}\right]_{\theta_1=0}d\theta_2 dtdx. \tag{5.15}$$

Since $\boldsymbol{D}_1$ and $\boldsymbol{D}_2$ are diagonal, we can further simplify the expression in (5.15) with the substitutions, $a_i = 1 + \theta_1 P_{i2} + \theta_2 P_{i2}$ and $b_i = \frac{1}{\sigma^2}P_{i1}\,(1 + \theta_1 P_{i2})$. Then, the integrand in (5.15), before differentiation, can be written as $\tilde{J}_0 = \frac{e^{-jtx}}{\prod_{i=1}^{n_R}(a_i - jtb_i)}$. Hence,

$$F_{\tilde{Z}}(z) = -\frac{1}{2\pi}\int_{0}^{z}\int_{-\infty}^{\infty}\int_{0}^{\infty}\left.\frac{\partial\tilde{J}_0}{\partial\theta_1}\right|_{\theta_1=0}d\theta_2 dtdx. \tag{5.16}$$

Since the limits of integration are independent of $\theta_1$, we can interchange the order of differentiation and first perform the integration over $t$. To obtain this integral, we use the partial fraction expansion of $\tilde{J}_0$ from (A.11) and apply the following integral identity from (A.19) to give the result,

$$F_{\tilde{Z}}(z) = -\int_{0}^{z}\int_{0}^{\infty}\left.\frac{\partial\tilde{J}_1}{\partial\theta_1}\right|_{\theta_1=0}d\theta_2 dx, \tag{5.17}$$

where $\tilde{J}_1 = \sum_{i=1}^{n_R} A_i e^{-\frac{a_i}{b_i}x}$, where

$$A_i = \frac{b_i^{n_R-2}}{\prod_{k\neq i}^{n_R}(b_i a_k - a_i b_k)}. \tag{5.18}$$

Differentiating $\tilde{J}_1$ term by term and setting $\theta_1 = 0$ gives

$$\left.\frac{\partial \tilde{J}_1}{\partial \theta_1}\right|_{\theta_1=0} = \sigma^2 \sum_{i=1}^{n_R} e^{-\tilde{\alpha}_i x - \tilde{\beta}_i x\theta_2} \times \left\{ \frac{P_{i1}^{n_R-2}\left(x\theta_2\sigma^2 P_{i2}^2 P_{i1}^{-1} + (n_R-2)P_{i2}\right)}{\prod_{k\neq i}^{n_R}(\tilde{n}_{ik}+\theta_2\tilde{m}_{ik})} - \frac{P_{i1}^{n_R-2}}{\prod_{k\neq i}^{n_R}\tilde{n}_{ik}+\theta_2\tilde{m}_{ik}} \left[\sum_{k\neq i}^{n_R} \frac{\tilde{\gamma}_{ik}+\theta_2\tilde{\delta}_{ik}}{\tilde{n}_{ik}+\theta_2\tilde{m}_{ik}}\right] \right\} \tag{5.19}$$

where

$$\tilde{\gamma}_{ik} = (P_{i1}-P_{k1})(P_{i2}+P_{k2}), \qquad \tilde{\delta}_{ik} = (P_{i1}-P_{k1})P_{i2}P_{k2}, \tag{5.20}$$

$$\tilde{n}_{ik} = (P_{i1}-P_{k1}), \qquad \tilde{m}_{ik} = (P_{i1}P_{k2}-P_{k1}P_{i2}), \tag{5.21}$$

$$\tilde{\alpha}_i = \frac{\sigma^2}{P_{i1}}, \qquad \tilde{\beta}_i = \frac{\sigma^2 P_{i2}}{P_{i1}}. \tag{5.22}$$

Using (A.11), the product in the denominator of (5.19) can be expanded as

$$\frac{1}{\prod_{k\neq i}^{n_R}(\tilde{n}_{ik}+\theta_2\tilde{m}_{ik})} = \sum_{k\neq i}^{n_R} \frac{\tilde{\eta}_{ik}}{\tilde{n}_{ik}+\theta_2\tilde{m}_{ik}}, \tag{5.23}$$

where

$$\tilde{\eta}_{ik} = \frac{\tilde{m}_{ik}^{n_R-2}}{\prod_{l\neq i,k}^{n_R}(\tilde{n}_{il}\tilde{m}_{ik} - \tilde{n}_{ik}\tilde{m}_{il})} \tag{5.24}$$

Substituting (5.23) in (5.19) gives (5.25)

$$\left.\frac{\partial \tilde{J}_1}{\partial \theta_1}\right|_{\theta_1=0} = \sigma^2 \sum_{i=1}^{n_R}\sum_{k\neq i}^{n_R} e^{-\tilde{\alpha}_i x - \tilde{\beta}_i x\theta_2} \left\{ \frac{x\theta_2\sigma^2 P_{i2}^2 P_{i1}^{n_R-3}\tilde{\eta}_{ik}}{(\tilde{n}_{ik}+\theta_2\tilde{m}_{ik})} - \frac{\tilde{\varphi}_{ik}}{(\tilde{n}_{ik}+\theta_2\tilde{m}_{ik})} - \frac{P_{i1}^{n_R-2}\tilde{\eta}_{ik}\tilde{\xi}_{ik}}{(\tilde{n}_{ik}+\theta_2\tilde{m}_{ik})^2} \right\}. \tag{5.25}$$

where the constants are given by

$$\tilde{\varphi}_{ik} = P_{i1}^{n_R-2}\left(\tilde{\Delta}_i\tilde{\eta}_{ik} - (n_R-2)P_{i2}\tilde{\eta}_{ik} + \tilde{\zeta}_{ik}\right), \tag{5.26a}$$

$$\tilde{\Delta}_i = \sum_{k\neq i}^{n_R} \frac{(P_{i1}P_{i2}P_{k2} - P_{k1}P_{k2}P_{i2})}{(P_{i1}P_{k2} - P_{i2}P_{k1})}, \tag{5.26b}$$

$$\tilde{\xi}_{ik} = \frac{(P_{i1}-P_{k1})\left(P_{i1}P_{k2}^2 - P_{k1}P_{i2}^2\right)}{(P_{i1}P_{k2} - P_{i2}P_{k1})}, \tag{5.26c}$$

$$\tilde{\zeta}_{ik} = \tilde{m}_{ik}\sum_{l\neq i,l\neq k}^{n_R} \frac{\tilde{\eta}_{ik}\tilde{\xi}_{il} + \tilde{\eta}_{il}\tilde{\xi}_{ik}}{(\tilde{n}_{il}\tilde{m}_{ik} - \tilde{n}_{ik}\tilde{m}_{il})}. \tag{5.26d}$$

Substituting $\left.\frac{\partial \tilde{J}_1}{\partial\theta_1}\right|_{\theta_1=0}$ from (5.25) in to the cdf expression in (5.17) gives (5.27).

$$F_{\tilde{Z}}(z) = -\sigma^2\int_0^z\int_0^\infty \sum_{i=1}^{n_R}\sum_{k\neq i}^{n_R} e^{-\tilde{\alpha}_i x - \tilde{\beta}_i x\theta_2} \times\left\{\frac{x\theta_2\sigma^2 P_{i2}^2 P_{i1}^{n_R-3}\tilde{\eta}_{ik}}{(\tilde{n}_{ik}+\theta_2\tilde{m}_{ik})} - \frac{\tilde{\varphi}_{ik}}{(\tilde{n}_{ik}+\theta_2\tilde{m}_{ik})} - \frac{P_{i1}^{n_R-2}\tilde{\eta}_{ik}\tilde{\xi}_{ik}}{(\tilde{n}_{ik}+\theta_2\tilde{m}_{ik})^2}\right\} d\theta_2 dx. \tag{5.27}$$

The desired cdf in (5.27) is rewritten in a compact form to obtain

$$F_{\tilde{Z}}(z) = \sigma^2\sum_{i=1}^{n_R}\sum_{k\neq i}^{n_R}\tilde{\varphi}_{ik}\tilde{I}_1\left(\tilde{n}_{ik},\tilde{\alpha}_i,\tilde{m}_{ik},\tilde{\beta}_i,z\right) + \tilde{\psi}_{ik}\tilde{I}_2\left(\tilde{n}_{ik},\tilde{\alpha}_i,\tilde{m}_{ik},\tilde{\beta}_i,z\right) + \tilde{\omega}_{ik}\tilde{I}_3\left(\tilde{n}_{ik},\tilde{\alpha}_i,\tilde{m}_{ik},\tilde{\beta}_i,z\right), \tag{5.28}$$

where $\tilde{\psi}_{ik} = \tilde{\eta}_{ik}\tilde{\xi}_{ik}P_{i1}^{n_R-2}$ and $\tilde{\omega}_{ik} = -P_{i1}^{n_R-3}\tilde{\eta}_{ik}P_{i2}^2$. Note that when $n_R = 2$, $\tilde{\zeta}_{ik} = 0$ and $\tilde{\eta}_{ik} = 1$ for all $i,k$. The cdf in (5.28) contains three types of double integral defined by

$$\tilde{I}_1(a,b,c,d,x) = \int_0^x\int_0^\infty \frac{e^{-bt-dt\theta}}{a+c\theta}d\theta dt, \tag{5.29}$$

$$\tilde{I}_2(a,b,c,d,x) = \int_0^x\int_0^\infty \frac{e^{-bt-dt\theta}}{(a+c\theta)^2}d\theta dt, \tag{5.30}$$

$$\tilde{I}_3(a,b,c,d,x) = \int_0^x\int_0^\infty \frac{t\theta e^{-bt-dt\theta}}{a+c\theta}d\theta dt. \tag{5.31}$$

Each double integral can be evaluated using standard methods in terms of a sum of exponential integral functions as shown in (5.35)-(5.37), where $E_1(x)$ is defined in (A.14). $\tilde{I}_1$ in (5.29) can be

solved by integrating over $t$ first and making use of the identity in [52]

$$\int_0^\infty \frac{e^{-\lambda\theta}}{\alpha+\beta\theta}d\theta = \frac{e^{\frac{\lambda\alpha}{\beta}}}{\beta}E_1\left(\frac{\lambda\alpha}{\beta}\right), \tag{5.32}$$

and identity in (A.20) to solve the resulting integral over $\theta$. Next, we note that $\tilde{I}_2$ follows directly from $\tilde{I}_1$ as $\tilde{I}_2 = -\frac{\partial \tilde{I}_1}{\partial a}$. Hence, by differentiating the expression for $\tilde{I}_1$ in (5.35), we obtain (5.36). In order to differentiate the exponential integral, we use Leibnitz's integration formula to give

$$\frac{\partial\left[E_1\left(\alpha a\right)\right]}{\partial a} = -\frac{e^{-\alpha a}}{a}. \tag{5.33}$$

$\tilde{I}_3$ in (5.31) can also be solved by a similar approach as in $\tilde{I}_1$ and making use of the following integral identity from [52] where necessary:

$$\int_0^x \frac{e^{-bt}}{t+d}dt = e^{bd}\left[E_1(bd) - E_1(bx+bd)\right]. \tag{5.34}$$

Hence, (5.28)-(5.37) give a closed form result for the cdf of the output SNR of a ZF receiver in a two-user macrodiversity environment.

$$\tilde{I}_1\left(a,b,c,d,x\right) = \frac{1}{bc-ad}\left[\ln\left(\frac{bc}{ad}\right) - e^{-bx}e^{\frac{adx}{c}}E_1\left(\frac{adx}{c}\right) + E_1\left(bx\right)\right], \tag{5.35}$$

$$\begin{aligned}\tilde{I}_2\left(a,b,c,d,x\right) = &\left[\frac{dx}{c\left(bc-ad\right)} + \frac{d}{\left(bc-ad\right)^2}\right]e^{-bx}e^{\frac{adx}{c}}E_1\left(\frac{adx}{c}\right)\\ &- \frac{d}{\left(bc-ad\right)^2}E_1\left(bx\right) - \frac{d+b\left(bc-ad\right)}{\left(bc-ad\right)^2}\ln\left(\frac{bc}{ad}\right) + \frac{1-e^{-bx}}{a\left(bc-ad\right)},\end{aligned} \tag{5.36}$$

$$\begin{aligned}\tilde{I}_3\left(a,b,c,d,x\right) = &\left[\frac{ax}{c\left(bc-ad\right)} + \frac{a}{\left(bc-ad\right)^2}\right]e^{-bx}e^{\frac{adx}{c}}E_1\left(\frac{adx}{c}\right)\\ &- \frac{a}{\left(bc-ad\right)^2}E_1\left(bx\right) - \frac{a}{\left(bc-ad\right)^2}\ln\left(\frac{bc}{ad}\right) + \frac{a\left(1-e^{-bx}\right)}{bc\left(bc-ad\right)} + \frac{1-e^{-bx}}{bcd}.\end{aligned} \tag{5.37}$$

### 5.2.3 MMSE Analysis

Let Z be the output SINR of an MMSE receiver given by (5.3). The cf of Z is [13, 10]

$$\phi_Z(t) \;=\; E\left\{e^{jtZ}\right\} = E\left\{e^{jt\boldsymbol{h}_1^H\boldsymbol{R}^{-1}\boldsymbol{h}_1}\right\}. \tag{5.38}$$

Next, by using the identity (A.18), the cf conditioned on $\boldsymbol{h}_2$ becomes

$$\phi_Z(t|\boldsymbol{h}_2) = \frac{1}{\left|\boldsymbol{I} - jt\boldsymbol{R}^{-1}\boldsymbol{P}_1\right|}. \tag{5.39}$$

Substituting $\boldsymbol{R}$ in (5.39) and rearranging gives

$$\phi_Z(t|\boldsymbol{h}_2) = \frac{\left|\sigma^2\boldsymbol{I} + \boldsymbol{h}_2\boldsymbol{h}_2^H\right|}{\left|\sigma^2\boldsymbol{I} + \boldsymbol{h}_2\boldsymbol{h}_2^H - jt\boldsymbol{P}_1\right|}. \tag{5.40}$$

This determinant ratio can be further simplified by applying the result $\left|\boldsymbol{I} + \boldsymbol{x}\boldsymbol{x}^H\right| = 1 + \boldsymbol{x}^H\boldsymbol{x}$ from (A.2) to obtain

$$\phi_Z(t|\boldsymbol{h}_2) = \frac{\sigma^2 + \boldsymbol{h}_2^H\boldsymbol{h}_2}{|\boldsymbol{D}|\left(\sigma^2 + \boldsymbol{h}_2^H\boldsymbol{D}^{-1}\boldsymbol{h}_2\right)}, \tag{5.41}$$

where $\boldsymbol{D} = \boldsymbol{I} - \frac{1}{\sigma^2}jt\boldsymbol{P}_1$. From [10] the full cf can be obtained by averaging the conditional cf in (5.41) over $\boldsymbol{h}_2$. Using Lemma 5.1, the full cf is given by

$$\phi_Z(t) = -K_0\int_0^\infty \left.\frac{\partial E\left\{e^{-\theta_1 z_1 - \theta_2 z_2}\right\}}{\partial\theta_1}\right|_{\theta_1=0} d\theta_2, \tag{5.42}$$

where $z_1 = \sigma^2 + \boldsymbol{h}_2^H\boldsymbol{h}_2$, $z_2 = \sigma^2 + \boldsymbol{h}_2^H\boldsymbol{D}^{-1}\boldsymbol{h}_2$ and $K_0 = 1/|\boldsymbol{D}|$. Note that the dummy variables are $\theta_1, \theta_2 \geq 0$ and we have used a slight variation of Lemma 5.1 in which the joint mgf has negative coefficients for convenience. Using the pdf of $\boldsymbol{h}_2$ in (5.7) to evaluate the expectation in (5.42) and using the Gaussian integral identity in (A.18) and a few simplifications, we can write the cf as

$$\phi_Z(t) = -\int_0^\infty \frac{\partial}{\partial\theta_1}\left[\frac{e^{-\sigma^2\theta_1 - \sigma^2\theta_2}}{|\boldsymbol{D}_1 - jt\boldsymbol{D}_2|}\right]_{\theta_1=0} d\theta_2, \tag{5.43}$$

where $\boldsymbol{D}_1 = \boldsymbol{I} + \theta_1\boldsymbol{P}_2 + \theta_2\boldsymbol{P}_2$ and $\boldsymbol{D}_2 = \frac{1}{\sigma^2}\boldsymbol{P}_1\,(\boldsymbol{I} + \theta_1\boldsymbol{P}_2)$. From [10], the pdf and cdf of Z are

$$f_Z(z) = \frac{1}{2\pi}\int_{-\infty}^{\infty}\phi_Z(t)e^{-jtz}dt, \tag{5.44}$$

and

$$F_Z(z) = \frac{1}{2\pi}\int_{0}^{z}\int_{-\infty}^{\infty}\phi_Z(t)e^{-jtx}dtdx. \tag{5.45}$$

By substituting (5.43) into (5.44) and (5.45), multiple integral forms for the pdf and cdf of Z are obtained as

$$f_Z(z) = -\frac{1}{2\pi}\int_{-\infty}^{\infty}\int_{0}^{\infty}\frac{\partial}{\partial\theta_1}\left[\frac{e^{-\sigma^2\,\theta_1-\sigma^2\theta_2\,-jtz}}{|\boldsymbol{D}_1 - jt\boldsymbol{D}_2|}\right]_{\theta_1=0} d\theta_2 dt, \tag{5.46}$$

$$F_Z(z) = -\frac{1}{2\pi}\int_{0}^{z}\int_{-\infty}^{\infty}\int_{0}^{\infty}\frac{\partial}{\partial\theta_1}\left[\frac{e^{-\sigma^2\nu-jtx}}{|\boldsymbol{D}_1 - jt\boldsymbol{D}_2|}\right]_{\theta_1=0} d\theta_2 dtdx, \tag{5.47}$$

where $\nu = \theta_1 + \theta_2$. Since $\boldsymbol{D}_1$ and $\boldsymbol{D}_2$ are diagonal, we can further simplify the expression in (5.47) with the following substitutions, $a_i = 1 + \theta_1 P_{i2} + \theta_2 P_{i2}$ and $b_i = \frac{1}{\sigma^2}P_{i1}\,(1 + \theta_1 P_{i2})$. Then, the integrand in (5.47) before differentiation can be written as $J_0 = \frac{e^{-\sigma^2\theta_1-\sigma^2\theta_2-jtx}}{\prod_{i=1}^{n_R}(a_i-jtb_i)}$. Hence,

$$F_Z(z) = -\frac{1}{2\pi}\int_{0}^{z}\int_{-\infty}^{\infty}\int_{0}^{\infty}\left.\frac{\partial J_0}{\partial\theta_1}\right|_{\theta_1=0} d\theta_2 dtdx. \tag{5.48}$$

Since the limits of integration are independent of $\theta_1$, we can interchange the order of differentiation. Hence, we first perform the integration over $t$. To obtain this integral, we use the partial fraction expansion of $J_0$ from (A.11) and applying integral identity in (A.19) to give the result,

$$F_Z(z) = -\int_{0}^{z}\int_{0}^{\infty} e^{-\sigma^2\theta_2}\left.\frac{\partial J_1}{\partial\theta_1}\right|_{\theta_1=0} d\theta_2 dx, \tag{5.49}$$

where $J_1 = \sum_{i=1}^{n_R} A_i e^{-\sigma^2\theta_1 - \frac{a_i}{b_i}x}$, where $A_i$ is given in (5.18). Differentiating $J_1$ term by term and setting $\theta_1 = 0$ gives

$$\left.\frac{\partial J_1}{\partial \theta_1}\right|_{\theta_1=0} = \sigma^2 \sum_{i=1}^{n_R} e^{-\alpha_i x-\beta_i x\theta_2} \times \left\{ \frac{P_{i1}^{n_R-2}\left(x\theta_2\sigma^2 P_{i2}^2 P_{i1}^{-1} + (n_R-2)P_{i2} - \sigma^2\right)}{\prod_{k\neq i}^{n_R}(n_{ik}+\theta_2 m_{ik})} - \frac{P_{i1}^{n_R-2}}{\prod_{k\neq i}^{n_R} n_{ik}+\theta_2 m_{ik}} \left[\sum_{k\neq i}^{n_R} \frac{\gamma_{ik}+\theta_2\delta_{ik}}{n_{ik}+\theta_2 m_{ik}}\right] \right\} \tag{5.50}$$

where,

$$\gamma_{ik} = \tilde{\gamma}_{ik}, \quad \delta_{ik} = \tilde{\delta}_{ik}, \quad n_{ik} = \tilde{n}_{ik}, \quad m_{ik} = \tilde{m}_{ik}, \quad \alpha_i = \tilde{\alpha}_i, \quad \beta_i = \tilde{\beta}_i. \tag{5.51}$$

Substituting (5.23) in (5.50) gives (5.52)

$$\left.\frac{\partial J_1}{\partial \theta_1}\right|_{\theta_1=0} = \sigma^2 \sum_{i=1}^{n_R}\sum_{k\neq i}^{n_R} e^{-\alpha_i x-\beta_i x\theta_2} \left\{ \frac{x\theta_2\sigma^2 P_{i2}^2 P_{i1}^{n_R-3}\eta_{ik}}{(n_{ik}+\theta_2 m_{ik})} - \frac{\varphi_{ik}}{(n_{ik}+\theta_2 m_{ik})} - \frac{P_{i1}^{n_R-2}\eta_{ik}\xi_{ik}}{(n_{ik}+\theta_2 m_{ik})^2} \right\}. \tag{5.52}$$

where $\varphi_{ik} = P_{i1}^{n_R-2}\left(\sigma^2\eta_{ik} + \Delta_i\eta_{ik} + \zeta_{ik} - (n_R-2)P_{i2}\eta_{ik}\right)$, $\eta_{ik} = \tilde{\eta}_{ik}$, $\xi_{ik} = \tilde{\xi}_{ik}$, $\Delta_i = \tilde{\Delta}_i$ and $\zeta_{ik} = \tilde{\zeta}_{ik}$. Substituting the simplified $\left.\frac{\partial J_1}{\partial \theta_1}\right|_{\theta_1=0}$ from (5.52) into the cdf expression in (5.49) gives (5.53).

$$F_Z(z) = -\sigma^2 \int_0^z \int_0^\infty \sum_{i=1}^{n_R}\sum_{k\neq i}^{n_R} e^{-\sigma^2\theta_2-\alpha_i x-\beta_i x\theta_2} \times \left\{ \frac{x\theta_2\sigma^2 P_{i2}^2 P_{i1}^{n_R-3}\eta_{ik}}{(n_{ik}+\theta_2 m_{ik})} - \frac{\varphi_{ik}}{(n_{ik}+\theta_2 m_{ik})} - \frac{P_{i1}^{n_R-2}\eta_{ik}\xi_{ik}}{(n_{ik}+\theta_2 m_{ik})^2} \right\} d\theta_2 dx. \tag{5.53}$$

The desired cdf in (5.53) is rewritten

$$F_Z(z) = \sigma^2 \sum_{i=1}^{n_R} \sum_{k \neq i}^{n_R} \varphi_{ik} I_1\left(\sigma^2 n_{ik}, \alpha_i, m_{ik}, \frac{\beta_i}{\sigma^2}, z\right) + \psi_{ik} I_2\left(\sigma^2 n_{ik}, \alpha_i, m_{ik}, \frac{\beta_i}{\sigma^2}, z\right) + \omega_{ik} I_3\left(\sigma^2 n_{ik}, \alpha_i, m_{ik}, \frac{\beta_i}{\sigma^2}, z\right). \quad (5.54)$$

where $\psi_{ik} = \sigma^2 P_{i1}^{n_R-2} \eta_{ik} \xi_{ik}$ and $\omega_{ik} = -P_{i2}^2 P_{i1}^{n_R-3} \eta_{ik}$. Note that when $n_R = 2$, $\zeta_{ik} = 0$ and $\eta_{ik} = 1$ for all $i, k$. The cdf in (5.54) contains three types of double integral defined by

$$I_1(a,b,c,d,x) = \int_0^x \int_0^\infty \frac{e^{-\theta - bt - dt\theta}}{a + c\theta} d\theta dt, \quad (5.55)$$

$$I_2(a,b,c,d,x) = \int_0^x \int_0^\infty \frac{e^{-\theta - bt - dt\theta}}{(a + c\theta)^2} d\theta dt, \quad (5.56)$$

$$I_3(a,b,c,d,x) = \int_0^x \int_0^\infty \frac{t\theta e^{-\theta - bt - dt\theta}}{a + c\theta} d\theta dt. \quad (5.57)$$

Each double integral can be evaluated using standard methods [52] in terms of a sum of exponential integral functions as shown in (5.58)-(5.60), where $E_1(x) = \int_x^\infty \frac{e^{-t}}{t} dt$.

$$I_1(a,b,c,d,x) = \frac{1}{bc - ad}\left[e^{\frac{a}{c}} E_1\left(\frac{a}{c}\right) - e^{\frac{b}{d}} E_1\left(\frac{b}{d}\right) + e^{\frac{b}{d}} E_1\left(\frac{b}{d} + bx\right) - e^{-bx} e^{\frac{(1+dx)a}{c}} E_1\left(\frac{(1+dx)\,a}{c}\right)\right]. \quad (5.58)$$

$$I_2(a,b,c,d,x) = \left[\frac{d}{(bc-ad)^2} + \frac{1+dx}{c\,(bc-ad)}\right] e^{-bx} e^{\frac{(1+dx)a}{c}} E_1\left(\frac{(1+dx)\,a}{c}\right) - \frac{cd + bc - ad}{c\,(bc-ad)^2} \times e^{\frac{a}{c}} E_1\left(\frac{a}{c}\right) + \frac{d}{(bc-ad)^2} e^{\frac{b}{d}}\left[E_1\left(\frac{b}{d}\right) - E_1\left(\frac{b}{d} + bx\right)\right] + \frac{1 - e^{-bx}}{a\,(bc-ad)}. \quad (5.59)$$

$$I_3(a,b,c,d,x) = \left[\frac{a}{(bc-ad)^2} + \frac{ax}{c\,(bc-ad)}\right] e^{-bx} e^{\frac{(1+dx)a}{c}} E_1\left(\frac{(1+dx)\,a}{c}\right) + \frac{ad^2 + abd - b^2 c}{d^2\,(bc-ad)^2} \times e^{\frac{b}{d}}\left[E_1\left(\frac{b}{d}\right) - E_1\left(\frac{b}{d} + bx\right)\right] - \frac{a}{(bc-ad)^2} e^{\frac{a}{c}} E_1\left(\frac{a}{c}\right) + \frac{1 - e^{-bx}}{d\,(bc-ad)}. \quad (5.60)$$

Hence, (5.54)-(5.60) give a closed form result for the cdf of the output SINR of an MMSE receiver in a two-user macrodiversity environment.

## 5.3 High SNR Approximations

In this section, we derive high SNR approximations for the SER of MMSE and ZF receivers. This is motivated by the complexity of the exact analysis and the importance of finding a simple, functional link between performance and the average link SNRs.

### 5.3.1 ZF Analysis

The conditional cf in (5.9) is a ratio of quadratic forms in $\boldsymbol{h}_2$. Hence, $\phi_{\tilde{Z}}(t) = E\{\phi_{\tilde{Z}}(t|\boldsymbol{h}_2)\}$ is the mean of a ratio of quadratic forms which can be approximated by the Laplace approximation [56] as

$$\phi_{\tilde{Z}}(t) \approx \frac{E\{\boldsymbol{h}_2^H \boldsymbol{h}_2\}}{|\boldsymbol{D}|\, E\left\{\boldsymbol{h}_2^H \boldsymbol{D}^{-1} \boldsymbol{h}_2\right\}} = \frac{\mathrm{Tr}\left(\boldsymbol{P}_2\right)}{|\boldsymbol{D}| \mathrm{Tr}\left(\boldsymbol{D}^{-1}\boldsymbol{P}_2\right)}. \tag{5.61}$$

Note that the second equality in (5.61) follows from the result, $E\{\boldsymbol{u}^H \boldsymbol{Q} \boldsymbol{u}\} = \mathrm{Tr}\left(\boldsymbol{Q}\right)$, where $\boldsymbol{u} \sim \mathcal{CN}\left(0, \boldsymbol{I}\right)$ and $\boldsymbol{Q}$ is a Hermitian matrix. Expanding the denominator of (5.61) gives

$$\phi_{\tilde{Z}}(t) \approx \frac{\mathrm{Tr}\left(\boldsymbol{P}_2\right)}{\sum_{i=1}^{n_R} P_{i2} \prod_{k \neq i}^{n_R} \left(1 - \frac{jt}{\sigma^2} P_{k1}\right)}, \tag{5.62}$$

which follows since $\boldsymbol{D}$ and $\boldsymbol{P}_2$ are diagonal and $|\boldsymbol{D}|$ is the product of the diagonal entries of $\boldsymbol{D}$. As the SNR grows, $\sigma^2 \to 0$ and keeping only the dominant power of $\sigma^2$ in (5.62) gives

$$\phi_{\tilde{Z}}(t) \approx \frac{\mathrm{Tr}\left(\boldsymbol{P}_2\right)}{|\boldsymbol{P}_1| \mathrm{Tr}\left(\boldsymbol{P}_1^{-1}\boldsymbol{P}_2\right)} \frac{\sigma^{2(n_R-1)}}{(-jt)^{n_R-1}}. \tag{5.63}$$

Defining $\vartheta\left(\boldsymbol{P}_1, \boldsymbol{P}_2\right) = \frac{\mathrm{Tr}\boldsymbol{P}_2}{|\boldsymbol{P}_1| \mathrm{Tr}\left(\boldsymbol{P}_1^{-1}\boldsymbol{P}_2\right)}$ gives a metric which encapsulates the effects of the power matrices $\boldsymbol{P}_1$ and $\boldsymbol{P}_2$. For many modulations, the SER can be evaluated as a single integral of the moment generating function of the SNR [9]. The mgf of the SNR is $\mathcal{M}_{\tilde{Z}}\left(s\right) = \phi_{\tilde{Z}}\left(-js\right)$. As an

example, for $M$-ary phase shift keying ($M$-PSK) the SER is [9, 8]

$$\tilde{P}_s = \frac{1}{\pi}\int_0^T \mathcal{M}_{\tilde{Z}}\left(-\frac{g}{\sin^2\theta}\right)d\theta, \tag{5.64}$$

where $g = \sin^2(\pi/M)$ and $T = \frac{(M-1)\pi}{M}$. Note that linear combinations of equations of the form given in (5.64) also give SERs for $M$-QAM in the usual way [9]. Substituting (5.63) in (5.64) gives the approximation

$$\tilde{P}_s^{\infty} \simeq \left(\tilde{G}_a\bar{\gamma}\right)^{-\tilde{G}_d}. \tag{5.65}$$

In (5.65), the average SNR is $\bar{\gamma} = \frac{1}{\sigma^2}$, and the diversity gain and array gain are given by

$$\tilde{G}_d = n_R - 1, \qquad \tilde{G}_a = \left(\vartheta(\boldsymbol{P}_1, \boldsymbol{P}_2)\,\tilde{\mathcal{I}}\right)^{-1/(n_R-1)}.$$

The constant integral, $\tilde{\mathcal{I}}$, is given by

$$\tilde{\mathcal{I}} = \frac{1}{\pi}\int_0^T \left(\frac{\sin^2\theta}{g}\right)^{n_R-1} d\theta. \tag{5.66}$$

Note that the simple representation in (5.65) shows the diversity order of $n_R - 1$ and the effect of the link powers on array gain controlled by the metric $\vartheta(\boldsymbol{P}_1, \boldsymbol{P}_2)$. The integral $\tilde{\mathcal{I}}$ can be solved in closed form and the final result is given in (5.67).

$$\tilde{\mathcal{I}} = \frac{1}{\pi g^{n_R-1}}\left\{\frac{T}{2^{2(n_R-1)}}\binom{2n_R-2}{n_R-1} + \frac{(-1)^{n_R-1}}{2^{2n_R-3}}\sum_{k=0}^{n_R-2}(-1)^k\binom{2n_R-2}{k}\frac{\sin\left(2\left(n_R-k-1\right)T\right)}{2\left(n_R-k-1\right)}\right\}, \tag{5.67}$$

### 5.3.2 MMSE Analysis

By using the Laplace approximation for the expectation of the conditional cf in (5.40), we obtain

$$\phi_Z(t) \approx \frac{\sigma^2 + \mathrm{Tr}\left(\boldsymbol{P}_2\right)}{|\boldsymbol{D}|\left(\sigma^2 + \mathrm{Tr}\left(\boldsymbol{D}^{-1}\boldsymbol{P}_2\right)\right)}. \tag{5.68}$$

As the SNR grows, $\sigma^2 \to 0$ and keeping only the dominant power of $\sigma^2$ in (5.68) gives

$$\phi_Z(t) \approx \frac{\mathrm{Tr}\left(\boldsymbol{P}_2\right)\left(\frac{1}{-jt\bar{\gamma}}\right)^{n_R-1}}{|\boldsymbol{P}_1|\left(\mathrm{Tr}\left(\boldsymbol{P}_1^{-1}\boldsymbol{P}_2\right)-jt\right)}. \tag{5.69}$$

As in the ZF analysis, the SER for $M$-PSK can be approximated by

$$P_s^{\infty} \simeq \left(G_a\bar{\gamma}\right)^{-G_d}, \tag{5.70}$$

where the diversity gain and array gain are given by

$$G_d = n_R - 1, \qquad G_a = \left(\vartheta\left(\boldsymbol{P}_1,\boldsymbol{P}_2\right)\mathcal{I}\left(\boldsymbol{P}_1,\boldsymbol{P}_2\right)\right)^{-1/(n_R-1)}. \tag{5.71}$$

In (5.71), $\mathcal{I}\left(\boldsymbol{P}_1,\boldsymbol{P}_2\right)$ is given by

$$\mathcal{I}\left(\boldsymbol{P}_1,\boldsymbol{P}_2\right) = \frac{1}{\pi}\int_0^T \frac{g^{-(n_R-1)}\sin^{2n_R}\theta}{g_0+\sin^2\theta}d\theta, \tag{5.72}$$

where $g = g_0\mathrm{Tr}\left(\boldsymbol{P}_1^{-1}\boldsymbol{P}_2\right)$. The integral, $\mathcal{I}\left(\boldsymbol{P}_1,\boldsymbol{P}_2\right)$, can be solved in closed form by expanding the ratio of $\sin^2\theta$ terms in (5.72) as a polynomial and integrating term by term to get the final result in (5.73).

$$\begin{aligned}\mathcal{I}\left(\boldsymbol{P}_1,\boldsymbol{P}_2\right) = (-1)^{n_R}\frac{g_0^{n_R-1}}{\pi g^{n_R-1}}\Bigg\{&\sqrt{\frac{g_0}{1+g_0}}\tan^{-1}\left(\sqrt{\frac{1+g_0}{g_0}}\tan T\right) - \sum_{i=0}^{n_R-1}(-1)^i\frac{1}{g_0^i}\\ &\times\left[\frac{T}{2^{2i}}\binom{2i}{i} + \frac{(-1)^i}{2^{2i-1}}\sum_{k=0}^{i-1}(-1)^k\binom{2i}{k}\frac{\sin\left(2\left(i-k\right)T\right)}{2\left(i-k\right)}\right]\Bigg\}.\end{aligned} \tag{5.73}$$

We note that, as expected, the diversity order of $n_R - 1$ is observed in both receiver types and the difference only appears in the array gains.

The approximate, high SNR result for ZF in (5.65) is particularly useful since it is simpler than the MMSE version in (5.70), and at high SNR the performance of the two schemes is similar anyway. Hence, (5.65) acts as a useful approximation for both ZF and MMSE and provides a remarkably compact relationship between SER and the link powers, via the single function, $\vartheta\left(\boldsymbol{P}_1,\boldsymbol{P}_2\right)$.

## 5.4 Exact High SNR Analysis

In this section, we derive exact high SNR results for the SER of MMSE and ZF receivers. The work in this section does not employ the Laplace type approximation used in (5.61) and (5.68) and hence produces exact asymptotics at the expense of increased complexity. The mathematical details are given in brief to avoid unnecessary detail.

### 5.4.1 ZF Analysis

The conditional cf in (5.9) is a ratio of quadratic forms in $\boldsymbol{h}_2$. As the SNR grows, $\sigma^2 \to 0$ and keeping only the dominant power of $\sigma^2$ in (5.9) gives

$$\phi_{\tilde{Z}}(t|\boldsymbol{h}_2) \approx \frac{\boldsymbol{h}_2^H \boldsymbol{h}_2}{|\boldsymbol{P}_1| \left(\boldsymbol{h}_2^H \boldsymbol{P}_1^{-1} \boldsymbol{h}_2\right)} \left(\frac{\sigma^2}{-jt}\right)^{n_R-1}. \tag{5.74}$$

Hence, the unconditional cf, when $\sigma^2 \to 0$, becomes

$$\phi_{\tilde{Z}}(t) = \tilde{K}_0 \left(\frac{\sigma^2}{-jt}\right)^{n_R-1} + o\left(\sigma^{2(n_R-1)}\right), \tag{5.75}$$

where $o(.)$ is the standard "little-o" notation and represents the fact that only the dominant power of $\sigma^2$ is used in the approximation and

$$\tilde{K}_0 = \frac{1}{|\boldsymbol{P}_1|} E\left\{\frac{\boldsymbol{h}_2^H \boldsymbol{h}_2}{\boldsymbol{h}_2^H \boldsymbol{P}_1^{-1} \boldsymbol{h}_2}\right\}. \tag{5.76}$$

Following the same mgf based procedure to obtain the SER as in Sec. 5.3, we arrive at the following expression

$$\tilde{P}_s^{\infty} = \left(\tilde{G}_{ea}\bar{\gamma}\right)^{-\tilde{G}_{ed}} + o\left(\bar{\gamma}^{-\tilde{G}_{ed}}\right), \tag{5.77}$$

where, the diversity and array gains are given by

$$\tilde{G}_{ed} = n_R - 1, \qquad \tilde{G}_{ea} = \left(\tilde{K}_0 \tilde{\mathcal{I}}\right)^{-1/(n_R-1)}.$$

The constant, $\tilde{K}_0$, can be found using Lemma 1 to obtain the final expression as in (5.78)

$$\tilde{K}_0 = \sum_{i=1}^{n_R} \Upsilon_i P_{i2} + \sum_{1 \le u \ne v \le n_R}^{n_R} (\Upsilon_u P_{v1} + \Upsilon_v P_{u1}) \left( \frac{\ln\left(\frac{P_{u1}}{P_{u2}}\right) - \ln\left(\frac{P_{v1}}{P_{v2}}\right)}{\frac{P_{u1}}{P_{u2}} - \frac{P_{v1}}{P_{v2}}} \right) \tag{5.78}$$

where

$$\Upsilon_i = \frac{P_{i2}^{n_R-2}}{\prod_{k \ne i}^{n_R} P_{k1} P_{i2} - P_{i1} P_{k2}}. \tag{5.79}$$

### 5.4.2 MMSE Analysis

Consider the expectation of the conditional cf expression in (5.40). As the SNR grows, $\sigma^2 \to 0$ and keeping only the dominant power of $\sigma^2$ in (5.40) gives

$$\phi_Z(t) = K_0(jt) \left( \frac{\sigma^2}{-jt} \right)^{n_R-1} + o\left(\sigma^{2(n_R-1)}\right), \tag{5.80}$$

where

$$K_0(s) = \frac{1}{|\boldsymbol{P}_1|} E\left\{ \frac{\boldsymbol{h}_2^H \boldsymbol{h}_2}{\boldsymbol{h}_2^H \boldsymbol{P}_1^{-1} \boldsymbol{h}_2 - s} \right\}. \tag{5.81}$$

Following the mgf based procedure in Sec. 5.3, the SER at high SNR becomes

$$P_s^{\infty} = \frac{1}{\pi} \int_0^T \left( \frac{\sigma^2 \sin^2\theta}{g} \right)^{n_R-1} K_0\left( -\frac{g}{\sin^2\theta} \right) d\theta. \tag{5.82}$$

From (5.82), the approximate SER can be written in terms of the diversity gain and array gain as

$$P_s^{\infty} = (G_{ea}\bar{\gamma})^{-G_{ed}} + o\left(\bar{\gamma}^{-G_{ed}}\right), \tag{5.83}$$

where

$$G_{ed} = n_R - 1, \qquad G_{ea} = \left(\mathcal{I}_e(\boldsymbol{P}_1, \boldsymbol{P}_2)\right)^{-1/(n_R-1)},$$

$$\mathcal{I}_e(\boldsymbol{P}_1, \boldsymbol{P}_2) = \frac{1}{\pi} \int_0^T \left( \frac{\sin^2\theta}{g} \right)^{n_R-1} K_0\left( -\frac{g}{\sin^2\theta} \right) d\theta. \tag{5.84}$$

Using Lemma 1, $K_0(-s)$ can be given by

$$K_0(-s) = -\int_0^\infty \frac{\partial}{\partial\theta_1}\left[\frac{e^{-s\theta_2}}{|\boldsymbol{P}_1+\theta_1\boldsymbol{P}_2\boldsymbol{P}_1+\theta_2\boldsymbol{P}_2|}\right]_{\theta_1=0} d\theta_2, \tag{5.85}$$

which can be simplified to obtain

$$K_0(-s) = \int_0^\infty e^{-s\theta_2}\left(\sum_{i=1}^{n_R}\frac{P_{i2}\Upsilon_i}{P_{i2}\theta_2+P_{i1}}\right)\left(\sum_{i=1}^{n_R}\frac{P_{i1}P_{i2}}{P_{i2}\theta_2+P_{i1}}\right)d\theta_2, \tag{5.86}$$

where $\Upsilon_i$ is given in (5.79). Equation (5.86) can be solved in closed form to give

$$K_0(-s) = \sum_{i=1}^{n_R}\left\{e^{s\frac{P_{i1}}{P_{i2}}}E_1\left(s\frac{P_{i1}}{P_{i2}}\right)(\Phi_i - s\Upsilon_i P_{i1}) + \Upsilon_i P_{i2}\right\}, \tag{5.87}$$

where

$$\Phi_i = \sum_{k\neq i}^{n_R}\frac{P_{i2}\Upsilon_i P_{k1}P_{k2} + P_{k2}\Upsilon_k P_{i1}P_{i2}}{P_{k1}P_{i2}-P_{k2}P_{i1}}. \tag{5.88}$$

Substituting $s = g/\sin^2\theta$ in (5.87) and then substituting $K_0\left(-\frac{g}{\sin^2\theta}\right)$ in (5.84) and integrating over $\theta$ gives the result in (5.89)

$$\mathcal{I}_e(\boldsymbol{P}_1,\boldsymbol{P}_2) = \tilde{\mathcal{I}}\left(\sum_{i=1}^{n_R}\Upsilon_i P_{i2}\right) + \frac{1}{\pi g^{n_R-1}}\sum_{i=1}^{n_R}\left\{\Phi_i H\left(n_R-1, g\frac{P_{i1}}{P_{i2}}\right) - \Upsilon_i P_{i1} H\left(n_R-2, g\frac{P_{i1}}{P_{i2}}\right)\right\} \tag{5.89}$$

where

$$H(m,a) = \int_0^T e^{\frac{a}{\sin^2\theta}}E_1\left(\frac{a}{\sin^2\theta}\right)\sin^{2m}\theta\, d\theta. \tag{5.90}$$

Clearly the exact asymptotics, especially for the MMSE case, are substantially more complex than the approximations in Sec. 5.3. Also, the relationship between SER and the link powers is far more involved.

## 5.5 Numerical Results

In this section, we verify the analysis by Monte Carlo simulations using the network MIMO scenario in Fig. 5.1 [74]. We also consider some special cases of $\boldsymbol{P}_1$ and $\boldsymbol{P}_2$ in order to investigate the effect of the macrodiversity powers on performance. For the two-user system in Fig. 5.1, we consider the desired user to be user 1 and parameterize the system by three parameters. The average received signal to noise ratio is defined by $\rho = \mathrm{Tr}(\boldsymbol{P}_1)/n_R\sigma^2$. The total signal to interference ratio is defined by $\varsigma = \mathrm{Tr}(\boldsymbol{P}_1)/\mathrm{Tr}(\boldsymbol{P}_2)$. The spread of the signal power across the three antennas is assumed to follow an exponential profile, as in [57], so that a range of possibilities can be covered with only one parameter. The exponential profile is defined by

$$P_{ik} = K_k(\alpha)\,\alpha^{i-1}, \tag{5.91}$$

for receive antenna i, source k where

$$K_k(\alpha) = \mathrm{Tr}(\boldsymbol{P}_k)/\left(1+\alpha+\alpha^2\right), \quad k = 1, 2, \tag{5.92}$$

and $\alpha > 0$ is the parameter controlling the uniformity of the powers across the antennas. Note that as $\alpha \to 0$ the received power is dominant at the first antenna, as $\alpha$ becomes large ($\alpha \gg 1$) the third antenna is dominant and as $\alpha \to 1$ there is an even spread, as in the standard microdiversity scenario. Although we consider microdiversity (S4 and S9), this is in the context of exploring the effect of different $\boldsymbol{P}$ matrix structures. Physically, it is not sensible to directly compare microdiversity with macrodiversity as they involve different system structures. In microdiversity, there may be multiple users communicating with a single array at a single BS. In macrodiversity, the users may be communicating with distributed antennas located at different BS sites which are back-hauled together to enable joint transmission/reception. In Figs. 5.2-5.3 we show cdf results for the ten scenarios given in Table 5.1. In Fig. 5.2, we see that S1 has the worst cdf since the sharply decaying power profile is identical for both desired and interfering source. Hence, there is reduced diversity, as most of the signal strength is seen at one antenna, and there is strong interference at each antenna. Scenario S3 is best at high SINR since in this interference limited

Table 5.1: Parameters for Figures 5.2 and 5.3

| | Decay Parameter | | |
|---|---|---|---|
| Sc. No. | Desired | Interfering | $\varsigma$ |
| S1 | $\alpha = 0.2$ | $\alpha = 0.2$ | 1 |
| S2 | $\alpha = 0.2$ | $\alpha = 1$ | 1 |
| S3 | $\alpha = 0.2$ | $\alpha = 5$ | 1 |
| S4 | $\alpha = 1$ | $\alpha = 1$ | 1 |
| S5 | $\alpha = 1$ | $\alpha = 0.2$ | 1 |
| S6 | $\alpha = 0.2$ | $\alpha = 0.2$ | 20 |
| S7 | $\alpha = 0.2$ | $\alpha = 1$ | 20 |
| S8 | $\alpha = 0.2$ | $\alpha = 5$ | 20 |
| S9 | $\alpha = 1$ | $\alpha = 1$ | 20 |
| S10 | $\alpha = 1$ | $\alpha = 0.2$ | 20 |

situation ($\varsigma = 1$) it is best to have at least one antenna where there is minimal interference. This occurs with S3 as the power profiles are opposing and the strongest desired signal aligns with the weakest interferer. At low SINR, scenarios S4 and S5 are slightly better than S3 as they have full diversity (equal power at each antenna) which is beneficial in this SINR region. In Fig. 5.3, similar results are observed with diversity being important at lower SINR (where S9 and S10 are the best) and interference reduction being important at high SINR (where S8 is best). In Fig. 5.4, we consider the effect of $\varsigma$ on two different macrodiversity scenarios in Table 5.1. In particular, we have shown results for S1 and S6 and S3 and S8. As expected, S1 and S3 have lower SINRs than S6 and S9 due to increased interference. However, S1 is far more sensitive to $\varsigma$ than S3. This is because S3 has opposing power profiles for the desired and interfering users so that the two sources are more orthogonal and interference plays a smaller part in performance.

Next, we consider the high SNR results in Secs. 5.3 and 5.4. In Fig. 5.5, the MMSE/ZF receivers are considered for four drops (D1, D2, D3 and D4) of two users in the shaded coverage area of Fig. 5.1. Each user is dropped at a different random location (uniformly generated over the coverage area) and random lognormal shadow fading and path loss is considered where $\sigma_{SF} = 8$dB (standard deviation of shadow fading) and $\gamma = 3.5$ (path loss exponent). Hence, each user has a different distance and shadow fade to each BS and each drop results in a new $\boldsymbol{P}$ matrix. The transmit power of the sources is scaled so that all locations in the coverage area have a maximum received SNR greater than 3dB, at least 95% of the time. The maximum SNR is taken over the 3

BSs. For all four drops, the high SNR approximations from Sec. 5.3 are shown to be very accurate for SERs below $10^{-2}$, although for drop D2 the results are less tight. Note that drop D2 has the greatest difference between the MMSE and ZF results. In general, the gap between MMSE and ZF results [83, 86] can be assessed by a comparison of (5.66) with (5.72). Here, it can be seen that the approximate asymptotics are the same for ZF and MMSE when $g_0 = 0$. Hence, scenarios where $g_0$ is large, i.e., $\mathrm{Tr}\left(\boldsymbol{P}_1^{-1}\boldsymbol{P}_2\right) \approx 0$, will create substantial differences between the two receivers. In Fig. 5.5, drop D2 had the smallest value of $\mathrm{Tr}\left(\boldsymbol{P}_1^{-1}\boldsymbol{P}_2\right)$ and hence showed the greatest difference. Note that for $\mathrm{Tr}\left(\boldsymbol{P}_1^{-1}\boldsymbol{P}_2\right)$ to be small, $P_{i1} \gg P_{i2}$ is required for $i = 1, 2, \ldots, n_R$. Hence, the power profiles for users 1 and 2 must be "parallel" in some sense, with any large value of $P_{i2}$ aligning with an even larger value of $P_{i1}$. In these "parallel" scenarios, MMSE and ZF results can exhibit greater differences.

This methodology is used again in Fig. 5.6 for three drops and ZF results are shown. Again, the asymptotic results show good agreement at SERs below $10^{-2}$. Furthermore, the difference between the approximations in Sec. 5.3 and the exact asymptotics in Sec. 5.4 is shown to be minor. Hence the simple SER forms in (5.65) and (5.70) are particularly useful. Note that the power matrices, $\boldsymbol{P}_1$ and $\boldsymbol{P}_2$, are completely general, with the sole constraint being $P_{ik} \geq 0$, $\forall i, k$. As a result, it is likely that some combinations of powers can be found that will cause the approximate SERs to lose accuracy. However, in all the scenarios considered and all random drops simulated (see also [74]) the approximations have shown similar accuracy to the results in Figs. 5.5 and 5.6.

In multiuser systems it is well-known that two users may be successfully detected if their channels are approximately orthogonal. In the context of a dual user system, where only the channel powers are considered, the analog would be that $\mathrm{Tr}\left(\boldsymbol{P}_1\boldsymbol{P}_2\right)$ is small. To investigate this relationship, we generate a large number of random power matrices with a fixed total power. For user 1, the powers are generated by (5.91) with $\alpha = 0.2$. For user 2, the powers are independent uniform random variables which are scaled so that $\varsigma = 1$. For each pair, $(\boldsymbol{P}_1, \boldsymbol{P}_2)$, we compute $\mathrm{Tr}\left(\boldsymbol{P}_1\boldsymbol{P}_2\right)$ and the approximate SER of user 1 using using (5.70). The results are plotted in Fig. 5.7. As expected, SER increases with $\mathrm{Tr}\left(\boldsymbol{P}_1\boldsymbol{P}_2\right)$, although there is wide variation in the band of SER results. In comparison, the new metric, $\vartheta\left(\boldsymbol{P}_1, \boldsymbol{P}_2\right)$, has a one-to-one relationship with the approximate SER

and carries far more information than ad-hoc measures such as $\mathrm{Tr}\,(\boldsymbol{P}_1\boldsymbol{P}_2)$.

## 5.6 Summary

In this chapter, we derived the exact cdf of the output SINR/SNR for MMSE and ZF receivers in the presence of a single interfering user with an arbitrary number of receive antennas. To the best of our knowledge, this represents the first exact analysis of linear combining in macrodiversity systems. Although not shown for reasons of space, the slightly simpler problem of obtaining the associated pdf can also be handled since the pdf expression in (5.12) is inherently computed en-route to the cdf in (5.13). Numerical examples demonstrate the validity of the analysis across arbitrary drops and channels. This suggests that the analysis is also numerically robust. A high SNR analysis reveals simple SER results for both MMSE and ZF which provide insights into both diversity and array gain. It also provides a functional link between the performance of the macrodiversity system and the link SNRs.

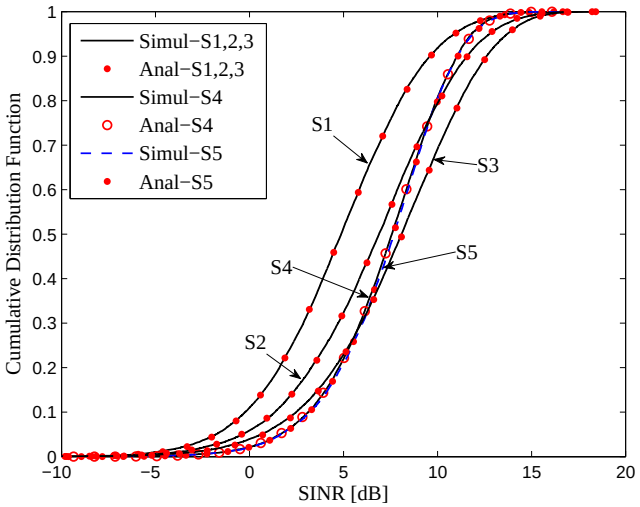


Figure 5.2: Analytical and simulated cdfs for the output SINR of an MMSE receiver for scenarios S1-S5 listed in Table 1 at $\rho = 5$ dB with $\varsigma = 1$.

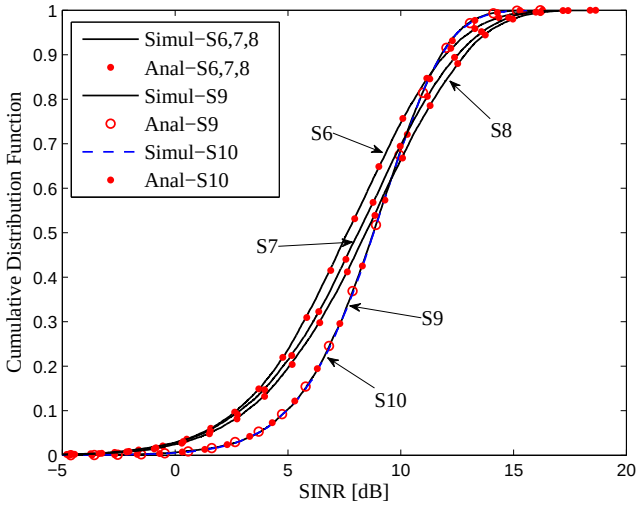


Figure 5.3: Analytical and simulated cdfs for the output SINR of an MMSE receiver for scenarios S6-S10 listed in Table 1 at $\rho = 5$ dB with $\varsigma = 20$.

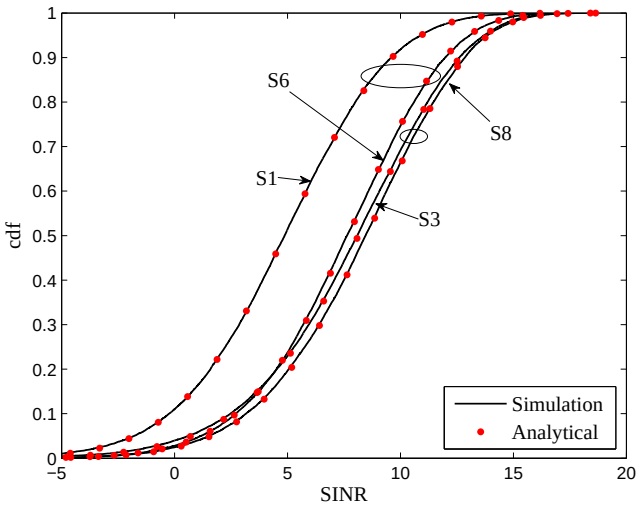


Figure 5.4: Analytical and simulated cdfs for the output SINR of an MMSE receiver for scenarios (S1,S6) and (S3,S8) in Table 1.

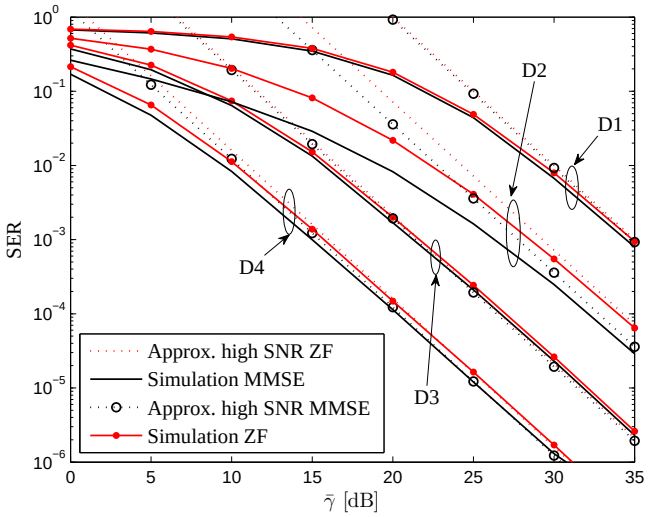


Figure 5.5: SER and high SNR approximations for MMSE/ZF receivers using QPSK modulation in flat Rayleigh fading for four arbitrary drops.

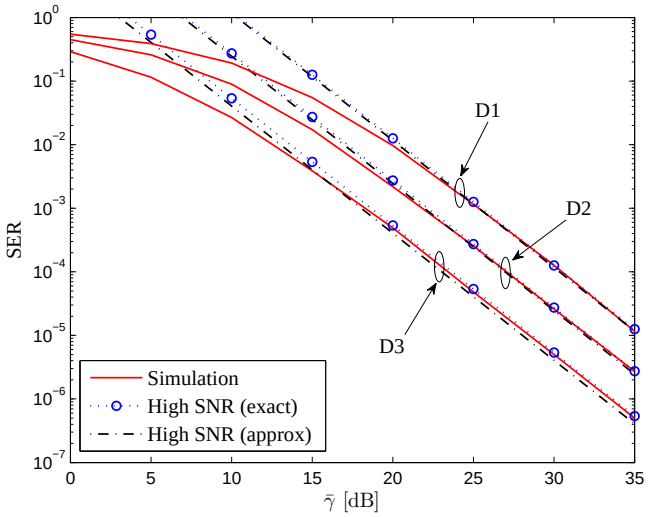


Figure 5.6: SER of a ZF receiver using QPSK modulation in Rayleigh flat fading for three arbitrary drops.

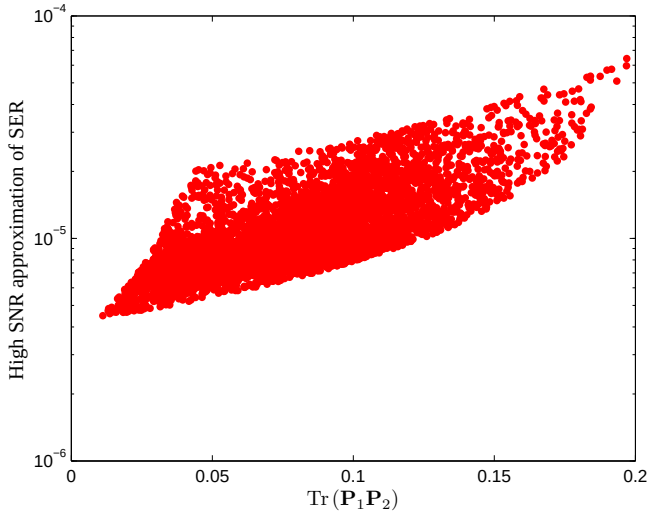


Figure 5.7: SER of a MMSE receiver for QPSK modulation in flat Rayleigh fading at $\bar{\gamma} = 35$ dB.

# Chapter 6

# Multiuser Macrodiversity MIMO Systems with Linear Receivers

In the previous chapter, we analyzed the SINR/SNR distribution of MMSE/ZF receivers in dual a source scenario with arbitrary numbers of receive antennas in a flat Rayleigh fading environment. We derived exact pdf results for both type of receivers. In this chapter, we extend the results derived in Chapter 5 to arbitrary numbers of users. We are able to derive the approximate probability distribution function and cumulative distribution function of the output SINR/SNR of MMSE/ZF receivers. We also derive high SNR SER results for MMSE/ZF receivers obtaining the diversity order and array gain of the users in a remarkably compact form. These expressions are useful for gaining further insights into the effects of channel distribution information on the performance of macrodiversity MIMO systems.

## 6.1 System Model

The multiuser MIMO system investigated in this chapter consists of $N$ distributed single antenna users communicating with $n_R$ distributed receive antennas in an independent flat Rayleigh fading environment. The $\mathcal{C}^{n_R \times 1}$ receive vector is given by

$$\boldsymbol{r} \;=\; \boldsymbol{H}\boldsymbol{s}+\boldsymbol{n}, \tag{6.1}$$

where the $\mathcal{C}^{N\times 1}$ data vector, $\boldsymbol{s}=(s_1,s_2,\ldots,s_N)^T$, contains the transmitted symbols from the $N$ users and it is normalized, so that $E\left\{|s_i|^2\right\}=1$ for $i=1,2,\ldots,N$. $\boldsymbol{n}$ is the $\mathcal{C}^{n_R\times 1}$ additive-white-Gaussian-noise vector, $\boldsymbol{n}\sim\mathcal{CN}\left(\boldsymbol{0},\sigma^2\boldsymbol{I}\right)$, which has independent entries with $E\left\{|n_i|^2\right\}=\sigma^2$, for $i=1,2,\ldots,n_R$. The channel matrix contains independent elements, $H_{ik}\sim\mathcal{CN}\left(0,P_{ik}\right)$, where $E\left\{|\boldsymbol{H}_{ik}|^2\right\}=P_{ik}$. A typical macrodiversity MU-MIMO multiple access channel is shown in Fig. 6.1, where it is clear that the geographical spread of users and antennas creates a channel matrix $\boldsymbol{H}$, which has independent entries with different $P_{ik}$ values. We define the $\mathcal{C}^{n_R\times N}$ matrix, $\boldsymbol{P}=\{P_{ik}\}$, which holds the average link powers due to shadowing, path fading, etc.

By assuming that perfect channel state information is available at the receiver side, we consider a

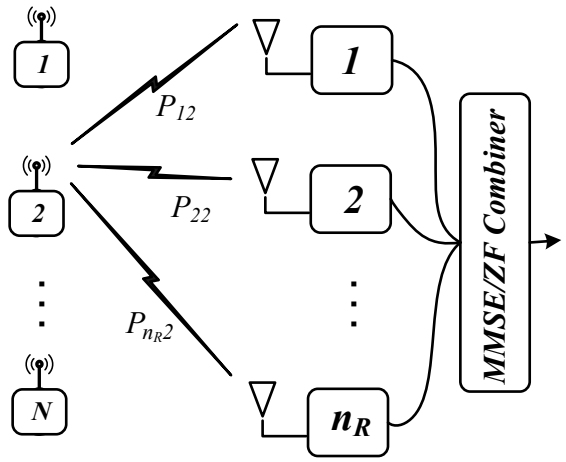


Figure 6.1: System diagram. To reduce clutter, only paths from a single source are shown.

system where channel adaptive linear combining is performed at the receiver to suppress multiple access interference [11]. Therefore, the $\mathcal{C}^{N\times 1}$ combiner output vector is $\tilde{\boldsymbol{r}}=\boldsymbol{V}^H\boldsymbol{r}$, where $\boldsymbol{V}$ is an $\mathcal{C}^{n_R\times N}$ weight matrix. In this work, we consider two well-known linear combining schemes: MMSE and ZF. The structure of $\boldsymbol{V}$ and the resulting output SINR/SNR for MMSE/ZF schemes are well-known and are given below. Without loss of generality, we assume that the index of the desired user is $i=1$. The combining vector and output SINR of the MMSE receiver for user 1 are given by [57, 87] as

$$\boldsymbol{v}_1=\boldsymbol{R}^{-1}\boldsymbol{h}_1, \tag{6.2}$$

$$\text{SINR} = \boldsymbol{h}_1^H \boldsymbol{R}^{-1} \boldsymbol{h}_1, \tag{6.3}$$

where

$$\boldsymbol{R} = \sum_{k \neq i}^{N} \boldsymbol{h}_k \boldsymbol{h}_k^H + \sigma^2 \boldsymbol{I}, \tag{6.4}$$

where $\boldsymbol{H} = (\boldsymbol{h}_1, \boldsymbol{h}_2, \ldots, \boldsymbol{h}_N)$, Defining $\boldsymbol{v}_2, \ldots, \boldsymbol{v}_N$ similarly gives $\boldsymbol{V} = (\boldsymbol{v}_1, \boldsymbol{v}_2, \ldots, \boldsymbol{v}_N)$. The vectors, $\boldsymbol{h}_k$, clearly play an important role in MMSE combining and it is useful to define the covariance matrix of $\boldsymbol{h}_k$ by $\boldsymbol{P}_k = E\left\{\boldsymbol{h}_k \boldsymbol{h}_k^H\right\} = \text{diag}(P_{1k}, P_{2k}, \ldots, P_{n_R k})$. From [33, 84], the combining matrix, $\boldsymbol{V}$, and output SNR of the ZF receiver for $n_R \geq N$ are given by

$$\boldsymbol{V} = \boldsymbol{H}\left(\boldsymbol{H}^H \boldsymbol{H}\right)^{-1} \tag{6.5}$$

and

$$\text{SNR} = \frac{1}{\sigma^2 \left[\left(\boldsymbol{H}^H \boldsymbol{H}\right)^{-1}\right]_{11}}. \tag{6.6}$$

where $[\boldsymbol{B}]_{11}$ indicates the $(1,1)^{th}$ element of matrix $\boldsymbol{B}$.

## 6.2 ZF Analysis

In this section, we derive an approximate cdf for the output SNR of a ZF receiver and a high SNR approximation to SER. The pdfs for the columns of the channel matrix $\boldsymbol{H}$ as given in (5.7) are used throughout the analysis.

### 6.2.1 CDF Approximations

The output SNR of a ZF receiver in (6.6) can be written as

$$\tilde{Z} = \frac{1}{\sigma^2} \boldsymbol{h}_1^H \left(\boldsymbol{I} - \boldsymbol{H}_1 \left(\boldsymbol{H}_1^H \boldsymbol{H}_1\right)^{-1} \boldsymbol{H}_1^H\right) \boldsymbol{h}_1 \tag{6.7}$$

$$= \frac{1}{\sigma^2} \boldsymbol{h}_1^H \boldsymbol{M} \boldsymbol{h}_1, \tag{6.8}$$

where $\boldsymbol{M} = \boldsymbol{I} - \boldsymbol{H}_1 \left(\boldsymbol{H}_1^H \boldsymbol{H}_1\right)^{-1} \boldsymbol{H}_1^H$ and $\bar{\boldsymbol{H}}_1$ is $\boldsymbol{H}$ with column $\boldsymbol{h}_1$ removed. Following the analysis in [74], the characteristic function of $\tilde{Z}$ is given by

$$\phi_{\tilde{Z}}(t) \quad = \quad E\left\{e^{jt\tilde{Z}}\right\} = E\left\{e^{\frac{jt}{\sigma^2}\boldsymbol{h}_1^H \boldsymbol{M} \boldsymbol{h}_1}\right\}. \tag{6.9}$$

Conditioning on $\boldsymbol{H}_1$, the expectation over $\boldsymbol{h}_1$ in (6.9) can be solved as in [74] to obtain

$$\phi_{\tilde{Z}}(t|\boldsymbol{H}_1) = \frac{1}{\left|\boldsymbol{I} - jt\frac{1}{\sigma^2}\boldsymbol{M}\boldsymbol{P}_1\right|}. \tag{6.10}$$

Substituting for $\boldsymbol{M}$ in (6.10) gives

$$\phi_{\tilde{Z}}(t|\boldsymbol{H}_1) = \frac{1}{\left|\boldsymbol{I} - \frac{jt}{\sigma^2}\boldsymbol{P}_1 + \frac{jt}{\sigma^2}\boldsymbol{H}_1 \left(\boldsymbol{H}_1^H \boldsymbol{H}_1\right)^{-1} \boldsymbol{H}_1^H \boldsymbol{P}_1\right|} \tag{6.11}$$

$$= \frac{1}{|\boldsymbol{D}| \left|\boldsymbol{I} + \frac{jt}{\sigma^2}\boldsymbol{H}_1 \left(\boldsymbol{H}_1^H \boldsymbol{H}_1\right)^{-1} \boldsymbol{H}_1^H \boldsymbol{P}_1 \boldsymbol{D}^{-1}\right|} \tag{6.12}$$

$$= \frac{\left|\boldsymbol{H}_1^H \boldsymbol{H}_1\right|}{|\boldsymbol{D}| \left|\boldsymbol{H}_1^H \boldsymbol{H}_1 + \frac{jt}{\sigma^2}\boldsymbol{H}_1^H \boldsymbol{P}_1 \boldsymbol{D}^{-1} \boldsymbol{H}_1\right|}, \tag{6.13}$$

where $\boldsymbol{D} = \boldsymbol{I} - \frac{1}{\sigma^2} jt\boldsymbol{P}_1$. Simplifying (6.13) gives

$$\phi_{\tilde{Z}}(t|\boldsymbol{H}_1) = \frac{\left|\boldsymbol{H}_1^H \boldsymbol{H}_1\right|}{|\boldsymbol{D}| \left|\boldsymbol{H}_1^H \boldsymbol{D}^{-1} \boldsymbol{H}_1\right|}. \tag{6.14}$$

The full cf can then be obtained by averaging the conditional cf in (6.14), to give

$$\phi_{\tilde{Z}}(t) = \frac{1}{|\boldsymbol{D}|} E\left\{ \frac{\left|\boldsymbol{H}_1^H \boldsymbol{H}_1\right|}{\left|\boldsymbol{H}_1^H \boldsymbol{D}^{-1} \boldsymbol{H}_1\right|} \right\}, \tag{6.15}$$

where expectation is over $\boldsymbol{H}_1$. An exact analysis of (6.15) is extremely cumbersome. However, for the dual source scenario where $N = 2$, (6.15) can be solved in closed form [88]. Even for $N = 2$, the resulting exact expressions are complex. Hence, for arbitrary $N$ we use a Laplace type approximation as in [74] to approximate and simplify the cf. This approximation has some

motivation in the work of [56] and [89]. It can also be thought of as a first order delta expansion [71]. This approach gives

$$\phi_{\tilde{Z}}(t) \simeq \frac{1}{|\boldsymbol{D}|} \frac{E\left\{\left|\boldsymbol{H}_1^H \boldsymbol{H}_1\right|\right\}}{E\left\{\left|\boldsymbol{H}_1^H \boldsymbol{D}^{-1} \boldsymbol{H}_1\right|\right\}}. \tag{6.16}$$

Applying Lemma 4.1 to (6.16) gives

$$\phi_{\tilde{Z}}(t) \simeq \frac{\operatorname{Perm}(\boldsymbol{Q}_1)}{|\boldsymbol{D}| \operatorname{Perm}\left(\boldsymbol{D}^{-1}\boldsymbol{Q}_1\right)}, \tag{6.17}$$

where the $n_R \times (N-1)$ matrix $\boldsymbol{Q}_1$ is defined by $\boldsymbol{Q}_1 = E\{\boldsymbol{H}_1 \circ \boldsymbol{H}_1\}$. $\boldsymbol{Q}_1$ is $\boldsymbol{P}$ with column $\boldsymbol{p}_1$ removed and $\boldsymbol{p}_1 = (P_{11}, P_{21}, \ldots, P_{n_R 1})^T$. From Appendix D.1, the denominator in (6.17) can be expanded as

$$|\boldsymbol{D}| \operatorname{Perm}\left(\boldsymbol{D}^{-1}\boldsymbol{Q}_1\right) = \sum_{i=0}^{L} (-jt)^i \, \tilde{\varphi}_i, \tag{6.18}$$

where

$$\tilde{\varphi}_i = \sum_{\sigma} \operatorname{Tr}_i\left((\boldsymbol{P}_1)_{\bar{\sigma}_{L,n_R}}\right) \operatorname{perm}\left((\boldsymbol{Q}_1)^{\{N-1\}}_{\sigma_{N-1,n_R}}\right) \left(\sigma^2\right)^{-i}. \tag{6.19}$$

Since $\operatorname{perm}\left((\boldsymbol{Q}_1)^{\{N-1\}}_{\sigma_{N-1,n_R}}\right)$ is independent of $t$, it is clear from (6.19) that $|\boldsymbol{D}| \operatorname{Perm}\left(\boldsymbol{D}^{-1}\boldsymbol{Q}_1\right)$ is a polynomial in $t$ of degree $L$. Hence, (6.17) becomes

$$\phi_{\tilde{Z}}(t) \approx \frac{\operatorname{Perm}(\boldsymbol{Q}_1)}{\sum_{i=0}^{L} (-jt)^i \, \tilde{\varphi}_i} \tag{6.20}$$

$$= \frac{\operatorname{Perm}(\boldsymbol{Q}_1)}{\tilde{\varphi}_L \sum_{i=0}^{L} \left(\frac{\tilde{\varphi}_i}{\tilde{\varphi}_L}\right) (-jt)^i} \tag{6.21}$$

$$= \frac{\operatorname{Perm}(\boldsymbol{Q}_1)}{\tilde{\varphi}_L \prod_{i=1}^{L} (\tilde{\omega}_i - jt)} \tag{6.22}$$

$$= \frac{\operatorname{Perm}(\boldsymbol{Q}_1)}{\tilde{\varphi}_L} \sum_{i=1}^{L} \frac{\tilde{\eta}_i}{\tilde{\omega}_i - jt}, \tag{6.23}$$

where $\tilde{\omega}_i > 0$ for all $i$ from Descartes rule of signs for the polynomial in (6.21) and

$$\tilde{\eta}_i = \frac{1}{\prod_{k\neq i}^{n_R} (\tilde{\omega}_k - \tilde{\omega}_i)}. \tag{6.24}$$

It is clear from (6.17) that $\phi_{\tilde{Z}}(0) = 1$, since $\boldsymbol{D} = \boldsymbol{I}$ when $t = 0$. Therefore, the cf will produce a valid pdf after inversion [90]. From [10], the pdf and cdf of $\tilde{Z}$ are given by

$$f_{\tilde{Z}}(z) = \frac{1}{2\pi} \int_{-\infty}^{\infty} \phi_{\tilde{Z}}(t) e^{-jtz} dt, \tag{6.25}$$

$$F_{\tilde{Z}}(z) = \frac{1}{2\pi} \int_{0}^{z} \int_{-\infty}^{\infty} \phi_{\tilde{Z}}(t) e^{-jtx} dt dx. \tag{6.26}$$

Substituting (6.23) in (6.25) gives the approximate pdf

$$\hat{f}_{\tilde{Z}}(z) = \frac{\mathrm{Perm}\,(\boldsymbol{Q}_1)}{2\pi\tilde{\varphi}_L} \sum_{i=1}^{L} \tilde{\eta}_i \int_{-\infty}^{\infty} \frac{e^{-jtz}}{\tilde{\omega}_i - jt} dt. \tag{6.27}$$

Applying the integral identity in (A.19), we obtain the approximate pdf of $\tilde{Z}$ as

$$\hat{f}_{\tilde{Z}}(z) = \frac{\mathrm{Perm}\,(\boldsymbol{Q}_1)}{\tilde{\varphi}_L} \sum_{i=1}^{L} \tilde{\eta}_i e^{-\tilde{\omega}_i z}, \tag{6.28}$$

and the approximate cdf of $\tilde{Z}$ becomes

$$\hat{F}_{\tilde{Z}}(z) = \frac{\mathrm{Perm}\,(\boldsymbol{Q}_1)}{\tilde{\varphi}_L} \sum_{i=1}^{L} \frac{\tilde{\eta}_i}{\tilde{\omega}_i} \left(1 - e^{-\tilde{\omega}_i z}\right). \tag{6.29}$$

The final pdf approximation in (6.28) has a remarkably simple form as a generalized mixture of $L$ exponentials where $L = n_R - N + 1$.

### 6.2.2 High SNR Approximations

The cf in (6.15) is a ratio of determinants, where $\boldsymbol{D} = \boldsymbol{I} - \frac{1}{\sigma^2} jt\boldsymbol{P}_1$. As the SNR grows, $\sigma^2 \to 0$ and keeping only the dominant power of $\sigma^2$ in (6.15) gives

$$\phi_{\tilde{Z}}(t) = \tilde{K}_0 \left( \frac{\sigma^2}{-jt} \right)^{n_R - N + 1}, \tag{6.30}$$

where

$$\tilde{K}_0 = \frac{1}{|\boldsymbol{P}_1|} E \left\{ \frac{\left| \boldsymbol{H}_1^H \boldsymbol{H}_1 \right|}{\left| \boldsymbol{H}_1^H \boldsymbol{P}_1^{-1} \boldsymbol{H}_1 \right|} \right\}. \tag{6.31}$$

Following the mgf based approach in [9], the SER of a macrodiversity ZF receiver can be evaluated for $M$-PSK modulation as

$$\tilde{P}_s = \frac{1}{\pi} \int_0^T \mathcal{M}_{\tilde{Z}} \left( -\frac{g}{\sin^2 \theta} \right) d\theta. \tag{6.32}$$

where $\mathcal{M}_{\tilde{Z}}(s) = \phi_{\tilde{Z}}(-js)$, $g = \sin^2(\pi/M)$ and $T = \frac{(M-1)\pi}{M}$. Note that linear combinations of equations of the form given in (6.32) also give SERs for $M$-QAM in the usual way [9]. Substituting (6.30) in (6.32) gives

$$\tilde{P}_s^{\infty} = \left( \tilde{G}_a \bar{\gamma} \right)^{-\tilde{G}_d} + o\left( \bar{\gamma}^{-\tilde{G}_d} \right), \tag{6.33}$$

where $o(.)$ is the standard little-o notation and the average SNR is $\bar{\gamma} = \frac{1}{\sigma^2}$. The diversity gain and array gain in (6.33) are given by

$$\tilde{G}_d = n_R - N + 1, \qquad \tilde{G}_a = \left( \tilde{K}_0 \tilde{\mathcal{I}} \right)^{-1/(n_R - N + 1)},$$

where $\tilde{\mathcal{I}}$ is given by

$$\tilde{\mathcal{I}} = \frac{1}{\pi} \int_0^T \left( \frac{\sin^2 \theta}{g} \right)^{(n_R - N + 1)} d\theta. \tag{6.34}$$

The high SNR expression derived in (6.33) will be exact, if and only if $\tilde{K}_0$ is exact. An exact calculation of $\tilde{K}_0$ for the $N = 2$ case is presented in [88] and shown to have a complex expression. This work suggests that in the general case an exact calculation is likely to be either excessively complicated or intractable. Hence, in this work, we use a Laplace type approximation for $\tilde{K}_0$ in (6.31) to obtain a more compact and insightful expression. Hence, we use the following approximation

$$\tilde{K}_0 \simeq \frac{1}{|\boldsymbol{P}_1|} \frac{E\left\{\left|\boldsymbol{H}_1^H \boldsymbol{H}_1\right|\right\}}{E\left\{\left|\boldsymbol{H}_1^H \boldsymbol{P}_1^{-1} \boldsymbol{H}_1\right|\right\}}. \tag{6.35}$$

Using Corollaries 4.2 and 4.3, (6.35) is given by

$$\tilde{K}_0 \simeq \frac{\mathrm{Perm}\left(\boldsymbol{Q}_1\right)}{|\boldsymbol{P}_1| \,\mathrm{Perm}\left(\boldsymbol{P}_1^{-1}\boldsymbol{Q}_1\right)}. \tag{6.36}$$

Note that when $N = 2$, approximate $\tilde{K}_0$ has simpler expression [74], which gives

$$\tilde{K}_0 \simeq \frac{\mathrm{Tr}\left(\boldsymbol{P}_2\right)}{|\boldsymbol{P}_1| \,\mathrm{Tr}\left(\boldsymbol{P}_1^{-1}\boldsymbol{P}_2\right)}. \tag{6.37}$$

## 6.3 MMSE Analysis

### 6.3.1 CDF Approximations

In this section, we derive the approximate cdf of the output SINR of an MMSE receiver and a high SNR approximation to the SER. Let Z be the output SINR of an MMSE receiver given by (6.3). Following the same procedure as in the ZF analysis, the cf of Z is

$$\phi_Z(t) \;=\; E\left\{e^{jtZ}\right\} = E\left\{e^{jt\boldsymbol{h}_1^H \boldsymbol{R}^{-1} \boldsymbol{h}_1}\right\}. \tag{6.38}$$

Next, the cf conditioned on $\boldsymbol{H}_1$ becomes [74]

$$\phi_Z(t|\boldsymbol{H}_1) = \frac{1}{\left|\boldsymbol{I} - jt\boldsymbol{R}^{-1}\boldsymbol{P}_1\right|}. \tag{6.39}$$

Since $\boldsymbol{R} = \sigma^2\boldsymbol{I} + \boldsymbol{H}_1\boldsymbol{H}_1^H$, the conditional cf in (6.39) becomes

$$\phi_Z(t|\boldsymbol{H}_1) = \frac{1}{\left|\boldsymbol{I} - jt\left(\sigma^2\boldsymbol{I} + \boldsymbol{H}_1\boldsymbol{H}_1^H\right)^{-1}\boldsymbol{P}_1\right|} \tag{6.40}$$

$$= \frac{\left|\sigma^2\boldsymbol{I} + \boldsymbol{H}_1\boldsymbol{H}_1^H\right|}{\left|\sigma^2\boldsymbol{I} - jt\boldsymbol{P}_1 + \boldsymbol{H}_1\boldsymbol{H}_1^H\right|}. \tag{6.41}$$

Using the determinant identity in (A.2) as $\left|\boldsymbol{I} + \boldsymbol{X}\boldsymbol{X}^H\right| = \left|\boldsymbol{I} + \boldsymbol{X}^H\boldsymbol{X}\right|$, where the rank of the identity matrix is obvious from the context, in (6.41) along with some simple algebra, we get

$$\phi_Z(t|\boldsymbol{H}_1) = \frac{\left|\sigma^2\boldsymbol{I} + \boldsymbol{H}_1^H\boldsymbol{H}_1\right|}{|\boldsymbol{D}|\left|\sigma^2\boldsymbol{I} + \boldsymbol{H}_1^H\boldsymbol{D}^{-1}\boldsymbol{H}_1\right|}, \tag{6.42}$$

where $\boldsymbol{D} = \boldsymbol{I} - \frac{1}{\sigma^2}jt\boldsymbol{P}_1$. Note the similarity of (6.42) with [74, eq. 14]. Then, the full cf can be solved by averaging the conditional cf in (6.42) over $\boldsymbol{H}_1$. Hence,

$$\phi_Z(t) = \frac{1}{|\boldsymbol{D}|}E\left\{\frac{\left|\sigma^2\boldsymbol{I} + \boldsymbol{H}_1^H\boldsymbol{H}_1\right|}{\left|\sigma^2\boldsymbol{I} + \boldsymbol{H}_1^H\boldsymbol{D}^{-1}\boldsymbol{H}_1\right|}\right\}. \tag{6.43}$$

Using a similar approach as in the ZF analysis we approximate (6.43) to get

$$\phi_Z(t) \simeq \frac{1}{|\boldsymbol{D}|}\frac{E\left\{\left|\sigma^2\boldsymbol{I} + \boldsymbol{H}_1^H\boldsymbol{H}_1\right|\right\}}{E\left\{\left|\sigma^2\boldsymbol{I} + \boldsymbol{H}_1^H\boldsymbol{D}^{-1}\boldsymbol{H}_1\right|\right\}}. \tag{6.44}$$

From (D.7) in Appendix D.2 we obtain the expectation in the numerator of (6.44) as

$$E\left\{\left|\sigma^2\boldsymbol{I} + \boldsymbol{H}_1^H\boldsymbol{H}_1\right|\right\} = \sum_{k=0}^{N-1}\sum_{\sigma}\mathrm{Perm}\left((\boldsymbol{Q}_1)^{\sigma_{k,N-1}}\right)\left(\sigma^2\right)^{N-k-1}. \tag{6.45}$$

The equation (D.11) in Appendix D.2 gives the denominator of (6.44) as

$$|\boldsymbol{D}|\,E\left\{\left|\sigma^2\boldsymbol{I} + \boldsymbol{H}_1^H\boldsymbol{D}^{-1}\boldsymbol{H}_1\right|\right\} = \sum_{i=0}^{n_R}(-jt)^i\,\varphi_i, \tag{6.46}$$

where

$$\varphi_i = \sum_{k=0}^{N-1} \hat{\varphi}_{ik} \left(\sigma^2\right)^{N-i-k-1}. \tag{6.47}$$

Substituting (6.45) and (6.46) in (6.44) we get,

$$\phi_Z(t) \simeq \frac{\sum_{k=0}^{N-1}\sum_{\sigma} \mathrm{Perm}\left(\left(\boldsymbol{Q}_1\right)^{\sigma_{k,N-1}}\right)\left(\sigma^2\right)^{N-k-1}}{\sum_{i=0}^{n_R}(-jt)^i \varphi_i} \tag{6.48}$$

$$= \frac{\Theta\left(\boldsymbol{Q}_1\right)}{\varphi_{n_R}\sum_{i=0}^{n_R}\left(\frac{\varphi_i}{\varphi_{n_R}}\right)(-jt)^i} \tag{6.49}$$

$$= \frac{\Theta\left(\boldsymbol{Q}_1\right)}{\varphi_{n_R}\prod_{i=1}^{n_R}(\omega_i - jt)}, \tag{6.50}$$

where $\tilde{\omega}_i > 0$ for all $i$ from Descartes rule of signs and

$$\Theta\left(\boldsymbol{Q}_1\right) = \sum_{k=0}^{N-1}\sum_{\sigma} \mathrm{Perm}\left(\left(\boldsymbol{Q}_1\right)^{\sigma_{k,N-1}}\right)\left(\sigma^2\right)^{N-k-1}. \tag{6.51}$$

The final expression for $\phi_Z(t)$ then becomes

$$\phi_Z(t) \approx \frac{\Theta\left(\boldsymbol{Q}_1\right)}{\varphi_{n_R}} \sum_{i=1}^{n_R} \frac{\eta_i}{\omega_i - jt}, \tag{6.52}$$

where

$$\eta_i = \frac{1}{\prod_{k\neq i}^{n_R}(\omega_k - \omega_i)}. \tag{6.53}$$

As in the ZF analysis, the pdf and cdf of $Z$ are given by

$$f_Z(z) = \frac{1}{2\pi}\int_{-\infty}^{\infty} \phi_Z(t) e^{-jtz} dt, \tag{6.54}$$

$$F_Z(z) = \frac{1}{2\pi}\int_{0}^{z}\int_{-\infty}^{\infty} \phi_Z(t) e^{-jtx} dt dx. \tag{6.55}$$

Using the identity in (A.19) to solve (6.54) and (6.55) we get the approximate pdf of $Z$ as

$$\hat{f}_Z(z) = \frac{\Theta\left(\boldsymbol{Q}_1\right)}{\varphi_{n_R}} \sum_{i=1}^{n_R} \eta_i e^{-\omega_i z}, \tag{6.56}$$

and the cdf of $Z$ becomes

$$\hat{F}_Z(z) = \frac{\Theta\left(\boldsymbol{Q}_1\right)}{\varphi_{n_R}} \sum_{i=1}^{n_R} \frac{\eta_i}{\omega_i} \left(1 - e^{-\omega_i z}\right). \tag{6.57}$$

In contrast to (6.28), where the ZF SNR is a generalized mixture of $L$ exponentials, (6.56) can be identified as a generalized mixture of $n_R \geq L$ exponentials. Since the MMSE SINR has more mixing parameters ($n_R$ rather than $L$) it might be expected that these increased degrees of freedom will result in a better approximation. Alternatively, the more concise ZF result may provide a simpler expression for use in system design and understanding. These issues are considered in Sec. 6.5.

### 6.3.2 High SNR Approximations

The cf in (6.44) is a ratio of determinants. As the SNR grows, $\sigma^2 \to 0$ and keeping only the dominant power of $\sigma^2$ in (6.44) gives

$$\phi(t) = K_0\left(-jt\right) \left(\frac{\sigma^2}{-jt}\right)^{n_R - N + 1}, \tag{6.58}$$

where

$$K_0\left(s\right) = \frac{1}{|\boldsymbol{P}_1|} E\left\{ \frac{\left|\boldsymbol{H}_1^H \boldsymbol{H}_1\right|}{\left|\boldsymbol{H}_1^H \boldsymbol{P}_1^{-1} \boldsymbol{H}_1 + s\boldsymbol{I}\right|} \right\}. \tag{6.59}$$

Hence, from (6.32), the SER at high SNR becomes

$$P_s^{\infty} = \frac{1}{\pi} \int_0^T \left(\frac{\sigma^2 \sin^2\theta}{g}\right)^{n_R - N + 1} K_0\left(\frac{g}{\sin^2\theta}\right) d\theta. \tag{6.60}$$

As in the ZF analysis, an exact calculation of $K_0$ appears difficult and we use the Laplace-type approximation again to give

$$K_0(s) \simeq \frac{1}{|\boldsymbol{P}_1|} \frac{E\left\{\left|\boldsymbol{H}_1^H \boldsymbol{H}_1\right|\right\}}{E\left\{\left|s\boldsymbol{I} + \boldsymbol{H}_1^H \boldsymbol{P}_1^{-1} \boldsymbol{H}_1\right|\right\}}. \tag{6.61}$$

From Corollaries 4.2 and 4.3 and Appendix D.2, we have

$$K_0(s) \simeq \frac{\operatorname{Perm}(\boldsymbol{Q}_1)}{|\boldsymbol{P}_1| \left(\sum_{i=0}^{N-1} \zeta_i \, s^{N-i-1}\right)}, \tag{6.62}$$

$$= \frac{\operatorname{Perm}(\boldsymbol{Q}_1) \left(\prod_{i=1}^{N-1} \vartheta_i\right)}{|\boldsymbol{P}_1| \left(\prod_{i=1}^{N-1} \vartheta_i\right) \prod_{i=1}^{N-1} (\vartheta_i + s)}, \tag{6.63}$$

$$= \frac{\operatorname{Perm}(\boldsymbol{Q}_1)}{|\boldsymbol{P}_1| \, \zeta_{N-1}} \sum_{i=1}^{N-1} \frac{\chi_i}{\vartheta_i + s}, \tag{6.64}$$

where $\zeta_i = \sum_\sigma \operatorname{Perm}\left(\left(\boldsymbol{P}_1^{-1}\boldsymbol{Q}_1\right)^{\sigma_{i,N-1}}\right)$ and $-\vartheta_i$ are the roots of $\sum_{i=0}^{N-1} \zeta_i \, s^{N-i-1}$. Since $\zeta_{N-1} = \operatorname{Perm}\left(\boldsymbol{P}_1^{-1}\boldsymbol{Q}_1\right)$, $K_0(s)$ in (6.64) becomes

$$K_0(s) \simeq \frac{\operatorname{Perm}(\boldsymbol{Q}_1)}{|\boldsymbol{P}_1| \operatorname{Perm}\left(\boldsymbol{P}_1^{-1}\boldsymbol{Q}_1\right)} \sum_{i=1}^{N-1} \frac{\chi_i}{\vartheta_i + s}, \tag{6.65}$$

where

$$\chi_i = \frac{\zeta_{N-1}}{\prod_{k \neq i}^{N-1} (\vartheta_k - \vartheta_i)}. \tag{6.66}$$

From (6.60) and (6.65), we obtain

$$P_s^\infty = (G_a \bar{\gamma})^{-G_d} + o\left(\bar{\gamma}^{-G_d}\right), \tag{6.67}$$

where the diversity order and array gain, $G_d$ and $G_a$ respectively, are given by

$$G_d = n_R - N + 1, \tag{6.68}$$

and

$$G_a = \frac{\mathrm{Perm}\left(\boldsymbol{Q}_1\right)}{|\boldsymbol{P}_1|\,\mathrm{Perm}\left(\boldsymbol{P}_1^{-1}\boldsymbol{Q}_1\right)}\mathcal{I}\left(\boldsymbol{P}\right), \tag{6.69}$$

where

$$\mathcal{I}\left(\boldsymbol{P}\right)=\frac{1}{\pi g^L}\sum_{i=1}^{N-1}\frac{\chi_i}{\vartheta_i}\int_0^T\frac{\left(\sin^2\theta\right)^{L+1}}{\frac{g}{\vartheta_i}+\sin^2\theta}d\theta. \tag{6.70}$$

The integrals in (6.70) can be solved in closed form as in [88]. Hence, the final result becomes

$$\mathcal{I}\left(\boldsymbol{P}\right)=\frac{1}{g^L}\sum_{i=1}^{N-1}\frac{\chi_i}{\vartheta_i}J_{L+1}\left(T,\frac{g}{\vartheta_i}\right), \tag{6.71}$$

where

$$J_m\left(c,a\right)=\frac{1}{\pi}\int_0^c\frac{\sin^{2m}\theta}{a+\sin^2\theta}d\theta. \tag{6.72}$$

## 6.4 Special Cases

In this section we present the special case where $n_R = N$, i.e., the system schedules as many simultaneous users as the number of receive antennas. In this particular scenario, the ZF cdf analysis in Sec. 6.2.1 has an intriguing form. From (6.17), the cf of $\tilde{Z}$ becomes

$$\phi_{\tilde{Z}}(t) \simeq \frac{\mathrm{Perm}\left(\boldsymbol{Q}_1\right)}{|\boldsymbol{D}|\,\mathrm{Perm}\left(\boldsymbol{D}^{-1}\boldsymbol{Q}_1\right)}. \tag{6.73}$$

When $n_R = N$, the denominator of (6.73) simplifies to give,

$$|\boldsymbol{D}|\,\mathrm{Perm}\left(\boldsymbol{D}^{-1}\boldsymbol{Q}_1\right)=\sum_{i=1}^{n_R}\left(1-\frac{jt}{\sigma^2}P_{i1}\right)\mathrm{perm}\left(\boldsymbol{Q}_{i1}\right), \tag{6.74}$$

where $\boldsymbol{Q}_{i1}$ is $\boldsymbol{Q}_1$ with the i$^{\text{th}}$ row removed. Then, (6.73) simplifies to

$$\phi_{\tilde{Z}}(t) \simeq \frac{\text{Perm}\left(\boldsymbol{Q}_1\right)}{\sum_{i=1}^{n_R} \text{perm}\left(\boldsymbol{Q}_{i1}\right) - \frac{jt}{\sigma^2} \sum_{i=1}^{n_R} P_{i1} \text{perm}\left(\boldsymbol{Q}_{i1}\right)}, \tag{6.75}$$

$$= \frac{\text{Perm}\left(\boldsymbol{Q}_1\right)}{\text{Perm}\left(\boldsymbol{Q}_1\right) - \frac{jt}{\sigma^2} \text{perm}\left(\boldsymbol{P}\right)}. \tag{6.76}$$

Inverting the cf expression in (6.76) gives the approximate pdf of $\tilde{Z}$ as the simple exponential

$$\hat{f}_{\tilde{Z}}(z) = \sigma^2 \theta e^{-\sigma^2 \theta z}, \tag{6.77}$$

where $\theta = \text{Perm}\left(\boldsymbol{Q}_1\right) / \text{perm}\left(\boldsymbol{P}\right)$.

## 6.5 Simulations and Numerical Results

In this section, we simulate the macrodiversity system shown in Fig. 5.1, where three base stations collaborate via a central backhaul processing in the shaded three sector cluster. This simulation environment was also used in [74] and is sometimes referred to as an edge-excited cell. We consider the three BS scenario having either a single antenna or two antennas each to give $n_R = 3$ or $n_R = 6$ respectively. In the shaded coverage area of this edge-excited cell, we drop three or four users uniformly in space giving $N = 3$ or $N = 4$. For each user, lognormal shadow fading and path loss is considered, where the standard deviation of the shadowing is 8dB and the path loss exponent is $\gamma = 3.5$. The transmit power of the sources is scaled so that the best signal received at the three BS locations is greater than 3dB at least 95% of the time. Even though the analysis in this chapter is valid for any set of channel powers, the above methodology allows us to investigate the accuracy of the performance matrices for realistic sets of channel powers.

In Figs. 6.2, 6.3 and 6.4, the case of three single antenna users and three distributed BSs with a single receiver antenna is considered. Here, we investigate both the approximate SINR distributions and the approximate SER results for an MMSE receiver. In Fig. 6.2, the approximate cdfs of the output SINR are plotted alongside the simulated cdfs. Results are shown for four random drops and, the results are for a particular user (the first of the three). The agreement between the cdfs

is shown to be excellent. Note that this agreement is good across all drops, from D1 which has a very poor SINR performance to D4 with a much higher SINR performance. The use of physically motivated drops rather than ad-hoc scenarios is useful as it assesses the accuracy of the analysis in plausible channel conditions.

In Fig. 6.3, the approximate SER curve is plotted alongside the simulated values. Results are shown for three drops and QPSK modulation. The agreement between the SER results is shown to be excellent across all three drops at SERs below $10^{-2}$. Again, this agreement is observed over a wide range with D1 having much higher SERs than D3. In Fig. 6.3 and also in Figs. 6.5-6.6 the SER is plotted against the transmit SNR, $\bar{\gamma}$. This is chosen instead of the receive SNR to separate the curves so that the drops are visible and not all superimposed which tends to happen when SER is plotted against receive SNR.

In Fig. 6.4, the approximate cdfs of the SNR are plotted alongside the simulated cdfs for a ZF receiver. Results are shown for four random drops. This is the companion plot to Fig. 6.2 with the same system but a ZF receiver rather than an MMSE receiver. The accuracy of the results in Fig. 6.2 and Fig. 6.4 is interesting, especially when you observe that the Fig. 6.2 analysis uses (6.57), a simple mixture of 3 exponentials, and Fig. 6.4 uses (6.29) which is a single exponential in this case.

In Fig. 6.5 and 6.6, the case of four single antenna users and six distributed receive antennas (two at each BS location) is considered. High SNR SER curves are plotted alongside the simulated values. Results are shown for both MMSE (Fig. 6.5) and ZF (Fig. 6.6) with QPSK modulation. The agreement between the simulated SER and the high SNR approximation is shown to be less accurate than in Fig. 6.3, with very close agreement requiring low error rates around $10^{-4}$. This is unsurprising, as the greater number of system dimensions gives greater freedom for the channel powers to vary substantially over the links.

## 6.6 Summary

The performance of MMSE and ZF receivers in a macrodiversity layout is a long-standing, unsolved research problem. In this chapter, we make the first major progress towards solving this problem

for the general case of an arbitrary number of transmit and receive antennas. The analysis is based on a derivation which targets the characteristic function of the output SINR. This leads to an expected value which is highly complex in its exact form, but can be simplified by the use of an extended Laplace type approximation. This methodology is able to produce approximate results for both the SINR distribution and the SER which are simple enough to be employed as the basis of a scheduling algorithm. Proportional fair (PF) ideas can be incorporated to overcome unfairness which can likely affect the CDI based scheduling methods. The SINR distribution is shown to have a remarkably simple form as a generalized mixture of exponentials. Also, the asymptotic SER results produce a remarkably compact metric which captures a large part of the functional relationship between the macrodiversity power profile and SER. In addition, since both SINR and SER results are available, scheduling can be performed on the basis of either metric.

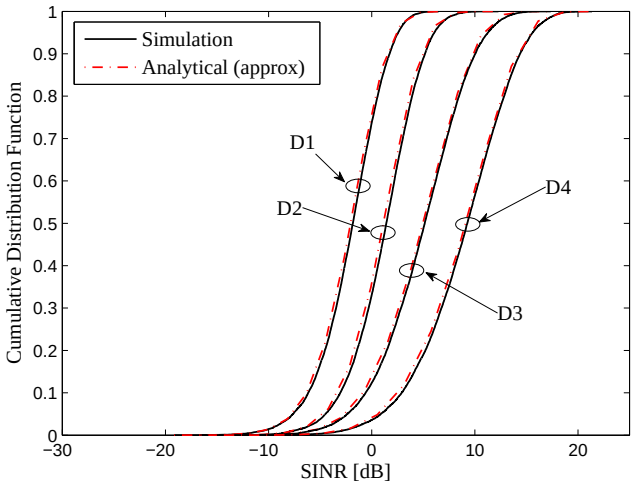


Figure 6.2: Approximate and simulated SINR cdf results for the $N = 3$, $n_R = 3$ scenario. Results are shown for the first of three users for four arbitrary drops and a MMSE receiver.

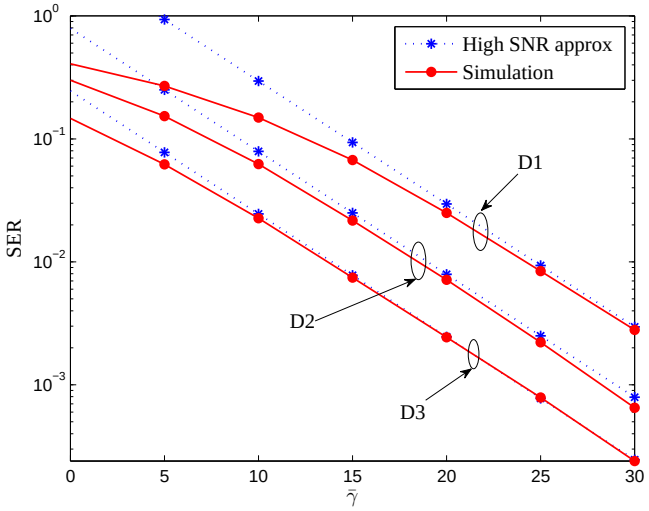


Figure 6.3: Approximate and simulated SER results for the $N = 3$, $n_R = 3$ scenario with QPSK modulation. Results are shown for the first of the three users for three arbitrary drops and a MMSE receiver.

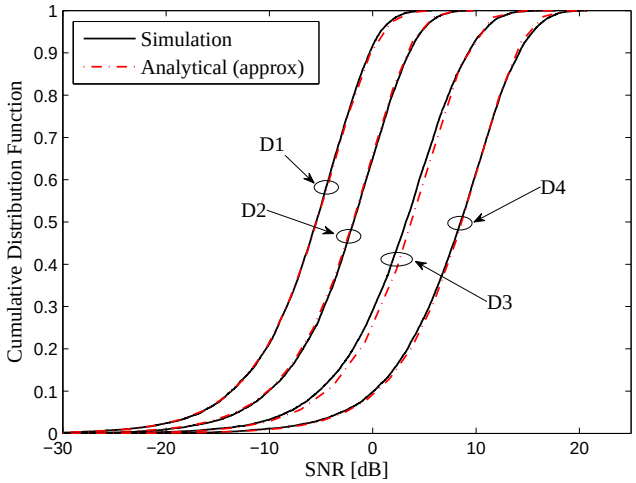


Figure 6.4: Approximate and simulated SNR cdf results for the $N = 3$, $n_R = 3$ scenario. Results are shown for the first of three users for four arbitrary drops and a ZF receiver.

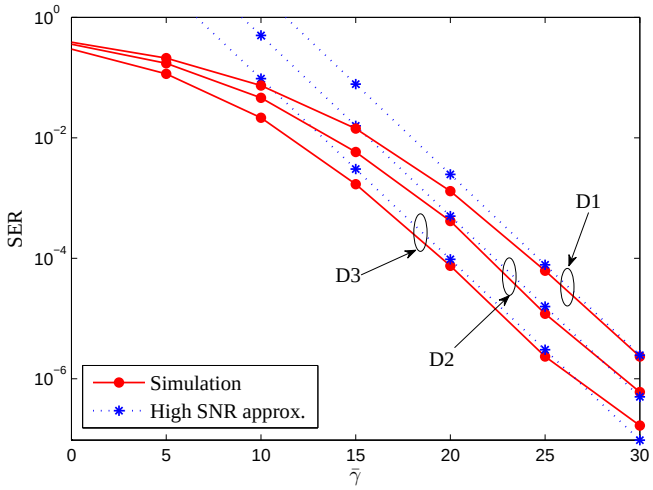


Figure 6.5: Approximate and simulated SER results for $N = 4$, $n_R = 6$, i.e., two receive antennas at each BS with QPSK modulation. Results are shown for the first of four users for three arbitrary drops and a MMSE receiver.

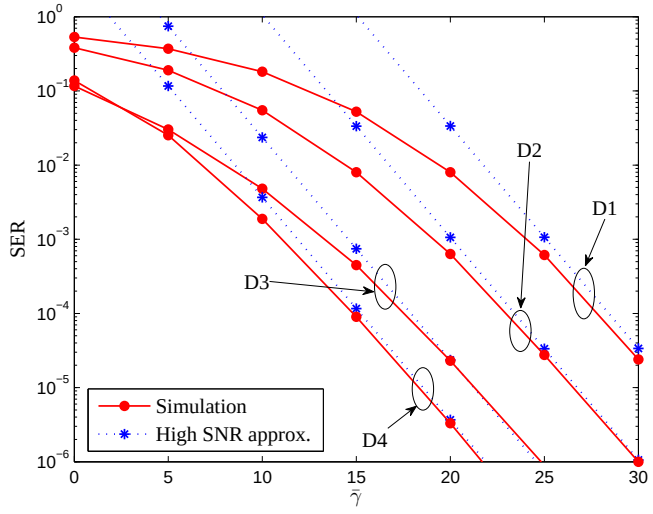


Figure 6.6: Approximate and simulated SER results for the $N = 4$, $n_R = 6$, i.e., two receive antenna at each BS scenario with QPSK modulation. Results are shown for the first of four users for four arbitrary drops and a ZF receiver.

# Chapter 7

# Maximum Likelihood Detection in Macrodiversity MIMO Systems

The performance of multiple input multiple output maximum likelihood detection (MLD) was considered in the classic paper by Zhu and Murch [91] for the case of independent and identically distributed (iid) Rayleigh channels. This work was extended to correlated Rayleigh channels in [92] and [93]. Note that [92] also considers cases where the noise is colored or a fixed transmit precoder is used. However, these effects can be accommodated by an equivalent change in the correlation structure. Hence, both [92] and [93] effectively consider two-sided Kronecker correlation models. In [94], performance analysis of MLD for space-time coding in correlated Ricean MIMO channels is considered. Work on MIMO MLD was motivated by the observation that "with small numbers of transmit antennas and low-order constellations, the complexity of MLD is not overwhelming" [91]. In [91]-[93], the performance analysis uses a union bound for the SER, based on an exact evaluation of the PEP.

In this chapter, the motivation and approach are the same, but the system is different. Here, we assume distributed transmit and receive antennas so that every path from a transmit antenna to a receive antenna has a different SNR. This assumption is a direct result of macrodiversity system architecture consider in this thesis. In this context, we derive the exact PEP which leads to a union bound for the SER in both flat Rayleigh and Rician fading environemnts. Further we analyze the

high SNR asymptotic for the PEP whereby producing a compact expressions for the analysis of the effect of macrodiversity power profiles on the performance of macrodiversity ML decoding.

## 7.1 System Model

Consider a MIMO system with $N$ sources and $n_R$ distributed receive antennas. The $N$ sources are assumed to be $N$ single-antenna users, but could equally well consist of fewer multiple antenna users or a single user with $N$ distributed antennas. The system equation is given by

$$\boldsymbol{r} \quad = \quad \boldsymbol{H}\boldsymbol{s} + \boldsymbol{n}, \tag{7.1}$$

where $\boldsymbol{r}$ is the $\mathcal{C}^{n_R \times 1}$ receive vector, $\boldsymbol{s}$ is the $\mathcal{C}^{N \times 1}$ transmit vector and $\boldsymbol{n}$ is the $\mathcal{C}^{n_R \times 1}$ vector of additive white Gaussian noise terms with $E\left\{|n_i|^2\right\} = \sigma^2$ for $i = 1, \ldots n_R$. The $\mathcal{C}^{n_R \times N}$ channel matrix, $\boldsymbol{H}$, corresponds to independent, but non-identical, fading and has entries which satisfy $\boldsymbol{H}_{ik} \sim \mathcal{CN}\left(0, P_{ik}\right)$ for Rayleigh fading and $\boldsymbol{H}_{ik} \sim \mathcal{CN}\left(\sqrt{\frac{K_{ik}P_{ik}}{1+K_{ik}}}\Omega_{ik}, \frac{P_{ik}}{1+K_{ik}}\right)$ for Rician fading. The $\Omega_{ik}$ term accounts for the complex LOS phase parameter and we assume $|\Omega_{ik}|^2 = 1$. The strength of the LOS component of the $ik^{th}$ path is governed by the K-factor given by $K_{ik}$. Hence, each link has a potentially different average SNR given by $P_{ik}/\sigma^2$. Assuming perfect channel state information at the receiver, the MLD approach estimates the transmit vector by [91]

$$\tilde{\boldsymbol{s}} = \arg\min_{\boldsymbol{s}} \|\boldsymbol{r} - \boldsymbol{H}\boldsymbol{s}\|^2, \tag{7.2}$$

where $\boldsymbol{s}$ ranges over all possible transmit vectors.

## 7.2 Pairwise Error Probability

The PEP is the probability that a transmitted codeword vector, $\boldsymbol{s}_i$, has a worse detection metric than another codeword vector, $\boldsymbol{s}_k$. In this section, we find the exact PEP for uncoded ML detection in macrodiversity systems. Let $\boldsymbol{s}_i$ be the complex transmitted code vector in baseband notation. The random event that some other code vector, $\boldsymbol{s}_k$, would be decoded in preference to

the transmitted vector, $\boldsymbol{s}_i$, is equivalent to the event $\mathcal{A}_{ik}$ where

$$\mathcal{A}_{ik} = \left\{ \|\boldsymbol{r} - \boldsymbol{H}\boldsymbol{s}_k\|^2 \leq \|\boldsymbol{r} - \boldsymbol{H}\boldsymbol{s}_i\|^2 \right\}. \tag{7.3}$$

Note that $\boldsymbol{s}_k$ may or may not be the final decoded vector, $\tilde{\boldsymbol{s}}$. Hence, the PEP defined in [95] is equal to

$$P_e\left(\boldsymbol{s}_i \rightarrow \boldsymbol{s}_k\right) = \Pr\left(\mathcal{A}_{ik}\right). \tag{7.4}$$

After some complex vector manipulations, we arrive at

$$\mathcal{A}_{ik} = \left\{ 2\mathrm{Re}\left(\boldsymbol{n}^H \boldsymbol{H}\boldsymbol{c}_{ik}\right) \leq -\boldsymbol{c}_{ik}^H \boldsymbol{H}^H \boldsymbol{H}\boldsymbol{c}_{ik} \right\}, \tag{7.5}$$

where the $\mathcal{C}^{N\times 1}$ vector, $\boldsymbol{c}_{ik}$, is the code-word difference vector, defined in [95] as $\boldsymbol{c}_{ik} = \boldsymbol{s}_i - \boldsymbol{s}_k$. Note that $2\mathrm{Re}\left(\boldsymbol{n}^H \boldsymbol{H}\boldsymbol{c}_{ik}\right)$ is Gaussian distributed, conditioned on $\boldsymbol{c}_{ik}$ and $\boldsymbol{H}$, with zero mean and variance $2\sigma^2 \boldsymbol{c}_{ik}^H \boldsymbol{H}^H \boldsymbol{H}\boldsymbol{c}_{ik}$. Therefore,

$$P_e\left(\boldsymbol{s}_i \rightarrow \boldsymbol{s}_k\right) = E_{\boldsymbol{H}}\left\{ Q\left( \sqrt{\frac{\boldsymbol{c}_{ik}^H \boldsymbol{H}^H \boldsymbol{H}\boldsymbol{c}_{ik}}{2\sigma^2}} \right) \right\}, \tag{7.6}$$

where $Q\left(x\right) = \frac{1}{\sqrt{2\pi}} \int_x^\infty e^{-\frac{t^2}{2}} dt$ is the Gaussian Q-function defined in [52] and $E_{\boldsymbol{H}}\left\{.\right\}$ denotes the expectation over the random matrix, $\boldsymbol{H}$. For notational simplicity we drop the subscripts of $\boldsymbol{c}_{ik}$ when it is clear from the context which codewords are involved.

Next, we decompose the channel matrix, $\boldsymbol{H}$, into a matrix of row vectors, where $\boldsymbol{H}^H$ becomes $\boldsymbol{H}^H = (\boldsymbol{v}_1, \boldsymbol{v}_2, \ldots, \boldsymbol{v}_{n_R})$, and the $N \times 1$ vector, $\boldsymbol{v}_r$, is multivariate Gaussian distributed. Let $Z$ be defined by

$$Z = \boldsymbol{c}^H \boldsymbol{H}^H \boldsymbol{H}\boldsymbol{c} = \sum_{r=1}^{n_R} \bar{X}_r X_r, \tag{7.7}$$

where the random variable, $X_r = \boldsymbol{v}_r^H \boldsymbol{c}$, for $r = 1, 2, \ldots n_R$.

### Rayleigh Fading

In Rayleigh fading, $\boldsymbol{v}_r$ is zero mean and has the diagonal covariance matrix, $\boldsymbol{D}_r = \text{diag}\left(P_{r1}, \ldots, P_{rN}\right)$, for $r = 1, 2, \ldots n_R$. Hence, $X_r$ is Gaussian distributed with

$$X_r \sim \mathcal{CN}\left(0, \boldsymbol{c}^H \boldsymbol{D}_r \boldsymbol{c}\right), \tag{7.8}$$

and $\bar{X}_r X_r$ has an exponential distribution with rate parameter, $\lambda_r$, given by

$$\lambda_r = \frac{1}{\boldsymbol{c}^H \boldsymbol{D}_r \boldsymbol{c}}. \tag{7.9}$$

Hence, $Z$ is a sum of $n_R$ independent exponential random variables. From [96], the expectation in (7.6) can be evaluated to give

$$P_e\left(\boldsymbol{s}_i \to \boldsymbol{s}_k\right) = \frac{\alpha}{2} \sum_{r=1}^{n_R} \frac{1}{\beta_r \lambda_r} \left(1 - \frac{1}{\sqrt{1 + 4\lambda_r \sigma^2}}\right), \tag{7.10}$$

where $\alpha = \prod_{l=1}^{n_R} \lambda_l$ and $\beta_r = \prod_{l \neq r}^{n_R} \left(\lambda_l - \lambda_r\right)$.

### Rician Fading

In Rician fading, $X_r$ is also Gaussian distributed, but with a non-zero mean. From the assumptions in Sec. 7.1,

$$E\left\{X_r\right\} = \Sigma_r, \tag{7.11}$$

$$E\left\{\bar{X}_r X_r\right\} = \boldsymbol{c}^H \tilde{\boldsymbol{D}}_r \boldsymbol{c} = 1/\tilde{\lambda}_r, \tag{7.12}$$

where $\Sigma_r = \left(\sqrt{\frac{K_{r1} P_{r1}}{1+K_{r1}}}\Omega_{r1}, \ldots, \sqrt{\frac{K_{rN} P_{rN}}{1+K_{rN}}}\Omega_{rN}\right)\boldsymbol{c}$ and $\tilde{\boldsymbol{D}}_r = \text{diag}\left(\sqrt{\frac{P_{r1}}{1+K_{r1}}}, \ldots, \sqrt{\frac{P_{rN}}{1+K_{rN}}}\right)$. First, the characteristic function (cf) of $Z$ is calculated to give [97]

$$\tilde{\phi}_Z\left(t\right) = \prod_{r=1}^{n_R} \frac{\exp\left(\frac{jt|\Sigma_r|^2}{1 - \frac{jt}{\tilde{\lambda}_r}}\right)}{1 - \frac{jt}{\tilde{\lambda}_r}}. \tag{7.13}$$

Note the use of $\sim$ notation to differentiate between Rayleigh results and Rician results in $\tilde{\boldsymbol{D}}_r$, $\tilde{\phi}_Z(t)$ and elsewhere. From [97], the cf in (7.13) can be expanded in an infinite series to give

$$\tilde{\phi}_Z(t) = \sum_{r=0}^{\infty} \frac{\eta_r}{(1-2jt\theta)^{n_R+r}}, \tag{7.14}$$

where $\theta > 0$ is a suitably chosen constant as in [97, pp. 169] and the coefficient, $\eta_r$, also defined in [97, pp. 170]. The cf in (7.14) can be inverted to obtain [52]

$$\tilde{f}_Z(z) = \sum_{r=0}^{\infty} \frac{\eta_r z^{n_R+r-1} e^{-\frac{z}{2\theta}}}{(2\theta)^{n_R+r}\,\Gamma(n_R+r)}. \tag{7.15}$$

The PEP in Rician fading can be calculated in closed form using (7.15) in (7.6) giving

$$P_e(\boldsymbol{s}_i \to \boldsymbol{s}_k) = \sum_{r=0}^{\infty} \int_0^{\infty} \frac{\eta_r Q\left(\sqrt{\frac{y\theta}{\sigma^2}}\right) y^{n_R+r-1} e^{-y}}{2\theta\Gamma(n_R+r)} dy, \tag{7.16}$$

where each term in the summation can be solved using the following generic integral solution from [98],

$$\int_0^{\infty} Q\left(\sqrt{\frac{y\theta}{\sigma^2}}\right) y^u e^{-y} dy = \Gamma(u)\left(\frac{1}{2}(1-\psi)\right)^{u+1} \sum_{k=0}^{u} \binom{u+k}{k} \left(\frac{1}{2}(1+\psi)\right)^k, \tag{7.17}$$

where $\psi = \sqrt{\frac{\theta}{\theta+2\sigma^2}}$. Hence, the Rician fading PEP can be computed in closed form using (7.16) in conjunction with (7.17). Details of the size of the remainder term in (7.16) when a finite version is used can be obtained from [97]. Although [97] specifically computes the remainder for the cdf of $Z$, $\tilde{F}_Z(z)$, since the Q-function in (7.6) is always less than 1 the remainder for $\tilde{F}_Z(z)$ upper bounds the remainder for (7.16). Due to the complexity of the PEP expression, we also consider a high SNR approximation PEP as shown in Sec. 7.3.1.

## 7.3 Performance Analysis

### 7.3.1 Diversity Order and High SNR Results

As in [91], the diversity order is equal to $n_R$, the number of receive antennas and is independent of $N$. This result follows from the work in [96] which can be applied to this problem.

#### Rayleigh Fading

The cf of $\frac{Z}{2\sigma^2}$ is given by [9]

$$\phi_Z(t) = \prod_{r=1}^{n_R} \frac{1}{1 - \frac{jt}{2\lambda_r \sigma^2}}. \tag{7.18}$$

At high SNR, that is when $\sigma^2 \to 0$, (7.18) simplifies to $\prod_{r=1}^{n_R} \frac{2\lambda_r \sigma^2}{-jt}$. By making use of the moment generating function, $\mathcal{M}_Z(s) = \phi_Z(-js)$, and using well-known techniques in [9], the PEP in Rayleigh fading at high SNR is obtained as

$$P_e(\boldsymbol{s}_i \to \boldsymbol{s}_j) \simeq \frac{2^{2n_R-1}\Gamma\left(n_R + \frac{1}{2}\right)^2 \alpha}{\pi (2n_R)!} \left(\sigma^2\right)^{n_R}. \tag{7.19}$$

#### Rician Fading

The cf of $\frac{Z}{2\sigma^2}$ in Rician fading can be calculated to give [9]

$$\tilde{\phi}_Z(t) = \prod_{r=1}^{n_R} \frac{\exp\left(\frac{\frac{jt}{2\sigma^2}|\Sigma_r|^2}{1-\frac{jt}{2\tilde{\lambda}_r\sigma^2}}\right)}{1 - \frac{jt}{2\tilde{\lambda}_r\sigma^2}}. \tag{7.20}$$

At high SNR, that is when $\sigma^2 \to 0$, (7.20) simplifies to

$$\tilde{\phi}_Z(t) = \prod_{r=1}^{n_R} \frac{\exp\left(-\tilde{\lambda}_r |\Sigma_r|^2\right)}{1 - \frac{jt}{2\tilde{\lambda}_r\sigma^2}}. \tag{7.21}$$

Using the moment generating function method as in the Rayleigh fading case, we obtain the high SNR approximation for the PEP given by

$$P_e\left(\boldsymbol{s}_i \to \boldsymbol{s}_j\right) \simeq \frac{2^{2n_R-1}\Gamma\left(n_R+\frac{1}{2}\right)^2 \tilde{\alpha}}{\pi\left(2n_R\right)!}\left(\sigma^2\right)^{n_R}, \tag{7.22}$$

where $\tilde{\alpha} = \prod_{r=1}^{n_R} \tilde{\lambda}_r \exp\left(-\tilde{\lambda}_r \left|\Sigma_r\right|^2\right)$.

### 7.3.2 Symbol Error Rate

A union bound for the SER of the $u^{th}$ user can be found by following similar arguments to those in [91]. Let $\{d_m, m = 1, 2, \ldots, M\}$ be the set of all possible symbols assuming an M-point constellation and $\{\boldsymbol{s}\}$ be the set of all $M^N$ symbol vectors that could be sent from the $N$ sources. Define $\{\boldsymbol{s}_{u,m}\}$ to be the subset of $\{\boldsymbol{s}\}$ containing $d_m$ as the symbol of user $u$. With this notation, the upper bound for the SER of user $u$ is given by

$$P_s \leq M^{-N} \sum_{m=1}^{M} \sum_{i} \sum_{j} P_e\left(\boldsymbol{s}_i \to \boldsymbol{s}_j\right), \tag{7.23}$$

where index $i$ runs over the set $\{\boldsymbol{s}_{u,m}\}$ and index $j$ runs over the complement, $j \in \{\boldsymbol{s}_{u,m}\}^c$. Hence, (7.23) covers all possible errors, for any symbol, $d_m$, from user $u$ and all vectors, $\boldsymbol{s}_i$, containing $d_m$ in the $u^{th}$ position and all vectors, $\boldsymbol{s}_j$, which do not contain $d_m$ in the $u^{th}$ position. The union bound in (7.23) is then computed using (7.10) or (7.16) or, if a high SNR approximation is desired, then (7.19) or (7.22) can be substituted in (7.23). For example, using (7.23) with (7.19) gives the following high SNR approximation for the SER of user 1 in Rayleigh fading for BPSK modulation and $n_R = N = 2$:

$$P_s \simeq \frac{3}{512}\left[\frac{\left(P_{11}+P_{12}\right)\left(P_{21}+P_{22}\right)+P_{11}P_{21}}{\left(P_{11}+P_{12}\right)\left(P_{21}+P_{22}\right)P_{11}P_{21}}\right]\left(\sigma^2\right)^{n_R}. \tag{7.24}$$

## 7.4 Numerical Results

In this section, we investigate the effect of macrodiversity, ie., the impact of the way in which the channel strengths are distributed. We begin with a microdiversity example as a baseline for comparison. Consider a single user microdiversity link where the transmitter and receiver both have three antennas. Here, $n_R = N = 3$ and all channels have the same powers. For this example, $\boldsymbol{P}$ is given by

$$\boldsymbol{P} = (3, 3, 3; 3, 3, 3; 3, 3, 3)\,. \tag{7.25}$$

We also consider the following macrodiversity scenarios for the same system size and the same value of $P_T = \sum_i \sum_j P_{ij}$. The average received signal to noise ratio is defined by $\rho = P_T/\sigma^2$. Since the SNR is varied by altering the value of $\sigma^2$, the actual size of the powers in $\boldsymbol{P}$ is irrelevant. It is the effect of the distribution of powers, the power profile, that is important. Hence, these scenarios allow us to consider the SER impact of the different channel power profiles. Note that the SER performance of user 1 is considered throughout.

- Scenario 1 (S1): Diagonal dominance

  Interpretation: Here, the 3 users are close to different receive antennas so that only one link is strong per user.

$$\boldsymbol{P} = \left(8, \frac{1}{2}, \frac{1}{2}; \frac{1}{2}, 8, \frac{1}{2}; \frac{1}{2}, \frac{1}{2}, 8\right). \tag{7.26}$$

- Scenario 2 (S2): Overloaded

  Interpretation: Here, the 3 users are close to one antenna so only the 3 links to a single receive antenna are strong.

$$\boldsymbol{P} = \left(8, 8, 8; \frac{1}{2}, \frac{1}{2}, \frac{1}{2}; \frac{1}{2}, \frac{1}{2}, \frac{1}{2}\right). \tag{7.27}$$

- Scenario 3 (S3): Opposite

  Interpretation: Here, the 3 users are distributed and the links have opposing trends across the

receive antennas.

$$\boldsymbol{P} = (5, 3, 1; 3, 3, 3; 1, 3, 5)\,. \tag{7.28}$$

- Scenario 4 (S4): Parallel

  Interpretation: Here, the 3 users are distributed and the links have parallel trends across the receive antennas.

$$\boldsymbol{P} = (5, 5, 5; 3, 3, 3; 1, 1, 1)\,. \tag{7.29}$$

In Figs. 7.1 and 7.2, the union bound in (7.23) using the PEP in (7.10) is verified by simulation. As expected, the union bound is tight with extremely accurate results below an SER of $10^{-2}$ and results for BPSK (Fig. 7.1) being tighter than QPSK (Fig. 7.2).

In terms of system performance, both Figs. 7.1 and 7.2 have the same ordering with microdiversity best, followed by S3 (opposite), S4 (parallel), S1 (diagonally dominant) and S2 (overloaded). This ordering is intuitive, with the lowest SER resulting from microdiversity, which maximizes the MIMO diversity, and the highest SER due to overloading, where there is little diversity and strong interference. In between, the opposite and parallel scenarios are second and third best as they maintain diversity with the opposite scenario being superior as it has less interference. Diagonal dominance is fourth best since it is essentially three single user links. Within this ordering, the major performance gap is between microdiversity, S3 and S4, with similar lower SERs, and scenarios S1 and S2, with similar higher SERs. The first group of three scenarios is superior to the second group due to diversity, with each user received with reasonable strength at more than one antenna.

In Fig. 7.3, the same scenarios are shown as in Fig. 7.2 and are compared to the high SNR approximation to the union bound. Results are obtained for QPSK and follow from (7.23) using the high SNR PEP given in (7.19). In all cases, results are reasonable for SERs below $10^{-3}$ and accurate below $10^{-4}$.

In Fig 7.4, three random drops are simulated incorporating random distances and shadow fading

according to the methodology in [74]. The Rician K-factors are uniformly generated in [0,8] for the nine links. Results are obtained for QPSK and follow from (7.23) using (7.22) for the high SNR PEP. Convergence of the results to the high SNR approximations is seen to be slower in the Rician case.

## 7.5 Summary

In this chapter, we have derived exact closed form results for the PEP in a macrodiversity MIMO context for both Rayleigh and Rician channels. These results have enabled an evaluation of SER results via the union bound and also high SNR approximations. The diversity order is shown to be equal to the number of receive antennas as in the microdiversity scenario. In terms of system performance, the importance of diversity (spreading the received powers over multiple receive antennas) is demonstrated. Also, channel power profiles which avoid strong interference for multiple sources are shown to be beneficial.

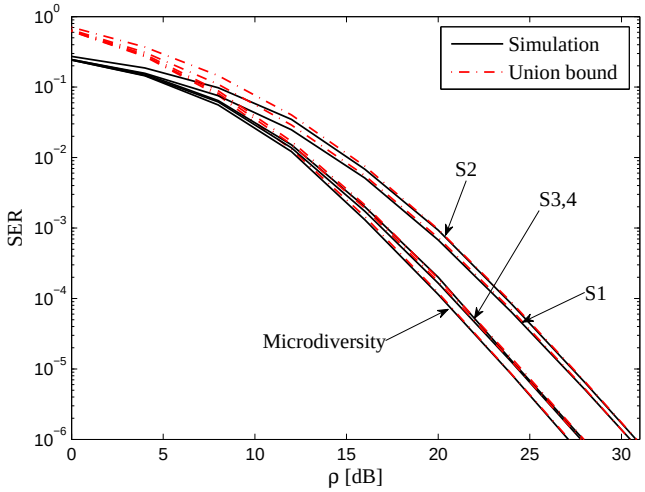


Figure 7.1: Simulated SER and union bound for an ML receiver with BPSK modulation in flat Rayleigh fading for scenarios S1-S4 with parameters: $n_R = K = 3$.

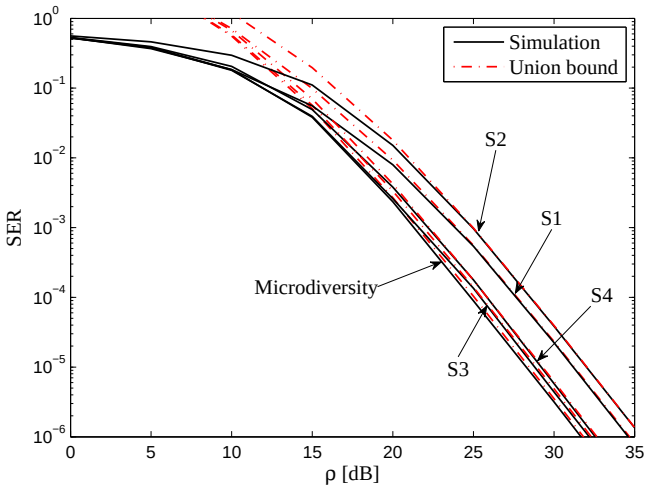


Figure 7.2: Simulated SER and union bound for an ML receiver with QPSK modulation in flat Rayleigh fading for scenarios S1-S4 with parameters: $n_R = K = 3$.

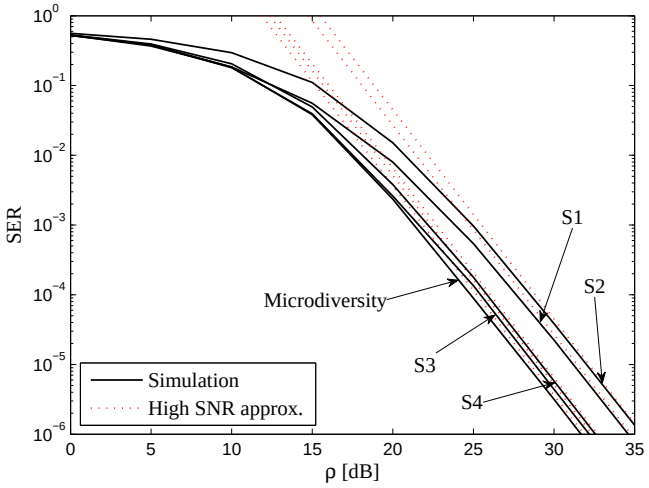


Figure 7.3: Simulated SER and high SNR approximations for an ML receiver with QPSK modulation in flat Rayleigh fading for scenarios S1-S4 with parameters: $n_R = K = 3$.

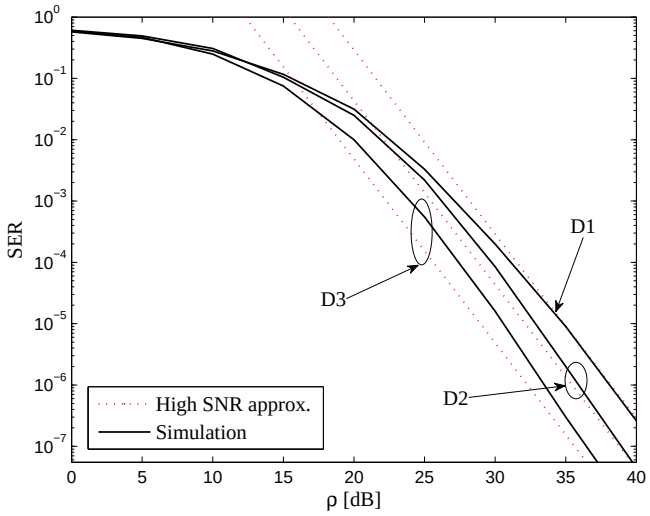


Figure 7.4: Simulated SER and high SNR approximations for an ML receiver with QPSK modulation in flat Rician fading for three arbitrary random power drops with $n_R = K = 3$.

# Chapter 8

# Uplink Macrodiversity MU-MIMO Scheduling

Conventional cellular mobile wireless systems, where, in a given cell site, many users are continuously trying to access radio resources need to manage these users intelligently. Managing users in such an environment has been investigated in [99], where the authors considered a single antenna BS scenario. In this work, the BS operates opportunistically to serve the best user (best user in the sense that its channel power is the best) out of all active users in the system hence extracting multiuser diversity. Managing users in this way or in a related manner is commonly referred to as user scheduling. The basic idea is that the user scheduler exploits the randomness of the wireless channel to select a good outcome. In [100], the performance of scheduling algorithms exploiting the multiuser selection diversity is studied comprehensively. From the service providers' point of view, user scheduling is a very important idea, but if BSs operate primarily on serving the best user, then some users may suffer from a lack of service. Hence, the two concepts of serving the best user and maintaining user fairness was incorporated in the Proportional Fair (PF) scheduling [101, 102, 103, 104]. In this chapter, we consider macrodiversity MU MIMO scheduling in the MIMO-MAC channel [105].

With the advent of multi-antenna technologies in multiuser environments, the concept of multiuser scheduling becomes very important. Unlike the case of a single antenna BS, multi-antenna BSs

can schedule multiple users in the same resource unit (i.e., the same time slot and frequency band) to improve the overall system throughput [30]. Since the macrodiversity MIMO-MAC also acts like a multi-antenna receiver, it can necessarily support simultaneous users. This gives rise to the application of multiuser scheduling ideas to macrodiversity MIMO systems.

The most straightforward and widely adopted uplink user scheduling approach is based on the use of instantaneous channel state information. However, in the MIMO-MAC channel, this approach may not scale as economically as in the conventional MIMO-MAC, because the CSI grows as the number of users grows and all CSI has to be transmitted to the BPU for making scheduling decisions [106, 107]. In a limited capacity backhaul network, this may not be possible. On the other hand, even with ideal backhaul in terms of the amount of data that can be transmitted, due to the geographical separation of distributed BSs, the CSI at the BPU will be a delayed version of the actual channel, which in turn may produce less accurate scheduling decisions.

One way to address the problems in using instantaneous CSI through backhaul networks is to use long term channel state information [108]. In some texts this is called channel distribution information [30]. CDI has certain advantages over instantaneous CSI in that it is simpler to obtain and relatively easy to communicate to the BPU. Furthermore, it is very robust to channel estimation errors and delays, and scales well with the size of the macrodiversity MIMO system. In LTE, scheduling methods are not fully specified. Hence, the methods proposed in this chapter have direct applications to these systems. Although CDI has many advantages, it has some disadvantages too. It is analytically, extremely difficult to formulate systematic scheduling metrics in terms of CDI. However, due to the contributions of this thesis, we are able to construct several novel approaches to metric construction. Also, where instantaneous CSI is available with minimal delay and estimation error, then it is always better than other alternatives such as CDI, if the backhaul overhead is neglected.

In this chapter, we consider scheduling in a macrodiversity MIMO-MAC. In order to give a practical focus to the discussion, we consider the uplink CoMP channel discussed in Sec. 2.3 [41].

## 8.1 System Model and Problem Statement

We consider $N_{MS}$ single-antenna distributed MSs attempting to communicate with $N_{BS}$ distributed BSs [38] each with a single receive antenna over an independent flat fading Rayleigh channel. Note that $N_{MS} >> N_{BS}$. An illustration of such an environment is shown in Fig. 8.1. In such a distributed environment, MSs can be served in many different ways. Some possible

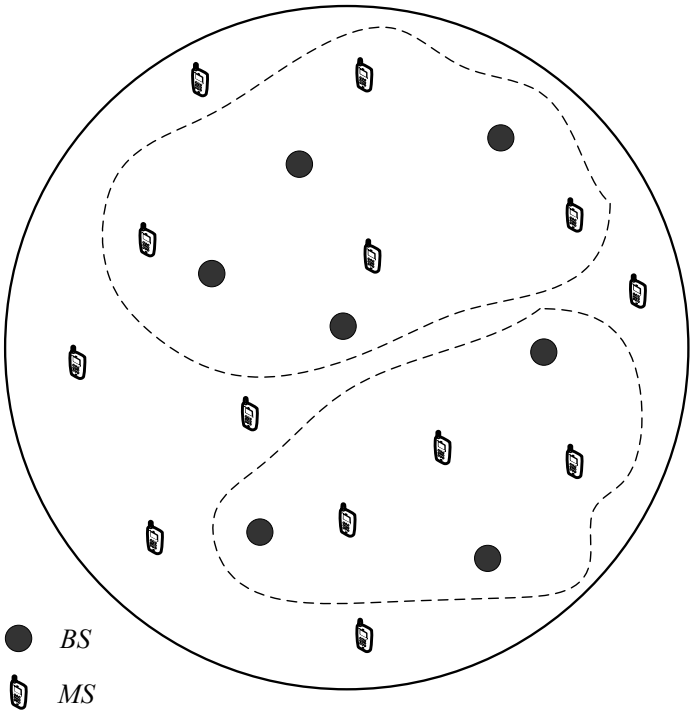


Figure 8.1: Illustration of a clustered CoMP.

scenarios are given below.

- Adaptive Cluster CoMP: In this scenario, in every scheduling interval, the BS set $\mathcal{M} = \{1, \ldots, N_{BS}\}$ is partitioned into $A$ disjoint non-empty subsets, $\mathcal{M}_i$, $i = 1, \ldots, A$ and the MS set $\{1, \ldots, N_{MS}\}$ is partitioned into $A$ disjoint non-empty subsets, $\mathcal{W}_i$, $i = 1, \ldots, A$. Then, all MSs in the $\mathcal{W}_i$ subset are served by BSs in the $\mathcal{M}_i$ subset. These partition structures may change across scheduling intervals. In this scenario a global backhaul network is essential to adjust the clustering structure dynamically.

- Fixed Cluster CoMP: This scenario is very similar to Adaptive Cluster CoMP, but the BS

clusters, defined by $\mathcal{M}_i$, are fixed across scheduling intervals. In contrast, MS partitions and their cardinalities may change. In this scenario, a global backhaul network is not needed, but as many local backhaul networks as the number of clusters are needed.

- Global CoMP: This scenario is similar to Adaptive Cluster CoMP, but with a single BS and MS partition, i.e., $A = 1$. This is only possible if all BSs are connected to a single BPU via backhaul interconnection links that cover the full coverage area.

Selecting the best MS subset and the best BS and MS partitions in cluster CoMP scenarios is a complex process. Algorithmic solutions using graph theory are possible, but this is outside the subject area of this thesis [109, 110]. Note that whatever the method we use in selecting the best partitions, at the center of any algorithm is a metric which states how well that particular partition of BSs serves a partition of MSs. In this chapter, we address this problem which is at the heart of any user scheduling algorithm using CDI [111, 108]. Without loss of generality, our system can be recast as follows.

Consider a single cluster as in Fig. 8.2, where $N$ single-antenna distributed MSs communicate with $n_R$ distributed BSs in the same time and frequency slot. Each MS and BS has a single receive antenna and an independent flat fading Rayleigh channel is assumed. In this chapter, we assume $N \leq n_R$, but generalization to $N > n_R$ is straightforward. In this system, we are interested in quantifying the performance of $N$ users in terms of CDI in a macrodiversity MIMO-MAC. The cluster in Fig. 8.2 may receive inter-cluster interference which is assumed to behave as extra AWGN.

## 8.2 Group vs Individual Metrics

According to the system description in Fig. 8.2, the $\mathcal{R}^{n_R \times N}$ power profile matrix $\boldsymbol{P} = (P_{ik})$ for $i = 1, \ldots, n_R$ and $k = 1, \ldots, N$ carries the full CDI for the system. Therefore, we call it the system power profile. On the other hand, the $\mathcal{R}^{n_R \times 1}$ column vectors $\boldsymbol{p}_k$ for $k = 1, \ldots, N$, where $\boldsymbol{P} = (\boldsymbol{p}_1, \boldsymbol{p}_2, \ldots, \boldsymbol{p}_N)$, are the user power profiles. Further, we define the diagonal $\mathcal{R}^{n_R \times n_R}$ matrices $\boldsymbol{P}_k = \text{diag}\,(\boldsymbol{p}_k) = (P_{1k}, \ldots, P_{n_R k})$. The interference power profile of user $k$ is given by $\boldsymbol{Q}_k$, where

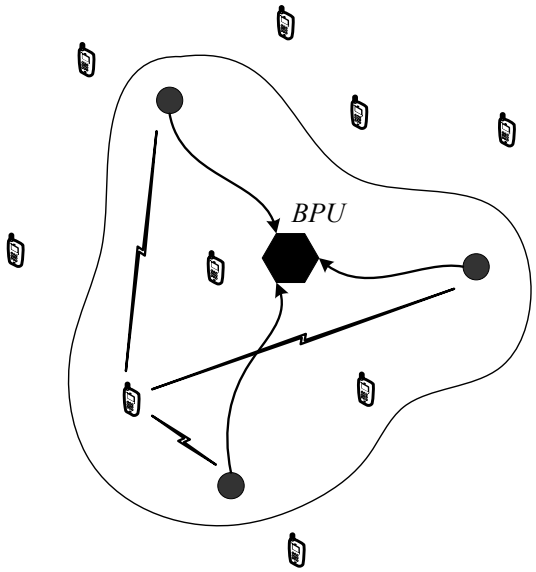


Figure 8.2: Illustration of a single CoMP cluster with $N = n_R = 3$.

$\boldsymbol{Q}_k$ is $\boldsymbol{P}$ with $\boldsymbol{p}_k$ removed. It is clear that after diversity combining, the $N$ co-channel users have different link level performance values. Therefore, we define individual scheduling metrics, $m_k$, for $k = 1, \ldots, N$. Furthermore, we are also interested in finding a group-wise scheduling metric, $M_g$. There are pros and cons between individual scheduling metrics and group-wise scheduling metrics. For example, $M_g$ may provide a simpler way to evaluate the performance of the user group, but it might not give any sense of the individual performance of the participating users. Therefore, any scheduling decision based solely on $M_g$ may lack fairness. Furthermore, individual scheduling metrics provide detailed information about the link level performance of the users in the MU-MIMO system. In this chapter, we consider both group-wise metrics and individual metrics. Due to the CDI based scheduling assumption, the scheduling metrics may be defined as

$$m_k = f\left(\boldsymbol{p}_k, \boldsymbol{Q}_k\right), \quad \text{for} \quad k = 1, \ldots, N, \tag{8.1}$$

$$M_g = f\left(\boldsymbol{P}\right). \tag{8.2}$$

The challenge of this approach is that an $n_R N$ dimensional variable (the $\boldsymbol{P}$ matrix) has to be mapped to a real variable in some systematic way which captures the spirit of the communication

system. There are crude approximations used in the literature [112], such as

$$m_k = \frac{\sum_{i=1}^{n_R} P_{ik}}{\sum_{i=1}^{n_R} \sum_{l \neq k}^{n_R} P_{il}}, \tag{8.3}$$

for $k = 1, \ldots, N$. Such scheduling metrics do not provide a direct link to any performance metric and are tractable ad-hoc measures built on basic SINR ideas.

## 8.3 Proposed Metrics Based on CDI

In this section, we provide several scheduling metrics based on CDI. These metrics are based on the analytical methods presented in previous chapters and are based on ergodic capacity, linear diversity combining and joint maximum likelihood decoding.

### 8.3.1 Information Theoretical Capacity Based Metrics

Sum capacity and rate regions are well known for the MIMO-MAC. Hence, it is straightforward to calculate the sum capacity and individual rates in terms of instantaneous CSI. However, due to the overheads associated with instantaneous CSI in macrodiversity systems, we adopt an approach based solely on CDI where ergodic values are employed.

#### Group Scheduling Metric

The instantaneous sum capacity has been widely used as a group scheduling metric [113]. The obvious extension using CDI is to use the mean sum capacity [62] which gives the metric

$$M_g = E\left\{\log_2 \left| \boldsymbol{I} + \frac{1}{\sigma^2} \boldsymbol{H}\boldsymbol{H}^H \right| \right\}. \tag{8.4}$$

In (8.4), $\boldsymbol{H}$ is the aggregate channel matrix of the macrodiversity MIMO-MAC and the expectation is over the multipath fading. Hence, $M_g$ is a function of the power profile. The expectation in

(8.4) can be calculated approximately, as in Chap. 4, to give the tight approximation

$$M_g = \frac{1}{\ln 2} \sum_{k=1}^{N} \left( \frac{\varphi_{k0}}{\varphi_{kn_R}} \sum_{l=1}^{n_R} \zeta_{kl} e^{\omega_{kl}} E_1 \left( \omega_{kl} \right) \right). \tag{8.5}$$

The constants in (8.5) are defined in Sec. 4.4. The sum capacity in (8.4) provides the fundamental MIMO-MAC capacity. Instead of using this theoretical limit, there may be practical interest in the link level sum capacity [114]. Such a metric can be easily found assuming independent MMSE linear combining at the BPU for every data stream. This gives

$$M_g = \sum_{k=1}^{N} E \left\{ \log_2 \left( 1 + \boldsymbol{h}_k^H \left( \sigma^2 \boldsymbol{I} + \boldsymbol{H}_k \boldsymbol{H}_k^H \right) \boldsymbol{h}_k \right) \right\}, \tag{8.6}$$

where the expectations in (8.6) inside the summation can be approximately computed using the approach described in Sec. 4.4, where $\boldsymbol{H}_k$ is $\boldsymbol{H}$ with column $\boldsymbol{h}_k$ removed.

### Individual Scheduling Metrics

Following the MMSE combining approach in (8.6), individual scheduling metrics can also be defined as

$$m_k = E \left\{ \log_2 \left( 1 + \boldsymbol{h}_k^H \left( \sigma^2 \boldsymbol{I} + \boldsymbol{H}_k \boldsymbol{H}_k^H \right)^{-1} \boldsymbol{h}_k \right) \right\}. \tag{8.7}$$

Using a combination of individual and group scheduling metrics, it is possible to balance individual user performance with group performance. This provides the opportunity to maintain fairness and boost overall system performance [101, 115].

## 8.3.2 Linear Receiver Based Metrics

The results in Chapters 3, 5 and 6 provide a functional link between the power profiles (CDI) and the performance of MRC, MMSE and ZF linear receivers. Hence, we are able to propose novel scheduling metrics based on CDI for systems employing linear receivers, e.g. 3GPP LTE-Advanced [39].

**Individual Scheduling Metrics/ZF**

From the analysis in Sec. 6.2.1, the approximate cdf of the output SNR of user $k$ after ZF combining is given by

$$\hat{F}_{\tilde{Z}_k}(z) = \frac{\text{Perm}\left(\boldsymbol{Q}_k\right)}{\tilde{\varphi}_L} \sum_{i=1}^{L} \frac{\tilde{\eta}_i}{\tilde{\omega}_i} \left(1 - e^{-\tilde{\omega}_i z}\right), \tag{8.8}$$

where the constants can be found using the approach described in Sec. 6.2.1 and $L = n_R - N + 1$. Scheduling metrics may be constructed based on these cdfs. The two obvious approaches are the outage probability at a given SNR threshold (say $\text{SNR}^{Th}$) and the SNR at which a certain outage probability threshold (say $q^{Th}\%$) occurs. We discuss both approaches in this section. Equation (8.8) allows us to directly calculate the approximate outage probability at $\text{SNR}^{Th}$ giving the following SNR threshold based individual scheduling metric as

$$m_k = \frac{\text{Perm}\left(\boldsymbol{Q}_k\right)}{\tilde{\varphi}_L} \sum_{i=1}^{L} \frac{\tilde{\eta}_i}{\tilde{\omega}_i} \left(1 - e^{-\tilde{\omega}_i \text{SNR}^{Th}}\right). \tag{8.9}$$

On the other hand, (8.8) allows us to calculate the approximate $q^{Th}\%$ outage SNR (e.g., 5 % outage SNR). The approximate $q^{Th}\%$ outage SNR can be calculated as, $z_k^*$, the solution of

$$\frac{\text{Perm}\left(\boldsymbol{Q}_k\right)}{\tilde{\varphi}_L} \sum_{i=1}^{L} \frac{\tilde{\eta}_i}{\tilde{\omega}_i} \left(1 - e^{-\tilde{\omega}_i z_k^*}\right) = \frac{q^{Th}}{100}. \tag{8.10}$$

Hence, we can define an individual scheduling metric based on an outage threshold as follows

$$m_k = z_k^*. \tag{8.11}$$

For $n_R = N$, equation (8.10) has analytical solution giving the outage threshold based metric, $m_k$, as

$$m_k = \frac{\left(2\ln\sigma + \ln\left(\text{Perm}\left(\boldsymbol{Q}_k\right)\right) - \ln\left(\text{perm}\left(\boldsymbol{P}\right)\right) - \ln q^{Th}\right) \text{perm}\left(\boldsymbol{P}\right)}{\sigma^2 \text{Perm}\left(\boldsymbol{Q}_k\right)}. \tag{8.12}$$

The SER analysis in Sec. 6.2.2 allows us to calculate another scheduling metric which is based on SER. From the analysis in Chapter 6, the SER of user k can be approximated by

$$\mathrm{SER}_k \simeq \left(\tilde{G}_a \bar{\gamma}\right)^{-\tilde{G}_d}, \tag{8.13}$$

where the diversity order and array gain of the SER of the $k$th user are given by

$$\tilde{G}_d = n_R - N + 1, \tag{8.14}$$

$$\tilde{G}_a = \left(\frac{1}{|\boldsymbol{P}_k|} \frac{\mathrm{Perm}\left(\boldsymbol{Q}_k\right)}{\mathrm{Perm}\left(\boldsymbol{P}_k^{-1}\boldsymbol{Q}_k\right)} \tilde{\mathcal{I}}\right)^{-1/(n_R-N+1)}. \tag{8.15}$$

In (8.15), the constant integral $\tilde{\mathcal{I}}$ is given in (6.34) and $\bar{\gamma}$ is the transmit SNR. It is clear from (8.13)-(8.15), that at a fixed transmit SNR

$$\mathrm{SER}_k \propto \frac{1}{|\boldsymbol{P}_k|} \frac{\mathrm{Perm}\left(\boldsymbol{Q}_k\right)}{\mathrm{Perm}\left(\boldsymbol{P}_k^{-1}\boldsymbol{Q}_k\right)}. \tag{8.16}$$

This observation permits us to define the following individual scheduling metric as

$$m_k = \frac{1}{|\boldsymbol{P}_k|} \frac{\mathrm{Perm}\left(\boldsymbol{Q}_k\right)}{\mathrm{Perm}\left(\boldsymbol{P}_k^{-1}\boldsymbol{Q}_k\right)}. \tag{8.17}$$

### Individual Scheduling Metrics/MMSE

In this section, we extend the scheduling metrics obtained in the last section to MMSE based metrics. Following a similar approach to the ZF case, we obtain the following metrics. The details are omitted due to the close relationship with the ZF result. The individual scheduling metric of user $k$, based on an SINR threshold, $\mathrm{SINR}^{Th}$, becomes

$$m_k = \frac{\Theta\left(\boldsymbol{Q}_k\right)}{\varphi_{n_R}} \sum_{i=1}^{n_R} \frac{\eta_i}{\omega_i} \left(1 - e^{-\omega_i \mathrm{SINR}^{Th}}\right), \tag{8.18}$$

where the constants can be found using the approach described in Sec. 6.3.1. Furthermore, the outage threshold based scheduling metric is found from the solution, $z_k^*$, of

$$\frac{\Theta\left(\boldsymbol{Q}_k\right)}{\varphi_{n_R}} \sum_{i=1}^{n_R} \frac{\eta_i}{\omega_i} \left(1 - e^{-\omega_i z_k^*}\right) = \frac{q^{Th}}{100}, \tag{8.19}$$

which gives $m_k = z_k^*$. Unlike the ZF receiver, the MMSE outage threshold based scheduling metric does not have a special case which gives simple results for $z_k^*$. The SER based scheduling metric becomes

$$m_k = \frac{\operatorname{Perm}\left(\boldsymbol{Q}_k\right)}{|\boldsymbol{P}_k| \operatorname{Perm}\left(\boldsymbol{P}_k^{-1}\boldsymbol{Q}_k\right)} \mathcal{I}\left(\boldsymbol{P}\right), \tag{8.20}$$

where $\mathcal{I}\left(\boldsymbol{P}\right)$ can be calculated using method described Sec. 6.3.2.

### Group Scheduling Metrics

In independent ZF decoding it is apparent that individual scheduling metrics can be derived fairly easily, but deducing a group scheduling metric is not trivial. However, we can obtain a simple yet powerful criterion as follows. For the system described in Sec. 6.1 with a ZF decoding criterion, the error covariance matrix $\boldsymbol{\Xi}$ is defined as

$$\boldsymbol{\Xi} = \sigma^2 \left(\boldsymbol{H}^H \boldsymbol{H}\right)^{-1}. \tag{8.21}$$

Using the classical *D-optimal* criterion [116] in statistics, it is straightforward to obtain the following group scheduling metric as

$$M_g = E\left\{\left|\boldsymbol{H}^H \boldsymbol{H}\right|\right\} = \operatorname{Perm}\left(\boldsymbol{P}\right). \tag{8.22}$$

From (8.22), the group of MSs and BSs which have the largest power matrix permanent is the best set to be scheduled together. This approach is further established in the analysis of Sec. 4.5. Hence, this approach gives a simple scheduling metric, although in comparison with (8.5) it is less tightly linked to system performance.

In the MMSE case we can also apply the *D-optimal* criterion on the error covariance matrix, $\boldsymbol{\Xi}$, of MMSE decoding. This result is very similar to the sum capacity criterion in (8.4) and is given by

$$M_g = E\left\{\left|\sigma^2\boldsymbol{I} + \boldsymbol{H}^H\boldsymbol{H}\right|\right\} = \sum_{i=0}^{N}\sum_{\sigma}\mathrm{Perm}\left((\boldsymbol{P})^{\sigma_{i,N}}\right)\left(\sigma^2\right)^{N-i}. \tag{8.23}$$

### 8.3.3 Maximum Likelihood Criterion Based Metrics

The optimum ML criterion is known to have high computational complexity and poor scaling with a growth in the number of users. However, it gives the best performance of all decoding algorithms. Whether or not ML decoding is actually employed, the theoretical performance of ML processing can still be used as a scheduling metric since good ML performance is likely to be linked with good performance of other sub-optimal approaches. Hence, we propose a group scheduling metric based on frame error rate (FER) and individual scheduling metrics based on the SER of each user.

#### Group Scheduling Metrics Based on FER

The frame defined in this chapter is the $N \times 1$ symbol vector transmitted by all the MSs. If the decoded vector, $\boldsymbol{s}_k$, is different (in the sense that any element of the vector is different from the corresponding element of the transmitted vector) from the transmitted vector $\boldsymbol{s}_i$, an error occurs. Following the same procedure for the SER in Sec. 7.3.2, the FER can be upper bounded to give

$$\mathrm{FER} \leq M^{-N}\sum_{i}\sum_{k\neq i}P_e\left(\boldsymbol{s}_i \rightarrow \boldsymbol{s}_k\right), \tag{8.24}$$

where $P_e\left(\boldsymbol{s}_i \rightarrow \boldsymbol{s}_k\right)$ is the pair wise error probability as defined in Sec. 7.2. In Chapter 7, $P_e\left(\boldsymbol{s}_i \rightarrow \boldsymbol{s}_k\right)$ has been calculated in closed form for both Rayleigh and Rician fading scenarios. However, these results are not particularly compact and may impose some unwanted computational burden in scheduling. Therefore, in this section we exploit the simple high SNR approximations for the scheduling metric derivations. This permits us to define the following group scheduling

metric for Rayleigh fading environment as

$$M_g = M^{-N} \sum_i \sum_{k \neq i} \alpha_{ik}, \tag{8.25}$$

where $\alpha_{ik} = \prod_{l=1}^{n_R} \lambda_l$, $M$ is the number of constellation points, and the $\lambda_l$ terms are defined as

$$\frac{1}{\lambda_l} = \boldsymbol{c}_{ik}^H \boldsymbol{D}_l \boldsymbol{c}_{ik}, \tag{8.26}$$

with the variables in (8.26) defined in Sec. 7.2. Both summations run over all possible $M^N$ transmit vectors. For a Rician fading environment, the corresponding metric is

$$M_g = M^{-N} \sum_i \sum_{k \neq i} \tilde{\alpha}_{ik}, \tag{8.27}$$

where $\tilde{\alpha}_{ik} = \prod_{r=1}^{n_R} \tilde{\lambda}_r \exp\left(-\tilde{\lambda}_r \left|\Sigma_r\right|^2\right)$ and the constants are defined in Sec. 7.2. The double summation in (8.25) and (8.27) can be regarded as an expectation operation over the discrete constellation points. Therefore, it is clear that $M_g$ is a function of the elements of the power profile matrix, $\boldsymbol{P}$.

### Individual Scheduling Metrics Based on SER

Individual scheduling metrics based on SER can be calculated following the same procedure as in Sec. 7.3.2. In the SER upper bound expression, the PEP is replaced by high SER approximations of PEP which give compact tractable expressions. These high SNR approximations are found in Sec. 7.3.1. For the sake of completeness, we provide the final result here. For Rayleigh fading,

$$m_k = M^{-N} \sum_{m=1}^{M} \sum_i \sum_k \alpha_{ik}, \tag{8.28}$$

and for Rician fading,

$$m_k = M^{-N} \sum_{m=1}^{M} \sum_{i} \sum_{k} \tilde{\alpha}_{ik}. \tag{8.29}$$

Note that the summations in (8.28) and (8.29) have a slightly different domain than the FER based scheduling metrics discussed in Sec. 7.3.2.

Note that the summations that appear in the group and individual metrics grow exponentially with the number the of users. Therefore, with larger numbers of users and BSs, ML criterion based scheduling metrics may become computationally inefficient. However, they are simple and efficient for small systems.

## 8.4 Summary

In this chapter, we have considered the idea of using long term CSI for user scheduling in a macrodiversity MU MIMO-MAC channel. In particular, CDI based user scheduling may be beneficial in CoMP systems where a limited backhaul interconnection network is present and the use of instantaneous CSI is restricted by delays and communication overheads. Despite the analytical difficulty in deriving scheduling metrics using CDI, in this chapter we have proposed user scheduling methods based on ergodic capacity, linear multiuser receivers and maximum likelihood decoding. Furthermore, we have derived several systematic group scheduling metrics and individual scheduling metrics.

# Chapter 9

# Conclusions and Future Work

Broadly speaking, the main focus of this thesis is the analytical investigation of fundamental performance measures for the macrodiversity MIMO-MAC. This investigation considers finite sized systems with completely arbitrary average link gain profiles, in contrast to simplified channel matrix assumptions, such as the classical Wyner model, widely used in network MIMO. Therefore, the results in this thesis may have applications in other areas where similar multivariate statistical problem arise. The analytical results can be useful in many different applications, such as:

- In contrast to previous ad-hoc approximations, our results reveal a direct functional link between fundamental performance measures and the average link gains. In some systems, the results give a remarkably simple, yet sophisticated relationship, while in other systems, the results may be rather complex. These functions gives system designers a greater range of options to optimize the performance of macrodiversity links.

- Analytical results can be used for efficient computation rather than using inefficient Monte-Carlo simulations which can greatly reduce the system design time. The exact results presented in the thesis can be used instead of simulation based methods for faster calculation of performance measures, even though analytical expressions are lengthy.

- If there is a requirement to further examine the statistical behavior over random average link gains (i.e., system level simulations involving averaging over the $\boldsymbol{P}$ matrix), our results save

hours of computation time. If Monte-Carlo simulation is used for averaging over both fast fading and slow fading, then this is highly inefficient. In contrast, the analytical results can be used for averaging over fast fading and simulation based methods can be used to average over slow fading.

- The analytical work fills a gap in our knowledge of wireless communication. The results are very attractive on some fronts, as far as their practical applications are concerned, while on other fronts, they turn out to be complex, but intriguing. We believe this will inspire future research for better, simpler and faster results in this area of communication and beyond.

More specific comments on the analytical methodologies and the results achieved in this research are summarized below followed by a brief description of potential future research.

## 9.1 Summary of Analysis and Key Results

### 9.1.1 MRC

Multiuser MRC receiver performance in a macrodiversity layout has been investigated in Chapter 3. We have considered a distributed antenna array performing MRC combining for a single antenna desired source in the presence of an arbitrary number of single antenna co-channel interferers. The analysis also covers the case where both the desired and interfering sources have multiple antennas. In particular, SER performance was derived in closed form for BPSK and QPSK modulations, but the analysis can be applied to $M$-QAM and a wide range of modulations where the SER can be written in terms of an expected value of the Gaussian $Q$-function and $Q^2$-function. Furthermore, the exact error floor and a simple power metric have been derived which provide some intuition about macrodiversity MRC performance. This analysis is based on identifying a simpler representation for the interference and noise terms in the combiner output. Analysis has shown that the macrodiversity MRC combiner can not resolve multiple interferers, but sense a single aggregate interferer, and the system performance is governed by the power trends of the desired user and aggregate interferer. In low SIR, the ratio of powers of the desired user against the aggregate

interferers plays the dominant role in SER performance. Here, good performance is achieved by opposing power trends which give some high ratios. However, in the high SIR scenario, greater diversity with an even spread of power across the antennas becomes more important. Even if some intuition concerning system performance can be gained using the power profiles, error floor and simple power metric, exact results are still necessary to provide an accurate performance measure. As a byproduct of the investigation of this chapter, we have presented two new probability integrals which have been solved in Appendix B.

### 9.1.2 Ergodic Sum Capacity

In Chapter 4, we have investigated the information theoretic capacity of the macrodiversity MU MIMO-MAC. In particular, the ergodic sum capacity has been considered in a Rayleigh flat fading environment with no CSI at the transmitter. The results obtained are shown to be valid for both independent channels and correlated channels, which may occur when some of the distributed transmit/receive locations have closely spaced antennas. The results remain valid for scenarios where the multiple antenna sources employ fixed per-antenna power control based on CDI. We derived exact results for the two-source scenario and approximate results for the general source case. Exact and approximate analytical results have been compared with simulation results and show good agreement. Furthermore, in the two-source scenario we have investigated the effect of macrodiversity on the ergodic capacity and found that, for equally strong (in the sense of the sum of the average link SNRs) users the ergodic sum capacity is greater than with very strong user and very weak user case. This suggests that balanced users (in the sense of link SNRs) may give better overall system performance. The general user approximations have a simple form and are shown to be very accurate over a wide range of channel powers. In addition, a simple upper bound is presented which demonstrates the importance of various channel power cross products in determining ergodic capacity. These bounds show that ergodic sum capacity is affected by the sum of the channel powers at low SNR, whereas at high SNR, the permanent of the channel power profile matric becomes important.

### 9.1.3 Dual User MMSE and ZF

In Chapter 5, we investigated more sophisticated linear combining systems, namely MMSE and ZF, in the macrodiversity MIMO-MAC. This diversity combining is particularly important because it has been proposed for future wireless standards such as those in 3GPP LTE-Advanced. However, the analytical investigation of MMSE/ZF receivers in a macrodiversity environment is a very difficult problem. Therefore, in Chapter 5, we have considered the dual user scenario with arbitrary numbers of distributed receive antennas where an exact analysis is possible. This analysis is possible for dual user scenarios because the characteristic function based analysis leads to an expected value of a ratio of correlated quadratic forms which can be calculated in closed form. For the dual user or dual source scenario, we have derived the exact cdf and pdf of the output SINR/SNR of MMSE/ZF receivers in a Rayleigh flat fading environment. Furthermore, we have presented exact and approximate high SNR SER performance results for commonly found modulation schemes which provide insights into both diversity and array gain. These high SNR SER results provide a sophisticated functional link between the performance of the macrodiversity system and the average link SNRs. Moreover, the approximate high SNR SER calculations revealed a compact power metric, in contrast to the exact high SNR SER results which gave an accurate, but relatively complex power metric. How the power trends of desired and interfering users interact with each other was investigated for some typical power trends to gain insight into system performance. Through the analysis, we identified that there is a considerable difference between the SER performance of MMSE and ZF receivers in the high SNR region before their performance converges at very high SNR values. This difference was successfully quantified through a metric and its accuracy was confirmed by simulation results. It was shown that parallel power trends for the users give greater differences in the SER performance of MMSE and ZF receivers in macrodiversity MIMO systems in Rayleigh flat fading.

### 9.1.4 Multi User MMSE and ZF

The analytical investigation in Chapter 6 extends the dual user results in Chapter 5 to arbitrary numbers of mutually interfering users. The exact performance of MMSE and ZF receivers in a macrodiversity MIMO layout is a long-standing, unsolved research problem. In this chapter, we made the first major progress towards solving this problem for the general case of an arbitrary number of transmit and receive antennas. The analysis was based on a derivation which targets the characteristic function of the output SINR. This led to an expected value which is highly complex in its exact form, but can be simplified by the use of an extended Laplace approximation. This methodology was able to produce approximate results for both the SINR distribution and the SER. The calculation of the SINR/SNR distributions of MMSE/ZF receivers allows us to calculate outage SINR/SNR and outage link level capacity with independent MMSE/ZF decoding. In addition, SER performance results for commonly found modulation schemes, provides insights into both diversity and array gain. The array gain results in turn have provided a direct functional link between the performance of the macrodiversity system and the link SNRs. We also investigated some special cases of the output SNR of ZF where the analysis collapses to simple forms revealing interesting links between the link SNRs and the SNR distribution. However, no such special cases could be found for the MMSE receiver performance. Furthermore, we have investigated the accuracy of the extended Laplace type approximation used at the heart of our analysis for both receiver types. We found that the MMSE receiver is more robust against extreme power profiles while the ZF results may be vulnerable to extreme link SNR scenarios. However, simulation results considered in this chapter show a similar accuracy for both receiver types under typical conditions. Note that the results presented in this chapter are simple enough to be employed as the basis of a scheduling algorithm. Since both SINR and SER results are available, scheduling can be performed on the basis of either metric.

### 9.1.5 MLD

In Chapter 7, we investigated the effect of macrodiversity on the performance of maximum likelihood detection. In particular, we considered the macrodiversity effect in Rayleigh and Rician fading environments. The analysis is based on the pairwise error probability. User SER performance has then been calculated using the exact PEP along with the well-known union bound for both Rayleigh and Rician fading. In order to get a simpler intuition about the link performance, high SNR approximations for the SER were also derived, which confirmed the well-known result that the diversity order of the ML receiver is equal to the number of receive antennas. Analytical results were checked with simulation results and shown to give good agreement. Various macrodiversity power profiles were compared through analysis and simulation and the behavior of the SER as a function of the power profiles was investigated. In terms of system performance, the importance of diversity (spreading the received powers over multiple receive antennas) is demonstrated. Also, channel power profiles which avoid strong interference for multiple sources are shown to be beneficial.

### 9.1.6 Multiuser Scheduling

Despite the analytical difficulty of analyzing macrodiversity MIMO systems, we have presented several performance results for the macrodiversity MIMO-MAC channel in terms of CDI. This opens up a mechanism to explore the performance of users in a macrodiversity system in terms of long term channel state information. Motivated by such results, in Chapter 8, we have extended the idea of using long term CSI for user scheduling in a macrodiversity MU MIMO-MAC channel. In particular, CDI based user scheduling is beneficial in CoMP systems where a limited backhaul interconnection network is present and the use of instantaneous CSI is restricted. We have proposed several user scheduling criteria based on information theoretical capacity, linear multiuser receivers and maximum likelihood decoding. Furthermore, we have presented several systematic group scheduling metrics and individual scheduling metrics which can be used at the heart of any scheduling algorithm. The suitability and applicability of these scheduling metrics requires further

investigation through large scale industry simulations, but it is likely that these metrics will perform well as they have a firm foundation and a strong functional relationship with fundamental performance measures like SER, SINR and information theoretic capacity.

## 9.2 Future Work

In this area, there are a vast number of additional problems which need further attention. Hence, we have identified below some particular topics that would be a useful basis for future work.

- **Explore Further Insights**: The analysis contained in the thesis covers a wide range of systems in modern wireless communication systems and reveals several insights. However, on some fronts, exploring further insights is restricted due to the complexity of the results. It will be exciting to explore methods to refine and simplify these results to obtain further insights.

- **Power Adaptation**: It is known that sum rate capacity can be further improved by a knowledge of CSI at the transmitters. Acquiring exact CSI is not realistic, but long term CSI can be acquired relatively easily. Therefore, further investigations to improve the ergodic sum rate by exploiting long term CSI such as the average link powers will be highly beneficial. This work will directly lead to power allocation methods in macrodiversity scenarios.

- **Limited Backhaul Systems**: Several distributed antenna elements are connected to form macrodiversity MIMO systems. In our system analysis, we have assumed that these links are perfect, high speed and lossless. In reality, these links will impose extra challenges for system analysis such as delays and other imperfections. It will be interesting to explore these factors and their effect on system performance.

- **Statistical Properties**: There are a large number of statistical properties of the macrodiversity channel matrix which are unknown. Eigenvalue and eigenvector distributions are two such examples. These statistical problems are very important in analyzing macrodiversity systems and beyond, but are known to be very difficult to tackle. Therefore, any statistical methods to deal with such random quantities will be invaluable.

# Appendix A

# Preliminary Mathematical Results

In this chapter we provide some basic results, concepts and related identities which are useful throughout this thesis.

## A.1 Matrix Identities

- *Laplace expansion of the determinant*: Let $\boldsymbol{X}$ be an $n \times n$ matrix with $(i,j)$th element $X_{i,j}$. Then the determinant

$$\det(\boldsymbol{X}) = \sum_{\{\alpha\}} (-1)^{\mathrm{per}(\alpha)} \prod_{k=1}^{n} X_{k,\alpha_k} \tag{A.1}$$

  where $\alpha = \{\alpha_1, \ldots, \alpha_n\}$ is a permutation of $\{1, \ldots, n\}$ with sign $(-1)^{\mathrm{per}(\alpha)}$, and the sum is over all such permutations. The expression $\mathrm{per}(\alpha)$ is the number of permutations needed to convert $\alpha$ in to its natural order.

- *Sylvester identity for the determinant*: Let $\boldsymbol{X}$ and $\boldsymbol{Y}$ be $n \times m$ and $m \times n$ matrices respectively. Then

$$\det(\boldsymbol{I}_n + \boldsymbol{XY}) = \det(\boldsymbol{I}_m + \boldsymbol{YX}). \tag{A.2}$$

- Let $\boldsymbol{X}$ and $\boldsymbol{Y}$ be $n \times n$ matrices. Then

$$\det(\boldsymbol{XY}) = \det(\boldsymbol{X})\det(\boldsymbol{Y}) = \det(\boldsymbol{YX}). \tag{A.3}$$

- Let $\boldsymbol{A}$ be an $n \times n$ matrix and $\boldsymbol{x}$ and $\boldsymbol{y}$ be $n \times 1$ vectors. Then, the following identity holds provided that the matrix $(\boldsymbol{A} + \boldsymbol{x}\boldsymbol{y}^H)$ is non-singular.

$$\det(\boldsymbol{A} \pm \boldsymbol{x}\boldsymbol{y}^H) = \det(\boldsymbol{A})(1 \pm \boldsymbol{y}^H\boldsymbol{A}^{-1}\boldsymbol{x}). \tag{A.4}$$

- Let $\boldsymbol{A}$, $\boldsymbol{B}$ and $\boldsymbol{C}$ be matrices of arbitrary dimension. Then

$$\mathrm{Tr}(\boldsymbol{ABC}) = \mathrm{Tr}(\boldsymbol{CAB}) = \mathrm{Tr}(\boldsymbol{BCA}) \tag{A.5}$$

- Let $\boldsymbol{A}$ be an $n \times n$ matrix and $\boldsymbol{x}$ and $\boldsymbol{y}$ be $n \times 1$ vectors. Then the following identity holds provided that the matrix $(\boldsymbol{A} + \boldsymbol{x}\boldsymbol{y}^H)$ is non-singular.

$$(A \pm \boldsymbol{x}\boldsymbol{y}^H)^{-1} = \boldsymbol{A}^{-1} \mp \frac{\boldsymbol{A}^{-1}\boldsymbol{x}\boldsymbol{y}^H\boldsymbol{A}^{-1}}{1 \pm \boldsymbol{y}^H\boldsymbol{A}^{-1}\boldsymbol{x}}. \tag{A.6}$$

## A.2 Permanent Identities

- Let $\boldsymbol{A} = (a_{ik})$ be an $m \times n$ matrix over the commutative ring, $m \leq n$. The permanent of $\boldsymbol{A}$, written $\mathrm{Perm}\,(\boldsymbol{A})$, is defined by

$$\mathrm{Perm}\,(\boldsymbol{A}) = \sum_{\sigma} a_{1,\sigma_1} a_{2,\sigma_2} \ldots a_{m,\sigma_m}, \tag{A.7}$$

  where the summation extends over all one-to-one functions from $\{1, \ldots, m\}$ to $\{1, \ldots, n\}$. The sequence $(a_{1,\sigma_1} a_{2,\sigma_2} \ldots a_{m,\sigma_m})$ is called a diagonal of $\boldsymbol{A}$, and the product $a_{1,\sigma_1} a_{2,\sigma_2} \ldots a_{m,\sigma_m}$ is a diagonal product of $\boldsymbol{A}$. Thus the permanent of $\boldsymbol{A}$ is the sum of all diagonal products of $\boldsymbol{A}$.

- Let $\boldsymbol{A}$ be an arbitrary $m \times n$ matrix, then

$$\sum_{\sigma} \mathrm{Perm}\left((\boldsymbol{A})_{\sigma_{k,m}}\right) = \sum_{\sigma} \mathrm{Perm}\left((\boldsymbol{A})^{\sigma_{k,n}}\right), \tag{A.8}$$

  where $\sigma_{k,n}$ is an ordered subset of $\{n\} = \{1, \ldots, n\}$ of length $k$ and the summation is over all

such subsets. $\sigma_{k,m}$ is also defined in similar fashion.

In general, $\boldsymbol{A}_{\sigma_{\ell,n}}^{\mu_{\ell,n}}$ denotes the submatrix of $\boldsymbol{A}$ formed by taking only the rows and columns indexed by $\sigma_{\ell,n}$ and $\mu_{\ell,n}$ respectively, where $\sigma_{\ell,n}$ and $\mu_{\ell,n}$ are length $\ell$ subsets of $\{1, 2, \ldots, n\}$. If either $\sigma_{\ell,n}$ or $\mu_{\ell,n}$ contains the complete set (i.e., $\sigma_{\ell,n} = \{1, 2, \ldots, n\}$ or $\mu_{\ell,n} = \{1, 2, \ldots, n\}$), the corresponding subscript/superscript may be dropped. When $\sigma_{\ell,n} = \mu_{\ell,n}$, only one subscript/superscript may be shown for brevity.

- Let $\boldsymbol{A}$ be an arbitrary $m \times n$ matrix, then

$$\sum_{\sigma} \text{Perm}\left((\boldsymbol{A})^{\sigma_{0,n}}\right) = \sum_{\sigma} \text{Perm}\left((\boldsymbol{A})_{\sigma_{0,m}}\right) = 1. \tag{A.9}$$

- For an empty matrix, $\boldsymbol{A}$,

$$\text{Perm}\left(\boldsymbol{A}\right) = 1. \tag{A.10}$$

## A.3 Algebraic Identities

- $$\frac{1}{\prod_{i=1}^{n_R}\left(a_i - jtb_i\right)} = \sum_{i=1}^{n_R} \frac{A_i}{\frac{a_i}{b_i} - jt}, \tag{A.11}$$

  where

$$A_i = \frac{b_i^{n_R-2}}{\prod_{k\neq i}^{n_R}\left(b_i a_k - a_i b_k\right)}.$$

- Let $e_k\left(X_1, X_2, \ldots, X_n\right)$ be the $k^{th}$ degree esf, then

$$e_k\left(X_1, X_2, \ldots, X_n\right) = \sum_{1\leq l_1<l_2<\cdots<l_k\leq n} X_{l_1} \ldots X_{l_k}. \tag{A.12}$$

  It is apparent from (A.12) that $e_0\left(X_1, X_2, \ldots, X_n\right) = 1$ and $e_n\left(X_1, X_2, \ldots, X_n\right) = X_1 X_2 \ldots X_n$. In general, the esf of degree $k$ in $n$ variables, for any $k \leq n$, is formed by adding together all distinct products of $k$ distinct variables.

- let $\boldsymbol{X}$ be an $n \times n$ complex symmetric positive definite matrix with eigenvalues $\lambda_1, \ldots, \lambda_n$. Then, the following identity holds.

$$e_k\left(\lambda_1, \lambda_2, \ldots, \lambda_n\right) = \mathrm{Tr}_k\left(\boldsymbol{X}\right),$$

where

$$\mathrm{Tr}_k\left(\boldsymbol{X}\right) = \begin{cases} \sum_\sigma \left|\boldsymbol{X}_{\sigma_{k,n}}\right| & 1 \leq k \leq n \\ 1 & k = 0 \\ 0 & k > n. \end{cases} \tag{A.13}$$

# A.4 Integral Identities

- *Exponential Integral*

$$E_1(x) = \int_x^\infty \frac{e^{-t}}{t} dt. \tag{A.14}$$

- *Gamma Function*

$$\Gamma(p) = \int_0^\infty t^{p-1} e^{-t} dt \qquad [\mathrm{Re}(p > 0)]. \tag{A.15}$$

- *Error Function*

$$\Phi(x) = \frac{2}{\sqrt{\pi}} \int_0^x e^{-t^2} dt. \tag{A.16}$$

- *Incomplete Gamma Function*

$$\Gamma(a, x) = \int_x^\infty t^{a-1} e^{-t} dt. \tag{A.17}$$

- *n-dimensional complex Gaussian integral*: Let $\boldsymbol{A}$ be an arbitrary $n \times n$ complex Hermitian

positive definite matrix. Then, the following integral identity holds.

$$\int_{-\infty}^{\infty} \dots \int_{-\infty}^{\infty} e^{-\boldsymbol{x}^H \boldsymbol{A} \boldsymbol{x}} dx_1 \dots dx_n = \frac{\pi^n}{|\boldsymbol{A}|}, \tag{A.18}$$

where $\boldsymbol{x}$ is a complex $n \times 1$ vector, $\boldsymbol{x} = [x_1, \dots, x_n]^T$ and $dx_i = dx_{iI} dx_{iQ}$, where $x_{iI} = \mathrm{Re}(x_i)$ and $x_{iQ} = \mathrm{Im}(x_i)$.

- $$\int_{-\infty}^{\infty} \frac{e^{-jpx}}{(\beta - jx)^v} dx = \begin{cases} \frac{2\pi p^{v-1} e^{-\beta p}}{\Gamma(v)} & p > 0 \\ 0 & p < 0, \end{cases}$$
$$[Re(v) > 0, Re(\beta) > 0]. \tag{A.19}$$

- $$\int_0^{\infty} \frac{dx}{(x+\alpha)(x+\beta)} = \frac{\ln(\beta/\alpha)}{\beta - \alpha}. \tag{A.20}$$

## A.5 Complex Gaussian Vector Distribution

Denote $\mathcal{CN}_n(\boldsymbol{\mu}, \boldsymbol{\Sigma})$ to be the n-variate complex Gaussian (Normal) distribution with mean vector, $\boldsymbol{\mu} \in \mathcal{C}^{n \times 1}$, and positive definite covariance matrix, $\boldsymbol{\Sigma} \in \mathcal{C}^{n \times n}$. Then, the complex Gaussian vector distribution is defined as below.

**Definition A.1.** *[13] The n-variate random vector $\boldsymbol{x}_n$ is said to have a multivariate vector Gaussian distribution with mean $\boldsymbol{\mu}$ and covariance $\boldsymbol{\Sigma}$ where $\boldsymbol{\Sigma} > 0$, if the elements of $\boldsymbol{x}_n$ have the joint pdf*

$$f(\boldsymbol{x}_n) = \frac{1}{\pi^n |\boldsymbol{\Sigma}|} e^{-(\boldsymbol{x}_n - \boldsymbol{\mu})^H \boldsymbol{\Sigma}^{-1} (\boldsymbol{x}_n - \boldsymbol{\mu})}. \tag{A.21}$$

# Appendix B

# Results for Chapter 3.

## B.1 Calculation of the cdf of $\gamma$

Since each term in the summation of (3.17) depends on the algebraic sign of $\beta_{ik}$, the final cdf has two parts as below

$$F_{\gamma}(r) = \sum_{i=1}^{n_R} \sum_{k \neq i}^{n_R} F_{ik}(r), \tag{B.1}$$

where $F_{ik}(r) = F_{ik}^{1}(r)$ for $\beta_{ik} > 0$ and $F_{ik}(r) = F_{ik}^{2}(r)$ for $\beta_{ik} < 0$. In subsection B.1.1 we derive $F_{ik}^{1}(r)$ followed by the derivation of $F_{ik}^{2}(r)$ in subsection B.1.2.

### B.1.1 Derivation of $F_{ik}^{1}(r)$

From the joint pdf in (3.17), when $\beta_{ik} > 0$, $F_{ik}^{1}(r)$ is given by

$$F_{ik}^{1}(r) = \iint_{\mathcal{F}_1} f_{X,Y}(x,y)\, dxdy, \tag{B.2}$$

where $\mathcal{F}_1 = \left\{x, y : x, y \geq 0, y - \frac{Q_i}{P_{i1}} x \geq 0, y - \frac{x^2}{r} \geq 0\right\}$. By using standard methods for 2-D integrals we arrive at

$$F_{ik}^1(r) = \frac{P_{i1}\xi_{ik}}{\beta_{ik}} - \xi_{ik} \int_{\frac{rQ_i}{P_{i1}}}^{\infty} \int_{\frac{xQ_i}{P_{i1}}}^{\frac{x^2}{r}} e^{-\frac{x}{P_{i1}}} e^{-\beta_{ik}\left(y - \frac{Q_i x}{P_{i1}}\right)} dy dx. \tag{B.3}$$

The final result then becomes

$$F_{ik}^1(r) = \frac{P_{i1}\xi_{ik}}{\beta_{ik}} \left(1 - e^{-\frac{rQ_i}{P_{i1}^2}}\right) + \frac{\xi_{ik}}{2\beta_{ik}} \sqrt{\frac{\pi r}{\beta_{ik}}} e^{\frac{r\omega_{ik}^2}{4\beta_{ik}}} \left(1 - \Phi\left(\sqrt{r\beta_{ik}}\alpha_{ik}\right)\right), \tag{B.4}$$

where

$$\omega_{ik} = \frac{1 - \beta_{ik} Q_i}{P_{i1}}, \tag{B.5a}$$

$$\alpha_{ik} = \frac{Q_i}{P_{i1}} + \frac{\omega_{ik}}{2\beta_{ik}}. \tag{B.5b}$$

The expression in (B.4) follows using standard methods of integration in (B.3) and employing the following integral identity [52] where necessary:

$$\int_{\alpha}^{\infty} e^{-\beta x^2} dx = \frac{1}{2}\sqrt{\frac{\pi}{\beta}} \left(1 - \Phi\left(\sqrt{\beta}\alpha\right)\right). \tag{B.6}$$

### B.1.2 Derivation of $F_{ik}^2(r)$

From the joint pdf in (3.17), when $\beta_{ik} < 0$, $F_{ik}^2(r)$ is given by

$$F_{ik}^2(r) = \iint_{\mathcal{F}_2} f_{X,Y}(x, y)\, dx dy, \tag{B.7}$$

where $\mathcal{F}_2 = \left\{x, y : x, y \geq 0, y - \frac{Q_i}{P_{i1}} x \leq 0, y - \frac{x^2}{r} \geq 0\right\}$. By using standard methods for 2-D integrals we arrive at

$$F_{ik}^2(r) = -\xi_{ik} \int_{0}^{\frac{rQ_i}{P_{i1}}} \int_{\frac{x^2}{r}}^{\frac{xQ_i}{P_{i1}}} e^{-\frac{x}{P_{i1}}} e^{-\beta_{ik}\left(y - \frac{Q_i x}{P_{i1}}\right)} dy dx. \tag{B.8}$$

The final result then becomes

$$F_{ik}^{2}(r)=\frac{P_{i1}\xi_{ik}}{\beta_{ik}}\left(1-e^{-\frac{rQ_{i}}{P_{i1}^{2}}}\right)-\frac{\xi_{ik}}{2\beta_{ik}}\sqrt{\frac{\pi r}{-\beta_{ik}}}e^{\frac{r\omega_{ik}^{2}}{4\beta_{ik}}}\left(\mathrm{erfi}\left(\sqrt{-r\beta_{ik}}\alpha_{ik}\right)+\mathrm{erfi}\left(\frac{1}{2}\sqrt{\frac{r}{-\beta_{ik}}}\omega_{ik}\right)\right), \tag{B.9}$$

where

$$\mathrm{erfi}(x)=\frac{\Phi(jx)}{j}. \tag{B.10}$$

The function erfi(.) is the error function with a complex argument defined in [52]. Note that the square roots appearing in (B.9) are the positive square root of $\beta_{ik}$. The expression in (B.9) follows using standard methods of integration and employing the following integral identity [52] where necessary:

$$\int e^{ax^{2}}dx=\frac{1}{2}\sqrt{\frac{\pi}{a}}\mathrm{erfi}\left(\sqrt{a}x\right). \tag{B.11}$$

## B.2 Derivation of the exact SER

The integral in (3.42) is required for the exact SER analysis. Substituting $F_{\gamma}\left(w^{2}/b\right)$ from (3.27) into (3.42) gives two new integrals involving $F_{ik}^{1}\left(w^{2}/b\right)$ or $F_{ik}^{2}\left(w^{2}/b\right)$, which are given in (B.4) and (B.9). These two integrals can be written in terms of known functions and two fundamental probability integrals that we denote $I_{1}(\alpha,\beta)$ and $I_{2}(\alpha,\beta)$. These integrals are computed below.

### B.2.1 Integral Form I

Consider the integral,

$$I_{1}(\alpha,\beta)=\int_{0}^{\infty}xe^{-\beta x^{2}}Q(x)\,\Phi(j\alpha x)\,dx. \tag{B.12}$$

Applying the integral forms of $Q(.)$ and $\Phi(.)$ gives

$$I_1(\alpha,\beta) = \frac{2j}{\pi}\int_0^{\infty}\int_{\frac{x}{\sqrt{2}}}^{\infty}\int_0^{\alpha x} x e^{-\beta x^2 - t_1^2 + t_2^2} dt_2 dt_1 dx. \tag{B.13}$$

Using the substitutions, $t_1 = r\cos\theta$ and $t_2 = r\sin\theta$, the integral then becomes

$$I_1(\alpha,\beta) = \frac{2j}{\pi}\int_0^{\infty}\int_0^{\phi}\int_{r_1}^{r_2} x r e^{-\beta x^2 - r^2 cos\,2\theta}\, dr d\theta dx, \tag{B.14}$$

where $\tan\phi = \alpha\sqrt{2}$, $r_1 = x/\sqrt{2}\cos\theta$ and $r_2 = \alpha x/\sin\theta$. Using standard methods of integration with some simplifications we obtain

$$I_1(\alpha,\beta) = \frac{j}{2\pi\beta}\int_0^{\alpha\sqrt{2}} \frac{dt}{t^2 - 1 - 2\beta} - \frac{j\alpha^2}{2\pi\beta}\int_0^{\alpha\sqrt{2}} \frac{dt}{(\alpha^2-\beta)\,t^2 - \alpha^2}. \tag{B.15}$$

Defining

$$I_{11}(\alpha,\beta) = \int_0^{\alpha\sqrt{2}} \frac{dt}{t^2 - 1 - 2\beta}, \tag{B.16}$$

$$I_{12}(\alpha,\beta) = \int_0^{\alpha\sqrt{2}} \frac{dt}{(\alpha^2-\beta)\,t^2 - \alpha^2}, \tag{B.17}$$

allows (B.15) to be rewritten as

$$I_1(\alpha,\beta) = \frac{j}{2\pi\beta} I_{11}(\alpha,\beta) - \frac{j\alpha^2}{2\pi\beta} I_{12}(\alpha,\beta). \tag{B.18}$$

The integral in (B.16) and (B.17) can be solved in closed form to give

$$I_{11}(\alpha,\beta) = -\frac{1}{\sqrt{2\beta+1}}\tanh^{-1}\left(\frac{\alpha\sqrt{2}}{\sqrt{2\beta+1}}\right) \tag{B.19}$$

and

$$I_{12}(\alpha,\beta) = \begin{cases} -\frac{\sqrt{2}}{\alpha} & \beta = \alpha^2 \\ -\frac{1}{\alpha\sqrt{\beta-\alpha^2}}\tan^{-1}\left(\sqrt{2\,(\beta-\alpha^2)}\right) & \text{otherwise.} \end{cases} \tag{B.20}$$

Note that some intermediate steps in the derivation show that $1+2\beta > 2\alpha^2$ is required for the existence of (B.12). This constraint is satisfied by the current problem. This can easily be seen by substituting the arguments of both $I_1(.,.)$ functions in (3.45) in to $1+2\beta > 2\alpha^2$ followed by simplifications using (B.5).

### B.2.2 Integral Form II

Consider the integral,

$$I_2(\alpha,\beta) = \int_0^\infty x e^{\beta x^2} Q(x)\left(1-\Phi(\alpha x)\right) dx. \tag{B.21}$$

Applying the integral forms of $Q(.)$ and $\Phi(.)$ we obtain

$$I_2(\alpha,\beta) = \frac{2}{\pi}\int_0^\infty \int_{\frac{x}{\sqrt{2}}}^\infty \int_{\alpha x}^\infty x e^{\beta x^2 - t_1^2 - t_2^2} dt_2 dt_1 dx. \tag{B.22}$$

Following the same procedure as in Appendix B.2.1 and with some simplifications we arrive at

$$I_2(\alpha,\beta) = \frac{\alpha^2}{2\pi\beta}\int_0^\phi \frac{d\theta}{\alpha^2 - \beta\sin^2\theta} + \frac{1}{2\pi\beta}\int_\phi^{\pi/2} \frac{d\theta}{1-2\beta\cos^2\theta} - \frac{1}{4\beta}, \tag{B.23}$$

where $\tan\phi = \sqrt{2}\alpha$. Making another substitution as $t = \tan\theta$ in (B.23) gives

$$I_2(\alpha,\beta) = \frac{\alpha^2}{2\pi\beta}\int_0^{\sqrt{2}\alpha} \frac{dt}{(\alpha^2-\beta)t^2+\alpha^2} + \frac{1}{2\pi\beta}\int_{\sqrt{2}\alpha}^\infty \frac{dt}{t^2+1-2\beta} - \frac{1}{4\beta}. \tag{B.24}$$

Defining

$$I_{21}(\alpha,\beta) = \int_0^{\sqrt{2}\alpha} \frac{dt}{(\alpha^2-\beta)t^2+\alpha^2}, \tag{B.25}$$

$$I_{22}(\alpha,\beta) = \int_{\sqrt{2}\alpha}^\infty \frac{dt}{t^2+1-2\beta}, \tag{B.26}$$

allows (B.24) to be rewritten as

$$I_2(\alpha,\beta) = \frac{\alpha^2}{2\pi\beta} I_{21}(\alpha,\beta) + \frac{1}{2\pi\beta} I_{22}(\alpha,\beta) - \frac{1}{4\beta}. \tag{B.27}$$

The integrals in (B.25) and (B.26) can be solved in closed form to give

$$I_{21}(\alpha,\beta)=\begin{cases}\frac{\sqrt{2}}{\alpha} & \alpha^2=\beta \\ \frac{1}{\alpha\sqrt{\alpha^2-\beta}}\tan^{-1}\left(\sqrt{2\left(\alpha^2-\beta\right)}\right) & \text{otherwise}\end{cases} \tag{B.28}$$

and

$$I_{22}(\alpha,\beta)=\begin{cases}\frac{1}{\sqrt{2}\alpha} & 1=2\beta \\ \frac{1}{\sqrt{2\beta-1}}\coth^{-1}\left(\frac{\sqrt{2}\alpha}{\sqrt{2\beta-1}}\right) & \text{otherwise.}\end{cases} \tag{B.29}$$

As for $I_1(\alpha,\beta)$ there is an associated region of validity, $1+2\alpha^2>2\beta$, which is satisfied by the problem.

# Appendix C

# Results for Chapter 4.

## C.1 Derivation of $I_b$

From (4.29), $I_b$ can be written as

$$I_b = \left.\frac{\partial \tilde{I}_b}{\partial \theta_1}\right|_{\theta_1=0}, \tag{C.1}$$

where

$$\tilde{I}_b = -\int_0^\infty\int_0^\infty \frac{e^{-\sigma^2 t-\sigma^2\theta_2}}{\prod_{i=1}^{n_R}(1+tP_{i2}+\theta_1 P_{i1}P_{i2}+\theta_2 P_{i1})}d\theta_2 dt. \tag{C.2}$$

From (C.2), $L_b$ becomes

$$L_b = \int_0^\infty\int_0^\infty \frac{e^{-\sigma^2 t-\sigma^2\theta_2}}{\prod_{i=1}^{n_R}\left(\theta_1+\frac{\theta_2}{P_{i2}}+\frac{t}{P_{i1}}+\frac{1}{P_{i1}P_{i2}}\right)}d\theta_2 dt. \tag{C.3}$$

Defining

$$L_b = -\left|\boldsymbol{P}_1\boldsymbol{P}_2\right|\tilde{I}_b, \tag{C.4}$$

we use a partial fraction expansion in $\theta_1$ to give

$$L_b = \sum_{i=1}^{n_R} \int_0^\infty \int_0^\infty \frac{A_i\left(\theta_2, t\right) e^{-\sigma^2 t - \sigma^2 \theta_2}}{\left(\theta_1 + \frac{\theta_2}{P_{i2}} + \frac{t}{P_{i1}} + \frac{1}{P_{i1}P_{i2}}\right)} d\theta_2 dt, \tag{C.5}$$

where

$$A_i\left(\theta_2, t\right) = \frac{1}{\prod_{k\neq i}^{n_R}\left(\alpha_{ik}\theta_2 + \beta_{ik}t + \gamma_{ik}\right)} \tag{C.6a}$$

$$\alpha_{ik} = \frac{1}{P_{k2}} - \frac{1}{P_{i2}} \tag{C.6b}$$

$$\beta_{ik} = \frac{1}{P_{k1}} - \frac{1}{P_{i1}} \tag{C.6c}$$

$$\gamma_{ik} = R_k - R_i \tag{C.6d}$$

$$R_i = \frac{1}{P_{i1}P_{i2}}. \tag{C.6e}$$

To compute (C.5), the following substitutions are employed

$$u = \sigma^2 t + \sigma^2 \theta_2 \tag{C.7a}$$

$$v_i = \frac{t}{P_{i1}} + \frac{\theta_2}{P_{i2}}. \tag{C.7b}$$

The Jacobian of the transformation in (C.7b) can be calculated as

$$J_i = \sigma^2 \left(\frac{1}{P_{i2}} - \frac{1}{P_{i1}}\right). \tag{C.8}$$

Substituting (C.7b) and (C.8) in (C.5) gives

$$L_b = \sum_{i=1}^{n_R} \int_0^\infty \int_{\frac{u}{P_{i1}\sigma^2}}^{\frac{u}{P_{i2}\sigma^2}} \frac{A_i\left(u, v_i\right) e^{-u}}{J_i\left(v_i + \theta_1 + R_i\right)} dv_i du, \tag{C.9}$$

where

$$A_i\left(u, v_i\right) = \frac{1}{\prod_{k\neq i}^{n_R}\left(a_{ik}v_i + b_{ik}u + \gamma_{ik}\right)} \tag{C.10a}$$

$$a_{ik} = \frac{\sigma^2}{J_i}\left(\alpha_{ik} - \beta_{ik}\right) \tag{C.10b}$$

$$b_{ik} = \frac{1}{J_i}\left(\frac{\beta_{ik}}{P_{i2}} - \frac{\alpha_{ik}}{P_{i1}}\right). \tag{C.10c}$$

The term $A_i\left(u, v_i\right)$ in (C.10a) can be written as a summation using partial fractions, to give

$$A_i\left(u, v_i\right) = \sum_{k\neq i}^{n_R} \frac{B_{ik}\left(u\right)}{v_i + q_{ik}u + r_{ik}}, \tag{C.11}$$

where

$$B_{ik}\left(u\right) = \frac{\left(a_{ik}\right)^{n_R-3}}{\prod_{l\neq i,k}^{n_R}\left(c_{ikl}u + d_{ikl}\right)} \tag{C.12a}$$

$$c_{ikl} = b_{il}a_{ik} - a_{il}b_{ik} \tag{C.12b}$$

$$d_{ikl} = a_{ik}\gamma_{il} - \gamma_{ik}a_{il} \tag{C.12c}$$

$$q_{ik} = \frac{b_{ik}}{a_{ik}} \tag{C.12d}$$

$$r_{ik} = \frac{\gamma_{ik}}{a_{ik}}. \tag{C.12e}$$

Substituting (C.11) in (C.9) and simplifying gives

$$L_b = \sum_{i=1}^{n_R}\sum_{k\neq i}^{n_R}\int_0^{\infty}\int_{\frac{u}{P_{i1}\sigma^2}}^{\frac{u}{P_{i2}\sigma^2}} \frac{B_{ik}\left(u\right)e^{-u}}{J_i}\,\frac{dv_i du}{\left(v_i + \theta_1 + R_i\right)\left(v_i + q_{ik}u + r_{ik}\right)}\,. \tag{C.13}$$

First, we integrate over $v_i$ in (C.13) to give

$$L_b = \sum_{i=1}^{n_R}\sum_{k\neq i}^{n_R}\int_0^{\infty}\frac{C_{ik}\left(u, \theta_1\right)e^{-u}}{J_i}\ln\left[\frac{\left(\frac{u}{P_{i2}\sigma^2} + \theta_1 + R_i\right)\left(\lambda_{ik}u + r_{ik}\right)}{\left(\frac{u}{P_{i1}\sigma^2} + \theta_1 + R_i\right)\left(\mu_{ik}u + r_{ik}\right)}\right]du, \tag{C.14}$$

where

$$C_{ik}\left(u,\theta_1\right)=\frac{B_{ik}\left(u\right)}{q_{ik}u+r_{ik}-\theta_1-R_i} \tag{C.15a}$$

$$\lambda_{ik}=\frac{1}{P_{i1}\sigma^2}+q_{ik} \tag{C.15b}$$

$$\mu_{ik}=\frac{1}{P_{i2}\sigma^2}+q_{ik}. \tag{C.15c}$$

Let

$$D_{ik}\left(u,\theta_1\right)=\ln\left[\frac{\left(\frac{u}{P_{i2}\sigma^2}+\theta_1+R_i\right)\left(\lambda_{ik}u+r_{ik}\right)}{\left(\frac{u}{P_{i1}\sigma^2}+\theta_1+R_i\right)\left(\mu_{ik}u+r_{ik}\right)}\right], \tag{C.16a}$$

then $B_{ik}\left(u\right)$ in (C.12a) can be rewritten as the summation

$$B_{ik}\left(u\right)=\sum_{l\neq i,k}^{n_R}\frac{\xi_{ikl}}{c_{ikl}u+d_{ikl}}, \tag{C.17}$$

where

$$\xi_{ikl}=\frac{\left(a_{ik}c_{ikl}\right)^{n_R-3}}{\prod_{z\neq i,k,l}^{n_R}\left(d_{ikz}c_{ikl}-c_{ikz}d_{ikl}\right)}. \tag{C.18}$$

Substituting (C.17) and (C.15c) in (C.14) gives

$$L_b=\sum_{i=1}^{n_R}\sum_{k\neq i}^{n_R}\sum_{l\neq i,k}^{n_R}\int_0^\infty D_{ik}\left(u,\theta_1\right)\frac{\xi_{ikl}}{J_i}\frac{du}{\left(c_{ikl}u+d_{ikl}\right)\left(q_{ik}u+r_{ik}-\theta_1-R_i\right)}. \tag{C.19}$$

Equation (C.19) can be further simplified to give

$$L_b=\sum_{i=1}^{n_R}\sum_{k\neq i}^{n_R}\sum_{l\neq i,k}^{n_R}\frac{\xi_{ikl}\left(M_{b_{ikl}}-N_{b_{ikl}}\right)}{J_i}, \tag{C.20}$$

where

$$M_{b_{ikl}}=\int_0^\infty\frac{D_{ik}\left(u,\theta_1\right)}{f_1\left(\theta_1\right)}\frac{du}{\left(u+\varepsilon_{ikl}\right)}, \tag{C.21}$$

$$N_{b_{ikl}} = \int_0^\infty \frac{D_{ik}\left(u, \theta_1\right)}{f_1\left(\theta_1\right)} \frac{du}{\left(u + f_2\left(\theta_1\right)\right)}, \tag{C.22}$$

and $\varepsilon_{ikl} = d_{ikl}/c_{ikl}$. Next, we introduce the following linear functions of $\theta_1$:

$$f_1\left(\theta_1\right) = n_{ikl} - c_{ikl}\theta_1 \tag{C.23}$$

$$f_2\left(\theta_1\right) = m_{ikl} - \frac{\theta_1}{q_{ik}}, \tag{C.24}$$

where

$$n_{ikl} = r_{ik}c_{ikl} - d_{ikl}q_{ik} - \frac{c_{ikl}}{R_i} \tag{C.25}$$

$$m_{ikl} = \frac{\gamma_{ik}}{b_{ik}} - \frac{1}{q_{ik}R_i}. \tag{C.26}$$

Next, we can differentiate $M_{b_{ikl}}$ and $N_{b_{ikl}}$ and integrate over $u$ to give the final result along with (C.1) and (C.4). Hence, from (C.23) and (C.16a) we get (C.27). Substituting (C.27) in (C.21) and (C.22) we get (C.28) and (C.29). (C.28) and (C.29) can be solved in closed form to give (C.30) and (C.31), where we have used the two integrals defined as follows

$$H_1\left(a, b, c\right) = \int_0^\infty \frac{e^{-t}\ln\left(ct + a\right)}{t + b} dt \tag{C.32}$$

$$H_2\left(a, b, c\right) = \int_0^\infty \frac{e^{-t}\ln\left(ct + a\right)}{\left(t + b\right)^2} dt \tag{C.33}$$

and the constants are given by

$$\varepsilon'_{ikl} = \frac{1}{\left(\varepsilon_{ikl} - \frac{\sigma^2}{P_{i1}}\right)}, \quad \varepsilon''_{ikl} = \frac{1}{\left(\varepsilon_{ikl} - \frac{\sigma^2}{P_{i2}}\right)},$$
$$m'_{ikl} = \frac{1}{\left(m_{ikl} - \frac{\sigma^2}{P_{i1}}\right)}, \quad m''_{ikl} = \frac{1}{\left(m_{ikl} - \frac{\sigma^2}{P_{i2}}\right)}.$$

Both $H_1$ and $H_2$ can be solved in closed form as

$$H_1\left(a, b, c\right) = e^b \left[E_1\left(b\right)\ln c + D_1\left(\frac{a}{c} - b, b\right)\right],$$

$$\frac{\partial}{\partial\theta_1}\left[\frac{D_{ik}\left(u,\theta_1\right)}{f_1\left(\theta_1\right)}\right]_{\theta_1=0}=\frac{c_{ikl}}{n_{ikl}^2}\ln\left[\frac{\left(\frac{u}{P_{i2}\sigma^2}+R_i\right)\left(\lambda_{ik}u+r_{ik}\right)}{\left(\frac{u}{P_{i1}\sigma^2}+R_i\right)\left(\mu_{ik}u+r_{ik}\right)}\right]+\frac{1}{n_{ikl}}\left[\frac{P_{i2}\sigma^2}{\left(u+\frac{\sigma^2}{P_{i1}}\right)}-\frac{P_{i1}\sigma^2}{\left(u+\frac{\sigma^2}{P_{i2}}\right)}\right] \tag{C.27}$$

$$\tilde{M}_{b_{ikl}}=\left.\frac{\partial M_{b_{ikl}}}{\partial\theta_1}\right|_{\theta_1=0}=\int_0^\infty\frac{\partial}{\partial\theta_1}\left[\frac{D_{ik}\left(u,\theta_1\right)}{f_1\left(\theta_1\right)}\right]_{\theta_1=0}\frac{du}{\left(u+e_{ikl}\right)} \tag{C.28}$$

$$\tilde{N}_{b_{ikl}}=\left.\frac{\partial N_{b_{ikl}}}{\partial\theta_1}\right|_{\theta_1=0}=\int_0^\infty\frac{\partial}{\partial\theta_1}\left[\frac{D_{ik}\left(u,\theta_1\right)}{f_1\left(\theta_1\right)}\right]_{\theta_1=0}\frac{du}{\left(u+m_{ikl}\right)}+\int_0^\infty\left[\frac{D_{ik}\left(u,\theta_1\right)}{f_1\left(\theta_1\right)}\right]_{\theta_1=0}\frac{1/q_{ik}}{\left(u+m_{ikl}\right)^2}du \tag{C.29}$$

---

$$\begin{aligned}\tilde{M}_{b_{ikl}}=&\frac{c_{ikl}}{n_{ikl}^2}\left[H_1\left(R_i,\varepsilon_{ikl},\frac{1}{P_{i2}\sigma^2}\right)+H_1\left(r_{ik},\varepsilon_{ikl},\lambda_{ik}\right)-H_1\left(R_i,\varepsilon_{ikl},\frac{1}{P_{i1}\sigma^2}\right)-H_1\left(r_{ik},\varepsilon_{ikl},\mu_{ik}\right)\right]\\&+\frac{\varepsilon'_{ikl}}{n_{ikl}}\left[e^{\frac{\sigma^2}{P_{i1}}}E_1\left(\frac{\sigma^2}{P_{i1}}\right)-e^{\varepsilon_{ikl}}E_1\left(\varepsilon_{ikl}\right)\right]-\frac{\varepsilon''_{ikl}}{n_{ikl}}\left[e^{\frac{\sigma^2}{P_{i2}}}E_1\left(\frac{\sigma^2}{P_{i2}}\right)-e^{\varepsilon_{ikl}}E_1\left(\varepsilon_{ikl}\right)\right],\end{aligned} \tag{C.30}$$

---

$$\begin{aligned}\tilde{N}_{b_{ikl}}=&\frac{c_{ikl}}{n_{ikl}^2q_{ik}}\left[H_2\left(R_i,m_{ikl},\frac{1}{P_{i2}\sigma^2}\right)+H_2\left(r_{ik},m_{ikl},\lambda_{ik}\right)-H_2\left(R_i,m_{ikl},\frac{1}{P_{i1}\sigma^2}\right)-H_2\left(r_{ik},m_{ikl},\mu_{ik}\right)\right]\\&+\frac{c_{ikl}}{n_{ikl}^2}\left[H_1\left(R_i,m_{ikl},\frac{1}{P_{i2}\sigma^2}\right)+H_1\left(r_{ik},m_{ikl},\lambda_{ik}\right)-H_1\left(R_i,m_{ikl},\frac{1}{P_{i1}\sigma^2}\right)-H_1\left(r_{ik},m_{ikl},\mu_{ik}\right)\right]\\&+\frac{m'_{ikl}}{n_{ikl}}\left[e^{\frac{\sigma^2}{P_{i1}}}E_1\left(\frac{\sigma^2}{P_{i1}}\right)-e^{m_{ikl}}E_1\left(m_{ikl}\right)\right]-\frac{m''_{ikl}}{n_{ikl}}\left[e^{\frac{\sigma^2}{P_{i2}}}E_1\left(\frac{\sigma^2}{P_{i2}}\right)-e^{m_{ikl}}E_1\left(m_{ikl}\right)\right],\end{aligned} \tag{C.31}$$

---

$$H_2\left(a,b,c\right)=\ln c\left[\frac{1}{b}-e^bE_1\left(b\right)\right]-2e^bD_1\left(\frac{a}{c}-b,b\right)+\frac{1}{\left(\frac{a}{c}-b\right)}\left[e^bE_1\left(b\right)-e^{\frac{a}{c}}E_1\left(\frac{a}{c}\right)\right],$$

where $D_1(a,b)$ is defined by

$$D_1(a,b)=\int_b^\infty\frac{e^{-t}\ln\left(t+a\right)}{t}dt,\quad\text{for}\quad b\neq0.$$

## C.2 Calculation of $E\left\{\left|\sigma^2\boldsymbol{I}+\tilde{\boldsymbol{H}}_k^H\tilde{\boldsymbol{H}}_k\right|\right\}$

Let $\lambda_1,\lambda_2,\ldots,\lambda_{k-1}$ be the ordered eigenvalues of $\tilde{\boldsymbol{H}}_k^H\tilde{\boldsymbol{H}}_k$. Since $n_R\geq(k-1)$, all eigenvalues are non zero. Then,

$$\begin{aligned}E\left\{\left|\sigma^2\boldsymbol{I}+\tilde{\boldsymbol{H}}_k^H\tilde{\boldsymbol{H}}_k\right|\right\}&=E\left\{\prod_{i=1}^{k-1}\left(\sigma^2+\lambda_i\right)\right\}\\&=E\left\{\sum_{i=0}^{k-1}\mathrm{Tr}_i\left(\tilde{\boldsymbol{H}}_k^H\tilde{\boldsymbol{H}}_k\right)\left(\sigma^2\right)^{k-i-1}\right\},\end{aligned}\tag{C.34}$$

where (C.34) is from (A.12) and (A.13). Therefore, the building block of this expectation is $E\left\{\mathrm{Tr}_i\left(\tilde{\boldsymbol{H}}_k^H\tilde{\boldsymbol{H}}_k\right)\right\}$. From (A.13)

$$\mathrm{Tr}_i\left(\tilde{\boldsymbol{H}}_k^H\tilde{\boldsymbol{H}}_k\right)=\sum_{\sigma}\left|\left(\tilde{\boldsymbol{H}}_k^H\tilde{\boldsymbol{H}}_k\right)_{\sigma_{i,k-1}}\right|.\tag{C.35}$$

Therefore, from Lemma 4.1,

$$E\left\{\mathrm{Tr}_i\left(\tilde{\boldsymbol{H}}_k^H\tilde{\boldsymbol{H}}_k\right)\right\}=\sum_{\sigma}\mathrm{Perm}\left(\left(\boldsymbol{Q}_k\right)^{\sigma_{i,k-1}}\right),$$

where the $n_R\times(k-1)$ matrix, $\boldsymbol{Q}_k$, is given by

$$E\left\{\tilde{\boldsymbol{H}}_k\circ\tilde{\boldsymbol{H}}_k\right\}=\boldsymbol{Q}_k.\tag{C.36}$$

Note that summation in (C.36) has $\binom{k-1}{i}$ terms. Then, the final expression becomes

$$E\left\{\left|\sigma^2\boldsymbol{I}+\tilde{\boldsymbol{H}}_k^H\tilde{\boldsymbol{H}}_k\right|\right\}=\sum_{i=0}^{k-1}\sum_{\sigma}\mathrm{Perm}\left(\left(\boldsymbol{Q}_k\right)^{\sigma_{i,k-1}}\right)\left(\sigma^2\right)^{k-i-1}.\tag{C.37}$$

## C.3 Calculation of $|\boldsymbol{\Sigma}_k| \, E\left\{\left|\sigma^2\boldsymbol{I}+\tilde{\boldsymbol{H}}_k^H\boldsymbol{\Sigma}_k^{-1}\tilde{\boldsymbol{H}}_k\right|\right\}$

A simple extension of (4.39) allows the expectation in the denominator of (4.38) to be calculated as

$$E\left\{\left|\sigma^2\boldsymbol{I}+\tilde{\boldsymbol{H}}_k^H\boldsymbol{\Sigma}_k^{-1}\tilde{\boldsymbol{H}}_k\right|\right\}=\sum_{i=0}^{k-1}\psi_{ki}\left(t\right)\left(\sigma^2\right)^{k-i-1}, \tag{C.38}$$

where

$$\psi_{ki}\left(t\right)=\sum_{\sigma}\mathrm{Perm}\left(\left(\boldsymbol{\Sigma}_k^{-1}\boldsymbol{Q}_k\right)^{\sigma_{i,k-1}}\right), \tag{C.39}$$

and (A.9)

$$\psi_{k0}\left(t\right)=1.$$

The term in (C.39) can be simplified using (A.8) to obtain

$$\psi_{ki}\left(t\right)=\sum_{\sigma}\frac{\mathrm{Perm}\left(\left(\boldsymbol{Q}_k\right)_{\sigma_{i,n_R}}^{\{k-1\}}\right)}{\left|\left(\boldsymbol{\Sigma}_k\right)_{\sigma_{i,n_R}}\right|}. \tag{C.40}$$

Then,

$$|\boldsymbol{\Sigma}_k| \, E\left\{\left|\sigma^2\boldsymbol{I}+\tilde{\boldsymbol{H}}_k^H\boldsymbol{\Sigma}_k^{-1}\tilde{\boldsymbol{H}}_k\right|\right\}=\sum_{i=0}^{k-1}\xi_{ki}\left(t\right)\left(\sigma^2\right)^{k-i-1}, \tag{C.41}$$

where $\xi_{ki}\left(t\right)=|\boldsymbol{\Sigma}_k|\,\psi_{ki}\left(t\right)$. From (C.40), we obtain

$$\xi_{ki}\left(t\right)=\sum_{\sigma}\left|\left(\boldsymbol{\Sigma}_k\right)_{\bar{\sigma}_{n_R-i,n_R}}\right|\mathrm{Perm}\left(\left(\boldsymbol{Q}_k\right)_{\sigma_{i,n_R}}^{\{k-1\}}\right), \tag{C.42}$$

where $\bar{\sigma}_{n_R-i,n_R}$ is the compliment of $\sigma_{i,n_R}$. Therefore, it is apparent that $\xi_{ki}\left(t\right)$ is a polynomial of degree $n_R-i$. Clearly $|\boldsymbol{\Sigma}_k| \, E\left\{\left|\sigma^2\boldsymbol{I}+\tilde{\boldsymbol{H}}_k^H\boldsymbol{\Sigma}_k^{-1}\tilde{\boldsymbol{H}}_k\right|\right\}$ is a polynomial of degree $n_R$, since $\xi_{k0}\left(t\right)=|\boldsymbol{\Sigma}_k|$

is the highest degree polynomial term in $t$ in (C.41). Then,

$$\left|(\boldsymbol{\Sigma}_k)_{\bar{\sigma}_{n_R-i,n_R}}\right| = \sum_{l=0}^{n_R-i}\left(\frac{t}{\sigma^2}\right)^l \mathrm{Tr}_l\left((\boldsymbol{P}_k)_{\bar{\sigma}_{n_R-i,n_R}}\right). \tag{C.43}$$

Hence, applying (C.43) in (C.42),

$$\xi_{ki}(t) = \sum_{\sigma}\sum_{l=0}^{n_R-i}\left(\frac{t}{\sigma^2}\right)^l \mathrm{Tr}_l\left((\boldsymbol{P}_k)_{\bar{\sigma}_{n_R-i,n_R}}\right)\mathrm{Perm}\left((\boldsymbol{Q}_k)^{\{k-1\}}_{\sigma_{i,n_R}}\right),$$

and $\xi_{ki}(t)$ becomes

$$\xi_{ki}(t) = \sum_{l=0}^{n_R-i}\left(\frac{t}{\sigma^2}\right)^l \hat{\varphi}_{kli} \tag{C.44}$$

$$= \sum_{l=0}^{n_R}\left(\frac{t}{\sigma^2}\right)^l \hat{\varphi}_{kli}, \tag{C.45}$$

where

$$\hat{\varphi}_{kli} = \sum_{\sigma}\mathrm{Tr}_l\left((\boldsymbol{P}_k)_{\bar{\sigma}_{n_R-i,n_R}}\right)\mathrm{Perm}\left((\boldsymbol{Q}_k)^{\{k-1\}}_{\sigma_{i,n_R}}\right),$$

and from (A.9), $\hat{\varphi}_{kl0}$ simplifies to give

$$\hat{\varphi}_{kl0} = \mathrm{Tr}_l(\boldsymbol{P}_k).$$

Equation (C.45) follows from (C.44) due to the fact that

$$\mathrm{Tr}_l\left((\bar{\boldsymbol{P}}_k)_{\bar{\sigma}_{n_R-i,n_R}}\right) = 0 \quad \text{for} \quad l > n_R - i.$$

Therefore, (C.38) can be written as

$$|\boldsymbol{\Sigma}_k|\, E\left\{\left|\sigma^2\boldsymbol{I} + \tilde{\boldsymbol{H}}_k^H\boldsymbol{\Sigma}_k^{-1}\tilde{\boldsymbol{H}}_k\right|\right\} = \sum_{i=0}^{k-1}\sum_{l=0}^{n_R} t^l\,\hat{\varphi}_{kli}\left(\sigma^2\right)^{k-l-i-1},$$

which in turn can be given as

$$|\boldsymbol{\Sigma}_k| \, E\left\{\left|\sigma^2 \boldsymbol{I} + \tilde{\boldsymbol{H}}_k^H \boldsymbol{\Sigma}_k^{-1} \tilde{\boldsymbol{H}}_k\right|\right\} = \sum_{l=0}^{n_R} t^l \, \varphi_{kl},$$

where

$$\varphi_{kl} = \sum_{i=0}^{k-1} \hat{\varphi}_{kli} \left(\sigma^2\right)^{k-l-i-1}. \tag{C.46}$$

## C.4 Extended Laplace Type Approximation

Note the well-known fact that, $\sigma^2 \boldsymbol{I} = E\left\{\boldsymbol{A}^H \boldsymbol{A}\right\}$, for an iid complex Gaussian matrix ensemble, $\boldsymbol{A}$, of $\mathcal{CN}\left(0, \frac{\sigma^2}{\kappa}\right)$ random variables, where $\boldsymbol{A}$ is a $\kappa \times k-1$ matrix as in [57]. This result can be rewritten in the limit to give $\sigma^2 \boldsymbol{I} = \lim_{\kappa \to \infty} \left\{\boldsymbol{A}^H \boldsymbol{A}\right\}$. Using this in (4.37) gives

$$\tilde{I}_k(t) = \frac{1}{|\boldsymbol{\Sigma}_k|} \lim_{\kappa \to \infty} E\left\{\frac{\left|\boldsymbol{A}^H \boldsymbol{A} + \tilde{\boldsymbol{H}}_k^H \tilde{\boldsymbol{H}}_k\right|}{\left|\boldsymbol{A}^H \boldsymbol{A} + \tilde{\boldsymbol{H}}_k^H \boldsymbol{\Sigma}_k^{-1} \tilde{\boldsymbol{H}}_k\right|}\right\}, \tag{C.47}$$

$$= \frac{1}{|\boldsymbol{\Sigma}_k|} \lim_{\kappa \to \infty} E\left\{\frac{\left|\left(\boldsymbol{A}^H, \tilde{\boldsymbol{H}}_k^H\right)\begin{pmatrix}\boldsymbol{A} \\ \tilde{\boldsymbol{H}}_k\end{pmatrix}\right|}{\left|\left(\boldsymbol{A}^H, \tilde{\boldsymbol{H}}_k^H \boldsymbol{\Sigma}_k^{-\frac{1}{2}}\right)\begin{pmatrix}\boldsymbol{A} \\ \boldsymbol{\Sigma}_k^{-\frac{1}{2}} \tilde{\boldsymbol{H}}_k\end{pmatrix}\right|}\right\}, \tag{C.48}$$

$$= \frac{1}{|\boldsymbol{\Sigma}_k|} \lim_{\kappa \to \infty} E\left\{\frac{\left|\boldsymbol{B}_k^H \boldsymbol{B}_k\right|}{\left|\boldsymbol{B}_k^H \bar{\boldsymbol{\Sigma}}_k \boldsymbol{B}_k\right|}\right\}, \tag{C.49}$$

where $\bar{\boldsymbol{\Sigma}}_k = \operatorname{diag}\left(\boldsymbol{I}, \boldsymbol{\Sigma_k}^{-\frac{1}{2}}\right)$ and $\boldsymbol{B}_k = \begin{pmatrix}\boldsymbol{A} \\ \tilde{\boldsymbol{H}}_k\end{pmatrix}$. Using the well-known fact

$$\left|\boldsymbol{B}_k^H \boldsymbol{B}_k\right| = \prod_{i=1}^{k-1} \boldsymbol{b}_{ki}^H \left(\boldsymbol{I} - \tilde{\boldsymbol{B}}_{ki} \left(\tilde{\boldsymbol{B}}_{ki}^H \tilde{\boldsymbol{B}}_{ki}\right)^{-1} \tilde{\boldsymbol{B}}_{ki}^H\right) \boldsymbol{b}_{ki}, \tag{C.50}$$

from standard linear algebra, where $\boldsymbol{b}_{ki}$ is the $i^{th}$ column of $\boldsymbol{B}_k$, $\tilde{\boldsymbol{B}}_{ki}$ is $\boldsymbol{B}_k$ with columns $1, 2 \ldots i-1$, $\left|\tilde{\boldsymbol{B}}_{k1}^H \tilde{\boldsymbol{B}}_{k1}\right| = 1$ and $\tilde{\boldsymbol{B}}_{k1}\left(\tilde{\boldsymbol{B}}_{k1}^H \tilde{\boldsymbol{B}}_{k1}\right)^{-1} \tilde{\boldsymbol{B}}_{k1}^H = \boldsymbol{0}$, we can approximate (C.49) by

$$\tilde{I}_k(t) \simeq \frac{1}{|\boldsymbol{\Sigma}_k|} \prod_{i=1}^{k-1} E\left\{ \frac{\boldsymbol{b}_{ki}^H \left( \boldsymbol{I} - \tilde{\boldsymbol{B}}_{ki}\left(\tilde{\boldsymbol{B}}_{ki}^H \tilde{\boldsymbol{B}}_{ki}\right)^{-1} \tilde{\boldsymbol{B}}_{ki}^H \right) \boldsymbol{b}_{ki}}{\boldsymbol{b}_{ki}^H \left( \bar{\boldsymbol{\Sigma}}_k - \bar{\boldsymbol{\Sigma}}_k \tilde{\boldsymbol{B}}_{ki}\left(\tilde{\boldsymbol{B}}_{ki}^H \bar{\boldsymbol{\Sigma}}_k \tilde{\boldsymbol{B}}_{ki}\right)^{-1} \tilde{\boldsymbol{B}}_{ki}^H \bar{\boldsymbol{\Sigma}}_k \right) \boldsymbol{b}_{ki}} \right\}, \tag{C.51}$$

where $\boldsymbol{b}_{ki}$ and $\boldsymbol{B}_k$ correspond to a large but finite value of $\kappa$. Approximation (C.51) assumes that the terms in the product in (C.50) are independent. This is only true when $\boldsymbol{b}_{ki}$ contains iid elements. However, in the macrodiversity case, all the elements of $\boldsymbol{b}_{ki}$ are not iid. Nevertheless, part of $\boldsymbol{b}_{ki}$ (the contribution from $\boldsymbol{A}$) is iid. This motivates the approximation in (C.51). Next, we apply the standard Laplace type approximation [56] in (C.51) to give

$$\tilde{I}_k(t) \simeq \frac{1}{|\boldsymbol{\Sigma}_k|} \prod_{i=1}^{k-1} \frac{E\left\{ \boldsymbol{b}_{ki}^H \left( \boldsymbol{I} - \tilde{\boldsymbol{B}}_{ki}\left(\tilde{\boldsymbol{B}}_{ki}^H \tilde{\boldsymbol{B}}_{ki}\right)^{-1} \tilde{\boldsymbol{B}}_{ki}^H \right) \boldsymbol{b}_{ki} \right\}}{E\left\{ \boldsymbol{b}_{ki}^H \left( \bar{\boldsymbol{\Sigma}}_k - \bar{\boldsymbol{\Sigma}}_k \tilde{\boldsymbol{B}}_{ki}\left(\tilde{\boldsymbol{B}}_{ki}^H \bar{\boldsymbol{\Sigma}}_k \tilde{\boldsymbol{B}}_{ki}\right)^{-1} \tilde{\boldsymbol{B}}_{ki}^H \bar{\boldsymbol{\Sigma}}_k \right) \boldsymbol{b}_{ki} \right\}}, \tag{C.52}$$

$$\simeq \frac{1}{|\boldsymbol{\Sigma}_k|} \frac{E\left\{ \prod_{i=1}^{k-1} \boldsymbol{b}_{ki}^H \left( \boldsymbol{I} - \tilde{\boldsymbol{B}}_{ki}\left(\tilde{\boldsymbol{B}}_{ki}^H \tilde{\boldsymbol{B}}_{ki}\right)^{-1} \tilde{\boldsymbol{B}}_{ki}^H \right) \boldsymbol{b}_{ki} \right\}}{E\left\{ \prod_{i=1}^{k-1} \boldsymbol{b}_{ki}^H \left( \bar{\boldsymbol{\Sigma}}_k - \bar{\boldsymbol{\Sigma}}_k \tilde{\boldsymbol{B}}_{ki}\left(\tilde{\boldsymbol{B}}_{ki}^H \bar{\boldsymbol{\Sigma}}_k \tilde{\boldsymbol{B}}_{ki}\right)^{-1} \tilde{\boldsymbol{B}}_{ki}^H \bar{\boldsymbol{\Sigma}}_k \right) \boldsymbol{b}_{ki} \right\}}, \tag{C.53}$$

$$= \frac{1}{|\boldsymbol{\Sigma}_k|} \frac{E\left\{ \left| \boldsymbol{B}_k^H \boldsymbol{B}_k \right| \right\}}{E\left\{ \left| \boldsymbol{B}_k^H \bar{\boldsymbol{\Sigma}}_k \boldsymbol{B}_k \right| \right\}}. \tag{C.54}$$

Hence, a combination of approximate independence, the Laplace approximation for quadratic forms and the limiting version in (C.47) gives rise to the approximation used in Sec. 4.4. The accuracy of this approach is numerically established in the simulation results in Sec. 4.6.

# Appendix D

# Results for Chapter 6.

## D.1 Calculation of $|\boldsymbol{D}|\,\mathrm{Perm}\left(\boldsymbol{D}^{-1}\boldsymbol{Q}_1\right)$

The permanent of the denominator in (6.17) can be expanded as

$$\mathrm{Perm}\left(\boldsymbol{D}^{-1}\boldsymbol{Q}_1\right)=\sum_{\sigma}\mathrm{perm}\left(\left(\boldsymbol{D}^{-1}\boldsymbol{Q}_1\right)^{\{N-1\}}_{\sigma_{N-1,n_R}}\right), \tag{D.1}$$

where $\sigma_{N-1,n_R}$ is an ordered subset of $\{n_R\}=\{1,2,\ldots,n_R\}$ of length $N-1$ and the sum is over all $\binom{n_R}{N-1}$ such subsets. Noting the fact that $\mathrm{perm}\left(\boldsymbol{\Sigma}\boldsymbol{X}\right)=|\boldsymbol{\Sigma}|\,\mathrm{perm}\left(\boldsymbol{X}\right)$, for a square diagonal matrix $\boldsymbol{\Sigma}$ and (A.8), (D.1) can be further simplified to give

$$\mathrm{Perm}\left(\boldsymbol{D}^{-1}\boldsymbol{Q}_1\right)=\sum_{\sigma}\frac{\mathrm{perm}\left(\left(\boldsymbol{Q}_1\right)^{\{N-1\}}_{\sigma_{N-1,n_R}}\right)}{\left|\boldsymbol{D}^{\{N-1\}}_{\sigma_{N-1,n_R}}\right|}. \tag{D.2}$$

Using (D.2), the denominator in (6.17) becomes

$$|\boldsymbol{D}|\,\mathrm{Perm}\left(\boldsymbol{D}^{-1}\boldsymbol{Q}_1\right)=\sum_{\sigma}\left|\boldsymbol{D}_{\bar{\sigma}_{L,n_R}}\right|\mathrm{perm}\left(\left(\boldsymbol{Q}_1\right)^{\{N-1\}}_{\sigma_{N-1,n_R}}\right), \tag{D.3}$$

where $\bar{\sigma}_{L,n_R}$ is the ordered subset of length $L$ of $\{1, 2, \ldots, n_R\}$ which does not belong to $\sigma_{N-1,n_R}$ and $L = n_R - N + 1$. Expanding $\left|\boldsymbol{D}_{\bar{\sigma}_{L,n_R}}\right|$ gives

$$\left|\boldsymbol{D}_{\bar{\sigma}_{L,n_R}}\right| = \sum_{i=0}^{L} \left(\frac{-jt}{\sigma^2}\right)^i \mathrm{Tr}_i\left(\left(\boldsymbol{P}_1\right)_{\bar{\sigma}_{L,n_R}}\right). \tag{D.4}$$

Substituting (D.4) in (D.3) gives the desired result

$$|\boldsymbol{D}|\,\mathrm{Perm}\left(\boldsymbol{D}^{-1}\boldsymbol{Q}_1\right) = \sum_{i=0}^{L} (-jt)^i\,\tilde{\varphi}_i, \tag{D.5}$$

where

$$\tilde{\varphi}_i = \sum_{\sigma} \mathrm{Tr}_i\left(\left(\boldsymbol{P}_1\right)_{\bar{\sigma}_{L,n_R}}\right) \mathrm{perm}\left(\left(\boldsymbol{Q}_1\right)^{\{N-1\}}_{\sigma_{N-1,n_R}}\right) \left(\sigma^2\right)^{-i}. \tag{D.6}$$

## D.2 Calculation of Expectations Required for MMSE Analysis

The expectation, $E\left\{\left|\sigma^2\boldsymbol{I} + \boldsymbol{H}_1^H\boldsymbol{H}_1\right|\right\}$, can be computed adapting Appendix C.2 to handle $\boldsymbol{H}_1$ instead of $\tilde{\boldsymbol{H}}_k$ to give

$$E\left\{\left|\sigma^2\boldsymbol{I} + \boldsymbol{H}_1^H\boldsymbol{H}_1\right|\right\} = \sum_{i=0}^{N-1}\sum_{\sigma} \mathrm{Perm}\left(\left(\boldsymbol{Q}_1\right)^{\sigma_{i,N-1}}\right)\left(\sigma^2\right)^{N-i-1}. \tag{D.7}$$

Following the same approach the expectation, $|\boldsymbol{D}|\,E\left\{\left|\sigma^2\boldsymbol{I} + \boldsymbol{H}_1^H\boldsymbol{D}^{-1}\boldsymbol{H}_1\right|\right\}$, can also be computed adapting Appendix C.3 using the substitutions

$$t \to -jt, \tag{D.8}$$

$$\boldsymbol{\Sigma}_k \to \boldsymbol{D}, \tag{D.9}$$

$$\tilde{\boldsymbol{H}}_k \to \boldsymbol{H}_1, \tag{D.10}$$

to give

$$|\boldsymbol{D}|\, E\left\{\left|\sigma^2\boldsymbol{I}+\boldsymbol{H}_1^H\boldsymbol{D}^{-1}\boldsymbol{H}_1\right|\right\}=\sum_{i=0}^{n_R}(-jt)^i\,\varphi_i, \tag{D.11}$$

where

$$\varphi_i=\sum_{k=0}^{N-1}\hat{\varphi}_{ik}\left(\sigma^2\right)^{N-i-k-1}. \tag{D.12}$$

# Bibliography


[1] G. J. Foschini and M. J. Gans, "On the limits of wireless communication in a fading environment when using multiple antennas," *Wireless Personal Commun.*, vol. 6, no. 3, pp. 311–335, Mar 1998.

[2] J. H. Winters, "Optimum combining in digital mobile radio with co-channel interference," *IEEE J. Select Areas in Commun.*, vol.SAC-2, pp. 528–539, July. 1984.

[3] G. J. Foschini, M. K. Karakayali, and R. A. Valenzuela, "Coordinating multiple antenna cellular networks to achieve enormous spectral efficiency," *IEEE Proc. Commun.*, vol. 153, no. 4, pp. 548–555, Aug. 2006.

[4] M. K. Karakayali, G. J. Foschini, and R. A. Valenzuela, "Network coordination for spectrally efficient communications in cellular systems," *IEEE Trans. on Wireless Commun. Mag.*, vol. 13, no. 4, pp. 56–61, Aug. 2006.

[5] H. Huang, C. B. Papadias, and S. Venkatesan, "*MIMO Communication for Cellular Networks*," 1st ed., Springer: New York, 2012.

[6] G. J. Foschini, D. Chizhik, M. Gans, C. Papadias, and R. A. Valenzuela, "Analysis and performance of some basic space time architectures," *IEEE J. Select. Areas Commun.*, pt. 1, vol. 21, pp. 303–320, 2003.

[7] E. Biglieri, J. G. Proakis, and S. Shamai, "Fading channels: Information-theoretic and communications aspects," *IEEE Trans. Inform. Theory*, vol. 44, no. 6, pp. 2619–2692, 1998.

[8] A. Goldsmith, "*Wireless Communication*," 4th ed, New York: McGraw-Hill, 2000.

[9] M. K. Simon and M. S. Alouini, "*Digital Communications over Fading Channels: A Unified Approach to Performance Analysis*," 1st ed, New York, NY, USA: John Wiley, 2000.

[10] J. G. Proakis, "*Digital Communications*," 4th ed, New York: McGraw-Hill, 2001.

[11] S. Verdu, "*Multiuser Detection*," 1st ed, Cambridge: Cambridge University Press, 1998.

[12] R. A. Horn and C. R. Johnson, "*Matrix Analysis*," Cambridge: Cambridge Univ. Press, 1985.

[13] R. J. Muirhead, "*Aspects of Multivariate Statistical Theory*," 1st ed, New York: John Wiley, 1982.

[14] N. R. Goodman, "Statistical analysis based on certain multivariate compex distribution," *Annals of Mathematical Statistics*, pp. 152–177, 1963.

[15] K. I. Gross and D. S. T. P. Richards, "Total positivity, spherical series and hypergeometric functions of matrix arguments," *J. Approx. Theory*, vol-59, pp. 224–226, 1989.

[16] A. Edelman, "Eigenvalues and condition numbers of random metrices," *PhD thesis*, Masachusetts Institute of Technology, 1989.

[17] J. Wishart, "Generalised product moment distribution in samples from a normal multivariate population," *Biometrika*, vol. 20A, no. 1/2, pp. 32–52, 1928.

[18] P. A. Bello, "Characterization of randomly time-variant linear channels," *IEEE Trans. Commun.*, vol. 11, pp. 360-393, Dec. 1963.

[19] B. Sklar, "Rayleigh fading channels in mobile digital communication systems. I. Characterization," *IEEE Commun. Mag.*, vol. 35, no. 9, pp. 136–146, 1997.

[20] A. A. Saleh and R. A. Valenzuela, "A statistical model for indoor multipath propagation," *IEEE J. Select. Areas Commun.*, vol. SAC-5, no. 2, pp. 128–137, 1987.

[21] T. S. Rappaport, "*Wireless Communications: Principles and Practice*," 2nd ed., Upper Saddle River, NY: Prentice-Hall, 2001.

[22] D. Tse and P. Viswanath, *Fundamentals of Wireless Communication*. Cambridge, UK: Cambridge University Press, 2005.

[23] C. Oestges and B. Clerckx, "MIMO wireless communications: From real-world propagation to space-time code design," Academic Press (Elsevier), Oxford, UK, Apr. 2007.

[24] D. Chizhik, J. Ling, P. W. Wolniansky, R. A. Valenzuela, N. Costa, and K. Huber, "Multiple-input-multiple-output measurements and modelling," *IEEE J. Select. Areas Commun.*, vol. 21, no. 3, pp. 321–331, 2003.

[25] 3GPP and 3GPP2., "SCM-103: Spatial channel model AHG," Jan 2003.

[26] A. J. Goldsmith, "Design and performance of high-speed communication systems over time-varying radio channels," Ph.D. dissertation, University of California at Berkeley, 1994.

[27] J. P. Kermoal, L. Schumacher, K. I. Pedersen, P. E. Mogensen, and F. Frederiksen, "A stochastic MIMO radio channel model with experimental validation," *IEEE J. Select. Areas Commun.*, vol. 20, no. 6, pp. 1211-1226, 2002.

[28] P. J. Smith and M. Shafi, "The impact of complexity in MIMO channel models," *Proc. IEEE Int'l. Conf. on Communications*, Paris, France, pp. 2924–2928, 2004.

[29] W. C. Jakes, "*Microwave Mobile Communications*," 1st ed, Wiley, New York, 1974.

[30] E. Biglieri, R. Calderbank, A. Constantinides, A. Goldsmith, A. Paulraj, and H. V. Poor, "*MIMO Wireless Communication*," 1st ed, Cambridge: Cambridge University Press, 2007.

[31] E. Telatar, "Capacity of multi-antenna Gaussian channels," *Europ. Trans. Telecomm.*, vol. 10, no. 6, pp. 585–595, Nov. 1999.

[32] G. J. Foschini, "Layered space-time architecture for wireless communication in a fading environment when using multiple antennas," *Bell Syst. Tech. J.*, vol. 1, no. 2, pp. 41–59, 1996.

[33] J. H. Winters, J. Salz, and R. D. Gitlin, "The impact of antenna diversity on the capacity of wireless communication systems," *IEEE Trans. Commun.*, vol. 42, no.2/3/4, pp.1740–1751, Feb/Mar/Apr. 1994.

[34] S. Alamouti, "A simple transmit diversity technique for wireless communications," *IEEE J. Select. Areas Commun.*, vol. 16, no. 8, pp. 1451–1458, Oct. 1998.

[35] J. H. Winters, "The diversity gain of transmit diversity in wireless systems with Rayleigh fading," *IEEE Trans. Veh. Technol.*, vol. 47, no. 1, pp. 119–123, 1998.

[36] A. Paulraj, R. Nabar, and D. Gore, "*Introduction to Space-Time Wireless Communication*," 1st ed, Cambridge: Cambridge University Press, 2007.

[37] B. Clerckx, A. Lozano, S. Sesia, C. V. Rensburg, and C. B. Papadias, "3GPP LTE and LTE Advanced," *EURASIP Journal on Wireless Communication and Networking* 2009.

[38] D. Lee, B. Clerckx, E. Hardouin, D. Mazzarese, S. Nagata, and K. Sayana, "Coordinated multipoint transmission and reception in LTE-Advanced: Deployment scenarios and operational challenges," *IEEE Commun. Mag.*, vol. 50, no. 2, pp. 148–155, 2012.

[39] M. Sawahashi, Y. Kishiyama, A. Moromoto, D. Nishikawa, and M. Tanno, "Coordinated multipoint transmission/reception techniques for LTE-Advanced," *IEEE Trans. Wireless Commun.*, vol. 17, no. 3, pp. 26–34, Nov. 2011.

[40] D. Gesbert, S. Hanly, H. Huang, S. Shamai, O. Simeone, and W. Yu, "Multi-cell MIMO cooperative networks: A new look at interference," *IEEE Journal on Selected Areas in Comm.*, vol. 28, no. 9, pp. 1380–1408, Dec. 2010.

[41] I. F. Akyildiz, D. M. Gutierrez-Estevez, and E. C. Reyes, "The evolution to 4G cellular systems: LTE-Advanced," *Elsevier Physical Commun.*, vol. 3, pp. 214–244, 2010.

[42] G. T. . V11.1.0, "Coordinated multi-point operation for LTE physical layer aspects," release 11, 2011.

[43] A. Sanderovich, O. Somekh, H. Poor, and S. Shamai, "Uplink macro diversity of limited backhaul cellular network," *IEEE Trans. Inform. Theory*, vol 55, no. 8, pp. 3457–3478, Aug. 2009.

[44] P. Marsch and G. Fettweis, "Uplink CoMP under a constrained backhaul and imperfect channel knowledge," *IEEE Trans. Wireless Commun*, vol 10, no. 6, pp. 1730–1742, Jun. 2011.

[45] Q. H. Ngo, E. G. Larsson, and T. L. Marzetta, "Uplink power efficiency of multiuser MIMO with very large antenna arrays," *Proc. Allerton Conf. on Communication, Control, and computing*, Illinois, USA, pp. 1272–1279, 2011.

[46] J. Zhu, Q. Li, and Q. Li, "Pragmatic adaptive MRC and MMSE MIMO-OFDM receiver algorithm," US Patent 20080310486, 18 Dec. 2008.

[47] J. Cui and A. U. H. Sheikh, "Outage probability of cellular radio systems using maximal ratio combining in the presence of multiple interferers," *IEEE Trans. Commun.*, vol. 47, No. 47, pp. 1121–1124, Aug. 1999.

[48] A. Akyildiz and B. D. Rao, "Maximum ratio combining performance with imperfect channel estimates," *Proc. ICASSP*, Orlando, FL, May 2002, pp. 2485–2488.

[49] K. S. Ahn and R. W. Heath, "Performance analysis of maximum ratio combining with imperfect channel estimation in the presence of cochannel interferences," *IEEE Trans. Wireless Commun.*, vol. 8, no. 3, pp. 1080–1085, Mar. 2009.

[50] V. A. Aalo and J. Zhang, "Performance analysis of maximal ratio combining in the presence of multiple equal-power cochannel interferers in a nakagami fading channel," *IEEE Trans. Veh. Technol.*, vol. 50, no. 2, pp. 497–503, Mar. 2001.

[51] C. Chayawan and V. A. Aalo, "On the outage probability of optimum combining and maximal ratio combining schemes in an interferencelimited rice fading channel," *IEEE Trans. Commun.*,vol. 50, no. 4, pp. 532–535, Apr. 2002.

[52] I. S. Gradshteyn and I. M. Ryzhik, "*Table of Integrals, Series, and Products*," 7th ed, Boston: Academic Press, 2000.

[53] P. J. Smith, "Exact performance analysis of optimum combining with multiple interferers in flat Rayleigh fading," *IEEE Trans. Commun.*, vol. 55, no. 9, pp. 1674–1677, Sep. 2007.

[54] K. S. Miller, "*Multidimensional Gaussian Distributions*," 1st ed, New York: John Wiley & Sons, 1964.

[55] A. Firag, P. J. Smith, H. Suraweera, and A. Nallanathan, "Beamforming in correlated MISO systems with channel estimation error and feedback delay," *IEEE Trans. on Wireless Commun.*, vol. 10, no. 8, pp. 2592–2602, 2011.

[56] O. Lieberman, "A Laplace approximation to the moments of a ratio of quadratic forms," *Biometrika*, vol. 81, no. 4, pp. 681–690, Dec 1994.

[57] H. Gao, P. J. Smith, and M. V. Clark, "Theoretical reliability of MMSE linear diversity combining in Rayleigh-fading additive interference channels," *IEEE Trans. Commun.*, vol. 46, no. 5, pp. 666–672, May. 1998.

[58] A. Goldsmith, S. A. Jafar, N. Jindal, and S. Vishwanath, "Capacity limits of MIMO channels," *IEEE J. Select. Areas Commun.*, vol. 21, no. 5, pp. 684-702, 2003.

[59] M. Kiessling and J. Speidel, "Mutual information of MIMO channels in correlated Rayleigh fading environments - a general solution," *IEEE ICC*, Paris, France, vol.2, pp. 814–818, 2004.

[60] C. Chuah, D. Tse, J. Kahn, and R. Valenzuela, "Capacity scaling in MIMO wireless systems under correlated fading," *IEEE Trans. Inform. Theory*, vol. 48, no. 7, pp. 637–650, 2002.

[61] J. S. E. M. N. Bacha and S. V. Hanly, "On the capacity of cellular networks with MIMO links," *IEEE ICC*, Istanbul, Turkey, pp. 1337–1342, June 2004.

[62] B. Z. O. Somekh and S. S. (Shitz), "Spectral efficiency of joint multiple cellsite processors for randomly spread DS-CDMA systems," *IEEE Trans. Inform. Theory*, vol. 53, no. 7, pp. 2625–2637, Jul. 2007.

[63] D. W. Bliss, K. W. Forsthe, and A. F. Yegulalp, "MIMO communication capacity using infinite dimension random matrix eigenvalue distributions," *Proc. 35th Asilomar Conf. Signals, Systems and Computers*, Pacific Grove, CA, vol. 2, pp. 969-974, Nov. 2001.

[64] S. Chatzinotas, M. A. Imran, and R. Hoshyar, "On the multicell processing capacity of the cellular MIMO uplink channel in correlated Rayleigh fading environment," *IEEE Trans. Wireless Commun.*, vol. 8, no. 7, pp. 3704–3715, Jul. 2009.

[65] W. Weichselberger, M. Herdin, H. Ozcelik, and E. Bonek, "A stochastic MIMO channel model with joint correlation of both link ends," *IEEE Trans. Wireless Commun*, vol. 5, no. 1, pp. 90–100, Jan 2006.

[66] M. G. D. Shiu, G. Foschini and J. Kahn, "Fading correlation and its effect on the capacity of multielement antenna systems," *IEEE Trans. Commun.*, vo1.48, no.3, pp. 502–513, Mar. 2000.

[67] A. M. Tulino, A. Lozano, and S. Verdu, "Impact of antenna correlation on the capacity of multiantenna channels," *IEEE Trans. Inform. Theory*, vol. 51, no. 7, pp. 2491-2509, Jul. 2005.

[68] H. Minc, "*Permanants*," 1st ed, Massachusetts: Addison-Wesley Publishing Company Inc, 1978.

[69] H. Lutkepohl, "*Handbook of Matrices*," 1st ed, USA: John Wiley, 1996.

[70] D. A. Basnayaka, P. J. Smith, and P. A. Martin, "Ergodic sum capacity of macrodiversity MIMO systems in at Rayleigh fading," *IEEE Trans. Inf. Theory*, submitted.

[71] A. Stuart and J. K. Ord, *Kendall's Advanced Theory of Statistics: Volume 1 Distribution Theory.* London, UK: Edward Arnold, 1994.

[72] T. M. Cover and J. A. Thomas, "*Elements of Information Theory*," 3rd ed., USA: John Wiley Sons, 1991.

[73] D. A. Basnayaka, P. J. Smith, and P. A. Martin, "Symbol error rate performance for macro-diversity maximal ratio combining in flat Rayleigh fading," *IEEE AusCTW*, Wellington, New Zealand, pp. 25–30, 2012.

[74] ——, "Exact dual-user macrodiversity performance with linear receivers in flat Rayleigh fading," to be presented *IEEE ICC*, Ottawa, Canada, Jun. 2012.

[75] J. H. Winters and J. Salz, "Upper bounds on the bit error rate of optimum combining in wireless systems," *IEEE Proc. Vehicul. Tech. Conf.*, pp. 942–946, June. 1994.

[76] H. V. Poor and S. Verdu, "Probability of error in MMSE multiuser detection," *IEEE Trans. Inform. Theory*, vol. 43, no. 3, pp. 858-871, 1997.

[77] D. Guo, S. Verdu, and L. K. Rasmussen, "Asymptotic normality of linear multiuser receiver outputs," *IEEE Trans. Inform. Theory*, vol. 48, no. 12, pp. 3080-3095, 2002.

[78] M. Kobayashi, M. Debbah, and J. C. Belfiore, "Outage efficient strategies for network MIMO with partial CSIT," *Proc. IEEE Int'l. Symp. Information Theory* 2009, Coex, Seoul, Korea, pp. 249–253, Jun/Jul. 2009.

[79] L. Hui and W. W. Bo, "Performance analysis of network MIMO technology," *IEEE APCC*, Shanghai, China, pp. 234–236, May 2009.

[80] R. K. Mallik, M. Z. Win, M. Chiani, and A. Zanella, "Bit-error probability for optimum combining of binary signals in the presence of interference and noise," *IEEE Trans. Wireless Commun.*, vol. 3, n. 2, pp. 395–407, Mar. 2004.

[81] M. R. McKay, A. Zanella, I. B. Collings, and M. Chiani, "Optimum combining of Rician-faded signals: Analysis in the presence of interference and noise," *Proc. IEEE Int'l. Conf. on Communications*, vol. 3, n. 2, pp. 1096–1101, 2007.

[82] Y. C. Liang, G. Pan, and Z. D. Bai, "Asymptotic performance of MMSE receivers for large systems using random matrix theory," *IEEE Trans. Inform. Theory*, vol 53, no. 11, pp. 4173–4190, Nov. 2007.

[83] Y. Jiang, M. K. Varanasi, and J. Li, "Performance analysis of ZF and MMSE equalizers for MIMO systems: An in depth study of the high SNR regime," *IEEE Trans. Inform. Theory*, vol. 57, no. 4, pp. 2008–2026, Apr. 2011.

[84] D. A. Gore, R. W. H. Jr., and A. J. Paulraj, "Transmit selection in spatial multiplexing systems," *IEEE Commun. Lett.*, vol. 6, no.11, pp. 491–493, Nov. 2002.

[85] T. Suwa, "Finite-sample properties of the k-class estimators," *Econometrica*, vol. 40, no. 4, pp. 653–680, Jul 1972.

[86] P. Li, D. Paul, R. Narasimhan, and J. Cioffi, "On the distribution of SINR for the MMSE MIMO receiver and performance analysis," *IEEE Trans. Inform. Theory*, vol. 52, no. 1, pp. 271-286, 2006.

[87] M. V. Clark, L. J. Greenstein, W. K. Kennedy, and M. Shafi, "Optimum linear diversity receivers for mobile communication," *IEEE Trans. Veh. Technol.*, vol. 43, no. 1, pp. 47–56, Feb. 1994.

[88] D. A. Basnayaka, P. J. Smith, and P. A. Martin, "Performance analysis of dual-user macro-diversity MIMO systems with linear receivers in flat Rayleigh fading," submitted to *IEEE Trans. Wireless Commun.*, Nov. 2011.

[89] ——, "Ergodic sum capacity of macrodiversity MIMO systems in flat Rayleigh fading," submitted to *IEEE Trans. Inform. Theory*, May. 2012.

[90] H. Cramer, "*Mathamatical Methods of Statistics*," 1st ed, Princeton: Princeton University Press, 1945.

[91] X. Zhu and R. D. Murch, "Performance analysis of maximum likelihood detection in a MIMO antenna system," *IEEE Trans. Commun.*, vol-50, no. 2, pp. 187–191, 2002.

[92] M. Kiessling, J. Speidel, and N. Geng, "Performance analysis of MIMO maximum likelihood receivers with channel correlation, colored Gaussian noise, and linear prefiltering," *IEEE ICC*, Istanbul, Turkey, vol. 5, pp. 3026–3030, May 2003.

[93] H. Liu, G. Li, X. Cheng, and D. Li, "Performance analysis framework of ML MIMO receiver over correlated Rayleigh fading channel," *IEEE ICC*, Istanbul, Turkey, vol. 9, pp. 4137–4142, May 2003.

[94] B. Clerckx and C. Oestges, "Finite-snr performance analysis of space-time coding in correlated ricean mimo channels," *IEEE Trans. Inform. Theory*, vol. 53, no. 12, pp. 4761–4777, Dec. 2007.

[95] V. Tarokh, N. Seshadri, and A. R. Calderbank, "Space-time codes for high data rate wireless communications: Performance criterion and code construction," *IEEE Trans. Inform. Theory*, vol. 44, no. 2, pp. 744–765, Mar. 1998.

[96] Y. Jeong and H. Shin, "Effect of joint spatial correlation on the diversity performance of space-time block codes," *IEEE Commun. Lett.*, vol. 13, no. 7, pp. 477–479, July 2009.

[97] N. L. Johnson and S. Kotz, "Continuous univariate distributions - 2," 1st ed, John Wiley: New York, 2000.

[98] L. M. Garth, P. J. Smith, and M. Shafi, "Exact symbol error probabilities for SVD transmission of BPSK data over fading channels," *IEEE ICC*, Seoul, South Korea, pp. 2271–2276, 2005.

[99] R. Knopp and P. A. Humblet, "Information capacity and power control in single cell multiuser communications," *Proc. IEEE Int'l. Conf. on Communications*, pp. 331-335, June 1995.

[100] L. Yang and M. S. Alouini, "Performance analysis of multiuser selection diversity," *IEEE Trans. Veh. Technol.*, vol. 55, no. 6, pp. 1848–1861, Nov. 2006.

[101] W. Ajib and D. Haccoun, "An overview of scheduling algorithums in MIMO-based fourth-generation wireless systems," *IEEE Network*, vol. 19, no. 5, pp. 43–48, Oct. 2005.

[102] M. Gidlund and J. C. Laneri, "Scheduling algorithms for 3GPP long term evolution systems: from a quality of service perspective," *IEEE ISSSTA*, Bologna, Italy, pp. 114-117, Aug. 2008.

[103] P. Visawanath, D. N. C. Tse, and R. Laroia, "Opportunistic beamforming using dumb antennas," *IEEE Trans. Inform. Theory*, vol. 48, no. 6, pp. 1277-1294, June 2002.

[104] L. Wand, Y. K. Kwok, W. C. Lau, and V. K. N. Lau, "On channel-adaptive fair multiple acess control," *Proc. IEEE Int'l. Conf. on Communications*, vol. 1, pp. 276–280, 2003.

[105] M. Al-Rawi, R. Jantti, J. Torsner, and M. Sagfors, "Opportunistic uplink scheduling for 3G LTE systems," *IEEE IIT*, Dubai, pp. 705-709, 2007.

[106] S. A. Ramprashad and G. Caire, "Cellular vs. network MIMO: A comparison including the channel state information overhead," *Proc. IEEE Int'l. Symp. on Personal, Indoor and Mobile Radio Communications*, pp. 878–884, 2009.

[107] ——, "Rethining network MIMO: Cost of CSIT, performance analysis, and architecture comparisons," *Information Theory and Applications Workshop*, pp. 1–10 , 2010.

[108] B. Bandemer and S. Visuri, "Capacity-based uplink scheduling using long-term channel knowledge," *Proc. IEEE Int'l. Conf. on Communications*, pp. 785–790, 2007.

[109] F. D. Calabrese, P. H. Michaelsen, C. Rosa, M. Anas, C. U. Castellanos, D. L. Villa, K. I. Pedersen, and P. E. Mogensen, "Search tree based uplink channel aware packet scheduling for UTRAN LTE," *IEEE VTC*, pp. 1949-1953, 2008.

[110] R. Zhang, "Scheduling for maximum capacity in SDMA/TDMA networks," *Proc. IEEE Int'l. Conf. on Acoustics, Speech, and Signal Processing*, vol. 3, pp. 2141–2144, 2009.

[111] R. Madan, S. P. Boyd, and S. Lall, "Fast algorithms for resource allocation in cellular networks," *IEEE/ACM Trans. Networking*, vol. 18, no. 3, pp. 973–984 , 2007.

[112] S. V. Hanly, "Capacity and power control in spread spectrum macrodiversity radio networks," *IEEE Trans. Commun.*, pp. 247-256, 1996.

[113] X. Zhang and J. Lee, "Low complexity MIMO scheduling with channel decomposition using capacity upper bound," *IEEE Trans. Commun.*, vol. 56, no. 6, pp. 871–876, 2008.

[114] O. Somekh, O. Simeone, Y. Bar-Ness, A. M. Haimovich, and S. Shamai, "Cooperative multi-cell zero-forcing beamforming in cellular downlink channels," *IEEE Trans. Inform. Theory*, vol. 55, no. 7, pp. 3206–3219, 2009.

[115] A. Reichman, "An overview of multi-mode multi-user adaptation and scheduling techniques in MIMO-based fourth generation wireless systems," *IEEE Network*, vol. 19, no. 5, pp. 43–48, Oct. 2005.

[116] F. Pukelsheim, *Optimal Design of Experiments*. New York, NY, USA: John Wiley, 1993.

# About The Author

(S'11,M'12) Dushyantha A. Basnayaka was born in 1982 in Colombo, Sri Lanka. He received the B.Sc.Eng degree with 1$^{st}$ class honors from the University of Peradeniya, Sri Lanka, in Jan 2006. He is currently working towards for his PhD degree in Electrical and Computer Engineering at the University of Canterbury, Christchurch, New Zealand.

He was an instructor in the Department of Electrical and Electronics Engineering at the University of Peradeniya from Jan 2006 to May 2006. He was a system engineer at MillenniumESP (a member company of London Stock Exchange group) from May 2006 to Jun 2009. Since Jul. 2009 he is with the communication research group at the University of Canterbury, New Zealand.

D. A. Basnayaka is a recipient of University of Canterbury International Doctoral Scholarship for his doctoral studies at UC. His current research interests include all the areas of digital communication, with a special emphasis on macrodiversity wireless systems. He holds one pending US patent as a result of his doctoral studies at UC.